ISSN 2538-6727 (online)

KAUNAS UNIVERSITY OF TECHNOLOGY
FACULTY OF MECHANICAL ENGINEERING AND DESIGN

INTERNATIONAL YOUNG RESEARCHERS' CONFERENCE

Industrial Engineering 2025

CONFERENCE PROCEEDINGS

Kaunas, 2025

Proceedings of the 12th International Young Researchers' Conference
Editors: Dr. Ginta Laureckienė
Dr. Laura Gegeckienė
Dr. Ingrida Venytė

The administrator of the conference website
https://iec.ktu.edu/
Dr. Ginas Čižauskas

The language of articles and abstracts is not corrected.

The published articles were reviewed by the following reviewers:

Algimantas Balčius, Regita Bendikienė,
Kęstutis Buinevičius, Ginas Čižauskas,
Antanas Čiuplys, Milda Dubosienė,
Laura Gegeckienė, Virginija Gylienė,
Ada Gulbinienė, Mindaugas Dagilis,
Virginija Daukantienė, Eglė Fataraitė-Urbonienė,
Jūratė Jablonskytė, Vaida Jonaitienė,
Lina Kavaliauskienė, Tomas Kuncius,
Eglė Kumpikaitė, Ginta Laureckienė,
Martynas Lendraitis, Monika Maziukienė,
Darius Mažeika, Daiva Mikučionienė,
Rimvydas Milašius, Linas Paukštaitis,
Darius Pauliukaitis, Inga Skiedraitė,
Kęstutis Vaitasius, Visvaldas Varžinskas,
Ingrida Venytė, Kristina Žukienė

doi:

COMMITTEES

SCIENTIFIC COMMITTEE

Algimantas Balčius, Assoc. Prof. (Lithuania)
Rodica Harpa, Prof. Habil. Dr. (Romania)
Roberts Joffe, Prof. (Sweden)
João Mateus, Prof. (Portugal)
Daiva Mikučionienė, Prof. (Lithuania)
Üyesi Abdulkerim Okbaz, Assoc. Prof. (Turkey)
Mária Omastová, Principal Research Scientist, Ing. (Slovakia)
Laurencas Raslavičius, Prof. (Lithuania)
Rūta Rimašauskienė, Assoc. Prof. (Lithuania)
Dariusz Szpica, Prof. (Poland)
Daiva Zeleniakienė, Prof. (Lithuania)

ORGANIZING COMMITTEE

Chairman – Dr. Sigita Urbaitė
Members:
Dr. Ginas Čižauskas
PhD. Mindaugas Dagilis
Dr. Laura Gegeckienė
Dr. Ginta Laureckienė
Dr. Monika Maziukienė
Dr. Ingrida Venytė

Preface

The 12th International Young Researchers' Conference on "Industrial Engineering 2025" is dedicated to developing the research competencies of young researchers, publicizing research relevant to industry, and developing sustainable production and consumption. This year, a thematic section, "Fashion engineering—future technologies," is included in the conference program.

The Conference covers a wide range of topics:

- Advanced Mechanical Technologies
- Fashion Engineering
- Industrial Design and Engineering
- Materials Science and Engineering
- Production Technologies and Engineering
- Sustainable Consumption and Business Management
- Sustainable Energy Systems
- Sustainable Food Systems and Agriculture
- Sustainable Urban and Rural Development
- Transport Engineering and Sustainable Mobility

The International Young Researchers Conference provides an excellent opportunity to get acquainted with the works of young researchers and the problems being solved, to discuss current topics and to assess the national and international importance of scientific achievements for industry and society.

Organizing Committee

INVITED SPEAKERS

Sandra Antanavičienė
(ECIU University Marketing and Communication Lead)
Twelve universities towards one European ambition: ECIU University experiences and opportunities

Rafał Stanik
(Technische Universität Dresden Institut für Leichtbau und Kunststofftechnik)
Green materials and energy-efficient processes for circular composite products by utilising regional potentials and pan-European partnerships – GreenCompas

Kęstutis Lekeckas
(Kaunas University of Technology)
Design in Engineering

Albert Langkamp
(Technische Universität Dresden Institut für Leichtbau und Kunststofftechnik)
Excellence in Lightweight Design – Institute of Lightweight Engineering and Polymer Technology

Olivier Sappin
(CATIA CEO)
Dassault Systèmes

CONTENT

MATERIALS SCIENCE AND ENGINEERING

SUSTAINABLE ENERGY SYSTEMS

SUSTAINABLE URBAN AND RURAL DEVELOPMENT

TRANSPORT ENGINEERING AND SUSTAINABLE MOBILITY

ADVANCED MECHANICAL TECHNOLOGIES

Analysis of the Interfacial Shear Strength of aBasalt Single Fibre and Polymer Matrix: Numerical and Experimental Approach

Emilija STANKUTĖ[1, 2*], Gediminas MONASTYRECKIS[1], Daiva ZELENIAKIENĖ[1]

1 Kaunas Technology University, Department of Mechanical Engineering

2 Lithuanian Energy Institute, Laboratory of Nuclear Installation Safety

** emilija.stankute@lei.lt*

Abstract

The mechanical performance of fibre-reinforced composites is strongly influenced by the quality of the fibre-matrix interface. This research aims to analyse the interfacial shear strength (IFSS) between a basalt fibre and a polymer matrix using combined experimental and numerical approaches. Micro-bond tests were conducted to measure the IFSS, while finite element modelling simulated stress distribution and failure process. The results showed that basalt fibres exhibited moderate interfacial strength with the polymer matrix, and numerical simulations accurately depict the overall pattern of the experimental load-displacement behaviour. The study confirms the potential of basalt fibres for high-performance composites and demonstrates that combining testing with numerical modelling is an effective strategy for characterising and understanding fibre-matrix interactions.

Keywords: basalt fibre, epoxy, polymer composite, interfacial shear strength, finite element modelling.

1. Introduction

Fibre reinforced polymer (FRP) composites have become crucial materials in engineering and structural applications due to their excellent strength-to-weight ratio, corrosion resistance and versatility. The performance and durability of these composites are largely influenced by the mechanical characteristics of the fibre-matrix interface, where load transfer is important to ensure structural functionality. Among the various interface-related parameters, the interfacial shear strength (IFSS) is significant. A strong and well-bonded interface ensures that applied stresses are effectively transferred from the polymer matrix to high-strength fibres, enhancing overall composite performance and delaying the onset of failure mechanisms such as fibre pull-out or interfacial debonding.

Increasing environmental awareness and the demand for sustainable materials, basalt has gained attention as an eco-friendly alternative to traditional reinforcements such as glass or carbon fibres [1]. Sourced from volcanic rock and produced through a relatively low-energy melting process without the use of additives, basalt fibres offer a low environmental footprint, high recyclability and abundant raw material availability [2, 3]. Their non-toxic production and high durability contribute to more sustainable composite solutions, especially in sectors aiming to reduce environmental impact without compromising performance, such as aerospace, automotive and construction industries. As industries move towards greener alternatives, understanding and optimising the interface behaviour of basalt fibre composites becomes crucial for their broader application.

Basalt (BF) and glass (GF) fibres reinforced with a polypropylene (PP) matrix were investigated by R. Zykaite et al. [4] by micro-debonding testing and evaluation of interfacial shear strength. PP films of different thicknesses were formed by screw extruder and cut in rectangular shape. Both

types of fibres were treated with a silane-based surface treatment. For the sample preparation, PP film was mounted on the fibre and heated in the oven to melt the film. It is noted that PP-GF systems have higher IFSS values than PP-BF systems, due to GF sizing was made to have excellent compatibility with PP, in contrast to BF, which sizing intended for epoxy resin. In comparison to microcomposites without a coupling agent, the IFSS of microcomposites with a coupling agent increases. Researchers claim that at very low speeds, new adhesion contacts between the fibre and matrix may develop, and polymeric chains may reorganize. As a result, IFSS values are constant. Z. Yang et al. [5] investigated the limitation of basalt fibre as a reinforcing material due to the brittleness of the fibre-matrix interface. To enhance the interfacial adhesion between BF and epoxy matrix, low-pressure O_2 and H_2-Ar plasma were used to surface activate the BF under various conditions. According to the findings, the optimal conditions for the surface activation of BF were found to be O_2 plasma modification, since O_2 plasma treatment demonstrated a greater IFSS improvement of 38.4% compared to the H_2-Ar plasma approach (14.4%) under ideal activation circumstances when compared to neat BF.
The aim of this study is to analyse the interfacial shear strength between a single basalt fibre and a polymer matrix using a combined experimental and numerical approach. By simulating stress distributions and failure mechanisms that are difficult to witness directly in addition to experimentally measuring IFSS, this hybrid methodology allows a greater comprehension of interfacial mechanics.

2. Experimental

2.1. Sample preparation

A bio-based diglycidyl ether of bisphenol A epoxy SR Greenpoxy 33 (Sicomin, France) with carbon content (~35 %) sourced from plant origins and solvent-free phenalkamine epoxy curing agent LITE 2401 (Cardolite, Belgium) sourced from cashew nutshell liquid technology with bio-content of ~33 % were used as the matrix material due to their lower environmental impact, high bio-based content and good mechanical and chemical properties. The use of SR Greenpoxy 33 and LITE 2401 reduces reliance on petroleum-based resources, maintains comparable performance to traditional epoxy systems, making them appealing for use in sustainable composite applications. Basalt fibres, supplied by Basaltex, Belgium, with an average diameter of 16 μm were used.
Basalt fibres were carefully mounted on a support frame, securing both ends with glue. A curing agent was then added according to the equivalent weight of the epoxy. Small polymer droplets were deposited onto individual fibres using a thin metal wire and then left to cure in a room temperature for 24 h and post-cured in the oven for 2 h at 80°C and 2 h at 120°C. For the micro-bond test (MBT), 50 μm of distance between blades was chosen, the resin microdroplet diameter was 100 μm, embedded length – 250 μm.

2.2. Testing

MBT, a commonly used method for describing fibre-matrix adhesion at the micro-scale, is used in the experimental portion of this work. In this method, a small droplet of polymer is placed onto a single fibre and shear force is applied until the droplet debonds. IFSS is computed using the force at debonding, fibre diameter and embedded droplet values. The IFSS was calculated using the equation (1):

$$\tau = \frac{F_{max}}{\pi l d}, \quad (1)$$

where F_{max} is the maximum load at debonding, d – fibre diameter, l – embedded length of the droplet.

The embedded microdroplet length was measured using the Dia-Stron LEX820 micro-bond tester (Andover, UK). The load cell of 2 N pulled the droplet at the speed of 0,09 mm/min (Fig. 1).

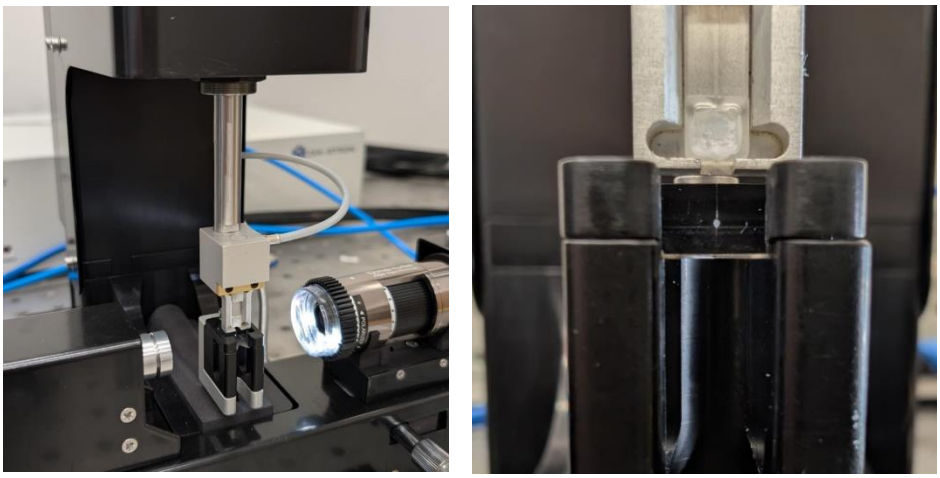

Fig. 1. Micro-bond test using Dia-Stron LEX820

3. Numerical modelling

A finite element model (FEM) was developed using ABAQUS software (Fig. 2). The model represented a single fibre embedded in a spherical polymer matrix. Fibre diameter – 16 µm, the surrounding interface was chosen 1 µm in thickness and the microdroplet diameter was 100 µm, while the embedded length – 250 µm. The fibre, interface, knives and the matrix were modelled using 3D solid elements. Elastic properties of basalt fibre (Young's modulus 90 GPa, Poisson's ratio 0,25), interface (Young's modulus 2 GPa, Poisson's ratio 0,3) and epoxy (Young's modulus 3,3 GPa, Poisson's ratio 0,3) droplet were implemented as linear isotropic. Model additionally had plastic properties, containing yield stress starting at 0,04 GPa and 0,025 GPa for epoxy and interface, respectively and damage evolution of 0,01 µm. The model is simulated using an explicit technique.

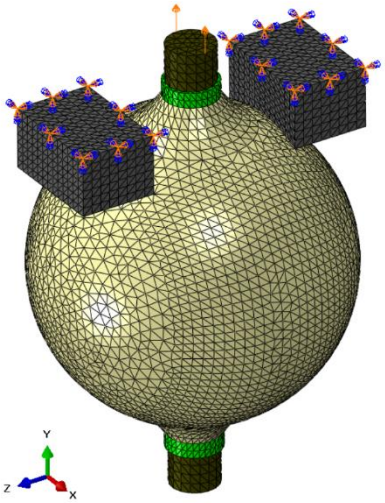

Fig. 2. Finite element model using ABAQUS software

Blades were fixed at the top surface, and a displacement-controlled load of 2 µm was applied to the fibre surface to simulate the micro-bond test. For model simulation, a tetrahedron mesh was chosen. The simulated load-displacement curve was compared with experimental results to validate the model.

4. Results

The finite element model successfully simulated the micro-bond test by replicating the mechanical response of a single basalt fibre embedded in a polymer matrix under axial loading. Simulation results show stress distribution in the fibre and microdroplet (Fig. 3). Stress starts where the knives embed the droplet and spreads down towards the fibre.

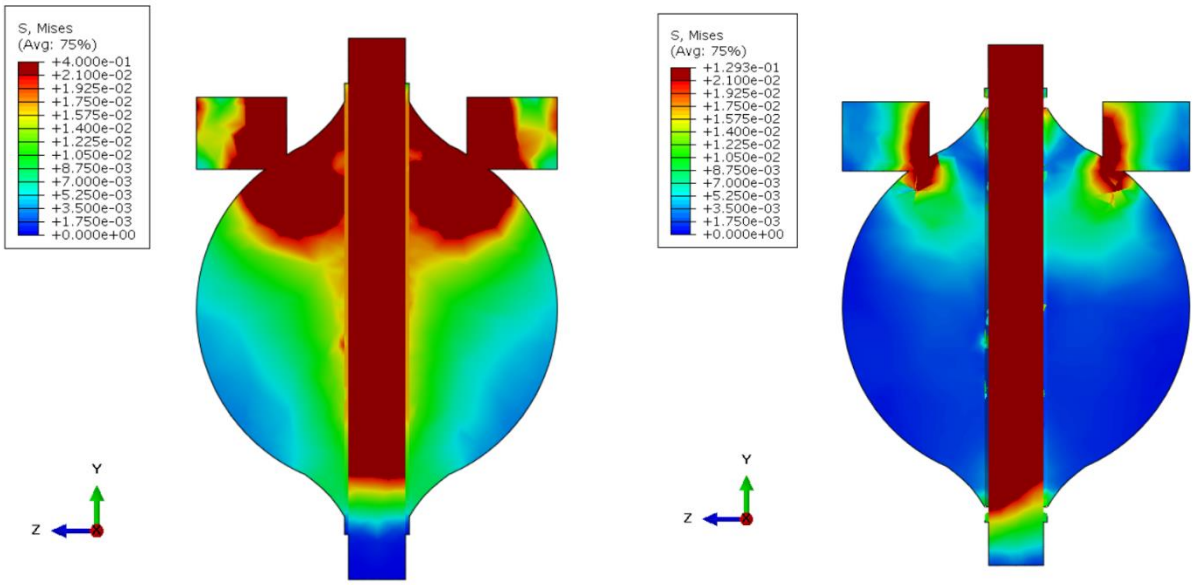

Fig. 3. Finite element model before and after the fracture, μm

Figure 4 reveals that the experimental graph is almost linear, reaching the highest point of 56.21 mN, where the droplet slips down the fibre. The numerical graph is a bit bent upwards, however, it follows the experimental graph well. Simulated microdroplet pull-out test reached the highest point of 58,90 mN. The reason for these deviations is that the current simulation findings are an initial calibration step and should be regarded as preliminary. It is anticipated that future model development will increase the agreement between numerical predictions and experimental findings.

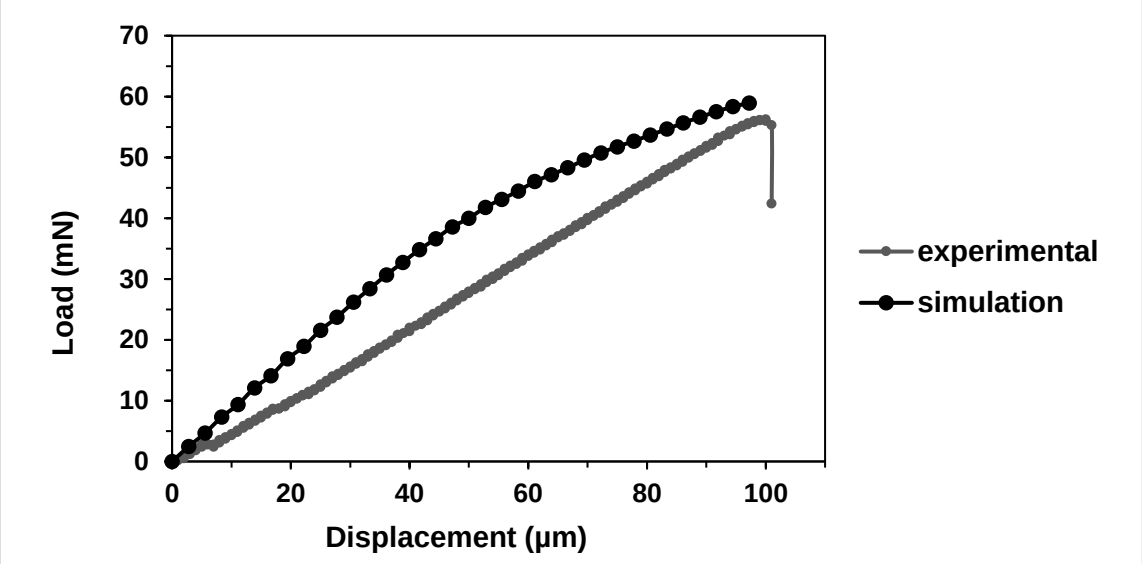

Fig. 4. Experimental and numerical load-displacement graph

IFSS was also calculated. Experimentally obtained average value is 9,66 MPa with 2,56 MPa of standard deviation, and numerical value is 9,38 MPa (Fig. 5).

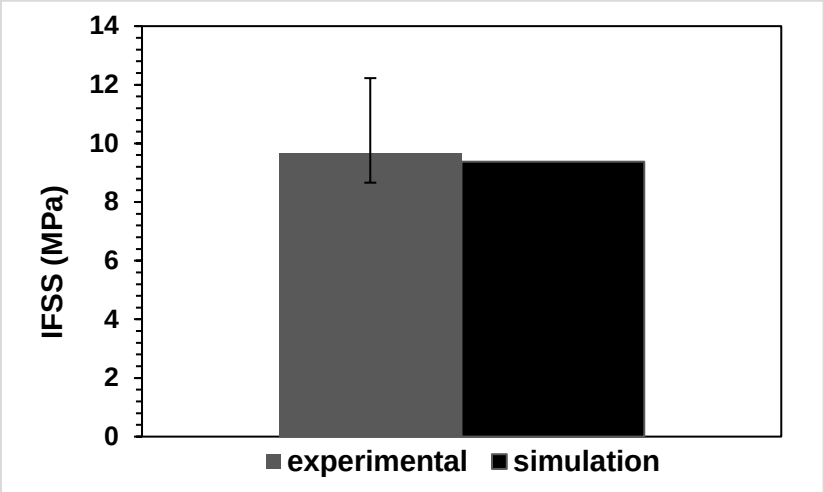

Fig. 5. Experimental and numerical values of IFSS

5. Conclusions

By accurately simulating the mechanical reaction of a single basalt fibre embedded in a polymer matrix under axial loading, the finite element model was able to replicate the micro-bond test.

1. The overall trends of the numerical and experimental load-displacement curves are similar; the reason for disparities is that the numerical model was created and parametrized before the entire experimental campaign was finished.
2. IFSS tests revealed good alignment between numerical and experimental results, with a 2.89% difference.

References

1. PATTI, A., et al. A Comparative Analysis on the Processing Aspects of Basalt and Glass Fibers Reinforced Composites. *Fibers and Polymers*, May 1, 2021, vol. 22, no. 5 [viewed Apr 29, 2025]. pp. 1449–1459. Available from: https://doi.org/10.1007/s12221-021-0184-x ISSN 1875-0052. DOI 10.1007/s12221-021-0184-x.
2. CHAIRI, M., PIPEROPOULOS, E., DI BELLA, G. and PROVERBIO, E. Mechanical Performance of Recycled Woven Basalt Fiber-Reinforced Composites for Sustainable Manufacturing Applications. *Applied Composite Materials*, April 8, 2025 [viewed Apr 29, 2025]. Available from: https://doi.org/10.1007/s10443-025-10332-6 ISSN 1573-4897. DOI 10.1007/s10443-025-10332-6.
3. FIORE, V., SCALICI, T., DI BELLA, G. and VALENZA, A. A Review on Basalt Fibre and its Composites. *Composites Part B: Engineering*, 2015, vol. 74 [viewed Apr 29, 2025]. pp. 74–94. Available from: https://www.sciencedirect.com/science/article/pii/S1359836815000062 ISSN 1359-8368. DOI 10.1016/j.compositesb.2014.12.034.
4. ZYKAITE, R., PURGLEITNER, B., STADLBAUER, W. and BURGSTALLER, C. Microdebond Test Development and Interfacial Shear Strength Evaluation of Basalt and Glass Fibre Reinforced Polypropylene Composites. *Journal of Composite Materials*, 2017, vol. 51, no. 29 [viewed Apr 29, 2025]. pp. 4091–4099. Available from: https://doi.org/10.1177/0021998317697810 ISSN 0021-9983. DOI 10.1177/0021998317697810.
5. GUO, G., et al. Surface Activation and Characterization of Basalt Fiber by Plasma Treatment and its Interfacial Adhesion with Epoxy. *Polymers*, 2024, vol. 16, no. 22 [viewed Apr 29, 2025]. pp. 3181. Available from: https://www.mdpi.com/2073-4360/16/22/3181 ISSN 2073-4360. DOI 10.3390/polym16223181.

Sustainable and Efficient Epoxy Curing for Enhanced Aviation Composite Bonding

Karina DRAGASIUTE*, Gediminas MONASTYRECKIS, Daiva ZELENIAKIENE

Kaunas University of Technology

* karina.dragasiute@ktu.edu

Abstract

This study investigates a more sustainable and energy-efficient alternative to conventional epoxy adhesive curing methods used in the aerospace and aviation industries. Instead of relying on traditional curing equipment, such as large ovens or autoclaves, the adhesive is reinforced with a carbon fibre chopped strand mat (CSM) to act as a conductive layer within the bonding area. The electrical resistance of CSM is characterised across three fabric layer orientations (0°, 45°, and 90°), confirming sufficient conductive homogeneity of the material, with 90° being the most conductive layer orientation. Single-lap shear tests demonstrate that CSM-reinforced specimens cured via Joule heating achieved a similar average shear strength (10.6 MPa) compared to oven-cured pure epoxy specimens (9.3 MPa). These results indicate that Joule heating using CSM is an energy-efficient and cost-effective alternative to conventional curing equipment.

Keywords: carbon fibre chopped strand mat (CSM), adhesives, Joule heating, localised curing, composite bonding.

1. Introduction

Traditional epoxy adhesive curing methods, particularly in the aviation and aerospace sectors, still face challenges related to efficiency and scalability [1, 2]. Conventional curing equipment, such as autoclaves and large ovens, typically requires an energy-intensive process [2, 3]. The low thermal conductivity of polymers imposes limitations on heating rates, leading to longer curing cycles and, thus, increased energy costs [3, 4]. The size of curing equipment also limits composite parts sizes, causing scalability issues when manufacturing large aircraft parts and highlighting the need for alternative curing processes [5].

To address these limitations, this research proposes an alternative bonding technology that utilises localised Joule heating. Joule heating (also known as Ohmic heating) is the process in which electrical energy applied to a conductive material is converted into heat due to the electrical resistance. In composite bonding applications, Joule heating can be used to cure adhesives directly in the bonding area. Generally, adhesives function as insulators; therefore, for Joule heating to be effective, this research suggests using a carbon fibre chopped strand mat (CSM) as a conductive layer. CSM material is selected because it is a commercially available option [6]. This type of application enables efficient localised curing without the need to heat the entire part. A significant aspect of this study is the implementation of a low-cost Arduino-controlled curing system, which regulates power input and monitors temperature fluctuations during curing cycles for each specimen. However, prior to integrating these CSM layers into the specimens, their electrical behaviour must be tested. Joule heating uniformity directly depends on the homogeneity of conductivity, therefore, it is important to ensure the suitability of the CSM for effective and even heat distribution [7, 8].

This study focuses on evaluating the electrical resistance of CSM in three different layer orientations (0 °, 45 ° and 90°) to determine its suitability as a reliable conductive layer within the bonding area under Joule heating and its potential implications for bonding performance in single-lap joint samples.

2. Materials and Methods

2.1. Conductive Homogeneity Evaluation of CSM

To evaluate the homogeneity of the 8 g/m^2 non-woven carbon fibre CSM (R&G Faserverbundwerkstoffe GmbH, Waldenbuch, Germany) and its suitability as a conductive interface for Joule heating, electrical resistance measurements were conducted on samples cut at nominal angles of 0°, 45°, and 90° relative to the fabric roll direction. Although it is considered that CSM fibres are randomly oriented within the fabric, as shown in Figure 1, these measurements allowed for the assessment of any potential anisotropy in the material's conductive behaviour caused by the manufacturing process.

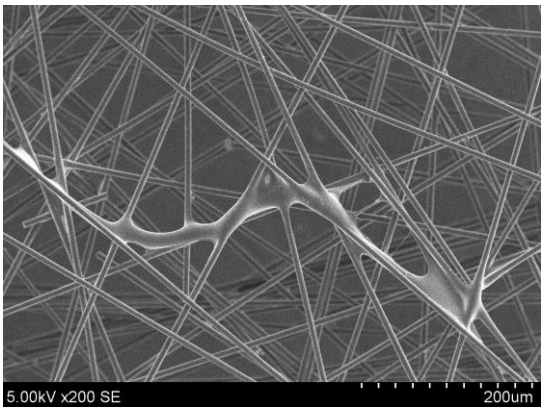

Fig. 1. SEM image of randomly oriented CSM fibres within the fabric

A Fluke 287 RMS multimeter (Fluke Corporation, Everett, WA, USA) was used to measure resistance. To ensure a stable connection between the CSM and multimeter probes, conductive copper foil tape was applied at each end of the specimen. Five specimens were prepared for each fabric layer orientation, and all specimens had a test area corresponding to the bonding area of a single-lap specimen (12.5 × 25.0 mm). Resistance was measured across the length of 12.5 mm, corresponding to the current path across the width of the bond.

2.2. Single-lap specimen preparation

Following the homogeneity assessment, single-lap shear test specimens were fabricated using the CSM layer oriented at a 90° angle as the embedded conductive layer. Lap joints were manufactured from glass fibre-reinforced polymer (GFRP) laminate, with measurements following the ISO 4587 standards, as shown in Figure 2 [9]. All bonding surfaces were cleaned with acetone before assembly to minimise contaminants.

The adhesive used for joint bonding was made from CHS 582 epoxy resin mixed with Telalit 0420 hardener (both from Spolchemie, Ústí nad Labem, Czech Republic) in a weight ratio of 100:25. CSM was coated with the prepared adhesive and placed in the bonding area (Figure 2). Additionally, pure epoxy specimens were prepared without a conductive layer to serve as a baseline.

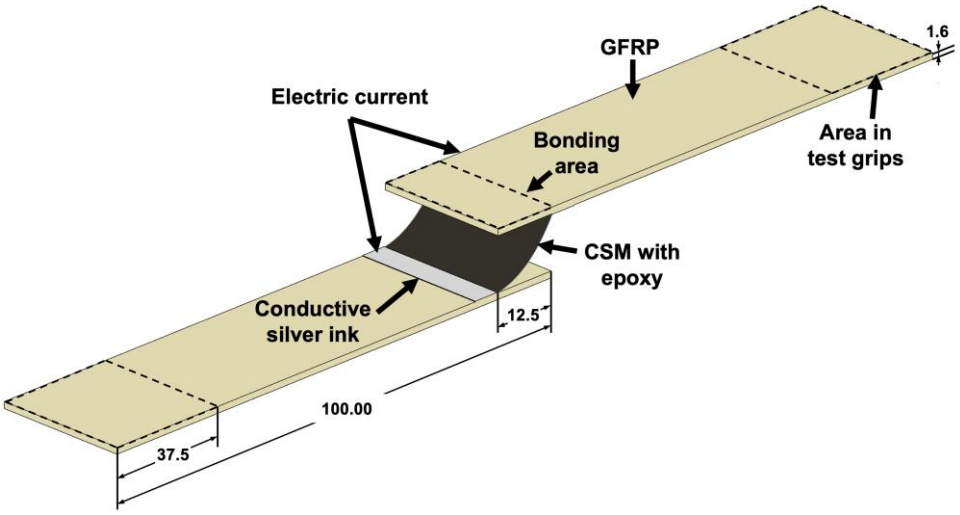

Fig. 2. Schematic of the single-lap shear specimen for local curing

The adhesive curing procedure for both specimen groups was carried out according to the manufacturer's recommendations: first, 24 hours cured at room temperature, followed by 2 hours at 50–60 °C, 1 hour at 80 °C, and finally, 1 hour at 120 °C. A total of six specimens per group were prepared. The pure epoxy specimens were cured in an oven, while the CSM specimens were cured using an Arduino-controlled Joule heating system, as described in Section 2.3. After curing at room temperature, conductive silver ink (Thermo Scientific, Karlsruhe, Germany) was applied to the contact areas of the CSM specimens to ensure good electrical contact.

2.3. Arduino-Controlled Curing System

Localised curing of the single-lap CSM joints was performed using a custom-built Arduino-based heating system. This system used temperature regulation via a digital control loop: temperature feedback from each specimen was continuously monitored and used to modulate power input. Since each specimen had different resistance values, they required different energy inputs. Therefore, a thermocouple sensor (LM35DZ TO92 (Texas Instruments, Dallas, USA)) was attached directly to the top of each bonding area to provide real-time data, which was also displayed on the computer screen to monitor temperature changes.

The curing system operated using a simple on-off control scheme, in which the Arduino microcontroller (Arduino, Turin, Italy) activated or deactivated semiconductor relay modules (Iduino, Shenzhen, China) to either resume or stop power input to each specimen individually. This approach allowed the system to maintain curing temperatures within the range of 50 °C to 120 °C by toggling current flow based on the measured temperature and the programmed setpoint.

All specimens were connected to the system simultaneously, using individual heating channels powered from a shared linear laboratory power supply (UNI-T, Dongguan, China). The system ensured consistent localised curing with minimal complexity and cost.

2.4. Mechanical Testing of Single-Lap Joints

The mechanical performance of the joints was evaluated using lap-shear testing conducted on a Tinius Olsen H10KT universal testing machine (Tinius Olsen, Horsham, USA), which is equipped with a 10 kN load cell and a crosshead speed of 0.5 mm/min. Shear strength tests were performed according to ISO 291, with each specimen being mounted in a way so that 37.5 mm of its length was gripped on both ends by the testing machine. The load and displacement data were recorded using QMAT 5.37 software.

3. Results

3.1. Results of Electrical Resistance Measurements of CSM

Figure 3 illustrates the electrical resistance of CSM in three different nominal angles of 0°, 45°, and 90°. The results of the CSM homogeneity evaluation show that the specimens with the nominal angle of 0° had the highest resistance values (28.80 Ω), followed by those at 45° (21.50 Ω), and the lowest values at 90° (17.48 Ω), as illustrated in Figure 3. When comparing the 0° and 90° groups, the electrical resistance in the nominal angle of 0° group is 1.7 times higher. This suggests that the electrical conductivity of the CSM material is not entirely isotropic. Since the effectiveness of Joule heating directly depends on the material's resistivity characteristics, CSM conductive pathways need to be uniform and free from anisotropic variations that could affect current distribution. However, the difference is too small to have any significant impact on Joule heating applications.

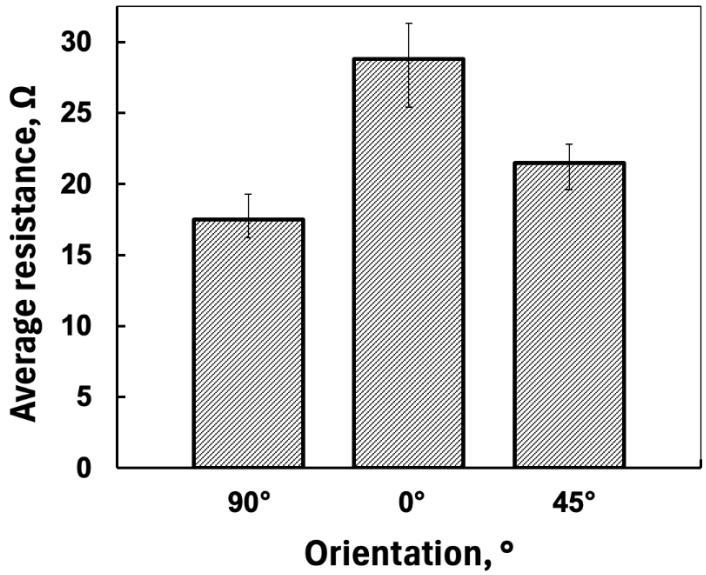

Fig. 3. Electrical resistance of CSM measured in three nominal angles of 0°, 45°, and 90°

The relatively small electrical resistance in all three nominal angles confirms the suitability of the CSM layer as a conductive interface for localised Joule heating, as it is expected to provide uniform heating within the bonding area.

3.2. Shear Strength Results of Single-Lap Joints

To evaluate the influence on single-lap mechanical performance, shear tests were performed. The average shear force sustained by both specimen groups is summarised in Figure 4. As shown in the graph, the GFRP specimens bonded with CSM had a slightly higher average shear strength (10.61 MPa) compared to the pure epoxy specimens (9.31 MPa). However, this improvement falls within the confidence intervals, making the difference statistically insignificant. Nevertheless, GFRP specimens, bonded with CSM, slight improvement in mechanical bond strength may indicate that inclusion of CSM could enhance mechanical bond performance and be suitable for cost-effective localised Joule curing. This enhancement is likely due to mechanical interlocking and an increased surface area at the bonding interface.

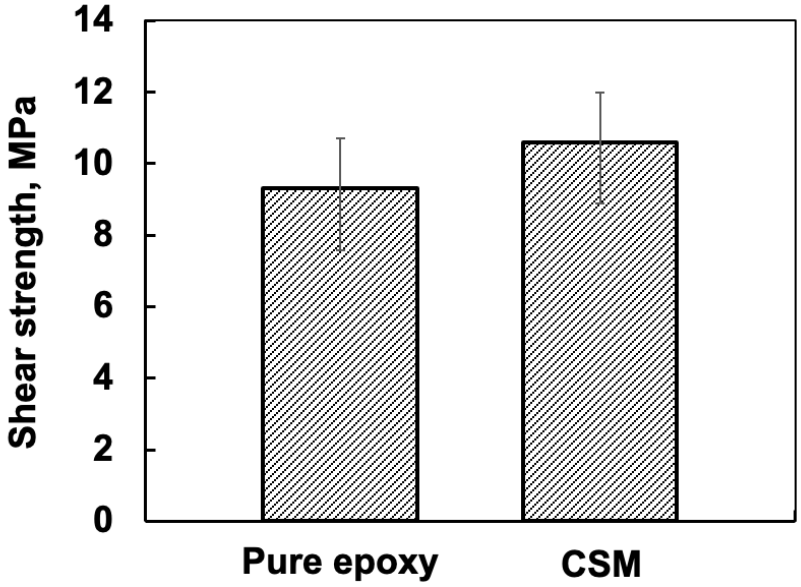

Fig. 4. Average shear strength of single-lap specimens: pure epoxy and CSM-reinforced adhesive

4. Conclusions

1. An automatic localised Joule heating system for single-lap specimen curing was developed with an Arduino microcontroller.
2. Carbon fibre CSM conductivity tests showed that the lowest resistance is in the 90° direction of the fabric.
3. Single-lap joints of GFRP reinforced with carbon fibre CSM exhibited a similar average shear strength of 10.61 MPa compared to pure epoxy specimens (9.31 MPa).

References

1. PROLONGO, S. G., GUDE, M. R., SANCHEZ, J. and UREÑA, A. Nanoreinforced Epoxy Adhesives for Aerospace Industry. *The Journal of Adhesion*, vol. 85 (2009), no. 4–5, pp. 180–199. ISSN 0021-8464. DOI: 10.1080/00218460902881766.
2. MAHDI, S., KIM, H.-J., GAMA, B. A., YARLAGADDA, S. and GILLESPIE, J. W. A Comparison of Oven-cured and Induction-cured Adhesively Bonded Composite Joints. *Journal of Composite Materials*, vol. 37 (2003), no. 6, pp. 519–542. ISSN 0021-9983. DOI: 10.1177/0021998303037006776.
3. AGHA, Akshat and ABU-FARHA, Fadi. Experimental methods to capture curing induced effects in adhesive bonded joints. *International Journal of Adhesion and Adhesives*. January 2021. Vol. 104, p. 102735. DOI: 10.1016/j.ijadhadh.2020.102735.
4. KOWATZ, Jannik, TEUTENBERG, Dominik and MESCHUT, Gerson. Optimization of inductive fast-curing of epoxy adhesive by model-based kinetics. *International Journal of Adhesion and Adhesives*. May 2023. Vol. 124, p. 103392. DOI: 10.1016/j.ijadhadh.2023.103392.
5. NOBLE, Thomas, DAVIDSON, James R., FLOREANI, Christophe, BAJPAI, Ankur, MOSES, William, DOOHER, Thomas, MCILHAGGER, Alistair, ARCHER, Edward, Ó BRÁDAIGH, Conchúr M. and ROBERT, Colin. Powder Epoxy for One-Shot Cure, Out-of-Autoclave Applications: Lap Shear Strength and Z-Pinning Study. *Journal of Composites Science*. 24 August 2021. Vol. 5, no. 9, p. 225. DOI: 10.3390/jcs5090225.
6. SHOKRIEH, M.M., SAEEDI, A. and CHITSAZZADEH, M. Evaluating the effects of multi-walled carbon nanotubes on the mechanical properties of chopped strand mat/polyester composites. *Materials & Design* (1980-2015). April 2014. Vol. 56, p. 274–279. DOI: 10.1016/j.matdes.2013.11.017.
7. MENZEL, Robert, BARG, Suelen, MIRANDA, Miriam, ANTHONY, David B., BAWAKED, Salem M., MOKHTAR, Mohamed, AL-THABAITI, Shaeel A., BASAHEL, Sulaiman N., SAIZ, Eduardo and

SHAFFER, Milo S. P. Joule Heating Characteristics of Emulsion-Templated Graphene Aerogels. *Advanced Functional Materials.* January 2015. Vol. 25, no. 1, p. 28–35. DOI: 10.1002/adfm.201401807.

8. LUNDSTRÖM, Fredrik, FROGNER, Kenneth, and ANDERSSON, Mats. A method for inductive measurement of equivalent electrical conductivity in thin non-consolidated multilayer carbon fibre fabrics. *Composites Part B: Engineering*. May 2018. Vol. 140, p. 204–213. DOI: 10.1016/j.compositesb.2017.12.027.
9. ISO 4587:2003. ISO. Available from: https://www.iso.org/standard/34852.html.

Smart Plaster Bandage After Forearm Bone Injury

Tautvydas GRUDYS, Gabrielius MARCINKUS, Arminas AMBRAZEVIČIUS, Ginas ČIŽAUSKAS, Irina KLIZIENĖ

Kaunas University of Technology, Kaunas, Lithuania

**tautvydas.grudys@ktu.edu*

Abstract

Forearm fractures are fairly common, accounting for 17% of all fractures [1]. Effective treatment and rehabilitation depend on timely and accurate monitoring of the fracture's healing process. However, these methods come with certain limitations in terms of real-time tracking. This gap in regular, detailed monitoring can delay medical intervention and negatively impact the healing outcomes. To tackle these flaws, we proposed an idea of having a smart plaster bandage imbedded with three types of sensors to properly evaluate if the wound is healing correctly.

Keywords: forearm fractures, effective treatment, gypsum.

1. Introduction

Forearm fractures are fairly common, accounting for 17% of all fractures [1]. These types of fractures can result from a variety of causes, including falls, direct trauma, or sports-related incidents, and often require careful management to ensure proper healing and restore full function. Bone strength depends on bone mineral density and bone geometry, including cross-sectional dimensions and mineral distribution [2]. Effective treatment and rehabilitation depend on timely and accurate monitoring of the fracture's healing process. Traditionally, healthcare professionals rely on X-rays and manual examinations to assess healing. However, these methods come with certain limitations in terms of real-time tracking, accessibility, and the need of frequent patient visits, not to mention the fact that manual examinations are relatively subjective and can't be used to find subtitle changes in the healing process. Additionally, the traditional monitoring methods put the healing process of the bone itself at the centre of attention and cannot achieve proper monitoring of the surrounding soft tissue during the healing process. In some cases, inflammation, infection, or incorrect tissue regeneration can go unnoticed until complications arise. This gap in regular, detailed monitoring can delay medical intervention and negatively impact the healing outcomes. To tackle these flaws, we proposed an idea of having a smart plaster bandage imbedded with three types of sensors to properly evaluate if the wound is healing correctly.

2. The methodology

The smart plaster cast is constructed out of a forearm cast and thermal, moisture and ultrasound sensors with the purpose of measuring the biometrics of the healing body part providing real time date of the healing prosses and helping to provide a more personalised and responsive treatment. The thermal sensor is used for monitoring the temperature of the tissue surrounding the healing bone, in theory creating a better chance of catching possible inflammation and bacterial infections. Inflammation is an important part of bone healing process, but unregulated acute and chronic inflammation can hider proper bone healing by stimulating the overproduction of osteoclasts leading to faster bone dissolvement and result in bone density loss, furthermore, prolonged inflammation has a link with creating other problems in human body, like rheumatoid arthritis, Crohn's disease, and bronchial asthma [3]. Traditional plaster casts, while effective for

immobilizing fractures, provide limited support for the healing process. Plaster casts are often soaked with sweat and moisture, creating a favourable environment for bacterial growth, which can delay healing. By integrating a moisture sensor, we can continuously check if there is no moisture under the plaster, and when there is, we can take measures to get rid of it. Ultrasound monitoring of damaged bone has several advantages. The alternative way to observe the healing process offers a cheaper, non-invasive way to track the healing process, offering high-resolution imaging. Furthermore, ultrasound is also safer than X-Ray on the fact that the recipient doesn't get a dose of ionized rays, making it a safer alternative for underaged and pregnant patients [4, 5]. Ultrasound frequency and dispersion speed are deciding factors for the quality and the resolution of the imaging. Ultrasound imagers work by transmitting a certain frequency of electromagnetic waves into the area of interest. Because of the different acoustic impedance (property of a material that describes how much resistance an ultrasound beam encounters as it passes through a tissue) of different tissues in the body, some of the energy of a transmitted wave is reflected back. The energy input is picked up by a transducer and converted into electrical impulses, creating an image of damaged tissues and making it easier to make a judgment about the healing process [5].

3. Sensor technology

Thermal sensor technology

The sensor is based on the fact that the Poly (3, 4-ethylenedioxythiophene) polystyrene sulfonate (PEDOT: PSS) is sensitive to the temperature Figure 1. As the temperature increases, the mobility of carriers in the material increases, resulting in a decrease in resistance. Despite its wide operating range, the sensor mainly operates between 30 °C and 50 °C. In this case, the temperature of the skin around the wound can be a possible indicator of the condition of the wound [6].

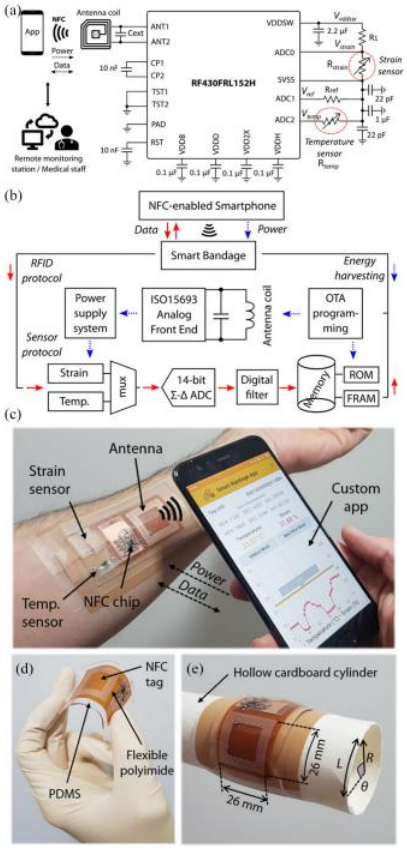

Fig. 1. a – circuit and system level; b – block diagram of the developed smart bandage for wireless strain and temperature monitoring; c – photographs of the NFC-based smart bandage attached on the arm as a proof of concept for wireless strain and temperature monitoring using the custom smartphone application, d – NFC tag fabricated in flexible polyimide and embedded in PDMS. (e) Smart bandage

attached on hollow cardboard cylinder for the bending tests [6].

To simplify on how this smart sensor works. Thermal sensors collect data from the skin. NFC chip inside this bandage powers the system and transmits data wirelessly. Then smartphone using a custom app reads the data. Having this kind of technology allows us to use this sensor in various medical applications for wireless monitoring of wounds and respiratory diseases, and transfer the data to a doctor wirelessly to reduce the number of visits and long lines to see a doctor.

Humidity sensor technology

The project uses a capacitive humidity sensor DHT11, which can measure moisture in the air Figure 2. It measures humidity in the change of capacitance between two electrodes separated by a moisture-absorbing substance. The changes in capacitance are converted into digital signals by means of an integrated circuit-usually.

This sensor also has a thermistor that measures the temperature according to the principle of a negative temperature coefficient, where resistance decreases upon temperature increments.

This sensor consequently helps in the regulation of humidity inside the splint, which in turn inhibits bacterial growth and necessarily maintains a proper healing state following surgery or trauma, within a smart splint system [7].

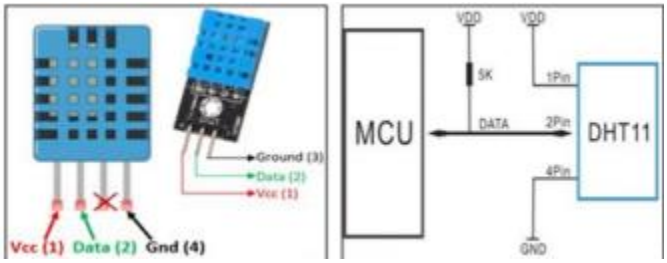

Fig. 2. DHT 11 Temperature and Humidity Sensor [7]

Ultrasound sensor technology

The most suitable method for examining fractures of long bones, such as the tibia and radius bone, is the axial transmission method. As a rule, the transmitter and receiver are placed in direct contact with the skin (percutaneous application) on either side of the fracture site, as shown in figure 3. The emitted ultrasound waves propagate from the transmitter to the receiver along the longitudinal axis of the bone. Distinct differences in the properties of bone tissue and cortical bone result in a change in ultrasound velocity at the fracture site compared to the baseline measurement on intact bone [8].

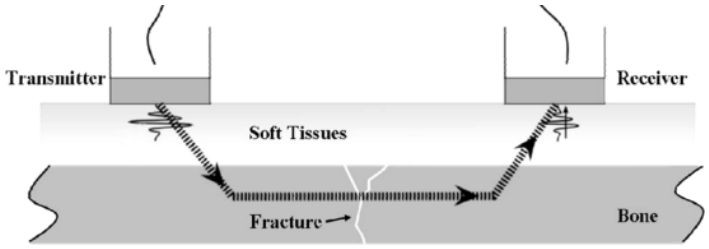

Fig. 3. The axial transmission technique used for the ultrasonic evaluation of fracture healing in long bones [8]

4. Conclusions

While standard casts offer a good and expectable quality of healing, the addition of thermal humidity and ultrasound sensors enhance the overall quality of healing. Real life monitoring of biometrics during the healing process, provided by sensors, lowers human error possibilities, helps to prevent complications such as inflammation, infection, rheumatoid arthritis or improper bone and tissue healing. The thermal sensor helps to catch abnormal body heat fluctuations

indicating inflammatory responses and prompting for medical intervention. The humidity sensor helps to monitor moisture inside the case and prevent bacterial buildup and skin irritation. Additionally, the use of ultrasound technology offers a lower-cost, non-invasive, and radiation-free method for keeping track of bone and surrounding tissue regeneration. Being radiation-free and a non-invasive way of tracking regeneration of bodily tissue also makes it a better alternative to X-rays for use with children and pregnant patients. By enabling wireless data transfer to a smartphone or remote system, the smart plaster bandage reduces the frequency of hospital visits and helps to create personalised treatment plans. This shift from reactive to proactive care could significantly improve patient outcomes and reduce healthcare burdens. The proposed smart plaster cast represents a forward-thinking approach to fracture management – one that embraces modern sensor technology to bridge existing gaps in patient monitoring and promote a safer, faster, and more informed healing process.

References

1. MARCEL A.N. de BRUIJN, L. A. van GINKEL and others. Ultrasound monitoring of bone healing in clinical and preclinical studies: A review. *Injury*, vol. 54, no. 12, 2023, pp. 2455–2465. ISSN 0020-1383. Available at: https://www.sciencedirect.com/science/article/pii/S0020138323006162.
2. KALKWARF, H.J., LAOR, T. & BEAN, J.A. Fracture risk in children with a forearm injury is associated with volumetric bone density and cortical area (by peripheral QCT) and areal bone density (by DXA). *Osteoporos* Int 22, 607–616 (2011). https://doi.org/10.1007/s00198-010-1333-z
3. MARUYAMA, M., et al. Modulation of the inflammatory response and bone healing. Frontiers in endocrinology, 2020, 11: 386. Frontiers | Modulation of the Inflammatory Response and Bone Healing
4. COCCO, G., et al. Ultrasound imaging of bone fractures. Insights into Imaging, 2022, 13.1: 189. https://link.springer.com/article/10.1186/s13244-022-01335-z
5. HIJAZY, A., et al. Quantitative monitoring of bone healing process using ultrasound. *Journal of the Franklin Institute*, 2006, 343.4-5: 495-500. https://www-sciencedirect-com.ezproxy.ktu.edu/science/article/pii/S001600320600072X
6. ESCOBEDO, P., et al. Smart bandage with wireless strain and temperature sensors and battery less NFC tag. *IEEE Internet of Things Journal*, 2020, 8.6: 5093-5100. https://ieeexplore.ieee.org/stamp/stamp.jsp?tp=&arnumber=9311219
7. HASHIM, W., et al. New Biomedical Applications Approach using Shape Memory Polymers for Muscles Rehabilitation and the Accompanying Wounds after Severe Bone Fractures. https://ijritcc.org/index.php/ijritcc/article/view/5838
8. PROTOPAPPAS, V. C., et al. Ultrasonic monitoring of bone fracture healing. Iee transactions on ultrasonics, ferroelectrics, and frequency control, 2008, 55.6: 1243-1255. https://pubmed.ncbi.nlm.nih.gov/18599412/

Study of Basketball Shooting Technique

Gintaras MICEVIČIUS*, Tomas IGNATAVIČIUS, Rojus RENEVIS, Ginas ČIŽAUSKAS, Kęstutis PILKAUSKAS, Nomeda PUODŽIŪNIENĖ

Kaunas University of Technology, Kaunas, Lithuania

** gintaras.micevicius@ktu.edu; www.ktu.edu*

Abstract

In this paper, basketball shots of different distances are investigated: close-range shots from standing position and long-range shots with vertical jump. Basketball shot is the main scoring method in the game of basketball. The ability to shoot the ball from different distances is the skill developed by athletes. The development of this skill requires a lot of time, practice, and excellent muscle memory. Assessment of shooting technique is difficult because each athlete performs his/her shot in a different way due to the complexity of the biomechanical aspects of the shot and different anthropometric data. Various factors can influence ball throw: symmetry between the sides of the body, fatigue, extraneous distractions, footwear or clothing, muscle soreness or tendon strain. As there is no single way to determine the correct technique, biomechanical analysis is used. The analysis can help to discover parts of the throw that are invisible to the naked eye, and which have an influence on the ball trajectory. Biomechanical analysis allows to see aspects of the throw that need to be addressed. Factors that are used to assess throwing technique of the ball are: symmetry between the body sides and regularity of the angles in different positions. Conclusions drawn from the analysis allow for improvement of the player's throwing technique and consequently the results. In this work, six subjects performed the throws. Angles through the ankle, knee, shoulder, and elbow joints and through the waist were recorded. Asymmetry between the left and right sides of the body and an increase in the angles of the athletes, regardless of the position, were observed throughout the study. Only one athlete (subject 1) showed exceptional regularity in the prevalence of increasing angles on one side, and two athletes (subject 3 and subject 5) were able to maintain symmetry for most positions. Shooting distance has no effect on the asymmetry and it was observed in all angles, in all positions and on both sides of the body. It is important to reduce asymmetry in the lower part of the body as it can affect stance or jump. It is allowed in the shoulder and elbow angles, due to unequal position of the left and right hands on the ball.

Keywords: basketball, ball shooting, close-range shooting, long-range shooting.

1. Introduction

In the game of basketball, the athletes' ability to handle and shoot the ball precisely is one of the key factors that makes a difference between elite players and amateurs in terms of team success and victory. Underneath every shot is a technique developed through years of training, and the complexity of biomechanical muscle memory and cognitive processes interplay. Understanding what makes the throwing technique correct is important not only for basketball players but also for team coaches and scientists who aim to develop an optimal training programme. This work focuses on the complex technique of shooting the basketball in order to determine what key elements differ between the athletes studied and their body sides when the external factor, distance to the basket, is varied. Using quantitative analysis and motion capture technology, movements of the athletes' feet, legs, pelvis, arms and hands, and angles between them, are analysed in order to determine the optimal sequence required for smooth and efficient shot

performance. Each ball throw is a unique challenge that requires a precise application of the technique. In basketball, shots are taken while the player is in a stationary position, i.e. standing. Of course, there are also shots in the game that are made on the run, but in this paper, only the shots made in a standing position are analysed.
The aim of the study is to analyse the throws of the athletes from two distances (close and far), and to compare their body sides and throws with each other.
To achieve this goal, the following objectives were set:

- to carry out analysis of basketball throwing parameters from short and long distances;
- to carry out kinematic analysis of the processes using the obtained data and to determine the dependencies between the results obtained;
- to evaluate different shooting positions.

2. Study

Subjects

Six athletes from a youth basketball team (starting five and one substitute) were selected for the study of basketball shooting technique. All of them have more than 9 years of experience in the sport. The level of a basketball player can be defined by the ability to play in a team, the number of successful shots, the number of rebounds, etc. These criteria are usually not assessed separately. The study consisted of two parts: free-throw shooting without jump and three-point shooting with jump. Due to the limitations of the laboratory, it was not possible to use a basketball hoop to record the success of the shots. Shooting from the free-throw line is easier as the distance is shorter and no additional jump movement is required. Shooting from longer distances is more difficult, as the athlete has to release the ball at the highest point to ensure the maximum possible angle between the trajectory of the ball and the hoop. Each player repeated both parts five times. Relevant anthropometric data from athletes are recorded and presented in Table 1.
Six males with height 202±6 cm, weight 96.5±5.72 kg and basketball training age 11.33±1.51 years participated in the study. All athletes have a dominant right leg and were in excellent physical condition and injury-free at the time of the study.

Table 1. Data of subjects

No	Subject	Height, cm	Weight, kg	Years of training experience
1	1 investigative	199	96	13
2	2 investigative	205	100	12
3	3 investigative	196	90	10
4	4 investigative	212	106	12
5	5 investigative	197	93	9
6	6 investigative	203	94	12
Average		202±6	96.5±5.72	11.33±1.51

Study methodology

Due to the complexity of the ball throwing motion, there are not many ways to study its throwing technique. The whole body is involved in the movement, with different limbs generating different magnitudes of force at different times. The most effective way to study throwing technique is by using a system of cameras and markers, which allows live tracking of the marked body parts and thus capturing values such as angles, velocities and accelerations of the measured body parts. The camera system captures full movement of an athlete, but does not capture muscle activity or force generated by the athlete. For a more detailed study, force plates can be used, or live electromagnetic measurements of muscle activity can be made. Muscle force is not measured in this study. Once a throw has been captured, three-dimensional model of the athlete can be analysed in software. It is viewed from different angles, at different points in time. This allows the movement to be analysed in more depth or broken down into phases.

The data of the players were recorded on arrival in the laboratory and they were informed about the progress of the test. The subjects' clothing consisted of: shorts, t-shirt, and basketball sneakers. After a 5-minute warm-up, reflective markers were placed on each athlete. They were applied to the ball and to both sides of the athletes' bodies in the following areas:

- the front of the sneakers;
- the ankles (on the far end of the fibula - lateral ankle);
- the centres of the outer knee joints (on the far end of the femur - lateral condyle);
- the hip joints (on the proximal end of the femur, the greater tuberosity);
- the deltoid muscle of the shoulder;
- and elbows (on the lateral condyle of the humerus);
- wrist (heel end of the dice).

Throws were recorded using Qualisys 5.6 and 7-series cameras for three-dimensional motion analysis. The cameras recorded displacements of the markers with an accuracy of 0.01 mm in the x, y and z planes at 200 Hz. After all athletes completed the test, data analysis was performed using Qualisys Track Manager software.

Course of the study

1. Each athlete made ten throws: five at close range without a jump and five at long range with a jump.
2. All throws are made from the same place.
3. No strict requirements for the throwing technique were imposed, as the aim of the study is to analyse the throwing technique and the differences in throws of an individual athlete.
4. After each shot, the players were given a 30-second break to prepare for the next shot and to rest, so that fatigue was not a factor.
5. The main requirement for the athletes was to make their throws as naturally and consistently as possible.

After the laboratory part of the study, the next step was to analyse each throw using Qualisys Track Manager software. In each throw, the joints were marked and the bones were connected (Figure 1). With the athlete's bar model, the kinematic results were analysed and compared with each other.

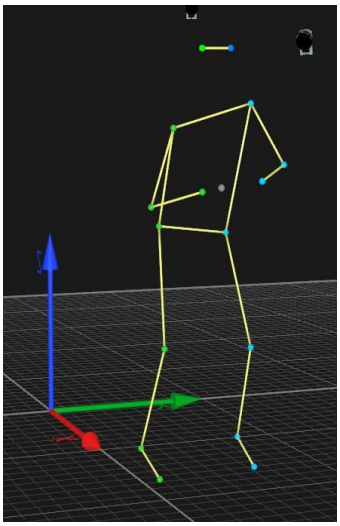

Fig. 1. Image of a subject in Qualisys Track Manager software

Shooting of the basketball can be divided into three main phases: preparation, execution and follow-through (Figure 2). In the preparation phase, the athlete starts the throwing motion by stopping in place and raising his/her arms. In the execution phase, the athlete jumps up and extends his/her arms. In the final follow-through phase, the ball is thrown, and the movement is completed.

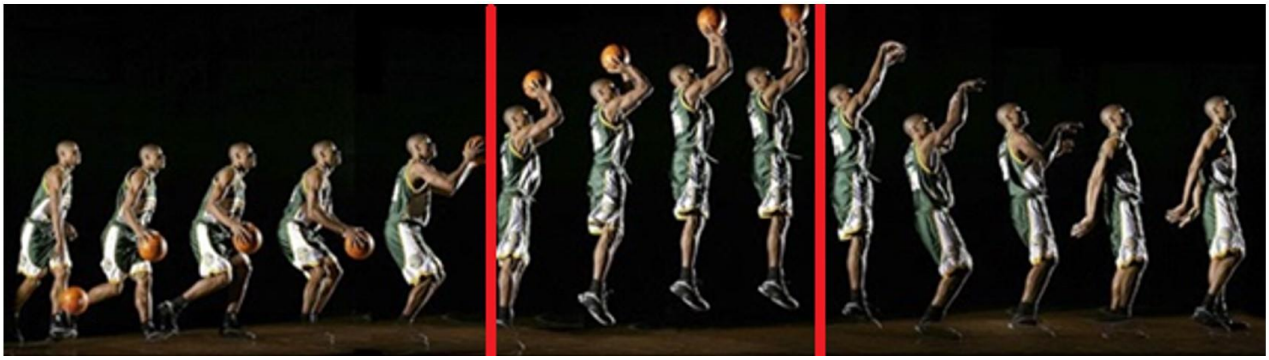

Preparation phase Implementation phase „Follow–through" phase

Fig. 2. Basketball shooting phases [23]

As movement in each phase takes place for several seconds and angles between the limbs vary in a wide range, for the kinematic analysis, three main positions were chosen:

- Position 1. The motion frame is captured when the athlete starts to raise his/her arms in the preparation phase (Figure 3, a);
- Position 2. The motion frame is captured when the athlete starts to extend his/her arms during the performance phase (Figure 3, b);
- Position 3. The shot is captured when the ball is thrown during the follow-through phase (Figure 3, c).

From the captured frames, the values of all the angles of the body analysed are obtained. Knowing the frame number ensures that all angle values are obtained at the same time. The five main body angles that affect throwing technique are analysed (Figure 3): α - angle between foot and calf; β - angle between calf and thigh; γ - angle between thigh and upper lumbar; δ - angle between upper lumbar and upper arm; ε - angle between arm and forearm.

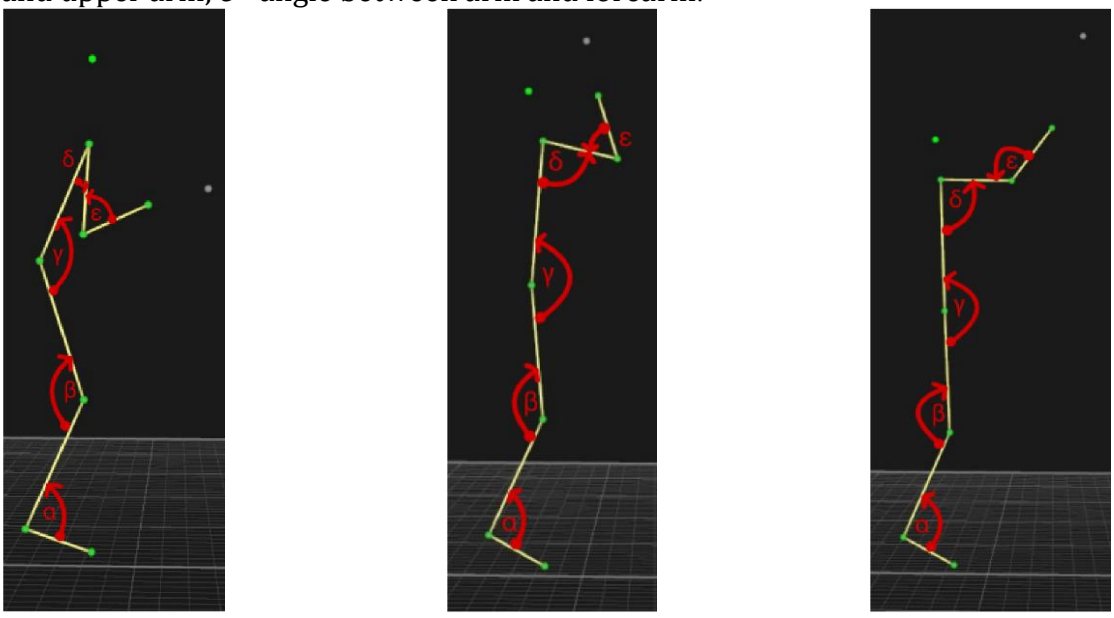

a b c

Fig. 3. Throwing positions and analysed angles: a – 1 position, b – 2 position, c – 3 position

3. Results

Results of close-range shots

The main criterion for judging an athlete's throwing technique is symmetry between the sides of the body. This is relevant for the angles: α (angle through the ankle joint), β (knee bend), and γ (angle through the pelvis). They determine the athlete's stance in the short-range throws and the jump in the long-range throws. If there is asymmetry between the sides of the athlete, it is likely that the athlete is standing in a twisted position, which may affect the trajectory of the throw.

Asymmetry is possible in δ (angle over the shoulder) and ε (angle over the elbow) because the hands are not held equally on the ball. The dominant hand holds the ball straight, and the nondominant hand is an auxiliary hand that holds the ball laterally (Figure 1.4). During the study, each athlete performed five close-range shots. The values of the analysed angles are recorded in three positions. Their averages per position are presented in Tables 3.1 to 3.3 (position 1 - Table 2, position 2 - Table 3, position 3 - Table 4). The angles tested are compared by body side and throwing position. The angles to be considered for both sides of the body must be the same in order for the throw to be performed correctly, i. e. symmetrically.

Table 2. Averages of the angles at close throws for position 1

Investigative	Body side	Position 1				
		α, °	β, °	γ, °	δ, °	ε, °
1 investigative	Right	77±3	125±3	122±5	13±1	78±1
	Left	83±1	128±4	124±5	16±2	95±2
2 investigative	Right	79±2	136±3	130±4	37±15	53±2
	Left	82±1	134±2	123±4	41±8	77±1
3 investigative	Right	83±1	136±1	127±2	16±1	71±2
	Left	90±1	138±2	122±3	25±1	99±1
4 investigative	Right	87±3	144±9	142±8	17±3	67±3
	Left	87±4	140±10	138±8	30±4	97±3
5 investigative	Right	91±2	144±4	146±4	16±3	117±3
	Left	83±2	144±4	146±5	13±1	95±3
6 investigative	Right	84±1	137±3	121±4	31±4	63±2
	Left	85±2	137±3	120±4	29±2	105±2

Table 3. Averages of the angles at close throws for position 2

Investigative	Body side	Position 2				
		α, °	β, °	γ, °	δ, °	ε, °
1 investigative	Right	87±4	138±8	162±2	75±2	39±2
	Left	99±1	146±3	162±3	93±2	87±2
2 investigative	Right	89±4	141±6	166±3	87±10	54±2
	Left	92±4	137±5	160±3	107±1	93±3
3 investigative	Right	102±6	161±4	175±2	95±3	47±2
	Left	106±5	160±3	176±3	102±3	93±6
4 investigative	Right	95±1	158±6	174±3	75±3	51±3
	Left	93±2	154±8	174±4	101±4	82±3
5 investigative	Right	90±1	145±4	175±1	98±2	79±1
	Left	84±2	148±4	177±2	101±2	61±1
6 investigative	Right	93±2	149±4	167±3	91±1	61±3
	Left	95±3	150±5	173±2	92±2	87±3

Table 4. Averages of the angles at close throws for position3

Investigative	Body side	Position 3				
		α, °	β, °	γ, °	δ, °	ε, °
1 investigative	Right	115±4	168±1	173±1	93±3	126±8
	Left	124±4	167±3	177±1	102±1	128±2
2 investigative	Right	121±5	170±2	177±1	101±7	125±6
	Left	121±5	163±1	171±1	115±1	140±2
3 investigative	Right	128±1	169±1	173±2	105±1	132±13

	Left	129±2	168±1	176±2	105±1	120±2
4 investigative	Right	96±1	160±5	176±3	79±4	111±10
	Left	93±1	158±7	174±1	100±3	110±5
5 investigative	Right	117±8	167±1	169±1	96±2	108±2
	Left	111±8	168±2	166±2	103±4	123±6
6 investigative	Right	116±2	167±1	174±1	108±4	139±9
	Left	115±4	165±2	177±1	95±2	108±1

Results of long-distance shots

The distance throws by position are shown in Tables 3.4 to 3.6 (position 1 - Table 5, position 2 - Table 6, position 3 - Table 7). The tested angles are compared according to body side and throwing position. The analysed angles on both sides of the body must be the same for correct, i. e. symmetrical, throw.

Table 5. Averages of the angles at distance throws for position 1

Investigative	Body side	Position 1				
		α, °	β, °	γ, °	δ, °	ε, °
1 investigative	Right	76±1	126±4	124±3	13±1	72±4
	Left	83±2	129±3	125±2	16±2	92±2
2 investigative	Right	84±1	151±5	147±7	27±2	51±2
	Left	85±1	147±4	139±6	28±5	81±3
3 investigative	Right	80±1	132±3	123±3	17±2	69±1
	Left	87±1	134±3	123±3	32±4	106±2
4 investigative	Right	82±2	130±5	129±5	19±2	68±4
	Left	81±2	126±5	125±4	30±5	97±5
5 investigative	Right	99±3	163±7	156±6	14±1	119±2
	Left	93±3	164±8	154±7	13±1	98±2
6 investigative	Right	95±3	139±2	111±3	30±3	59±1
	Left	91±2	135±1	110±4	32±1	103±3

Table 6. Averages of the angles at distance throws for position 2

Investigative	Body side	Position 2				
		α, °	β, °	γ, °	δ, °	ε, °
1 investigative	Right	100±7	146±4	169±4	70±1	40±2
	Left	113±11	148±5	169±4	88±1	89±5
2 investigative	Right	85±5	136±5	166±2	83±2	53±2
	Left	88±5	132±4	159±3	109±1	94±3
3 investigative	Right	116±13	155±13	172±4	99±3	48±2
	Left	117±14	156±13	175±5	103±3	100±4
4 investigative	Right	116±7	156±7	163±3	78±4	54±2
	Left	112±4	146±7	163±2	103±4	87±2
5 investigative	Right	82±3	124±4	164±2	103±1	79±2
	Left	76±3	127±4	168±4	105±1	60±1
6 investigative	Right	91±3	131±1	169±1	95±2	59±2
	Left	87±4	133±2	176±1	93±1	86±3

Table 7. Averages of the angles at distance throws for position 3

Investigative	Body side	Position 3				
		α, °	β, °	γ, °	δ, °	ε, °
1 investigative	Right	124±5	162±2	172±2	89±1	134±8
	Left	128±3	160±3	174±1	97±2	128±3
2 investigative	Right	124±2	167±2	177±1	92±1	119±6
	Left	129±1	159±3	168±3	116±2	143±2
3 investigative	Right	127±1	172±1	175±1	103±2	116±24
	Left	130±2	168±2	178±2	105±3	119±6
4 investigative	Right	118±4	161±3	170±3	86±5	122±6
	Left	115±4	154±6	170±3	104±3	120±3
5 investigative	Right	132±4	163±3	173±2	97±2	115±3
	Left	130±1	167±3	175±2	104±1	126±2
6 investigative	Right	122±3	160±1	168±2	102±3	101±3
	Left	126±3	161±2	175±1	97±1	109±2

4. Conclusions

1. In the short- and long-distance throws, regardless of the throwing position, almost all athletes showed asymmetry in all the angles considered. With the exception of subject 3 and subject 5 who showed symmetry in six positions. Excluding the shoulder and elbow angles from all thirty positions, 18 positions are left in which symmetry is important. The best-performing athletes were able to maintain symmetry in only one third of the positions considered.
2. Regardless of throwing distance and position, the tendency to increase angles is observed in almost all athletes. Differences in angles are not significant when comparing long-range and short-range shots. It is observed that in short- and long-distance throws, higher angles are recorded for the left side, although the dominant side for all athletes is the right. A consistent trend of increasing angles was observed for 1 subject. 70% of the angle measurements showed the tendency in each position. For the remaining athletes, only 20% of the measurements showed this tendency.

References

1. CABARKAPA, D., ANDREW C., FRY, D., CABARKAPA, C. Differences in Biomechanical Characteristics between Made and Missed Jump Shots in Male Basketball Players. USA, Kansas, 2022. Available from: https://www.mdpi.com/2673https://www.mdpi.com/2673-7078/2/3/287078/2/3/28. [viewed 02 May 2024]
2. YUKI, U., MASANORI, H. Basketball free-throw training with augmented reality-based optimal shot trajectory for novice shooters. Japan, Kanagawa, 2024. Available from: https://www.nature.com/articles/s41598-024-51190-9. [viewed 02 May 2024]
3. RISING, H. and TREMBLAY, R. How to Shoot a Three Pointer. 2024. Available from: https://www.wikihow.com/Shoot-a-Three-Pointer. [viewed 02 May 2024]
4. HUDSON, J.L., Biomechanical Analysis by Skill Level of Free Throw Shooting in Basketball. Available from: https://ojs.ub.uni-konstanz.de/cpa/article/view/885. [viewed 02 May 2024]
5. GAETANO, R. and D'ISANTO, T. Descriptive Shot Analysis in Basketball. Spain, Alicante, 2016. Available from: https://www.redalyc.org/pdf/3010/301051045017.pdf. [viewed 2024-05-02]
6. SLEGERS, N., LEE, D. and WONG, G. The Relationship of Intra-Individual Release Variability with Distance and Shooting Performance in Basketball. USA, Oregon, 2021. Available from: https://www.ncbi.nlm.nih.gov/pmc/articles/PMC8256521/. [viewed 02 May 2024]
7. OKAZAKI, V.H.A., RODACKI, A.L.F. Increased Distance of Shooting on Basketball Jump Shot. Brazil, Londrina, 2012. Available from: https://www.ncbi.nlm.nih.gov/pmc/articles/PMC3737873/. [viewed 02 May 2024]

8. FRANÇA, C., GOUVEIA, É.R., COELHO-E-SILVA, M.J. and GOMES, B.B. A Kinematic Analysis of the Basketball Shot Performance: Impact of Distance Variation to the Basket. Portugal, Madeira, 2022. Available from: https://www.researchgate.net/publication/359588331_A_kinematic_analysis_of_the_basketball_shot_performance_impact_of_distance_variation_to_the_basket. [viewed 2024-05-02]
9. OKUBO, H., HUBBARD, M. Comparison of shooting arm motions in basketball. USA, California, 2016. Available from: https://www.sciencedirect.com/science/article/pii/S187770581630649X?ref=pdf_download&fr=RR-2&rr=87def9927dd9c03f. [viewed 02 May 2024]
10. PAKOSZ, P., DOMASZEWSKI, P., KONIECZNY, M., BĄCZKOWICZ, D. Muscle activation time and free-throw effectiveness in basketball. Poland, Opole, 2021. Available from: https://www.nature.com/articles/s41598-021-87001https://www.nature.com/articles/s41598-021-87001-88. [viewed 02 May 2024]
11. Basketball Tips: How to Shoot a Free Throw. 2016. Available from: https://www.coachup.com/nation/articles/how-to-shoot-a-free-throw. [viewed 2024-05-02].
12. ZHEN, L., WANG, L. and HAO, Z. A Biomechanical Analysis of Basketball Shooting. China, Hebei, 2015. Available from: https://ijssst.info/Vol-16/No-3B/paper1.pdf. [viewed 02 May 2024].
13. VELJOVIC, F., SECIC, D., BEGIC, E. and ČAUŠEVIĆ, D. Biomechanical Analysis of Three Point Shot in Basketball. Bosnia, Sarajevo, 2021. Available from: https://www.researchgate.net/publication/350959965_Biomechanical_analysis_of_threehttps://www.researchgate.net/publication/350959965_Biomechanical_analysis_of_three-point_shot_in_basketballpoint_shot_in_basketball. [viewed 02 May 2024].
14. De MONDRAGON, G. Human Height. 2021. Available from: https://distributionofthings.com/human-height/. [viewed 02 May 2024].
15. EZIS, D., MITTON, T. What are the biomechanics of a basketball jump shot when aiming for optimal accuracy? Available from: https://biomechanicsbasketballjumpshot.blogspot.com/2015/06/blog-post.htmlA. [viewed 02 May 2024].

FASHION ENGINEERING – FUTURE TECHNOLOGIES

Sustainable Fashion's Unseen Challenge: Reduced Fabric Strength of Recycled Textiles

Muhammad Sohaib ANAS*, Daiva MIKUČIONIENĖ

Kaunas University of Technology, Kaunas, Lithuania

**Muhammad.anas@ktu.edu*

Abstract

Sustainable fashion is increasingly gaining prominence as the fashion industry struggles with its environmental impact. A key aspect of sustainable fashion is the use of recycled textiles, particularly post-consumer textiles, to reduce waste and conserve resources. However, one of the lesser-discussed challenges of using recycled textiles is the issue of fabric strength. Textiles that have been recycled from post-consumer waste often exhibit compromised mechanical properties, particularly in fabric strength, which can limit their practical applications in garments. This study examines the bursting strength of single jersey fabrics made from blended yarns containing post-consumer recycled cotton denim fibers and chemically recycled polyester fibers, analysing how different fiber ratios, twist levels, and spinning methods (ring vs. rotor) affect fabric strength.

Keywords: Sustainable fashion, post-consumer waste, recycling, durability, bursting.

1. Introduction

The global textile industry generates approximately 92 million tons of waste annually, with less than 15% being recycled (1). To combat this, brands are trying to incorporate post-consumer recycled (PCR) textiles into their products. However, mechanical recycling processes often weaken fibers, leading to reduced tensile strength, pilling, and poor durability (2).

The recycling of post-consumer textiles typically involves mechanical, chemical, or thermal processes that break down the fabric into smaller fibers (3). Mechanical recycling is the most common method and involves shredding the fabric into fibers, which are then spun into yarns(4). Chemical recycling, on the other hand, involves breaking down the fibers chemically to regenerate the original material. While these methods allow for the reuse of textile waste, the mechanical integrity of the fibers is often compromised during the recycling process (5). Mechanical recycling, while cost-effective and widely used, can significantly impact the strength of recycled fabrics. The repeated shredding, carding, and spinning of fibers often result in a reduction of fiber length and alignment, which can lead to weakened fabric strength. Mechanical recycling can degrade the fiber's physical structure, making the fabric less durable. Studies have shown that recycled fibers exhibit lower tensile strength, elongation, and abrasion resistance compared to virgin fibers, limiting their usefulness in durable applications such as outerwear and activewear (6).

Despite the growing importance of textile recycling, there is still a significant gap in understanding of how specific factors, such as the waste percentage, twist level, and spinning methods (ring or rotor), affect fabric strength and durability, particularly those derived from post-consumer waste. This paper addresses this gap by investigating how varying these processing parameters impacts the mechanical properties of fabric, i.e., strength.

2. Materials and Methods

A total number of 12 samples of 12/s yarn were produced, with varying material ratios to determine their properties. The material ratios used were 90 % recycled polyester and 10 % recycled cotton, 80 % recycled polyester and 20 % recycled cotton, and 70 % recycled polyester and 30 % recycled cotton. The samples were developed using two different spinning techniques, ring spinning and rotor spinning and two twist levels were applied - for ring yarns (12.0±0.5 TPI) and for rotor yarns (13.0±0.5 TPI) called as medium and high twist. The sample codes represent yarns produced using ring (Ri) or rotor (Ro) spinning with 10 %, 20 %, or 30 % post-consumer waste content, (MT) for medium twist and (HT) for high twist, i.e., Ri10HT abbreviates ring spun yarn with 10 % post-consumer waste and high twist level.
The figures and tables shall be numbered and have a self-contained caption. Figure captions shall be below the figures (Fig. 1 and Fig. 2); table captions shall be above the tables (Table 1). Please avoid placing figures and tables before their first mention in the text.

2.1. Fabric Development

Single jersey fabric (**Fig. 1**) was produced on the 14E gauge Stoll CMS 530 HP, Germany, knitting machine. The stitch length was maintained constant for all samples at approximately. 2.9 mm, ensuring consistency in the fabric structure. Take down tension was also kept uniform throughout the knitting process. The fabric was knitted at a carriage speed of 0.5 m/s, with the constant yarn tension from the cones to the needles by the machine's integrated tension control system.

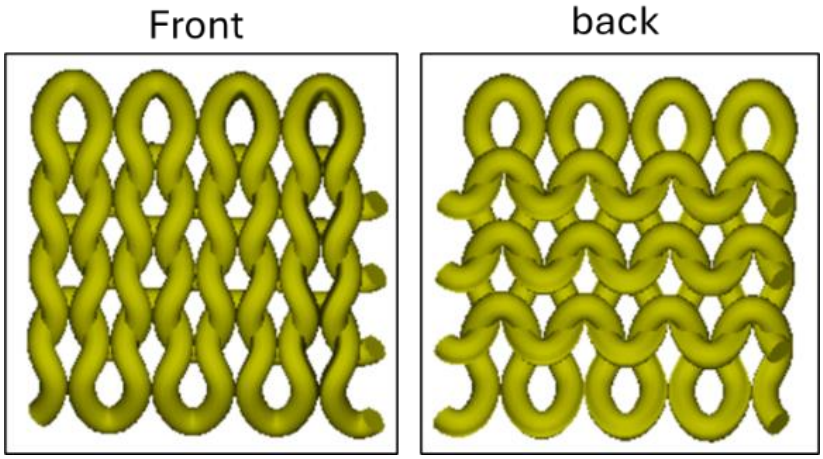

Fig. 1. Illustration of single jersey fabric structure.

3. Characterization

Bursting strength
Bursting strength is defined as the maximum perpendicular force required to rupture a textile material when subjected to multidirectional stress. This property is particularly critical for knitted fabrics, as their looped structure distributes tension differently compared to woven materials, making uniaxial tensile tests insufficient for comprehensive strength assessment. Using the standard procedure of ASTM-D-3786, the samples were cut to a size of 112 mm^2 for examination. Cut samples were clamped over the rubber diaphragm, and fluid pressure was gradually increased until the fabric burst during testing. Pressure exerted and time taken on each sample were recorded (7).

4. Results and discussion

From Fig. 2, the bursting strength analysis of fabrics manufactured from recycled denim yarns reveals significant variations influenced by spinning technology, recycled content, and twist level.

Ring-spun fabrics demonstrated superior bursting strength compared to rotor-spun counterparts, with Ri10HT achieving the highest performance (320 kPa) versus Ro10 MT (199.73 kPa). This difference is due to the more compact structure and better fiber alignment characteristic of ring-spun yarns (8). Increasing recycled content from 10 % to 30 % consistently reduced bursting strength across all samples, with Ri30MT (222.9 kPa) showing a 28 % decrease from Ri10MT, attributable to fiber damage and shorter staple lengths in recycled materials. High-twist variants consistently outperformed medium-twist samples, with Ro30HT (266.66 kPa) exhibiting a particularly notable 54% improvement over Ro30MT, demonstrating twist's compensatory effect on fiber weakness (9). Burst time measurements correlated positively with strength values, where stronger fabrics like Ri10HT (41.6 s) resisted deformation longer than weaker variants. The results indicate that while ring spinning maintains better mechanical properties, rotor-spun high-twist yarns offer a viable alternative, particularly at lower recycled contents. These findings have important implications for sustainable textile production, suggesting optimal configurations of ≤20 % recycled content in ring-spun or high-twist rotor-spun yarns for applications requiring substantial bursting strength.

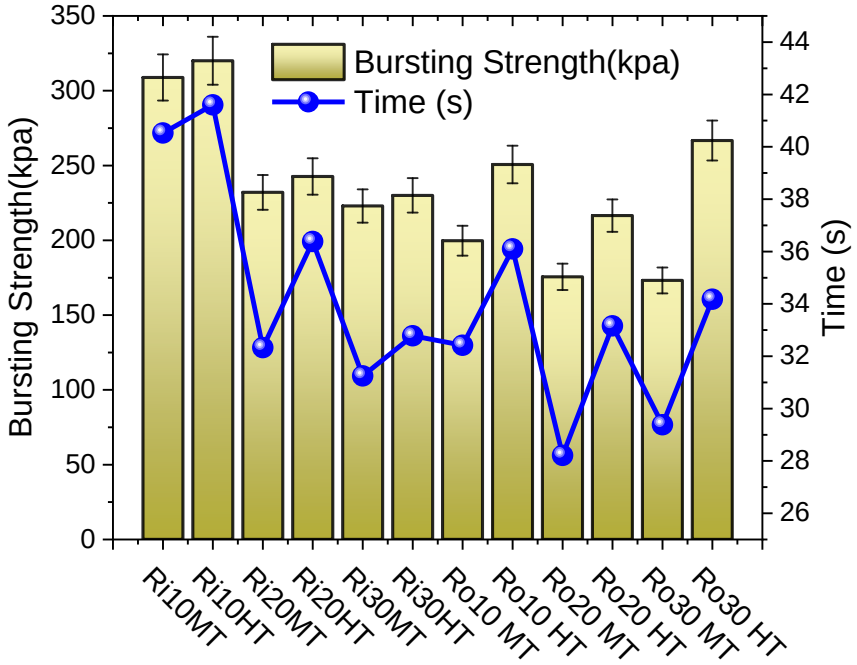

Fig. 2. Results of the bursting strength of developed fabrics

5. Conclusion

The challenge of low fabric strength in post-consumer recycled textiles represents a significant barrier to the widespread adoption of recycled materials in sustainable fashion. While the recycling of textiles holds great promise for reducing waste and conserving resources, the mechanical properties of recycled fabrics, particularly their strength, are often compromised. Balancing environmental sustainability, economic feasibility, and fabric performance is a critical challenge. Continued research and innovation are needed to overcome these obstacles and unlock the full potential of recycled textiles in sustainable fashion.

References

1. ZHANG, Z., HUANG, J., YAO, Y., PETERS, G., MACDONALD, B., LA ROSA, A.D., et al. Environmental impacts of cotton and opportunities for improvement. *Nat Rev Earth Environ*. 2023 Oct 1;4(10):703–15.
2. PENSUPA, N. Recycling of end-of-life clothes. *Sustainable Technologies for Fashion and Textiles.* 2019 Jan 1;251–309.

3. PERIYASAMY, A.P, TEHRANI-BAGHA, A. A review on microplastic emission from textile materials and its reduction techniques. *Polym Degrad Stab*. 2022 May 1,199:109901.
4. BROEGA, A.C., JORDÃO, C., MARTINS, S.B. Textile sustainability: Reuse of clean waste from the textile and apparel industry. *IOP Conf Ser Mater Sci Eng*. 2017 Nov 8;254(19).
5. DISSANAYAKE, D.G.K., WEERASINGHE, D.U. Fabric Waste Recycling: a Systematic Review of Methods, Applications, and Challenges. *Materials Circular Economy,* 2021 3:1 [Internet]. 2021 Oct 22 [cited 2025 Apr 22];3(1):1–20. Available from: https://link.springer.com/article/10.1007/s42824-021-00042-2
6. BALOYI, R.B., GBADEYAN, O.J., SITHOLE, B., CHUNILALL, V. Recent advances in recycling technologies for waste textile fabrics: a review. *Textile Research Journal* [Internet]. 2024 Feb 1 [cited 2025 Apr 22];94(3–4):508–29. Available from: https://journals.sagepub.com/doi/10.1177/00405175231210239
7. SARWAR, M.E., ANAS, M.S., JAMSHAID, H. Engineering an eco-friendly hybrid bi-layer fabric having inherently flame-resistant & antibacterial characteristics for children's protective clothing. *Thermal Science and Engineering Progress*. 2024 Mar 1;49.
8. ANAS, M.S., ABBAS, A., AWAIS, H., SARWAR, M.E., HASSAN, T.U., ABBAS, H. A study on the effect of material type, structure tightness and finishing process on the physical and thermo-physiological properties of sandwich terry socks for winter wear. *J Eng Fiber Fabr*. 2023 Jan 1;18.
9. ABBAS, A., ANAS, M.S., AZAM, Z. In vitro experimental study on the effect of fiber denier, yarn doubling, and speciality treatments on physical and thermal behaviors of knitted sports socks. *J Eng Fiber Fabr*. 2023 Jan 1;18.

Jackquard Weaving: History, Equipment, Structure, Properties

Darshan Puttaswamy[1*], Eglė KUMPIKAITĖ[2 **]

[1]*Kaunas, Lithuania,*

[2]*Kaunas University of Technology, Kaunas, Lithuania,*

[*]*darshanputtaswamy99@gmail.com*

[**]*egle.kumpikaite@ktu.lt*

Abstract

Fabrics made with jacquard patterns have a rich history of evolution from manual weaving to modern technological advancements. During the 19th century, Jacquard looms revolutionized textile production by automating complex designs with punched cards. The advancement of CAD/CAM systems has enabled Jacquard looms to create multilayer, customizable fabrics with the ability to control pattern design, texture, and colour precisely. As a result of the integration of digital tools, adjustments can be made in real time, production can be more efficient, and design possibilities can be expanded. In addition to improving design flexibility, this transition has also made Jacquard textiles more durable and desirable for interior and fashion design applications.

Keywords: Jacquard weaving, digital design, CAD/CAM systems, pattern design, loom automation.

1. Introduction

Fabrics made from jacquard have been a staple of the textile industry for centuries because of their intricate patterns and luxurious appearance. The distinctive quality of this fabric comes from the ability to weave complex designs directly into the fabric rather than relying on printed patterns. In the past, Jacquard fabrics were used to make upscale garments, upholstery, and decorative textiles due to their fine workmanship. In fashion and interior design, these fabrics have elaborate motifs, including floral, geometric, and damask patterns, which add texture and depth to the material [1]. As modern digital technologies are integrated into Jacquard weaving, the trend has evolved significantly. Nowadays, designers can experiment with multi-layered, highly detailed fabric designs using CAD/CAM systems, allowing them to create both traditional and contemporary patterns more precisely and personally [2]. A growing demand for personalized and sustainable textiles has further boosted the popularity of Jacquard fabrics since they can be adapted to a variety of design aesthetics and functional requirements.

2. History and Evolution of the Jacquard Machine

The origins of jacquard fabrics can be traced to Lyons, France, a centre of silk weaving in the early 19th century. To create intricate patterns faster, artisans had to overcome the limitations of drawlooms. In response to this, Joseph-Marie Jacquard developed a loom with programmable warp threads, thus enabling automated control of warp threads for efficient and precise pattern weaving [1]. Based on earlier work by Bouchon, Falcon, and Vaucanson, the Jacquard machine was introduced in 1804. Silk production in Lyon was revolutionized by this technology, which reduced labour by a considerable amount while increasing output. This influence extended beyond textiles to programmable systems, such as Babbage's Analytical Engine, the forerunner of the modern computer. By 1834, more than 30,000 looms were in use in Lyons alone, despite resistance and destruction after Jacquard's death [2].

During the 1818-1832 period, Jacquard looms evolved in England, introducing a shedding system using hooks and punched cards. Jacquard machines of the early 20th century included features such as claw mechanisms, stabilizing hook frames, and spring-loaded needle boxes, as shown in Figure 1.

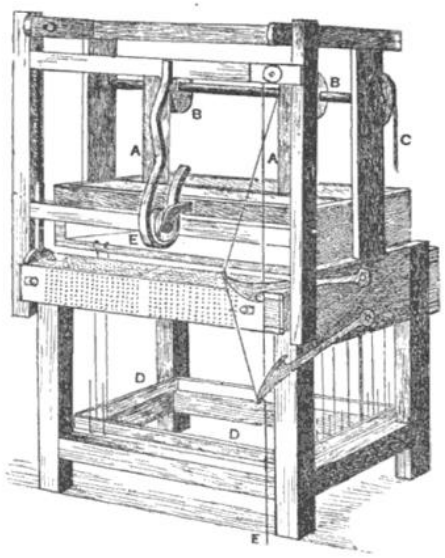

Fig. 1. Jacquard Loom [3]

While the basic concept remains unchanged, warp threads can now be lifted independently, and machines typically support 200 to 600 hooks. Jacquard loom types include single-acting, double-acting, and twilling, with single-acting types becoming obsolete due to their slow performance [3]. In traditional Jacquard fabric design, three phases are involved: design of pattern and colour, design of weave structure, and crafting (including point paper drawing and card cutting). Although this method requires deep technical knowledge, it is limited by the one-to-one correspondence principle, which restricts colour variation and demands laborious, repetitive efforts. To achieve optimal results when reproducing image-based colour effects, multiple iterations are often necessary. Figure 2 illustrates these limitations in colour flexibility and process efficiency [4].

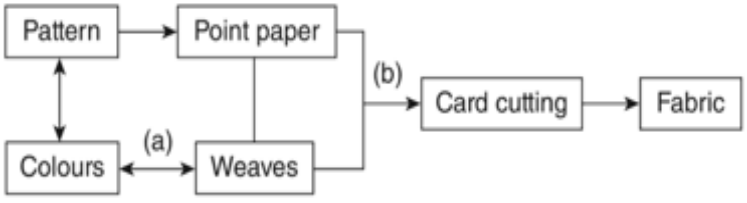

Fig. 2. Single-plane jacquard fabric design processes [4]

The manipulation of weft threads against fixed warp colours is a common way to achieve tonal variations in historical woven designs, such as Chinese brocades and Western tapestries. Despite the possibility of numerous colour combinations, manual limitations limited the number of distinctions to 100. Due to the advent of CAD tools, efficiency improved, but the plane design mode remained, limiting the potential for full-colour designs. Historically, structural stability determined colour consistency; deviations caused unpredictable results. Combining traditional craftsmanship with contemporary techniques, the layered combination design mode offers a digitally enhanced alternative for creating complex, scalable Jacquard fabrics that take advantage of contemporary digital design possibilities [4].

3. Jacquard Weaving Principle and Equipment

Jacquard weaving has dramatically evolved from its early mechanical form, invented by Joseph Jacquard in the early 19th century [5], into sophisticated digital systems that have transformed textile manufacturing. Jacquard's original mechanical loom used punched cards and harness mechanisms to precisely control the warp and weft yarns, enabling the creation of intricate patterns [5]. In Japan, Jacquard looms were adapted for kimono production by integrating European machinery with punch cards and computer software, allowing for digital archiving and cost-effective duplication of designs [6].

The introduction of binary image processing and dither masks by Toyoura, Igarashi, and Mao to manage tonal effects and warp-weft interaction allowed for the segmentation of input images to produce personalized and complex designs (Fig. 3) [7].

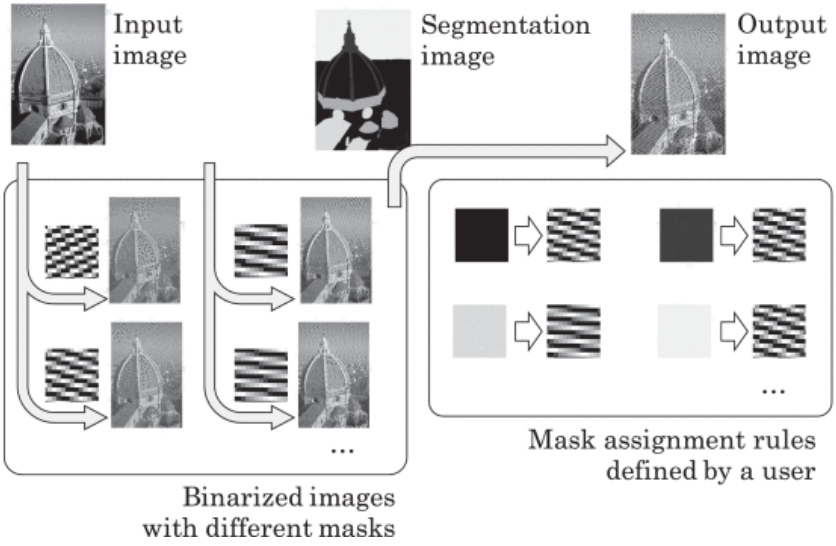

Fig. 3. Replication of Visual Impression using Binary Approach [7]

Modern Jacquard weaving now widely uses CAD/CAM technology, significantly reducing the design and manufacturing cycle. Miura, Nakajyo, and Suzuki underscore the move from human-operated processes to computer-driven ones, enhancing efficiency and flexibility in pattern creation [8]. Wang's research on seamless woven fashion (SWF) indicates that Jacquard technology, along with expanded material options and CAD design software, facilitates the production of form-fitting garments (Fig. 4) [9].

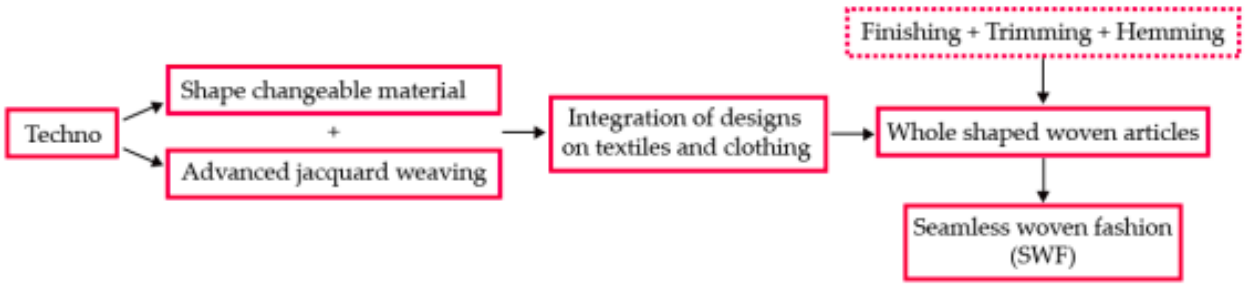

Fig. 4. Concept of Seamless Woven Fabrics [9]

Mitra illustrates how CAD/CAM technology is now essential for designing complex patterns, and technologies like Jacquard design management systems and laser cutters have further mechanized the process (Fig. 5) [10]. ArahWeave, as described by Arnăutu and Cioara, supports a wide array of weave structures and colour schemes and offers real-time 2D/3D simulation [11].

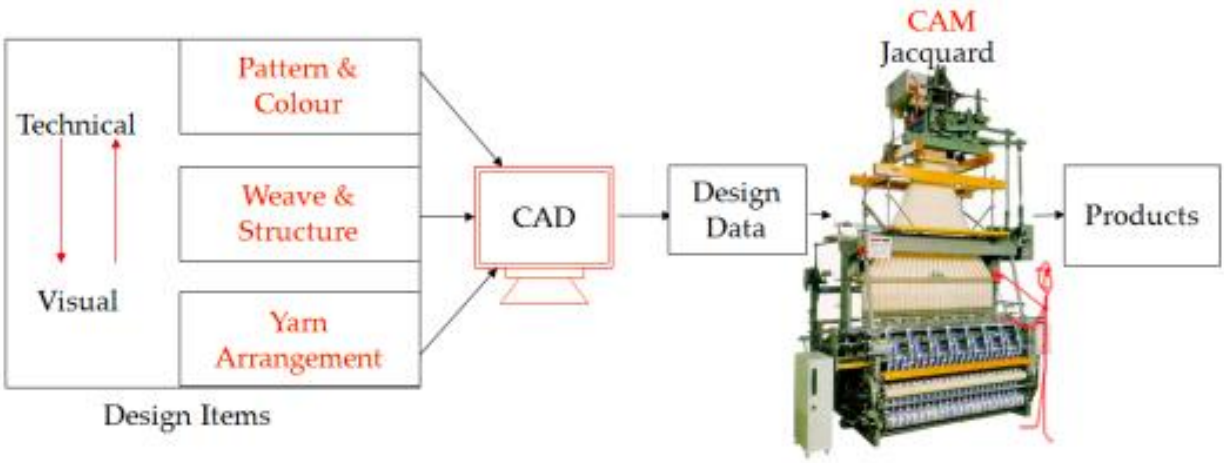

Fig. 5. CAD/CAM Technologies in Jacquard Weaving [10]

Arnăutu further explores ArahWeave's ability to create fabric with added wefts, producing cutting edges and decorative effects, and enabling functional modification through 3D simulation software [12]. Through digital image processing algorithms, Ng and Zhou highlight tonal contrast and texture over colour usage [13]. This allows designers to experiment with light and shadow for enhanced visual depth. Zhou, Ng, and Szeto propose a multi-layer design process alternating between colourless and colourful modes to generate photo-realistic multi-layered fabrics. Their method creates depth and richness in Jacquard fabrics, particularly when used with ArahWeave's software for visualization [14]. The integration of traditional craft techniques with computer technology remains central to textile design in Jacquard weaving.

4. Structure of Jacquard Fabrics

The jacquard fabric has evolved from mechanical looms to advanced electronic systems capable of producing complex, multi-layered textiles. Jacquard mechanisms control warp threads individually, resulting in intricate patterns. Kaddar points out that Jacquard weaves have versatile structural properties and aesthetic value in a variety of fabrics such as furniture, clothing, upholstery, and decorative fabrics like damask and brocade. In today's weaving industry, electronic Jacquard machines with digital controls are used with documented quality systems, as shown in a case study of a national textile company that adheres to ISO 9001:2008. Consistency and quality are determined by every element, from raw materials to machine calibration [15]. The textiles that depict Suleiman the Magnificent's life are a good example of how Jacquard weaving can be used as a medium for cultural storytelling, according to Arslan et al. In the weaving process, warp and weft interlace to create a narrative form, which combines culture and craftsmanship [16]. Digital tools, particularly layered-combination techniques, enhance precision and creativity in structural design, according to Zhou and Frankie. By using these tools, designers can separate colours, simulate weaves, and optimize paths, minimizing errors [17]. Accordingly, Ng and Zhou classify digital Jacquards as either colourless (single-layer) or colourful (multi-layer), both of which offer high structural flexibility and hyper-realistic textures. Through layered approaches, textile surfaces can be created with photographic detail and intricate patterns that are not possible with traditional methods [18]. The design of jacquard fabrics now integrates quality management, cultural narratives, and digital innovation. As a result of this combination of tradition and technology, Jacquard textiles serve both aesthetic and functional purposes.

5. Colour and Structure in Jacquard Fabrics

Jacquard fabric design has evolved remarkably since the advent of CAD technologies and innovative modelling systems. According to Akpinarli and Arslan, CAD could be used for the rapid creation of multiple Jacquard designs, but they noted that mass production would result in design

repetition [19]. The geometrical model developed by Mathur et al. was combined with various colour mixing techniques – including the Kubelka-Munk model – to accurately predict the visual outcome of yarn blends in Jacquard weaving [20]. A deeper dive into colour perception was taken by Chae, who explored both physical and visual colour prediction in jacquard textiles. Chae tested various colour prediction models on CMY-based Jacquard samples and determined that the optimized Warburton-Oliver (W-O) model was the most accurate at predicting fabric colour, especially when neighbouring yarn colours affected visualization [21]. By arranging yarns in structured proportions, Ng and Zhou proposed a full-colour compound structure with layered design modes that enhanced surface colour gradation and fabric richness [22]. Zhou developed layered-combination technology to simulate multi-layered colour effects and create novel textures like double-faced figured fabrics in a major departure from traditional Jacquard designs as shown in Fig 6 [23].

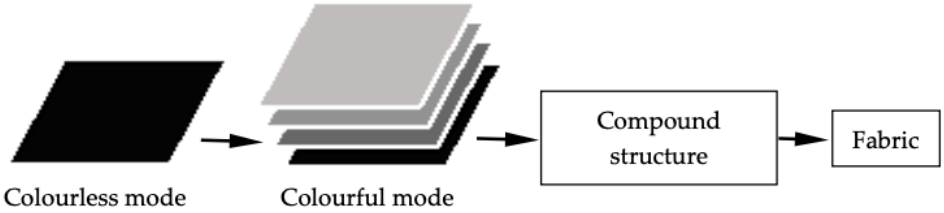

Fig. 6. Layered-Combination Technology [23]

Mathu investigated colour rendering in tapestry-style Jacquard weaving, proving that geometric colour tools can predict shade effects accurately without physical samples, reducing costs [24]. According to Kim et al. CMYK regions were segmented and shaded structures aligned for precise image reproduction [25]. Mathur et al. developed a colour/weave structure database for generating high-fidelity digital images that mimic actual fabric output. By combining digital innovation and structured weave modelling, these studies demonstrate how Jacquard's design is redefining colour control and visual complexity [26]. The use of CAD technologies and colour prediction models has improved colour-structure integration in Jacquard fabrics, reducing the need for physical sampling. Layered design and structured modelling produce textiles that are more dynamic and visually rich. The use of digital tools is transforming Jacquard's production both technically and creatively by addressing physical aspects of colour as well as perceptual ones.

6. Properties of Jacquard fabrics

A Jacquard fabric's structure and performance are determined by the weave composition, fibre types, and design elements. Warp crimp remained constant at 18.80% in both single-layer and double-layer Jacquard fabrics with minimal variation (~4%), ensuring dimensional stability across setups [27]. Air permeability tests revealed that interchanging double weaves were more airtight than self-stitched ones, while thermal conductivity tests revealed that larger motifs and specific yarns were more thermally conductive. In contrast, UV protection is solely dependent on raw materials [28]. Jacquard fabrics are tactile and mechanically responsive when optical fibres and metallic yarns are integrated. In addition to becoming softer and more transformable, optical fibre fabrics also had a reduced shear recovery and were rated unevenly and heavily by visually impaired users [29]. When used in higher percentages, metallic yarns make fabrics thicker, stiffer, and glossier, making them suitable for memory applications. However, they decreased flexibility and crease resistance [30]. Fabric performance in Jacquard weaving is influenced by structural design, materials, and functional enhancements. Jacquard textiles are versatile and functional when they balance comfort, strength, and aesthetics.

7. Conclusions

1. During the early 19th century, Joseph-Marie Jacquard's invention of punched cards revolutionized loom automation, boosting Lyon's productivity and influencing early computing. As of 1834, over 30,000 Jacquard looms had been installed.
2. The switch to digital looms, powered by CAD/CAM systems like Arah Weave, allows real-time pattern adjustments, thereby reducing errors and creating intricate, multicoloured fabrics.
3. Jacquard looms with digital design tools and quality management systems to enable the creation of precise, multi-layered fabrics, enhancing pattern design and yarn simulation.
4. By using CAD technologies, Jacquard fabrics can be created with multi-layered designs that have accurate results through models such as Kubelka-Munk and Warburton-Oliver, giving designers greater control over colour and texture.
5. Jacquard fabrics have unique properties, such as dimensional stability (18.80% crimp) and air permeability, which depend on weave structure, yarn type, and materials like optical fibres and metallic threads. In balancing aesthetics and function, metallic yarns add stiffness and thickness while reducing flexibility.

References

1. ESSINGER, James. *Jacquard's web: How a hand-loom led to the birth of the information age.* Oxford: OUP Oxford, 2004. ISBN 0192805789.
2. POSSELT, Emanuel A. *The Jacquard Machine Analyzed and Explained: with an Appendix on the preparation of Jacquard cards, and practical hints to learners of Jacquard designing.* London: Forgotten Books, 2022. ISBN 026017792X.
3. BELL, T. F. *Jacquard weaving and designing.* London: Longmans, Green, and Co, 1895. ISBN 1539672328.
4. NG, Frankie ir ZHOU, Jiu. *Innovative jacquard textile design using digital technologies.* Oxford: Woodhead Publishing, 2013. ISBN 978-1-84569-711-2.
5. BAITAB, Danish M. and NASREEN, Adeela. Textile Structures for Jacquard Weaving. In: NAWAB, Yasir; SHAKER, Khubab and HAMDANI, Syed Talha Ali, ed. *Structural Textile Design*, pp. 123–136. Islamabad: Higher Education Commission, 2017. ISBN 978-969-417-193-7.
6. UEDA, Kaori ir VOORWINDEN, Milou. The Innovative Development of the Jacquard*. The Journal of the Asian Conference of Design History and Theory*, Vol. 4 (2022), pp. 62–73.
7. TOYOURA, Masahiro; IGARASHI, Tetsuya ir MAO, Xiaoyang. Generating jacquard fabric pattern with visual impressions*. IEEE Transactions on Industrial Informatics*, Vol. 15 (2018), no. 8, pp. 4536–4544. DOI: 10.1109/TII.2018.2886795.
8. MIURA, Yoshito; NAKAJYO, Yoshinosuke ir SUZUKI, Kunio. The Jacquard Machine*. Journal of the Textile Machinery Society of Japan*, Vol. 10 (1964), no. 4, pp. 159–164. DOI: 10.4188/JTE1955.10.159.
9. WANG, Xueqin. *Creation of seamless woven fashion via Jacquard technology*. Hongkong: Open Archives Initiative, 2010.
10. MITRA, Ashis. CAD/CAM support for jacquard-based textile industry. Fibre2fashion. Available from: https://static.fibre2fashion.com/articleresources/PdfFiles/59/5891.pdf. [viewed 2025-03-30].
11. ARNAUTU, Irina ir CIOARA, Lucica. Digital Design of Jacquard Weaves Based on ArahWeave. In: *The International Scientific Conference eLearning and Software for Education*, pp. 453. Bucharest: Gheorghe Asachi Technical University of Iaşi, 2016. DOI:10.12753/2066-026X-16-244.
12. ARNĂUTU, Irina. Jacquard Fabric Simulation with Extra Wefts in Arahweave. In: *Creativitate Tehnologie Marketing*, pp. 102–107. Chisinau: Technical University of Moldova, 2023.

13. NG, Frankie MC ir ZHOU, Jiu. Digital jacquard textile design in a colorless mode*. Research Journal of Textile and Apparel*, Vol. 10 (2006), no. 2, pp. 36–42. DOI: 10.1108/RJTA-10-02-2006-B005.
14. ZHOU, Jiu; NG, Man Ching Frankie; SZETO, Y. C. ir HUI, Chi Leung. Innovative principle and method for digital jacquard fabric designing*. Journal of Donghua University (English Edition)*, Vol. 24 (2007), no. 3, pp. 341–346.
15. KADDAR, Eng Taher Rajab. *Quality Assurance in Weaving Technology of Jacquard Fabrics*. Syrian Arab Republic: AL-Baath University, 2010.
16. ANA, Pınar ARSLAN Hatice Feriha AKPINARLI ir FERREIRA, Margarida. Innovative Jacquard Weaving Fabric Design: Suleiman Ottoman Sultan'Life Story As The Cultural And Sustainable Ground For Creativity*. Social Sciences Studies Journal (SSSJournal)*, Vol. 5 (2024), no. 31, pp. 1092–1099. DOI: 10.26449/sssj.1189
17. ZHOU, J. ir NG, Man Ching Frankie. Essence of innovative designs on digital jacquard fabric*. Journal of textile research*, Vol. 28 (2007), no. 7, pp. 33–37. DOI: 10.13475/j.fzxb.2007.07.010
18. NG, Man Ching Frankie ir ZHOU, J. Innovative layered-combination mode for digital jacquard fabric design*. Textile Research Journal*, Vol. 79 (2009), no. 8, pp. 737–743. DOI: 10.1177/0040517508090482
19. FERIHA AKPINARLI, H. ir ARSLAN, Pınar. Implementation of New Designs through the Jacquard System in Fabric Patterning. *Journal of International Social Research*, Vol. 9 (2016), no. 44, pp. 603–609. DOI: 10.1002/col.20494.
20. MATHUR, Kavita; HINKS, David; SEYAM, Abdel-Fattah M. ir DONALDSON, Robert Alan. Towards automation of color/weave selection in jacquard design: Model verification*. Color Research & Application*, Vol. 34 (2009), no. 3, pp. 225–232. DOI: 10.1002/col.20494.
21. CHAE, Youngjoo. Color and color appearance prediction for jacquard woven fabrics. Available from: https://theses.lib.polyu.edu.hk/handle/200/8478. [viewed 2025-03-30].
22. NG, Man Ching Frankie ir ZHOU, J. Full-colour compound structure for digital jacquard fabric design*. Journal of the Textile Institute*, Vol. 101 (2010), no. 1, pp. 52–57. DOI: 10.1080/00405000802231291.
23. ZHOU, Jiu. Reinventing jacquard textile design via the deployment of digitisation technology towards innovative ends, Available from: file:///C:/Users/Egle/Downloads/b22396937-1.pdf. [viewed 2025-03-30].
24. MATHUR, Kavita. Advancements in pattern coloration for Jacquard Woven Tapestry Fabrics*. Journal of Textile and Apparel, Technology and Management*, Vol. 10 (2018), no. 4, 59558663.
25. NG, Frankie; KIM, Ken Ri; HU, Jinlian ir ZHOU, Jiu. Patterning technique for expanding color variety of Jacquard fabrics in alignment with shaded weave structures*. Textile Research Journal*, Vol. 84 (2014), no. 17, pp. 1820–1828. DOI: 10.1177/0040517514527377.
26. MATHUR, K.; DONALDSON, A.; HINKS, D. ir SEYAM, A. M. Color on demand for jacquard fabrics*. Research Journal of Textile and Apparel*, Vol. 9 (2005), no. 4, pp. 26–37. DOI: 10.1108/RJTA-09-04-2005-B003
27. KUMPIKAITĖ, Eglė; LAPELYTĖ, Eglė and PETRAITIENĖ, Stasė. Method of Predicting the Crimp of Jacquard-Woven Fabrics*. Materials*, Vol. 14 (2021), no. 18, pp. 5157. DOI: 10.3390/ma14185157.
28. KOSTAJNŠEK, Klara ir BIZJAK, Matejka. Estimation of permeability properties of technologically developed jacquard fabrics: Original scientific paper*. Hemijska Industrija (Chemical Industry)*, Vol. 77 (2023), no. 3, pp. 191–202. DOI: 10.2298/HEMIND221017008K.
29. ROH, Eui Kyung; SONG, Byung Kab ir KIM, Min Su. Mechanical properties and sensibility evaluation of jacquard fabric with optical fiber*. Fashion & Textile Research Journal*, Vol. 19 (2017), no. 2, pp. 240–248. DOI: 10.5805/SFTI.2017.19.1.240
30. KANG, Duck-Hee ir LEE, Jung-Soon. Physical performance of metallic jacquard fabrics*. Journal of the Korean Society of Clothing and Textiles*, Vol. 33 (2009), no. 1, pp. 149–159. DOI: 10.5850/JKSCT.2009.33.1.149

The Influence of Recycled PES on the Properties of Welf-knitted Fabrics

Vykintė TRAKŠELYTĖ[1, 2*], Erika ADOMAVIČIŪTĖ[1]**

[1] Kaunas University of Technology, Kaunas, Lithuania

[2] SRIC FTMC Department of Textile Technologies, Kaunas, Lithuania

[*] vykinte.trakselyte@ktu.edu

[**] erika.adomaviciute@ktu.lt

Abstract

The textile industry is contributing significantly to environmental degradation and greenhouse gas emissions. In response, the EU has launched a circular economy strategy to reduce the environmental impact of textile production, which includes promoting the use of recycled fibers. This research aims to compare the structural and performance properties of weft-knitted fabrics made from commercially available virgin polyester (PES) and recycled polyester (rPES). The structure parameters as wale and course density, surface density of weft knits was measured, air permeability testing, and puncture resistance, were investigated. The results revealed that PES knits had higher wale and course densities, leading to increased surface density and air permeability. However, rPES exhibited greater bursting strength despite its looser structure. These findings contribute to a better understanding of the performance of recycled polyester textiles and support ongoing efforts toward more sustainable fabric development.

Keywords: Polyester, recycled polyester, weft knits

1. Introduction

The textile industry is the third highest area of consumption for water and land use, and one of the main sources of greenhouse gas emissions. To reduce this impact, the EU has initiated a circular economy strategy, which includes the reduction of microplastics and increased producer responsibility [1]. Also, the developed strategy includes increasing the use of recycled fibres [2]. There are three methods of textile recycling – mechanical, chemical and biological. Mechanical textile recycling is the most used method for recycling synthetic fibres, as it is economical and environmentally friendly. The main disadvantage of this recycling method is the loss of fibre quality, as mechanical recycling cannot maintain the original properties of the materials due to the breaking of the polymer chains [3– 6].

Several scientific publications are comparing the properties of woven fabrics, knits from virgin (PES) and recycled polyester (rPES) yarns. A. Majumdar with coauthors [3] had analysed woven fabrics from recycled PET. It was concluded that the thermal resistance of woven fabric reduces as the proportion of recycled PET in woven fabric increases. The same results were obtained and analysing air permeability and tensile properties tests of woven fabrics with recycled PET. In the research article by M. Hatamlou with coauthors [4] liquid moisture management properties of knitted fabrics from PES and rPES were tested. The results showed that both analysed fabrics are classified as fast absorbing and quick drying. In the research article by G. Albini with coauthors [5] mechanical properties of knitted and woven fabrics made from PES and rPES were tested. Results showed that both knitted and woven rPES fabrics had excellent performance in mechanical tests (tensile strength, tear resistance) comparable to PES fabrics results.

Analysing the literature review about the influence of recycled PES on the properties of textile materials, it was noticed that the results of studies are controversial. It is possible to do an assumption that the polymer type of recycled PES had an influence on the results, i.e. it is not the same polymer as in virgin PES yarns.

This research aims to investigate the difference between the properties of weft knitted fabrics from commercially available virgin polyester and recycled polyester.

2. Materials

From 16.5 tex virgin PES (PES) and recycled PES (rPES) yarn samples of combined interlock structure were knitted. Looping diagram of analysed knits is presented in Figure 1. The dots in the image represent the front and back needle beds. The samples were knitted with a 20E gauge 30" diameter Orizio (Italy) knitting machine in the company UAB "Omniteksas fabrics".

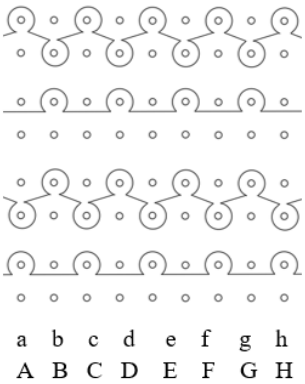

Fig. 3. Looping diagram of a knitted combined interlock structure fabric

3. Testing methodology

Before the experiments, all the materials had been kept in standard atmospheric conditions (temperature (20±2)˚C, relative humidity (64±4%) according to the LST EN ISO 139 standard.

Structure analysis of weft knits. Wale P_h (cm^{-1}) and course P_v (cm^{-1}) density coefficients of the knit fabrics were determined per unit length and width using a textile magnifier according to ISO 7211-2:2024 standards B method. P_h and P_v were calculated in five different parts of each knitted fabric.

The surface density was determined by the LST EN ISO 12127: 1999 standard. Five samples of each of an area of 100 cm^2 were cut and weighed using the analytical balance GX -200 (A&D, Japan)

Estimation of air permeability of weft knits. Air permeability was determined by the LST EN ISO 9237: 1997 standard using the Frazier Low Differential Pressure FAP-1034-LP (Frazier Precision Instrument Company Inc., JAV) air permeability measuring device. Ten samples of an area of 20 cm^2 were cut out. The direction of the air flow through the material was through the good side. The diameter of the measuring hole was 11 mm. Pressure difference: 100 Pa.

Estimation of puncture resistance of weft knits. Puncture resistance was determined by the LST EN ISO 13938-1: 2020 standard using the hand-held puncture tester T-50 (Mesdan Lab., Italy). Five samples with an area of 100 cm^2 were cut out. One test is performed for (20±5) s.

4. Results and discussion

4.1. Loop density of knits and surface density

The raw material of yarns and, structure of knits has an influence on the structure, physical, and mechanical properties of weft knitted fabrics [10, 11]. Table 1 shows wale and course densities of analyzing knits. From the results presented, it may be seen that knits from PES have higher loop density. Such results may be influenced by the unevenness of rPES yarns. In the study of K. Križmančić with coauthors [6] it was estimated that the structure of the loops (stitches) of virgin polyester is strictly vertically aligned, and the units are clearly visible. In contrast, the structure of rPES fabric does not have a clear vertical orientation, and the stitches are not uniformly shaped properties.

Table 1. Density parameters of weft knits

Type of knits raw materials	P_v, cm^{-1}	P_h, cm^{-1}
PES	16	23
rPES	15.5	22.5

Determination of surface density results is shown in Figure 2.

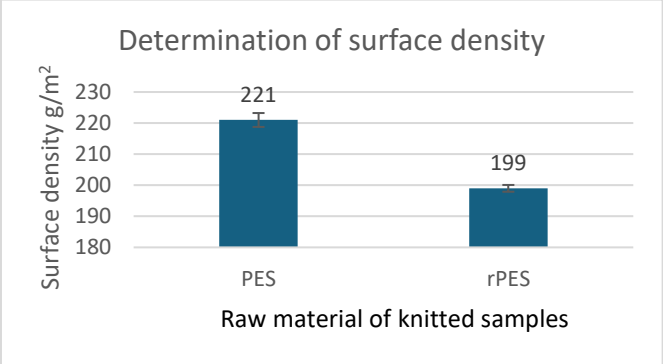

Fig. 4. Determination of surface density test results

Surface density of knits from PES was measured at 212.0 ± 2.2 g/m^{2,} and the surface density of rPES was measured at 199.0 ± 1.1 g/m^2. Wale and course density determine the surface density of the knitted fabric [7], consequently surface density of knits from PES was non-significant: 6.5% higher than knits from rPES.

4.2. Air permeability of weft knitted fabrics

The air permeability of knitted fabric is primarily influenced by the structure. Factors such as yarn type, density, loop length, tension, fabric thickness, and finishing processes determine how easily air can pass through knitted fabric [14, 15]. The air permeability test result in Figure 3 indicates that knits from rPES have lower air permeability.

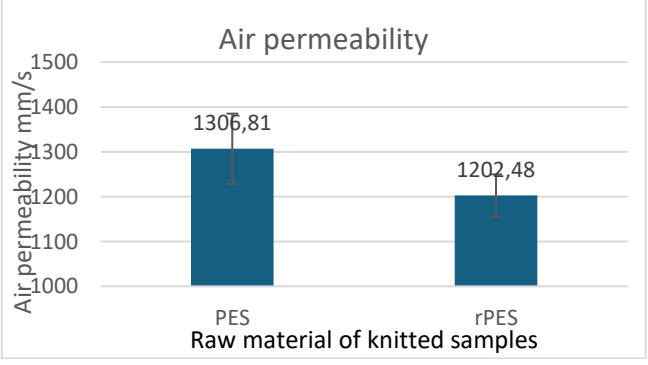

Fig. 5. Air permeability test results

Knits from PES have air permeability at 1306.8 ± 78.4 mm/s, and the air permeability of rPES was measured at 1202.5 ± 47.2 mm/s, i.e. 8% lower knitted fabrics from PES have slightly higher surface density (6.5%) than rPES, but air permeability of rPES knits has tendency to decrease. The result may be influenced by the unevenness of rPES yarns. These morphological obstacles may have increased airflow resistance [8].

4.3. Punch(ing) test of weft knitted fabrics

Bursting strength is influenced by fabric type, knit type, wale and course density, loop length and fabric extensibility [17, 18]. Punching test results are shown in Figure 4.

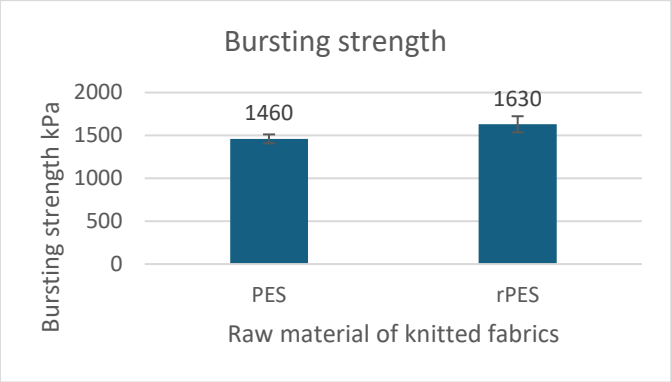

Fig. 6. Punching test results

Bursting strength of knits PES was measured at 1460 ± 52 kPa, while the bursting strength of the rPES was 1630 ± 94 kPa. Knitted fabrics from rPES have 11.6% higher bursting strength than knitted fabrics from PES, even if the surface density of knitted fabrics from PES was slightly higher (6.5%). It is important to note that none of the samples used in the experiment snapped, and both went back to their initial states during the test.
As mentioned earlier, the higher wale and course density of PES should have made it have a higher bursting strength than rPES, however, this was not the case, and further investigation should be conducted.

5. Conclusions

In this study properties of combined interlock knits from commercially available virgin polyester (PES) and recycled polyester (rPES) were analysed.

1. The analysis of wale and course density revealed that knits from PES had a slightly higher loop density (16 wales/cm and 23 courses/cm) compared to rPES (15.5 wales/cm and 22.5 courses/cm). Respectively, the surface density of knits from PES is 6.5% higher than rPES. This is directly linked to the higher wale and course density in PES.
2. Air permeability testing indicated that knitted fabrics from PES had greater airflow (8.7%) than knits from rPES, this difference, although within the allowable error margin, indicates that the unevenness of rPES yarns may have influence on air permeability of the knitted fabric.
3. Contrary to expectations based on structural density, the knitted rPES fabric demonstrated a higher bursting strength (1630.0 ± 94.2 kPa) than the virgin PES (1460.0± 52.0 kPa), however in all prior experiments the properties of rPES were inferior. To find out why, more tests are required for more accurate comparison of the samples.

References

1. *Textiles Strategy - European Commission.* [2024-12-10]. Available from: https://environment.ec.europa.eu/strategy/textiles-strategy_en. [viewed Apr 10, 2025].

2. *Full Overview of the EU Textile Strategy and Regulations.* Available from: https://www.carbonfact.com/blog/policy/eu-regulations-for-textile-brands. [viewed Apr 10, 2025].
3. *European Environment Agency. Recycling.* Available from: https://www.eea.europa.eu/help/glossary/eea-glossary/recycling.
4. MURINGAYIL JOSEPH, Tomy; AZAT, Seitkhan; AHMADI, Zahed; MOINI JAZANI, Omid; ESMAEILI, Amin, et al. Polyethylene terephthalate (PET) recycling: A review. *Case Studies in Chemical and Environmental Engineering*, vol. 9 (2024), pp. 100673. Available from: https://www.sciencedirect.com/science/article/pii/S2666016424000677..
5. RIBUL, Miriam; LANOT, Alexandra; TOMMENCIONI PISAPIA, Chiara; PURNELL, Phil; MCQUEEN-MASON, Simon J., et al. Mechanical, chemical, biological: Moving towards closed-loop bio-based recycling in a circular economy of sustainable textiles. *Journal of Cleaner Production*, vol. 326 (2021), pp. 129325. Available from: https://www.sciencedirect.com/science/article/pii/S0959652621035101..
6. DAMAYANTI, Damayanti; WULANDARI, Latasya Adelia; BAGASKORO, Adhanto; RIANJANU, Aditya and WU, Ho-Shing. Possibility Routes for Textile Recycling Technology. *Polymers*, vol. 13 (2021), no. 21, pp. 3834. Available from: https://www.mdpi.com/2073-4360/13/21/3834. [viewed Apr 10, 2025].
7. MAJUMDAR, Abhijit; SHUKLA, Sandeep; SINGH, Anshu Anjali and ARORA, Sanchi. Circular fashion: Properties of fabrics made from mechanically recycled poly-ethylene terephthalate (PET) bottles. *Resources, Conservation and Recycling*, vol. 161 (2020), pp. 104915. Available from: https://www.sciencedirect.com/science/article/pii/S0921344920302330..
8. MEHDI HATAMLOU NILGÜN ÖZDİL ARIF TANER ÖZGÜNEY GAMZE SÜPÜREN MENGÜÇ. Performance of recycled PET and conventional PES fibers in case of water transport properties, pp. 7. Available from: http://revistaindustriatextila.ro/images/2020/6/004%20MEHDI%20HATAMLOU_Industria%20Textila%206_2020.pdf. [viewed Dec 20, 2024].
9. ALBINI, Giulia; BRUNELLA, Valentina; PLACENZA, Bartolomeo; MARTORANA, Brunetto and GUIDO LAMBERTINI, Vito. Comparative study of mechanical characteristics of recycled PET fibres for automobile seat cover application. *Journal of Industrial Textiles*, vol. 48 (2019), no. 6, pp. 992–1008. Available from: https://doi.org/10.1177/1528083717750887. [viewed Apr 15, 2025].
10. HOQUE, Md Saiful; HOSSAIN, Md Jakir; RAHMAN, Md Mahbubur and RASHID, Md Mizanur. Fiber types and fabric structures influence on weft knitted fabrics. *Heliyon*, vol. 8 (2022), no. 6. Available from: https://www.cell.com/heliyon/abstract/S2405-8440(22)00893-3. [viewed Apr 15, 2025].
11. SANTOS, Thiago F.; SANTOS, Caroliny M.; ZILIO, Lucas; DIAS, Mariana; JAGADEESH, Praveenkumara, et al. Impact of yarn compositions, loop length, and float stitches on the mechanical behavior of knitted fabrics via full factorial design and RSM. *Heliyon*, vol. 9 (2023), no. 8, pp. e18784. Available from: https://www.sciencedirect.com/science/article/pii/S2405844023059923. [viewed Apr 15, 2025].
12. KATIĆ KRIŽMANČIĆ, Ines; SALOPEK ČUBRIĆ, Ivana; POTOČIĆ MATKOVIĆ, Vesna Marija and ČUBRIĆ, Goran. Changes in Mechanical Properties of Fabrics Made of Standard and Recycled Polyester Yarns Due to Aging. *Polymers*, vol. 15 (2023), no. 23, pp. 4511. Available from: https://pubmed.ncbi.nlm.nih.gov/38231927/. [viewed Apr 15, 2025].
13. MENG, Shuo; PAN, Ruru; GAO, Weidong; ZHOU, Jian; WANG, Jingan, et al. Woven Fabric Density Measurement by Using Multi-Scale Convolutional Neural Networks. *IEEE Access*, vol. PP (2019), pp. 1–1. Available from: https://www.researchgate.net/publication/333742446_Woven_Fabric_Density_Measurement_by_Using_Multi-Scale_Convolutional_Neural_Networks. [viewed Dec 20, 2024].

14. IVANOVSKA, Aleksandra; RELJIC, Mirjana; KOSTIC, Mirjana; ASANOVIC, Koviljka and AND MANGOVSKA, Biljana. Air Permeability and Water Vapor Resistance of Differently Finished Cotton and Cotton/Elastane Single Jersey Knitted Fabrics*. Journal of Natural Fibers*, vol. 19 (2022), no. 13, pp. 5465–5477. Available from: https://doi.org/10.1080/15440478.2021.1875383. [viewed Apr 17, 2025].
15. DEBEBE, Endalkachew and YILMA, Baye B. Thermo-physiological comfort properties of structurally and enzymatically modified knitted fabric for sportswear*. Journal of Industrial Textiles*, vol. 55 (2025), pp. 15280837251328299. Available from: https://doi.org/10.1177/15280837251328299. [viewed Apr 17, 2025].
16. LI, Ling; SHI, Qianqian; ZHANG, Yuze; DING, Qian and WANG, Jun. Transforming recycled polyester/cotton (*Gossypium hirsutum L.*) fibers into dye-free and eco-friendly denim fabrics: Preparation, properties evaluation, and feasibility analysis*. Industrial Crops and Products*, vol. 221 (2024), pp. 119308. Available from: https://www.sciencedirect.com/science/article/pii/S0926669024012858. [viewed Apr 18, 2025].
17. Factors Influencing Bursting Strength of Single Jersey Knitted Fabrics. Available from: https://www.researchgate.net/publication/365955874_Factors_Influencing_Bursting_Strength_of_Single_Jersey_Knitted_Fabrics. [viewed Apr 18, 2025].
18. AMIN, Md Ruhul; MAHMUD, Md Arif and ANANNYA, Ferdausee Rahman. Structural Impact on Some Common Physical Properties of Single Jersey Weft Knit Fabric*. AATCC Journal of Research*, vol. 8 (2021), no. 4, pp. 36–46. Available from: https://doi.org/10.14504/ajr.8.4.6. [viewed Apr 18, 2025].

Problem-Based Learning in the Course of Fashion Product Exploitation Modelling: A Case of Bending Stiffness Testing

Urtė Marija ČESONIENĖ*, Mehedi HASAN, Natalija PIGINA, Virginija DAUKANTIENĖ

Kaunas University of Technology, Kaunas, Lithuania

** urte.cesoniene@ktu.edu*

Abstract

The research presents the problem-based learning process (PBL) implemented in the course of 'Fashion product exploitation modelling', realised on the practical testing of bending stiffness of woven and laminated fabrics. The FAST-2 testing methodology was applied. The areas of problem and the disadvantages of the testing method were highlighted. The problem area related to specimen cutting showed the disadvantage of being manual, inconsistent, and time-consuming. The testing procedure required manual handling and variable pressure. Data collection was manual, slow, and with a risk of human error. In the laboratory, the environment (humidity, temperature, etc.) was not controlled. Automation of specimen cutting, pushing using the sensor, and standardised pressure application can improve the accuracy of bending stiffness measurements. The learning results achieved in this PBL project revealed that students developed an understanding of textile behaviour under bending stiffness and critically evaluated testing method limitations based on the analysed areas of the problem, and suggested the conception of a method improvement (prototype).

Keywords: problem-based learning (PBL), fashion product, bending stiffness, testing method, textile.

1. Introduction

In university engineering education, classical teaching methods are being intensively replaced by innovative ones such as design thinking, problem-based learning, and others. They require high didactic competencies and full immersion of the students in the learning process [1]. Problem-based learning (PBL) applied in this research is defined as 'a method of education in which the student is at the centre and the teacher is the guide on the side' [1]. When applying this learning method, students are responsible for their learning process and have a certain degree of control over the choice of literature [1].

Innovative problem-based learning was applied in the study module 'Fashion Product Exploitation Modelling', in which students gained knowledge of standard and original testing methods suitable for evaluating the behaviour of materials throughout the clothing system. Evaluation of bending stiffness is one of the topics of the course. Cantilever bending test is considered one of the simplest and most widely applied methods suitable for evaluating the bending stiffness of textiles [2]. The well-known cantilever bend testing tests are the Shirley stiffness tester [3], the bending metre FAST-2 (Fabric Assurance by Simple Testing) [4, 5], KES-FB (Kawabata Evaluation System) [6], the Leitz bending length tester [7], the TF113 Shirley fabric stiffness tester [8]. The Leitz bending length tester is a well-known tool in the textile manufacturing universe to measure the bending length and structural rigidity of fabrics because those characteristics recognise the properties of the drape and handle [7]. The Leitz tester consists of a horizontal platform with a clamp to hold the specimen, a smooth sliding surface for specimen movement forward, and a reference line to measure the bending length of the specimen

according to ASTM D1388. The specimen will be multiple with accurate data in warp and weft directions. It is capable of testing various types of textiles, for example, woven, knitted, nonwoven, and other materials such as paper or leather. Shirley's stiffness tester provides a quick way to determine the stiffness of all types of fabric, such as woven, laminated, knitted, pile, etc. The pressure plate of this device has scales that allow tracking movement in real time [8] and determining the bending height, flexural rigidity, and bending modulus of textiles according to the standard ISO 9073-7. The Kawabata Evaluation System (KES-F) is a set of sophisticated instruments to characterise the low-stress mechanical properties of the fabric, including the properties of tensile, shear, bending, compression, and surface properties [9]. All the discussed methods are constantly improved. For example, Broberg *et al.* suggested a novel method to automatically evaluate non-constant textile bending stiffness that can produce the moment–curvature relationship from a single image of the cantilevered specimen [5]. The moment and curvature at each point can be calculated using the deflection curve and the weight of the textile [2]. Therefore, the objective of this learning project was to define the problem related to the simplest test method FAST-2 suitable for evaluating the bending stiffness of textiles and to suggest the conception of its improved prototype by going through all the necessary steps of problem-based learning (PBL).

2. Tested materials and testing methods

Methodology of the PBL method

The problem-based learning (PBL) methodology, adapted according to Camp et al. [1], was applied in seven steps shown in Figure 1.

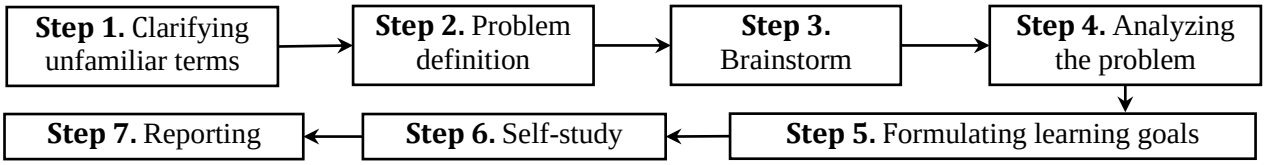

Fig. 1. The problem-based learning (PBL) methodology

To gain the necessary knowledge and skills related to the bending stiffness testing required to undergo the PBL process, experimental tests were performed to evaluate the bending stiffness of woven and laminated fabrics.

Tested materials and their characterisation

The 90% PES, 10 EL woven fabric of 210.0±11.0 g/m^2 area density (determined according to LST ISO 3801:1998 [10]) and 62 cm^{-1} warp and 31 cm^{-1} weft densities manufactured by JSC 'Textilis' (Lithuania) was investigated. For fabric laminating, the polyester-based adhesive film of the PAF-110 series ('Adhesive Films, INC'), most commonly used for the bonding of polyester, polycotton, and cotton fabric, was applied. In this PBL process, combined with the experimental testing activities necessary to gain research competencies of the students, this film was applied to simulate the behaviour of bending stiffness of laminated textiles. The characteristics of the adhesive film were: 100 PES content, 0.05±0.00 mm thickness, 55.8±0.01 g/m^2 area density, and a melting point of 130-135 C. 156±2C pressing temperature and 15 min pressing duration were applied for the lamination with the press device 'Stirovap' (Reggio Emilia, Italy). Thickness measurements were carried out with two thickness meters. J-40-T meter is applied for textiles and nonwovens ISO 5084:1996 [11] (Fig. 2 b). J-40-L meter is applied for leather according to the standard ISO 2589:2016 [12] (Fig. 2 c). They applied both woven fabric and laminated fabric to gain a deeper understanding of why the specified instruments must be applied for a particular material when the standard conditions are required to be strictly followed (Table 1).

Methodology of bending stiffness testing

The bending stiffness of the woven and laminated fabric was evaluated according to the FAST-2 method (Fig. 2 d). Five specimens of 50 mm width and 150 mm length were used in each warp and weft direction for both fabric sides to test the bending stiffness of the woven fabric. During the bending stiffness test, the length of the bent part of specimen 2c was determined for each specimen.

a b c d

Fig. 2. Testing devices: weights EG420-3NM (Kern&Sohn, Germany) (a); thickness meter J-40-T (SCHMIDT control instruments, Germany) (under 1.0 kPa pressure; 20 cm^2 pressure area) (b); thickness meter J-40-L (under 49.1 kPa pressure; 0.785 cm^2 pressure area) (c); the FAST-2 bending stiffness tester (FAST-2 prototype made and approved by scientists of the KTU) (d)

The bending stiffness characteristic was calculated according to the following formula:

$$B = w \times c^3 \times 9.81 \times 10^{-6} \text{ (μNm)}, \quad (1)$$

where: w – area density of the material, g/m^2, c – half the length of the inclined part, mm.

3. Results and discussion

In the first PBL step entitled 'Clarifying unfamiliar terms', it was determined whether all team members had the same understanding of the definitions related to the problem being solved and whether they had acquired sufficient knowledge of the study field being studied to solve the problem. For this, the literature was reviewed individually, and theoretical knowledge about the definition of the bending stiffness property, evaluation methods, and factors that influence this property of textiles was studied during lectures. Theory studies, real laboratory tests, practical analysis of fabric structure, specimen cutting, and testing of bending stiffness helped to gain the same understanding of the problem context. Results of the literature analysis of the bending stiffness evaluation are presented in the introduction chapter of this research. The preparation of the woven and laminated fabric specimens (Fig. 3) was analysed with respect to the required duration of the applied manual procedures. Totally, it was spent approximately 2476 seconds for the preparation of specimens.

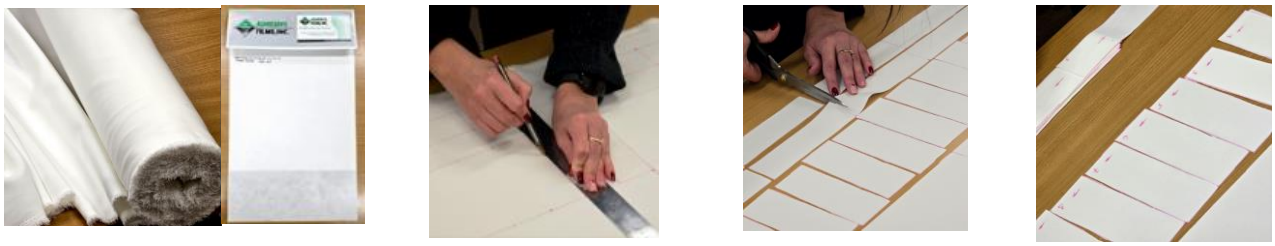

a b d e

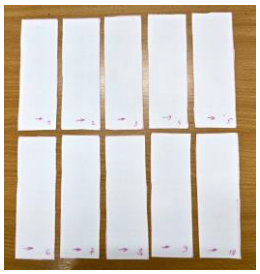
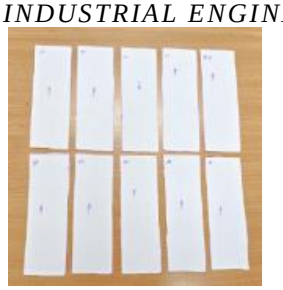
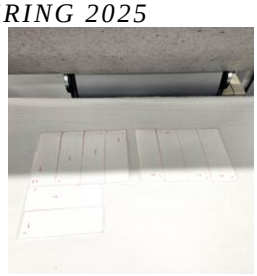
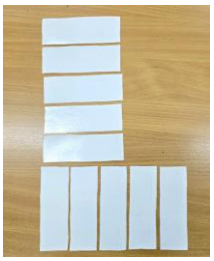

f g h

Fig. 3. Specimen preparation: a – investigated woven fabric and adhesive film used for the lamination; b – specimen marking; c –specimen cutting; d – specimen coding; e – weft specimens cut from woven fabric; f – warp specimens cut from woven fabric; g – lamination; h –laminated specimens

The influence of lamination on the thickness (Table 1) and bending stiffness (Table 2) of the woven fabric was evaluated. The thickness of the laminated fabric measured with J-40-T thickness meter under a 1.0 kPa pressure in the 20 cm^2 specimen area was lower than that of the woven fabric itself. Supposedly, it happened due to the fixing of the warp and weft yarns of the fabric in the compressed state by the penetrated adhesive in the space between the fibres and the yarns. The thickness value measured with the J-40-T thickness meter under the 49.1 kPa pressure in the 0.785 cm^2 specimen area was lower for laminated fabric as well, but this difference was not significant as it varied within the limits of measurement errors.

Table 1. Thicknesses of the tested woven and laminated fabrics

Fabric	Thickness, mm	
	J-40-T (1.0kPa pressure)	J-40-L (49.1 kPa pressure)
Woven	0.68±0.01 mm	0.69±0.03 mm
Laminated	0.64±0.01 mm	0.67±0.05 mm

The results of the bending stiffness *B* tests presented in Table 2 show that the bending stiffness varies from 6.933 μNm up to 9.810 μNm for woven fabric and from 25.618 μNm up to 70.573 μNm for laminated fabric. The stiffness of the laminated fabric is higher from 3.7 times to 8.8 times that one of the woven fabrics, depending on the direction of the fabric (warp and weft) and side (face and back). For the woven fabric, the bending stiffness is higher in the weft direction for both the face and the back sides. For all tested cases, the bending stiffness was higher for the weft direction than for the warp direction, with the exception of the back side of the laminated fabric.

Table 2. Bending stiffness *B* of woven and laminated fabrics

Sample	Bending stiffness *B*, μNm			
	Woven fabric		Laminated fabric	
Direction	Face side	Back side	Face side	Back side
Warp	6.933	8.003	25.618 (3.7 times higher)	70.573 (8.8 times higher)
Weft	9.810	8.813	64.748 (6.6 times higher)	54.561 (6.2 times higher)

In the second PBL step entitled 'Brainstorm', the knowledge and experience accumulated by the students were activated after conducting real scientific research. On the basis of the acquired competencies, many arguments, explanations, new ideas, and assumptions were generated for the critical evaluation of the applied bending stiffness method. In this step, the ideas generated by all team members were collected. Several problem areas and disadvantages of the FAST-2 method were identified during the brainstorming process (Table 3).

Table 3. Test method problem areas and method disadvantages

Problem area	Disadvantage
Specimen cutting	Manual, inconsistent, time-consuming
Testing procedure	Manual handling, variable pressure
Data collection	Manual, slow, risk of human error
Environment	Not controlled (humidity, temperature, etc.)

First, the specimens must be cut by hand, which requires a lot of manual work and time. The process cannot handle multiple specimens at once, leading to inefficiency in time. The results are collected manually, increasing the risk of human error and delays. In the cases where the specimen is not woven in plain weave, additional tests are required at both ends of the specimen, which complicates the procedure. Environmental factors, such as temperature and humidity, that were not controlled in the laboratory or considered further, affect the accuracy of the bending stiffness testing results. Variability in manual pressure applied during the test procedure, as well as differences in technique between technicians (students), contribute further to inconsistent results. It was difficult to test the bending stiffness of the laminated fabric face-sided specimens because they did not slide easily. The method is not only time-consuming but also unreliable and shows the need for improvements.

In the third PBL step entitled 'Problem definition', the problem was defined in the form of the question: What innovative solutions of the testing method could help to evaluate the bending stiffness of textiles more accurately, reliably, and effectively than practically implemented the simplified FAST-2 system meter used in the learning laboratory? The applied device lacks automation and precision. Movement is carried out manually, showing inconsistencies in speed and pressure.

In the fourth PBL step entitled 'Analysing the problem', an in-depth analysis was carried out, ideas were presented, explained in more detail, grouped and linked to each other. To improve the accuracy and efficiency of the bending stiffness test method, several practical suggestions were discussed. The lamination of the warp and weft specimens was performed separately; this must be done in one operation. The marking of the specimens and their cutting performed in this research using scissors should be replaced by the sharp cutting metal templates (cutters) placed on top of the multiple layers of fabrics and cut by using the pressing device. This decision would increase the accuracy of a specimen and the efficiency of their preparation process. In the laboratory test applied with the FAST-2 (Fig. 2, d), the specimen was moved by hand until the bent edge reached the inclined surface. The specimen would slide with smoothness on the surface of the device if it were installed in automatic transportation of a specimen at a constant rate (Fig. 3). Using an automatic pusher with a higher and constant weight that ensures a consistent push speed would help eliminate the variability caused by manual pressure. It is difficult to ensure that the same sliding velocity and pressure reach the inclined surface at the end of the sample strip. In addition, it is complicated to be very accurate in fixing that moment with human eyes. This makes it difficult to draw conclusions or compare them with different textile samples, especially when they are laminated. Visual fixation on the end of the specimen that touches the inclined surface could be changed with the electronic sensor that detects the edge of the specimen, allowing highly precise measurements, up to a millimetre, to be triggered by sensor signals. After the discussion in the team, the sketch of the improved testing device was suggested (Fig. 4).

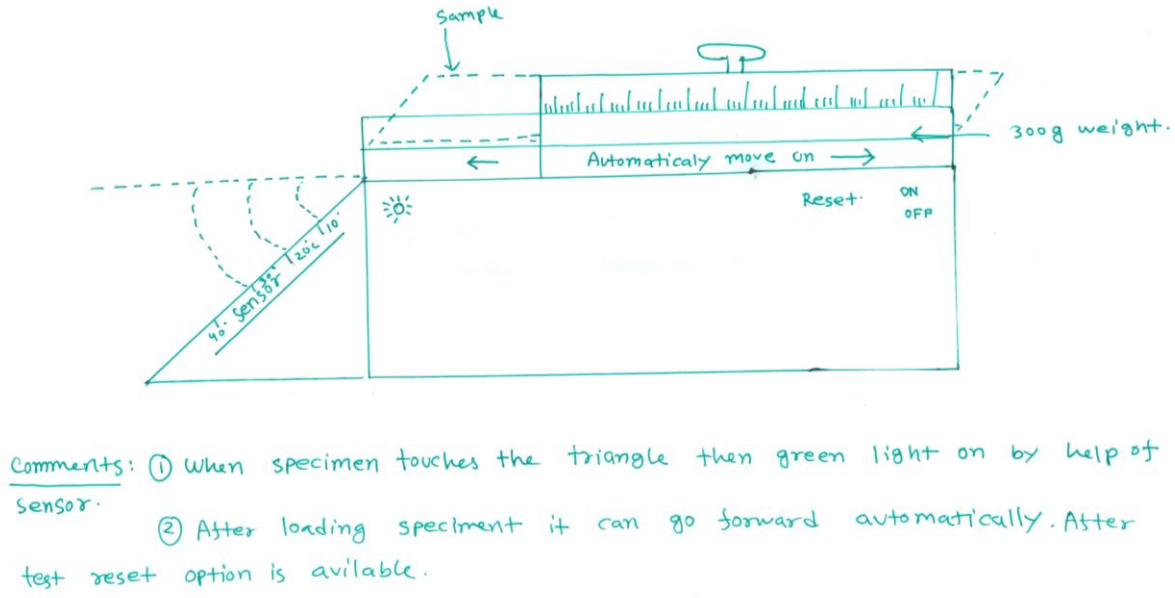

Fig. 4. The sketch of the improved testing device (prototype)

In the fifth PBL step entitled 'Formulating learning goals (preliminary discussion)', new clarification questions were raised, based on which the study activities of the team were continued. It became evident that not all team members are sufficiently familiar with the possible methods of testing bending stiffness and the devices used to implement them, and thus, the literature analysis was carried out, the results of which are presented in the Introduction chapter of this article.

In the sixth step of PBL entitled 'Self-study', the team members independently collected, studied and analysed the scientific literature. After that, they prepared individual study reports and presented them at a seminar between the student team and the lecturer-tutor.

In the last step of the PBL process, 'Reporting', a team prepared the report referring to all activities (literature analysis, tests, results analysis, and conclusions), reflecting the skills obtained. In this case, the typical reporting was changed in the form of a scientific article and reflection by presenting it at the conference, demonstrating their learning outcomes.

4. Conclusions

1. In this PBL learning process, a team developed an understanding of textile behaviour under cantilever bending and critically evaluated the alternatives of the bending stiffness testing methods, their limitations and disadvantages. Real testing of bending stiffness allowed one to gain new knowledge in the field of material engineering.
2. The FAST-2 bending stiffness testing method was found to be inaccurate, not efficient, and not reliable due to specimen preparation, manual operation, and possible human errors.
3. The conception (prototype) of improving the bending stiffness testing method was suggested. Automated specimen cutting and transport equipped with a sensor that fixes the moment the end of the specimen touches the inclined surface of the device, and standardised pressure application can increase the accuracy, reliability, and efficiency of bending stiffness measurements.
4. The PBL method effectively involved students in the research and innovation process, where they could generate ideas based on critical analysis and real testing experience.

References

1. CAMP, Gino, et al. PBL: step by step. *The Netherlands. Erasmus University*, 2014. Available from: https://www.eur.nl/sites/corporate/files/PBL_step_by_step_guide_0.pdf. [viewed 03-02-2025].
2. BROBERG, Peter Hede, et al. One-click bending stiffness: Robust and reliable automatic calculation of moment–curvature relation in a cantilever bending test. *Composites Part B: Engineering*, 2023, 260: 110763. Available from: https://www.sciencedirect.com/science/article/pii/S1359836823002664 [viewed 17-02-2025].
3. SUN, M. N. A new tester and method for measuring fabric stiffness and drape. *Textile Research Journal*, 2008, 78.9: 761-770. Available from: https://journals.sagepub.com/doi/abs/10.1177/0040517507084284 [viewed 03-03-2025].
4. Fabric Assurance by Simple Testing (FAST). Available from: https://www.slideshare.net/kotharivr/fast-5257119 [viewed 03-03-2025].
5. GIORGIO MINAZIO, Pier. FAST–fabric assurance by simple testing. *International Journal of Clothing Science and Technology*, 1995, 7.2/3: 43-48. Available from: https://doi.org/10.1108/09556229510087146 [viewed 03-03-2025].
6. HSU, Xiao-Yong, et al. Fabric handling evaluation of woven shirting fabrics by the fabric touch tester. *Textile Research Journal*, 2024, 94.15-16: 1786-1797. Available from: https://journals.sagepub.com/doi/abs/10.1177/00405175241231811 [viewed 03-03-2025].
7. Saville, B.P. 1999. *Physical testing of textiles*. Cambridge: Woodhead Publishing. Available at: https://books.google.lt/books?hl=en&lr=&id=4-uiAgAAQBAJ&oi=fnd&pg=PR2&dq=Physical+Testing+of+Textiles&ots=8dd6B1TvDY&sig=bt4yap2rVIkat0myRjstDXzWZeI&redir_esc=y#v=onepage&q=Physical%20Testing%20of%20Textiles&f=false [viewed 11-04-2025]
8. Shirley Stiffness Tester. Available from: https://lt.testextextile.com/product/fabric-stiffness-tester-tf113/ [viewed 03-03-2025].
9. Kawabata Evaluation System. Available at: https://www.sciencedirect.com/topics/engineering/kawabata-evaluation-system [viewed 07-04-2025].
10. INTERNATIONAL ORGANIZATION FOR STANDARDIZATION (ISO). LST ISO 3801:1998. Woven fabrics. Determination of mass per unit length and mass per unit area. Available from: https://lsd.lt/. [viewed 05-02-2025].
11. INTERNATIONAL ORGANIZATION FOR STANDARDIZATION (ISO). ISO 5084:1996 Textiles -- Determination of thickness of textiles and textile products. Available from: https://lsd.lt/. [viewed 05-02-2025].
12. INTERNATIONAL ORGANIZATION FOR STANDARDIZATION (ISO). ISO 2589:2016 Leather. Physical and mechanical tests. Determination of thickness. Available from: https://lsd.lt/. [viewed 05-02-2025].

Transforming Textile Waste into Biochar: A Climate-Positive Recycling Solution

Judita PANOVIENĖ*, Daina KLIAUGAITĖ**

Kaunas University of Technology, Institute of Environmental Engineering, Lithuania

**judita.panoviene@ktu.lt,*

***daina.kliaugaite@ktu.lt*

Abstract

The global fashion and textile industries generate enormous volumes of waste, most of which is currently landfilled or incinerated, contributing to greenhouse gas emissions. This study explores the use of biochar production as a negative emission technology (NET) to transform textile waste into a stable carbon sink and mitigate climate change. A laboratory experiment was conducted using a natural-fibre sweater, and the resulting biochar was analysed for its carbon sequestration potential. Based on empirical data and published scientific and market information, the process was evaluated in terms of its environmental, economic, and social benefits. The findings suggest that biochar production from textile waste can significantly reduce CO_2 emissions, generate financial value, and contribute to societal well-being.

Keywords: textile waste, biochar, carbon sequestration

1. Introduction

Textile production and consumption have risen sharply in recent decades, placing increasing pressure on environmental systems. Over the past 15 years, with the rise of fast fashion, global clothing output has nearly doubled, while the average lifespan of garments has significantly dropped [1]. This accelerating throughput of textiles leads to massive waste generation, with approximately 73% of discarded garments currently incinerated or landfilled [1].

The textile industry, with its current production, consumption, and disposal patterns, is also one of the major contributors to global warming, widely regarded as the most critical environmental issue of the 21st century. According to the Intergovernmental Panel on Climate Change (IPCC), global average temperatures have already increased by approximately 1.1 °C above pre-industrial levels [2]. If emission levels are not significantly reduced in the coming years, the planet is expected to exceed 1.5 °C of warming between 2030 and 2052, leading to severe climate disruptions such as extreme weather events, sea level rise, and loss of biodiversity [3]. In response, the Paris Agreement (2015) aims to limit temperature rise to well below 2 °C and strive for 1.5 °C, requiring carbon neutrality by mid-century [4].

One solution for climate change mitigation identified by the IPCC is the deployment of Negative Emission Technologies (NETs) - approaches that remove carbon dioxide from the atmosphere and store it in stable forms. Among them, biochar - a carbon-rich solid produced through pyrolysis of biomass in a low-oxygen environment - has recently gained attention for its dual benefits in carbon sequestration and soil enhancement [3]. The biochar production process, potential feedstocks, and applications are illustrated in Figure 1.

According to the standard of the European Biochar Certificate, textiles from cotton, cellulose, hemp, sisal, and other natural fibres are a suitable feedstock for biochar production [5]. Given the

rapidly growing challenge of global textile waste, this approach offers a promising opportunity to repurpose natural fibre-based textiles for climate change mitigation.

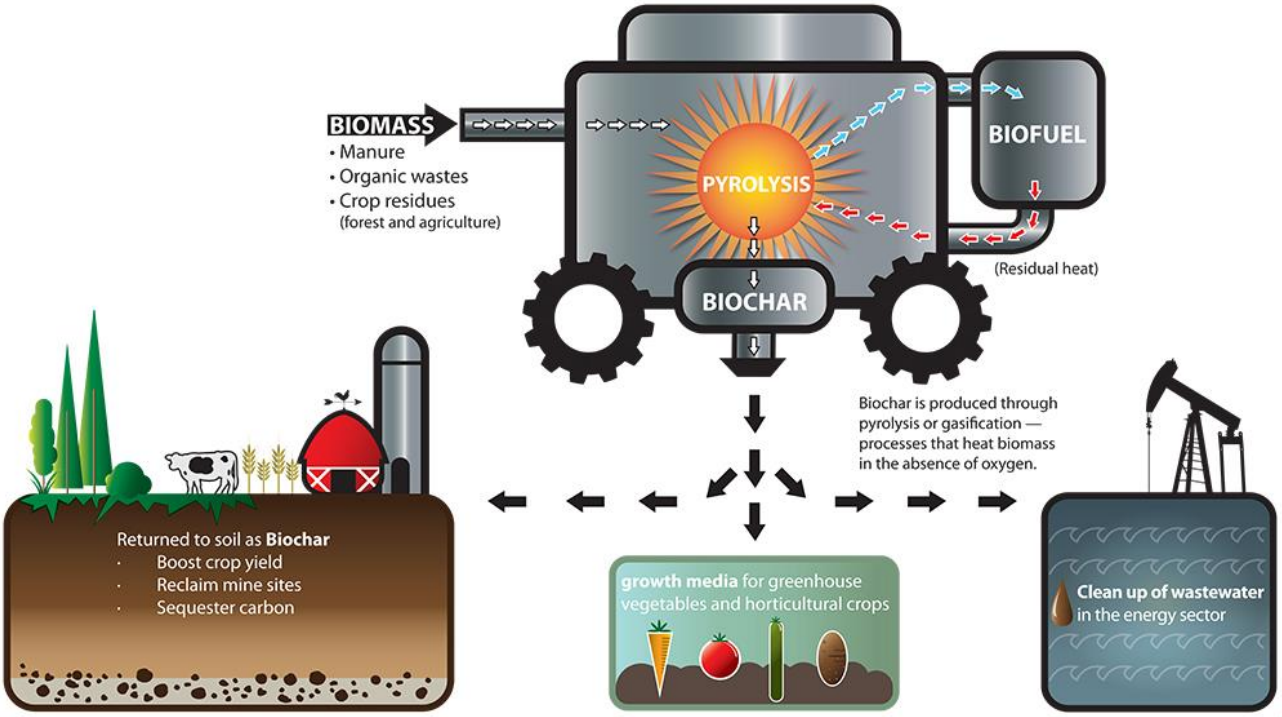

Fig. 1. The biochar production process, potential feedstocks, and applications [6]

Biochar has emerged as a growing focus of research in the fields of environmental science and materials engineering. Many studies focus on the production process itself and how different feedstock parameters and pyrolysis conditions influence the quality of biochar. There is also growing interest in the applications of biochar, including those derived from textile waste. However, there is a notable absence of life cycle assessment (LCA) studies that explore biochar as an end-of-life option for textiles and evaluate its effects across different environmental impact categories, especially its impact on climate change.
This study evaluates whether converting natural-fibre textile waste into biochar as a NET can provide climate benefits and deliver economic and societal value. The analysis draws on experimental data and established carbon accounting methodologies to quantify potential impacts.

2. Methods

This section presents the methods used to assess the environmental and economic potential of converting textile waste into biochar.

2.1. Biochar production and analysis

A knitted jersey sweater weighing 0,309 kg composed of Tencel™ lyocell (68%), wool (19%), and hemp (13%) was pyrolyzed at the Laboratory for Biochar Environmental Technologies at Vilnius Tech University. The biochar was produced at a temperature of 450°C under slow pyrolysis conditions in a tube furnace SNOL 0.7/1250. Nutrient content and potentially toxic elements were determined using the ICP–OES method, pH was measured using the 0.01M $CaCl_2$ method (ISO 10390), the FT-IR spectrum was analyzed with a Thermo Fisher Nicolet iS50 spectrometer (Waltham, MA, USA), porosity was analyzed using the Nova 4200e instrument (Quantachrome, USA), and CHNS composition was analyzed with the Vario Macro CHNSO analyzer (Germany).

The chemical composition of the biochar was analyzed to assess its suitability for soil enhancement, while its organic carbon content and stability characteristics were evaluated to estimate its carbon sequestration potential.

2.2. Carbon sequestration estimation

A methodology developed by "Puro.earth", a verified carbon removal registry, was used to calculate the amount of CO_2 potentially sequestered over a 100-year time horizon by the produced biochar [7]. According to this methodology, the following formula was applied (1):

$$E_{stored} = Q_{biochar} \times C_{org} \times F_p^{TH,T_S} \times \frac{44}{12} \quad (1)$$

where: E_{stored} is the amount of CO_2 sequestered over a 100 year time horizon by the amount of biochar produced, $Q_{biochar}$ is the amount of biochar produced, C_{org} is the organic carbon content of the biochar produced, F_p^{TH,T_s} is biochar carbon stability at a given time horizon in a given soil temperature, the factor $\frac{44}{12}$ is the ratio between the molar mass of carbon dioxide and the molar mass of carbon. This factor converts an amount of carbon to its corresponding amount of carbon dioxide.

2.3. Economic assessment

To assess the economic potential of textile waste-derived biochar, market data on biochar pricing were gathered from published market reports and industry analyses [8,9]. Carbon credit values were based on voluntary market trends reported by recognized market intelligence platforms [10,11]. The estimated revenue was calculated by multiplying the biochar yield by these price ranges. Carbon credit revenue was estimated by multiplying the calculated sequestration potential by the carbon credit price range.
This assessment provides indicative revenue potential but does not include biochar production costs such as energy use, labor, transportation, or textile shredding. These exclusions mean the results should be considered preliminary and serve primarily to illustrate potential market value rather than net profitability.

3. Findings

The experimental study aimed to evaluate the properties and benefits of biochar produced from textile waste under controlled slow pyrolysis conditions. The textile input material – 309 g sweater sample composed of Tencel™ lyocell, wool, and hemp fibers - was subjected to pyrolysis at 450 °C in a tube furnace. The resulting biochar yield was approximately 25% of the input textile mass, confirming the potential for efficient material conversion under the selected conditions. The findings of this study highlight the multifaceted value of converting textile waste into biochar, demonstrating its potential to enhance soil health, mitigate climate impact through carbon sequestration, generate economic returns, and deliver broader societal benefits.

3.1. Soil enhancement

The experiment concluded that the concentration of potentially toxic elements in the textile biochar sample did not exceed the threshold values set by the European Biochar Certificate (EBC) for use in organic farming, indicating that its application would pose no risk to soil health (Table 1).

Table 1. Concentrations of potentially toxic elements (mg/kg dry matter) compared with EBC – Agro Organic

Element	Concentration (mg/kg DM)	EBC Limit (mg/kg DM)
Zinc (Zn)	60.23 (±3.63)	<200
Nickel (Ni)	1.544 (±0.30)	<25
Copper (Cu)	12.79 (±0.35)	<70
Chromium (Cr)	6.48 (±0.12)	<70
Lead (Pb)	7.95 (±0.25)	<45
Cadmium (Cd)	<LOQ (limit of quantification)	<0.7
Arsenic (As)	<LOQ (limit of quantification)	<13
Mercury (Hg)	<LOQ (limit of quantification)	<0.4

When applied to soil, the textile biochar would enhance its fertility by enriching it with essential nutrients. The specific concentrations of these nutrients measured in the biochar sample are provided in Table 2.

Table 2. Nutrient content (mg/kg dry matter)

Nutrient	Amount, mg/kg DM
Magnesium (Mg)	569.18 (±5.31)
Calcium (Ca)	2792.89 (±50.14)
Potassium (K)	108.60 (± 9.50)
Iron (Fe)	128.47 (±9.27)
Phosphorus (P)	237.58 (±10.75)

The sample's pH was measured at 6.16 ± 0.02, indicating a slightly acidic to near-neutral character, which provides a good balance for microbial activity, nutrient availability, and overall soil health.
Elemental analysis revealed that the biochar sample contains total carbon (C) at 74.46 ± 0.89%, hydrogen (H) at 3.78 ± 0.18%, nitrogen (N) at 7.31 ± 0.80%, and sulfur (S) at 0.24 ± 0.06%, indicating a high carbon content with relatively low sulfur levels, suitable for soil enrichment purposes.

3.2. Climate Impact

Based on the experimental results, which indicated a biochar yield of 25%, it can be estimated that processing 1 tonne of textile waste could produce around 250 kg of biochar. Utilizing the selected carbon sequestration estimation methodology from "Puro.earth", this quantity of biochar could effectively sequester approximately 683 kg of CO_2 equivalent (CO_2e). Compared to incineration — the conventional method of treating textile waste in many economically developed countries, which emits approximately 3 kg of CO_2e per tonne — biochar production offers a significant improvement [12]. Replacing incineration with biochar production thus transforms the textile waste management process from carbon-positive into carbon-negative, providing substantial climate mitigation benefits by actively reducing atmospheric greenhouse gases.

3.3. Economic Benefit

Biochar is a versatile product with economic potential due to its wide range of applications — including use in agriculture (as a soil fertiliser), landscaping, water purification, construction materials, and increasingly, in carbon credit markets. Market data shows that biochar prices vary widely depending on quality, feedstock, and end use, typically ranging from EUR 300 to over EUR 2600 per tonne [8,9]. This translates to a potential revenue of approximately EUR 75 to EUR 700 per tonne of textile waste, based on an average biochar yield of 25%.

In the carbon market, biochar has gained attention for its role in long-term carbon sequestration. Biochar-based carbon credits are actively traded in the voluntary market, typically priced between EUR 100 and EUR 200 per tonne of CO_2 equivalent [10,11]. These credits are valued for their permanence and co-benefits, making them attractive to companies seeking credible climate offsets.

In this study, processing 1 tonne of textile waste is estimated to produce 250 kg of biochar, which could sequester 683 kg of CO_2e - equivalent to a potential revenue of EUR 68 to EUR 137 from carbon credits.

Although these figures may not represent a major income stream on their own, the combined revenues from biochar sales and carbon credits can help offset processing costs or be reinvested into sustainability initiatives, making textile waste conversion both environmentally and economically advantageous.

3.4. Societal Value

Beyond emissions reduction and enhanced soil health, biochar also contributes to water retention and pollution mitigation. These ecological benefits translate into long-term public health and well-being gains, particularly in urban or degraded rural areas where soil restoration is needed.

4. Conclusions

1. This study demonstrates that biochar production from natural-fibre textile waste is technically feasible under slow pyrolysis conditions at 450°C, achieving a biochar yield of approximately 25%.
2. The resulting biochar meets European Biochar Certificate (EBC) safety standards and provides essential nutrients beneficial for soil enhancement.
3. Biochar offers a climate-positive alternative to incineration, capable of sequestering up to 683 kg CO_2e per tonne of textile waste.
4. The economic assessment suggests potential combined revenues ranging from EUR 143 to 837 per tonne of textile waste, derived from two revenue streams: the sale of biochar for industrial products and the generation of carbon credits.
5. Biochar provides broader societal benefits, including soil restoration, water retention, and resource circularity.
6. Further research is needed to assess long-term soil effects, optimize production processes, and evaluate the scalability of biochar integration into waste management systems.

References

1. ELLEN MACARTHUR FOUNDATION. A new textiles economy: Redesigning fashion's future. Online. 2017. Available from: https://www.ellenmacarthurfoundation.org/a-new-textiles-economy. [viewed 5 April 2025].
2. INTERGOVERNMENTAL PANEL ON CLIMATE CHANGE (IPCC). Climate Change 2023: Synthesis Report. Online. 2023. Available from: https://www.ipcc.ch/report/ar6/syr. [viewed 5 April 2025].
3. IPCC. Summary for Policymakers. In: Global Warming of 1.5°C: An IPCC Special Report. Cambridge: Cambridge University Press, 2018, pp. 3–24. ISBN 9781009157940. DOI: https://doi.org/10.1017/9781009157940.001.
4. UNITED NATIONS. Paris Agreement. Online. 2015. Available from: https://unfccc.int/sites/default/files/english_paris_agreement.pdf. [viewed 5 April 2025].
5. EUROPEAN BIOCHAR CERTIFICATE. Positive list of permissible biomasses for the production of biochar. Online. Available from: https://www.carbon-standards.com/docs/transfer/4000095EN.pdf. [viewed 6 April 2025].

6. ALBERTA BIOCHAR INITIATIVE. Biochar for environmental remediation. Online. In: Environmental Science & Engineering Magazine. Available from: https://esemag.com/hazmat-remediation/biochar/. [viewed 6 April 2025].
7. PURO.EARTH. Biochar methodology: Edition 2022 V3. Online. 2024-02-01. Available from: https://7518557.fs1.hubspotusercontent-na1.net/hubfs/7518557/Supplier%20Documents/Puro.earth%20Biochar%20Methodology.pdf. [viewed 11 April 2025].
8. THENGANE, Shweta. California Biochar Market Report. Online. Sacramento: California Board of Forestry and Fire Protection, 2021. Available from: https://bof.fire.ca.gov/media/oobbtosm/thengane_2021_ca_biochar_market-002-_ada.pdf. [viewed 14 April 2025].
9. SEVERY, M. Biochar Quality and Market Assessment: Comparing Physical Properties to Market Value. Biochar 2018 Conference. Available from: https://archive.biochar-us.org/presentation/biochar-quality-and-market-assessment-comparing-physical-properties-market-value [viewed 14 April 2025].
10. LYTHOUSE. Carbon credit costs: What drives prices and how businesses can manage them. Online. Available from: https://www.lythouse.com/blog/carbon-credit-costs-what-drives-prices-and-how-businesses-can-manage-them. [viewed 15 April 2025].
11. QC INTEL. Biochar carbon credit prices need to rise, not fall. Online. Available from: https://www.qcintel.com/carbon/article/feature-biochar-carbon-credit-prices-need-to-rise-not-fall-while-producers-of-the-substance-need-buyers-36047.html. [viewed 15 April 2025].
12. SCHMIDT, Anders. Gaining benefits from discarded textiles: LCA of different treatment pathways. Copenhagen: Nordic Council of Ministers, 2019. 87 p. (TemaNord; 2019:510). ISBN 9789289361921. Available from: http://dx.doi.org/10.6027/TN2016-537. [viewed 15 April 2025].

Influence of Yarn Twist on Microfibre Release

Emilija SADAUSKAITĖ[1]*, Ieva POŠKUTĖ[1], Tuser BISWAS[2], Virginija DAUKANTIENĖ[1], Maria PERSSON[2], Ginta LAURECKIENĖ[1]

[1]Kaunas University of Technology, Kaunas, Lithuania

[2] Swedish School of Textiles, Boras, Sweden

** emilija.sadauskaite@ktu.edu*

Abstract

This study aimed to determine the impact of yarn twist on microfibre release during washing. Determination of microfibre release was conducted on polyester fabrics knitted using low, medium, and high twist yarns. Three different yarn twist fabrics were knitted, washed, and the washing liquid was filtered later. The results obtained revealed that different yarn twists did not have an essential impact on microfibre release during laundering. But low yarn twist showed show lowest microfibre release results. The findings showed minimal differences between the chosen yarn twists.

Keywords: microfibre, yarn twist, microplastics, knitted fabric, washing.

1. Introduction

Microplastic fibres (MFs) are considered to be one of the emerging contaminants observed in ecosystems. Due to the risks posed in the textile and clothing industry, many studies are carried out in order to minimise this threat. Researchers Zhu and Yang, in their study [1], investigated how microplastics could be reduced in textile wastewater using different water treatment techniques. The efficiency of microplastic removal was analyzed by the laser direct infrared (LDIR) and liquid chromatography tandem mass spectrometry methods. The finding showed that each technique had limitations, but could be combined effectively. The adopted liquid chromatography tandem mass spectrometry method removed only 68.7% of PET, 71.4 % of PA6.6 and only 38.4 % of PC from wastewater [1].

Juntarasakul, Julapong, and Srichonphaisarn investigated microplastic fibre emission quantities from three weave structures: plain, twill, and satin [2]. The obtained results showed that during the first laundry process, MFs volumes were the highest, regardless of the weaving structures. Overall, the satin weave appeared to release the most microplastic fibres compared to the other two weaves [2].

Cui and Xu explored the relationship between microplastic shedding and fabric structure [3]. The study used knitted polyester fabric, plain woven, twill and satin fabric and examined external factors such as washing time, temperature, and steel balls. The results obtained revealed that under the same washing conditions, the knitted fabric released a greater amount of MFs compared to woven fabrics. The chosen washing scheme was 80 min, temperature – 50°C and 30 stainless steel balls. These proportions show that choosing a different washing temperature does not affect microfibre release. The research also analyzed weave structures and satin fabric showed the largest amounts of microfibre release, plain weave fabric – the lowest [3].

Periyasamy [4] discusses mechanical and chemical finishes that could be a potential solution to microfibre pollution in the textile industry. The singeing finishing method uses an open flame to burn away the tiny fibres from the fabric surface to get a smooth and even appearance. Chemical

finishing using enzymatic treatment has been known to have a positive impact on microfibre shedding. The enzyme coating modifies the surface levels of the fabric, improving the appearance of the fabric, resulting in a reduction in microfibre generation [4].

In general, no specific literature has been found that analyzes the influence of different yarn twists on microfibre release.
In this investigation, three different polyester yarn twists were analyzed to confirm whether the twist in the yarn has an impact on microfibre shedding from knitted textiles. The research consisted of yarn twisting and knitting processes, and microfibre release tests were explored according to the ISO 4484 standard [5]. The quality and technical parameters of the twisted yarns were examined. The spun yarns were subjected to hairiness and evenness tests, actual confirmation of yarn twist was tested, and microscope pictures were taken. Gathered results showed that the choice of different twists for knitted textiles did not provide higher microfibre release findings, and the tests for yarn hairiness and evenness indicated quite different results. The actual and theoretical twist of the yarn turned out to be significantly diverse.

2. Materials and methods

In this investigation, three different twists of polyester yarns obtained from PT. Indo-Rama Synthetics Tbk. Indonesians were spun. To do so, the yarn twist per meter and alpha index must be determined. All studied yarn twists were calculated starting with already made 51/1 Nm yarn (Fig. 1), which was considered as a low twist yarn with 600 m^{-1} and α index – 2.7. Using the same calculation method, medium yarn twist was estimated – 700 m^{-1} r and α index – 3.3. For a high twist yarn, twist was 819 m^{-1} with α index – 3.8.

Fig. 1. Polyester yarn 51/1 Nm

After the yarn spinning process, three different yarn twist fabrics of single jersey pattern were knitted using Harry Lucas' cylindrical knitting machine. The fabrics were washed to remove any leftover dirt and oil according to ISO 6330 at 40 °C [6].

The study continued with sample preparation for washing tests; three specimens of different yarn twists were cut into 15 x 29 cm pieces according to the ISO 4484- 1 standard.

The samples were washed using a Gyrowash washing machine in separate metal containers with distilled water and 50 metal balls at 40 °C for 45 minutes. This washing method allowed for the collection of all released microfibres. Collected water with shedded microfibres was filtered with glass fibre filters. Finally, filters with microfibres were carefully dried and weighed to determine the amount of microfibres released during washing.
The research also investigated the quality and technical parameters of the spun yarns. Yarn hairiness and evenness tests were also studied; actual yarn twist results were compared with

theoretical ones. To visualize the research, microscope pictures of twisted yarns were taken using a Nikon Eclipse microscope.

3. Findings and arguments

Microfibre determination during washing

The findings carried out according to the ISO 4484 standard represent the impact of different yarn twists on microfibre release (Fig. 2). The obtained results show that the release of microfibres varies within a range of errors.

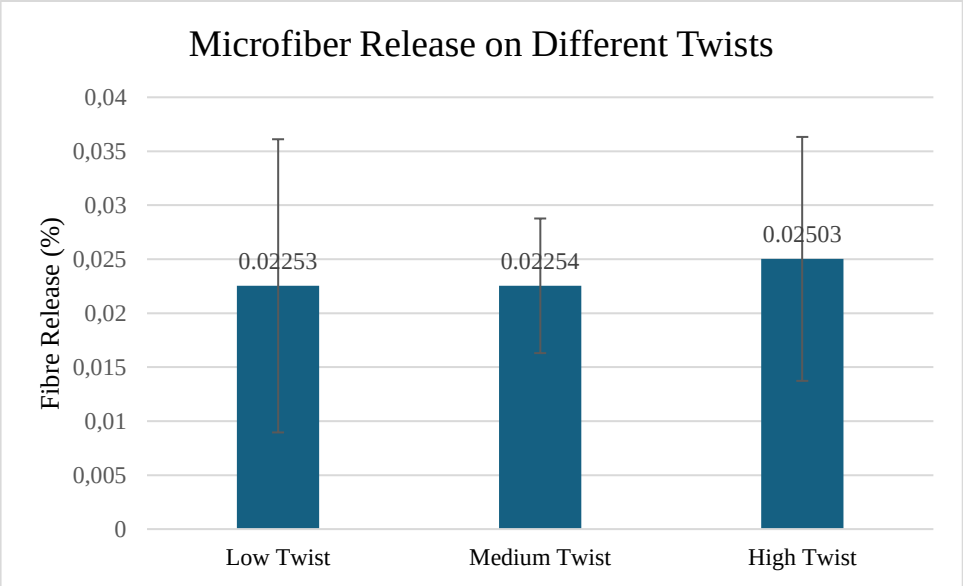

Fig. 2. Microfibre release results

The graph in Figure 2 shows that there is some tendency between yarn twist and microfibre shedding, but to obtain more accurate results, the range of tests must be extended to reduce the magnitude of errors.

Confirmation of Yarn Twist

The confirmation test of the actual twist of the yarn compared to the calculated theoretical ones illustrates different findings, which are sometimes common in the textile industry (Table 1).

Table 1. Theoretical and practical yarn twist comparison results

Theoretical results		**Practical results**	
TPM 600	α - 2.7	TPM 656	α - 3.04
TPM 711	α - 3.3	TPM 802	α - 3.72
TPM 819	α - 3.8	TPM 876	α - 4.06

Yarn Evenness and Hairiness

In the study, the unevenness and hairiness qualities of low, medium and high twist yarns were compared (Table 2). High-twist fibre showed the lowest coefficient of variation (CV) – 12.03%, which indicates the most uniform yarn structure. The medium twist had the highest CV–13.28 %, which means the lowest evenness. When it comes to hairiness, the low twist appeared to have the lowest hairiness, meaning the most refined surface.

Table 2. Yarn evenness and hairiness results

Samples	Yarn linear density	CV (%)	Hairiness (*H*)
Low twist	19.6 tex	12.84	1.75±0.03
Medium twist	19.6 tex	13.28	1.94±0.023
High twist	19.6 tex	12.03	1.88±0.05

Microscope images of low (Fig. 3), medium (Fig. 4), using 10x magnification, and high (Fig. 5), using 4x magnification, twist yarns visually highlight the differences in their structural characteristics. In the case of low-twist, the fibre appears to be quite loose, with a more open structure. Medium-twist shows a more balanced structure, and as for high-twist fibres, the yarn exhibits a tightly spun structure.

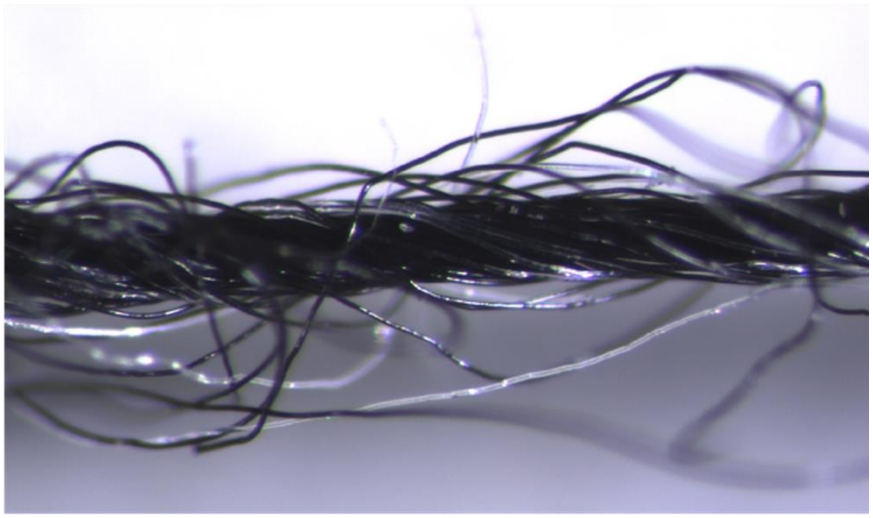

Fig. 3. Low twist fibre

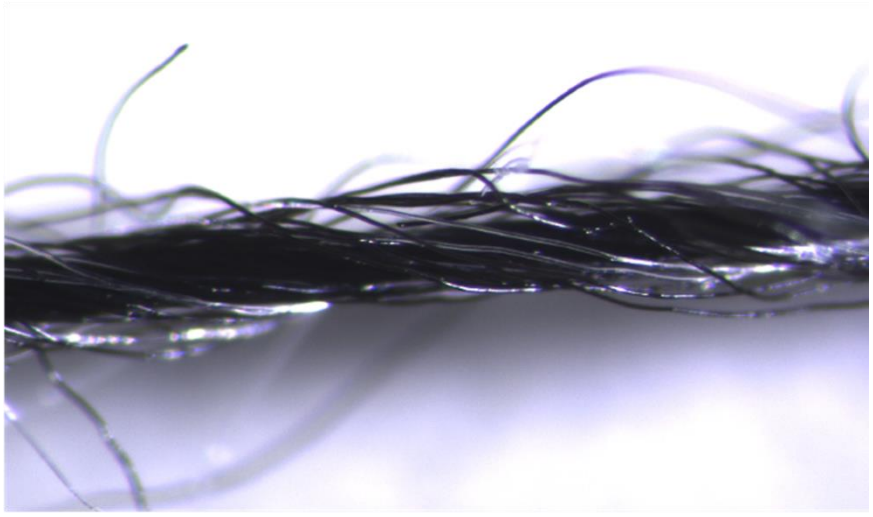

Fig. 4. Medium twist fibre

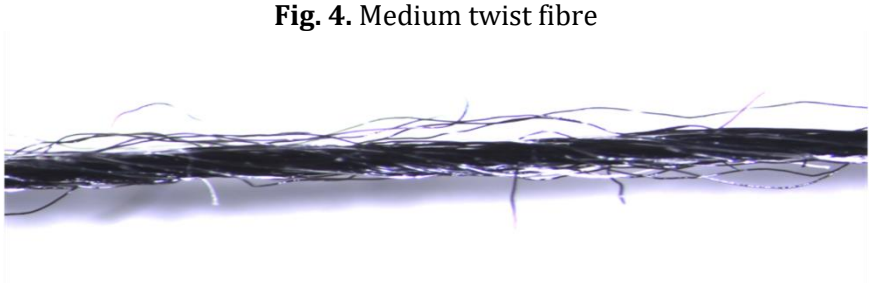

Fig. 5. Hight twist fibre

Microscope images visually underscore how twist levels significantly affect the structural integrity of the twisted yarns.

Conclusions

1. The research revealed that yarn twist has a minor impact on microfibre release during washing. Low twist yarn fabric released slightly fewer microfibres compared to medium and high twist yarn fabrics. However, the differences were not significant.
2. Yarn structural properties differed quite. The high-twist fibre showed the most uniform yarn structure. Low twist yarn appeared to have the lowest hairiness, meaning the most refined surface.
3. The actual values of the twist of the yarn deviated compared to theoretical calculations, which is considered quite common in the textile industry.
4. The microscope images revealed structural variations between twists. The low twist appeared looser, the medium structure quite stable and the high twist – tightly spun appearance.
5. When concluding, the research confirms that while yarn twist properties have little effect on microfibre release, it still must be taken into consideration when analysing the microfiber release issue in textiles.

References

1. ZHU, Yanjing, et al. Investigation of Removal Efficiency of Microplastics at Different Process Stages of a Wastewater Treatment Plant in the Textile Industry in Southern China. *Water*, 2025, 17.4: 574.
2. JUNTARASAKUL, O., JULAPONG, P., SRICHONPHAISARN, P. *et al.* Weave structures of polyester fabric affect the tensile strength and microplastic fiber emission during the laundry process. *Sci Rep,* 2025, 15, 2272.
3. CUI, Hong, and Changquan XU. Study on the Relationship between Textile Microplastics Shedding and Fabric Structure. *Polymers,* 2022, 14, no. 23: 5309. https://doi.org/10.3390/polym14235309
4. PERIYASAMY, A. P. Environmentally Friendly Approach to the Reduction of Microplastics during Domestic Washing: Prospects for Machine Vision in Microplastics Reduction. *Toxics*, 2023, 11 (7), 575. https://doi.org/10.3390/toxics11070575
5. INTERNATIONAL ORGANIZATION FOR STANDARDIZATION. ISO 4484-1:2023. Textiles and Textile Products -Microplastics from Textile Sources -Part 1: Determination of Material Loss from Fabrics during Washing, 2023.
6. INTERNATIONAL ORGANIZATION FOR STANDARDIZATION. ISO 6330:2021. Textiles – Domestic washing and drying procedures for textile testing. 2021. 59.080.01.

Analysis of Fashion Product Design and Manufacturing Technologies and Their Impact on Fashion Sustainability

Urtė Marija ČESONIENĖ*, Virginija DAUKANTIENĖ

Kaunas University of Technology, Kaunas, Lithuania

** urte.cesoniene@ktu.edu*

Abstract

The research aims to analyse the feasibility of increasing the sustainability of fashion products by implementing innovative solutions in the design and manufacturing of fashion products. Therefore, in this research, the idea of using textile waste left from the manufacture of interior textile products (curtains) (in this study named decor fabrics) for decorating dresses in the form of adhesive bonding appliqués was analysed. Following this idea, a test of the peeling strength of adhesive textile bonds was carried out. Adhesive bonds were created using strips of main woven fabric cut in three fabric directions (warp, weft, and bias) with strips of decor fabrics cut in the same three fabric directions. The peeling strength testing results have shown that the tested adhesive bonds with all three decorative fabrics have the lowest peeling strength along the warp fabric direction, the highest strength was for the bias fabric direction, with the exception of the third decorative fabric, which created the strongest adhesive bond along the weft direction. This third fabric also showed the strongest adhesive bonds along all directions of the fabric compared to the other two fabrics.

Keywords: fashion, sustainability, adhesive bonding, peeling strength, mechanical testing.

1. Introduction

Sustainable fashion is the practices and approaches of the fashion industry that aim to increase social responsibility by reducing textile waste and saving resources, reducing negative environmental impacts, and changing the linear economy approach to that of the circular one. One way to ensure sustainability is to personalise products using different design technologies: printing (digital printing, transfer printing, sublimation, etc.), embroidery, or appliqué. This article analyses in more detail the creation of a personalised dress design using industrial textile waste from the production of interior textiles, such as curtains, etc. Industrial waste will be used to produce appliqués for the decoration of a garment using adhesive bonding technology.

The delamination of adhesive bonds is an important factor in evaluating the strength and durability of the adhesive bond, especially in the textile and clothing industry. Pressing temperature, pressure, duration, and direction of the fabric are the key factors influencing the peeling strength of the adhesive bonds [1-5]. The optimisation of these parameters is essential to achieve the best properties of the adhesive bonds. As the pressing temperature increases, the delamination strength increases, but only up to a certain limit; too high a temperature can reduce the quality of the bond due to too deep of a penetration of adhesive [1]. Temperature and duration affect not only the mechanical properties of the adhesive bond, but also its ageing processes: too long or too high temperatures can cause the polymer structure to degrade [2]. The optimal temperature is around 150–160 °C, and the highest strength is achieved in the wale fabric direction [1].

The deformation of the fabric in the bias direction is greater than in one of the warp and weft directions, confirming that bias-aligned fabrics are more flexible and prone to deformation under

load [6]. This mechanical behaviour may influence the performance of the adhesive in bonded fabrics as well.

Thus, the aim of this research is to evaluate the peeling strength of the adhesive textile bonds designed pairing the main warp, weft, and bias-orientated woven fabric tapes selected for dress production and the tapes of textile waste left from the manufacture of interior textile products suitable for dress decorating in the form of adhesive bonding appliqués.

2. Materials and methods

The woven fabric manufactured by JSC 'Textilis' (Lithuania), suitable for the production of dresses, was chosen as the main fabric (A) and fabrics D1, D2, and D3 taken in the form of industrial waste intended for decoration to design adhesive bonds (Table 1).

Table 1. Characteristics of the tested woven fabrics

Fabric and code	Fiber content, %	Weave type	Thickness, mm		Area density, g/m²	Fabric density, cm⁻¹		Yarn linear density, tex	
			h_1	h_2		warp	weft	warp	weft
Main (A)	90 PES, 10 EL	Plain	0.69±0.01	0.66±0.01	210.0±11.0	62	31	11.0±0.0	11.2±0.0
Decor (D1)	100 PES	Jacquard	0.76±0.11	0.63±0.05	242.0±4.0	87	41	8.7±0.0	36.0±0.0
Decor (D2)	100 PES	Twill	0.76±0.01	0.70±0.00	249.0±5.0	35	25	43.5±0.0	42.6±0.0
Decor (D3)	100 PES	Satin	0.64±0.01	0.61±0.01	204.0±4.0	61	26	18.1±0.0	33.3±0.0

Notes: PES – polyester. EL – elastane. The area density of textile materials was measured according to the standard LST ISO 3801:1998 [8]. h_1 is the thickness of the fabric measured with J-40-T under a pressure of 1 kPa according to the standard ISO 5084:1996 [9]. h_2 is the thickness of the fabric measured with J-40-T under a pressure of 1.6 kPa. The linear density of the woven fabric was determined according to the standard ISO 7211-5: 2020 [10].

Mechanical properties such as strength, elongation, and bending stiffness are relevant properties for the prediction of dress performance. Thus, a uniaxial tensile test was performed to assess the strength and elongation of the main woven fabric (A) according to LST EN ISO 13934-1:2013 [11]. A computerised tensile machine H10KT (Tinius Olsen Ltd., UK) was applied at a rate of 100 mm/min with a preload of 5 N. Five fabric strips of 50 mm width and 300 mm length (200 mm gauge length) were cut in each sample group (warp, weft, and bias). The same directions of the fabric (A) were tested for bending stiffness by applying the cantilever bending performed according to the FAST methodology. Three specimens (50 mm × 150 mm) in each sample were tested. The length of the 2c bent part of the strip-shaped specimens was measured six times to calculate its average value and to determine the bending stiffness B:

$$B = \mathrm{w} \times \mathrm{c}^3 \times 9.81 \times 10^{-6}\ (\mu\mathrm{Nm}), \quad (1)$$

where: w – area density of the fabric, g/m², c – half the length of the inclined specimen part, mm.

Adhesive bonding technology is an effective way to join two layers of fabrics with the application of thermo-adhesive polymeric polyurethane (PU) or polyester (PES)-based tapes [3]. 100% PES-based 0.88 mm thickness adhesive film with 130-135 °C melting point manufactured by the company 'Adhesive Films, INC' was used in this investigation. It is most suitable for the bonding of polycotton and polyester fabrics in applications such as appliques, labels on woven and printed fabrics. The fabric strips used to produce the adhesive bonds had dimensions 20 mm (width)

× 80 mm (length). The sizes of the adhesive films used to bond the woven fabric samples with the application of the press device were 10 mm (width) × 50 mm (length). The number of specimens in each sample group was 5. During the bonding that was applied in two steps, the technological parameters, such as pressure, temperature, and duration, were controlled. Pressure and duration were taken from the results of previous research [1, 3-5, 7]. From these results, it was seen that even the 140 °C lowest applied temperature can ensure the appropriate values of the peeling strength *F*. Therefore, considering sustainability issues related to the saving of energy resources, it was selected for the second step of bonding. 110 °C pressing temperature and 15 s duration were parameters of the first step of bonding. After pre-bonding was applied in the first step, the silicon paper was peeled off in 5 s. The 5.6 kPa pressure for the pressing duration of 20 s was a parameter of the second bonding step. For a thin, 10–200 μm adhesive layer, tensile forces will dominate [2]. Therefore, the peeling strength test *F* (N/mm) was performed with the same H10KT tensile machine at a rate of 50 mm/min. The peeling strength was calculated automatically from experimental delamination curves. The penetration of the adhesive into the fabric structure strongly depends on the softness index of a fabric. Therefore, it was calculated using the thickness values h_1 and h_2 measured at different pressures (Table 1) and the formula:

$$\Delta h = \frac{h_1 - h_2}{h_1} \cdot 100\%. \quad (2)$$

3. Results and discussion

The results of the strength and elongation tests of the main woven fabric are presented in Table 2. It is seen that the fabric is strongest in the warp direction (1008.00 N). The bias direction offers the greatest stretch and flexibility (Table 3), which is useful in applications where fabric drape ability and elasticity are required. The weft direction is the weakest and least stretchable.

Table 2. Uniaxial tensile test results of the main woven fabric (fabric code A)

Warp (AM sample code)		Weft (AA sample code)		Bias (AI sample code)	
Maximal force F_{max}, N	Elongation at maximal force ε_{max}, %	Maximal force F_{max}, N	Elongation at maximal force ε_{max}, %	Maximal force F_{max}, N	Elongation at maximal force ε_{max}, %
1008.00±154.00	48.67±19.77	412.00±72.00	37.33±4.07	425.00±115.00	75.90±12.12

Table 3 presents the results of the bending stiffness testing of the A main woven fabric. The results show that weft fabric direction has the highest bending stiffness (9.81μNm). The warp direction shows intermediate stiffness, and the bias direction has the lowest (2.25 μNm), which shows the highest fabric flexibility.

Table 3. Bending stiffness results of the A main woven fabric

Fabric side	Bending stiffness *B*, μNm		
	Warp (AM sample code)	Weft (AA sample code)	Bias (AI sample code)
Face side	6.933	9.810	5.068
Back side	8.003	8.813	2.250

The results of the peeling strength test are presented in Table 4. The D1 decor-woven fabric shows the highest peeling strength in the bias direction (0.1444 N/mm), while the warp direction has the lowest one (0.0425 N/mm). In the bond created between the main fabric A and the D1 decor fabric, good adhesion occurred only in areas where there were more protruding yarns. The more yarns there were, the better bonding, but the overall result was poor, indicating very poor film and fabric adhesion.

Table 4. Peeling strength results (the highest values of bending stiffness are highlighted in bold)

Fabric code	Peeling strength *F*, N/mm		
D1	AM-P1-D1M (Warp)	AA-P1-D1A (Weft)	AI-P1-D1I (Bias)
	0.0425±0.0296	0.1011±0.0778	**0.1444±0.1428**
			
D2	AM-P1-D2M (Warp)	AA-P1-D2A (Weft)	AI-P1-D2I (Bias)
	0.0203±0.0170	0.0928±0.0992	**0.1309±0.1784**
			
D3	AM-P1-D3M (Warp)	AA-P1-D3A (Weft)	AI-P1-D3I (Bias)
	0.0525±0.0337	**1.1280±0.2236**	0.2203±0.0724
			

The bias direction of the D2 décor-woven fabric, similar to the D1 fabric, shows the highest peeling strength, and the warp direction shows the lowest. The D3 decor-woven fabric demonstrates the highest peeling strength in the weft direction, suggesting a stronger bond or higher resistance in that direction. In all tested bond cases, the warp direction consistently shows the lowest peeling strength across all types of fabrics.

When summarising the research results, it can be seen that the adhesive bonds with all three decor fabrics have the lowest peeling strength along the warp fabric direction, the highest strength was for the bias fabric direction, and only the D3 decor fabric created the strongest adhesive bond along the weft direction. The D3 decor fabric showed the strongest adhesive bonds along all directions of the fabric compared to the other two fabrics, and the weakest ones – the D2 fabric. In the weft direction of the D3 decor fabric, the peeling strength reached the maximum value (1.1280 N/mm), but it appears to be lower than previously determined (6.12 N/mm) by other investigations [1, 3-5]. This difference can be attributed to variations in fabric construction (especially of the back side of the D1 décor fabric), a low thickness of the adhesive film, and improper bonding conditions.

The summary of the results of the fabric softness index Δh is presented in Table 5. This index indicates the porosity of the fabric. It is likely that with higher porosity of the fabric, the adhesive penetrates deeper into the fabric.

Table 5. Fabric softness indexes

Parameter	Woven fabric			
	A	D1	D2	D3
Softness Δh, %	4.35	17.11	7.89	4.69

From the results presented in Table 5, it is seen that the D1 fabric, which has the highest softness index (17.11%), demonstrated the intermediate peeling strength, and the D3 fabric with the lowest softness index (4.69%) – the highest peeling strength (Table 4). Fabrics A and D3 are the least soft (4.35–4.69%). They are denser and stiffer in surface feel. The D2 fabric has moderate softness (7.89%). The more protruding yarns of the D1 fabric demonstrated better bonding in the localised areas. Notwithstanding this, in general, the adhesion of the film was poor since the adhesive was distributed unevenly, thus weakening the adhesion.

4. Conclusions

1. In this investigation, the peeling strength of the adhesive bonds designed from the main woven fabric (A) with the appropriate mechanical properties, such as strength, elongation, and bending stiffness, selected for dress sewing and three decor fabrics (D1, D2, and D3) was tested.
2. The research results revealed that fabric structure, surface characteristics, and direction influence peeling strength. In three tested groups of samples, the warp direction demonstrated the weakest adhesion, while the bias direction had the highest peeling strength in most cases. The fabric pair composed of A main fabric and D3 decor fabric had the strongest adhesion, especially in the weft direction, achieving 1.1280N/mm peeling strength value, and maintained strong adhesion in all directions.
3. The determined peeling strength values were significantly lower than required for the main joining of the garment pieces, but, supposedly, sufficient for the decoration of the dress with appliqués. Therefore, in the future, the influence of laundering on the peeling strength of adhesive bonds must be analysed to assess the exploitation behaviour, and the reasons influencing the low values of peeling strength must be explored in more detail, including the fact that a too high variation of the initial testing results was obtained.

References

1. ZMITRULEVIČIUS, Edvinas. *Influence of the Bonding Temperature and Printing on the Strength of Knitted Fabric's Adhesive Bonds*. PhD Thesis. M. Sc. Thesis. Available from: https://epubl.ktu.edu/object/elaba:29040057/ [viewed 17-02- 2025].
2. PETHRICK, Richard A. Design and ageing of adhesives for structural adhesive bonding–a review. *Proceedings of the Institution of Mechanical Engineers, Part L: Journal of Materials: design and applications*, 2015, 229.5: 349-379. Available from: https://www.researchgate.net/publication/273599663_Design_and_ageing_of_adhesives_for_structural_adhesive_bonding_-_A_review [viewed 15-02- 2025].
3. DAUKANTIENĖ, Virginija; DANILOVAS, Paulius Pavelas; MIKALAUSKAITĖ, Gerda. Study of temperature impact on the behaviour of fibre polymer materials′ and their adhesive bonds. *The Journal of the Textile Institute*, 2021, 112.2: 313-321. Available from: https://doi.org/10.1080/00405000.2020.1746011 [viewed 25-02- 2025].

4. DAUKANTIENĖ, Virginija; VADEIKĖ, Giedrė. Evaluation of the air permeability of elastic knitted fabrics and their assemblies. *International Journal of Clothing Science and Technology*, 2018, 30.6: 839-853. Available from: https://www.researchgate.net/publication/328329346_Evaluation_of_the_air_permeability_of_elastic_knitted_fabrics_and_their_assemblies [viewed 27-02- 2025].
5. MIKALAUSKAITĖ, Gerda; DAUKANTIENĖ, Virginija. Influence of technological parameters on the adhesion strength of adhesive bonded textile seams. In: *AUTEX 2016: 16th World Textile Conference: Book of Abstracts, University of Lubljana, Slovenia*. 2016. p. 218-220. Available from: https://www.researchgate.net/publication/322635931_Influence_of_technological_parameters_on_the_adhesion_strength_of_adhesive_bonded_textile_seams [viewed 16-03- 2025].
6. TAKATERA, Masayuki; ISHIZAWA, Ken; KIM, KyoungOk. Effect of adhesive interlining on the creep behavior of woven fabric under low stress in the bias direction. Available from: https://d1wqtxts1xzle7.cloudfront.net/119965618/ [viewed 18-03- 2025].
7. MIKALAUSKAITĖ, Gerda; DAUKANTIENĖ, Virginija. Investigation of the influence of bonding and thermal ageing duration on the peeling strength of knitted materials' bonds. *Materials science*, 2020, 26.2: 225-232. Available from: https://matsc.ktu.lt/index.php/MatSc/article/view/21666 [viewed 20-02- 2025].
8. INTERNATIONAL ORGANIZATION FOR STANDARDIZATION (ISO). LST ISO 3801:1998. Woven fabrics. Determination of mass per unit length and mass per unit area. Available from: https://lsd.lt/ . [viewed 05-02-2025].
9. INTERNATIONAL ORGANIZATION FOR STANDARDIZATION (ISO). ISO 5084:1996 Textiles-Determination of thickness of textiles and textile products. Available from: https://lsd.lt/ . [viewed 08-02-2025].
10. INTERNATIONAL ORGANIZATION FOR STANDARDIZATION (ISO). ISO 7211-5:2020 Textiles — Methods for analysis of woven fabrics construction — Part 5: Determination of linear density of yarn removed from fabric. Available from: https://lsd.lt/ . [viewed 15-02-2025].
11. INTERNATIONAL ORGANIZATION FOR STANDARDIZATION (ISO). LST EN ISO 13934-1:2013. Textiles. Tensile properties of fabrics - Part 1: Determination of maximum force and elongation at maximum force using the strip method (ISO 13934-1:2013). Available from: https://lsd.lt/. [viewed 05-02-2025].

Development of Compression Knitwear Materials with Shielding Properties Against Ultraviolet Radiation

Maria KRAVCHUK[1], Liudmyla HALAVSKA[1*], Daiva MIKUČIONIENĖ[2], Arsenii ARABULI[1]**

[1] Kyiv National University of Technologies and Design, Kyiv, Ukraine

[2]Kaunas University of Technology, Kaunas, Lithuania

** galavska.ly@knutd.com.ua*

***daiva.mikucioniene@ktu.lt*

Abstract

The work is devoted to developing knitted materials and tubular products based on them, which will provide effective protection from ultraviolet radiation of intact areas of the human body during quartzization of wound surfaces. During the research, a structure of a tubular knitted material with an elastomeric yarn arrangement in the soil structure was developed in the form of a tuck stitch and float stitch. The surface modification provided the knitted materials with shielding properties against ultraviolet radiation. It has been experimentally shown that using the proposed method makes it possible to create textile screens that effectively protect against ultraviolet radiation.

Keywords: compression knit, shielding textile material, UV protection.

1. Introduction

In the surgical practice of mobile hospitals, using ultraviolet radiation is appropriate as an effective means of disinfection and healing of wound surfaces, treatment of purulent and trophic wounds, ulcers and burns. This electromagnetic radiation, which is invisible to the human eye and occupies the spectral region between visible and X-ray radiation, has a bactericidal (antimicrobial) effect and, under its influence, leads to the death of a microbial cell in the first or next generation. It was established that electromagnetic radiation of the ultraviolet range of wavelengths in the interval from 200 to 320 nm has a bactericidal effect, therefore, it is used in surgical operations. However, in large quantities, it is dangerous for the human body. Therefore, it is important to regulate the intensity of bactericidal radiation and the surface dose of irradiation [1, 2].

The primary methods of obtaining textile materials for electromagnetic radiation shielding are the use of metallized fibers and threads or modification of textile fabrics, which consists in the chemical reduction of metal ions to metals directly in the structure of the textile material and on its surface. Depending on the further application, metallized textile materials are produced on various bases: cotton, polyester, polyamide, para-aramid, glass, basalt, etc. The metallized coating applied to the surface of the material, together with shielding properties, can provide an antibacterial effect. Today, there are many studies by scientists [3–6] related to the development and research of textiles with a high UV protection factor (UPF).

The issue of developing functional knitwear materials for rehabilitation purposes with a combination of compression and antimicrobial action and specified physical and mechanical characteristics to protect intact body parts from electromagnetic radiation of the ultraviolet wavelength range during physiotherapy procedures of wound surfaces in the pre- and

postoperative periods has not yet been considered and is a promising direction for the development of the textile industry in the context of war and a significant number of wounded among the military [7-9].

2. Results and discussion

During the research, a structure of a tubular knitted material with an elastomeric yarn arrangement in the soil structure was developed in the form of a tuck stitch and float stitch with a 1+1 and 1+3 laying report. The prototypes were produced on a gauge 13E circular hosiery machine with a cylinder diameter of 3.75 inches. In the knitting process, the knitting density was changed vertically at three levels. At the same time, the feed rate of the elastomeric thread into the soil structure remained unchanged and was controlled by the rotation speed of the wheel that feeds it into the knitting zone. Table 1 shows characteristics of the developed samples of knitted materials.

Table 1. Characteristics of the tested knitted samples are given

Sample code	Speed of wheel supplying elastomeric inlay-yarn v, min^{-1}	Wale density P_w, cm^{-1}	Course density P_c, cm^{-1}	Area density, M, g/m^2	Loop length of plating cotton yarn, mm	Loop length of textured-elastomeric PA-EL ground yarn, mm	Average length of textured-elastomeric PA-EL inlay-yarn per one wale, mm
the pattern repeat 1×1							
1×1/11/110	110	8.5	11	402.4	5.6	5.2	1.1
1×1/10/110			10	397.6	6.2	5.8	1.2
1×1/9/110			9	400.8	6.8	6.4	1.1
the pattern repeat 1×3							
3×1/11/110	110	9.0	11	450.0	6.1	5.5	1.2
3×1/10/110			10	456.8	6.7	6.1	1.3
3×1/9/110			9	417.6	7.3	6.7	1.2

To provide knitted materials with shielding properties against ultraviolet radiation, their surface modification was performed. The essence of the method of “modification with metal nanoparticles” is the chemical reduction of metal ions to metals directly in the structure of the textile material and on its surface. The research was conducted with copper sulfate. Hydrazine sulfate was used as a reducing agent. The ability of textile materials to shield UV radiation was evaluated by the values of the Transmittance in a certain wavelength range (Transmission, %) using a UV-Vis spectrophotometer DU-8800D (Drawell International Technology Ltd). The device is designed to determine the shielding properties of textile materials against non-ionising electromagnetic radiation in the wavelength range of 190-1100 nm (ultraviolet, visible and infrared spectrum).

The studies revealed that the surface modification of samples with a 1+3 elastomeric yarn layout leads to a significant decrease in the ability of the fabrics to transmit UV rays both in the UV-B (280-315 nm) and UV-A (315-400 nm) regions. This is due to a better penetration of the modifying solution into the structure of the knitted material due to its loose, embossed surface, which is formed due to the laying of the elastomeric yarn 1+3. In turn, the modification of samples with a 1+1 elastomeric yarn laying report also helps to reduce the ability of fabrics to transmit UV rays, both in the UV-B (280-315 nm) and UV-A (315-400 nm) regions. However, it should be noted that this decrease is not as significant as in the samples of the first series.

It has been experimentally proved that the use of the proposed method makes it possible to create textile screens that are effective in protecting against harmful ultraviolet radiation. It has been found that the shielding properties of a modified knitted material with a compression effect are influenced by the report of elastomeric yarn insertion into the soil structure.

3. Conclusions

The surface modification of the developed samples of knitted materials was carried out in the course of the research. The shielding properties were achieved by chemical reduction of metal ions to metals directly in the structure of the textile material and on its surface.
The developed knitted materials are recommended for the protection of intact areas of the human body during wound quartzing in the first phase of the wound process, as well as in the final phase and after the patient is discharged from the hospital for the prevention and treatment of infectious complications.

4. Acknowledgements

This research was carried out within the framework of a joint Lithuanian–Ukraine science and research project, “Functional textile materials and products for the needs of the military, doctors, hospitalists and civilians (ORTOKNIT)”, supported by the Ministry of Education and Science of Ukraine and the Research Council of Lithuania (LMT).

5. References

1. KOLOBRODOV, V. G. Wave optics. Part 1. Electromagnetic theory of light and interference: Textbook for students. Online. Place: Kyiv, NTUU "KPI named after I. Sikorsky", 2017. Available from: https://ela.kpi.ua/server/api/core/bitstreams/79210ae1-8a14-4a85-8bf3-9c3e8cf899a2/content
2. ZABETAKIS, A. Textiles for protection against solar UVR, weather conditions and fire, Proceedings of 1st International Textile, Clothing & Design Conference, 152-157, ISBN 953-96408- 8-1, Dubrovnik, October 2002, University of Zagreb, Faculty of Textile Technology, Zagreb, Croatia.
3. VISILEANU, E. Influence on the UPF level of the content and type of nanoceramics used in the textile treatment. Proceedings of the International Conference TexTeh IX "Advanced Textiles for a Better World", INCDTP-ICPI, Romania, Bucharest, Vol. 9, 24-25 October 2019, p. 187-190. Available from: https://paper.researchbib.com/view/paper/241714
4. WILSON, C. A., BEVIN, N. K., LAING, R. M., & NIVEN, B. E. Solar protection – Effect of selected fabric and use characteristics on ultraviolet transmission. *Textile Research Journal,* 2008, Vol. 78, p. 95–104. Available from: https://journals.sagepub.com/doi/10.1177/0040517508089660
5. SINGH, M. K., & SINGH, A. Ultraviolet protection by fabric engineering. *Journal of Textiles*, 2013, Vol. 16, p.21-32. Available from: https://onlinelibrary.wiley.com/doi/10.1155/2013/579129
6. VLASENKO, V., SMERTENKO, P., BEREZNENKO, S., ARABULI, S., KUCHERENKO, V. Synthesis of metals nano-particles in the porous structure of textiles for UV-shielding. *Vlakna a textil, Fibres and textiles*, vol. 24, 2017, no.4, pp.30-33. ISSN 1335-0617 Available from: http://vat.ft.tul.cz/2017/4/VaT_2017_4_5.pdf
7. MIKUCIONIENE, D., HALAVSKA, L., LAURECKIENE, G., MELNYK, L., ARABULI, S., & MILAŠIUS, R. Development of Knitted Compression Covers for Amputated Limbs. *Fibers*, 2024, 12(10), 80. Available from: https://www.mdpi.com/2079-6439/12/10/80
8. MELNYK, L., HALAVSKA, L., MIKUCIONENE, D., DUDNYK, I. Assortment and Manufacturing Methods of Stump Socks Proceedings of 11th International Young Researchers Conference INDUSTRIAL ENGINEERING 2024 – from Zero to Hero, 2024, pp.129-131. Available from: https://ebooks.ktu.edu/pdfreader/international-young-researchers-conference-industrial-engineering-2024--from-zero-to-hero.-proceedings
9. ARABULI, S., TRUBA, A., ARABULI, A., MIKUCIONIENE, D. Improvement of UV protection properties of the cotton fabric by chemical treatments. Book of Abstracts 15th Joint International Conference on Innovation in Clothing - Clotech 2024, Dresden, Germany, 5th - 6th September 2024, pp.28-30. https://tud.qucosa.de/landing page/https%3A%2F%2Ftud.qucosa.de%2Fapi%2Fqucosa %253A92640%2Fmets%2F/?L=1

Eco-Design Challenge in Fashion

Emilija MIELIAUSKAITĖ*, Kotryna Marija LIEKYTĖ, Daiva MIKUČIONIENĖ

Kaunas University of Technology, Kaunas, Lithuania

** emilija.mieliauskaite@ktu.edu*

Abstract

The textile and fashion industry is known as one of the largest polluters in the world. And this pollution does not only occur during the production stage, but even more pollution is created during the consumption stage and at the end-of-life cycle of textile and fashion products. This study aimed to create and discuss business ideas on how to reduce the industrial and post-consumer textile waste. The ideas are based on eco-design and circular economy principles. New materials and technologies in the field of textiles are the key innovations that can also meet a variety of societal challenges. By transforming waste into new products or wearable art, eco-design businesses combat overproduction, reduce resource consumption, and empower a new generation of conscious consumers – all while ensuring sustainability and a stylish look.

Keywords: eco design, fashion, textiles, waste reduction, entrepreneurship.

1. Introduction

As is known, textiles are essential in people's lives, both due to the need to wear clothes and due to the expansion of their areas of use, such as in the automotive industry, construction, medicine, agriculture, etc. [1]. The textile and fashion sector is an important part of the European manufacturing industry, playing a crucial role in the economy and social well-being in many regions of Europe. The textiles and fashion industry is also one of the second largest polluters in the world, and the environmental damage is increasing as the industry grows [2]. During the entire life-cycle of textile products, they generate multiple sources of waste and pollution in the air, water, and soil, noise, and visual pollution and significantly contribute to global climate change [3]. Textile and fashion sector's waste can mainly be classified into three groups: production waste, pre-consumer waste, and post-consumer waste. Production waste is scraps of fibers, yarns, fabrics, fabric roll ends, etc. Pre-consumer waste consists of products manufactured with some fabric, design or color mistakes. Post-consumer waste consists of any type of household articles or garments that an owner does not requires anymore and has decided to discard.

Eco-design in fashion incorporates a variety of sustainable actions to minimize the environmental impact of the fashion industry. Eco-design not only aims to reduce environmental impact but also seeks to improve aesthetic and functional aspects of a product. It also includes the consideration of social and ethical needs. Solutions of the eco-design of a product deal effectively with both the product's functionality and the three dimensions of sustainability – environmental, economic and social [4]. Eco-design choices have an impact on various stages of the life-cycle of materials and products. Eco-designers need to focus on customers' needs and create social and ecological value [5]. They are key drivers in enabling more circularity in products as they facilitate novel business models, enable re-use and recycling, and provide opportunities for upcycling, i.e., integrating re-used parts or recycled material into new products. The aim of this work was to show good examples of how new business ideas can contribute to the reduction of textile and fashion waste.

2. Methods

The development of business ideas in eco-design covers the following aspects:

- Core Concept: The need for the eco-design business and the purpose of entrepreneurship.
- Ecological Impact: specific environmental benefits of the eco-design business idea.
- Necessity: reasons justifying the importance and necessity of the eco-design business idea.
- Innovation: unique aspects and added value of the idea.
- Feasibility and Sustainability: Evidence that the eco-design business idea is feasible and has a lasting impact.

Two eco-design business ideas are presented in this paper: the 1st idea *TyreesCoat* is developed by Emilija Mieliauskaitė, and the 2nd idea, *Reborn Threads,* is developed by Kotryna Marija Liekytė. Turning waste into new products or wearable art, new eco-design business ideas help combat overproduction, reduce resource consumption and empower a new generation of conscious consumers, while ensuring sustainability and style.

3. Eco-design business ideas

TyreesCoat

The 1st business idea was to combine non-woven fabric' waste and recycled tire rubber for outerwear production. About 1 billion end-of-life tires are generated annually, and a great part of them end up in landfills. Scientists have already found various solutions for recycling, reusing, and refurbishing the tires for a new life. There are already companies that make shoes from recycled tires and contribute to sustainability by repurposing various materials with a completely different approach. These discoveries have inspired to develop a new ecological business idea - to combine non-woven fabric waste and recycled tire rubber for outerwear production. The fashion industry generates a high number of fabrics and yarns waste, which can be recycled into non-woven fabrics, which can be used, for instance, as lining for clothing. Recycled tire rubber can be used for waterproofing of external textile fabrics. These two major waste materials would be made into high-quality products – rainproof coats. These coats would not only be rainproof, they are also designed to insulate and maintain warmth. *TyreesCoat* would reduce waste over time and provide new ways to recycle and upcycle. *Tyreescoat* is targeted at people who are passionate about outdoor activities in rainy weather conditions. Also, this product is suitable for residents in a cold and rainy climate.

The proposed idea is to produce a coat by devulcanizing scrap tires and making a mixture of recycled rubber, latex, glycerine and Ethylene Vinyl Acetate that will serve as a laminate on a nonwoven fabric. Firstly, scrap tires will be teared into small bits and all additional components are removed. Then, the bits will be devulcanized into rubber granules and mixed with mentioned above materials. Non-woven fabric will be made by tearing wool, cotton yarns and fabrics into separate fibers and by the needle punching technique, garment pieces will be formed directly without cutting. Finally, the waterproof rubber mixture will be laminated on the fabric pieces and delivered to the sewing.

TyreesCoat delivers an unusual, innovative solution for designing outerwear. Most raincoats we see in markets are usually very thin and serve only one purpose – to protect from rain. They do not provide warmth, lots of them are even one-time use and are disposed after. *TyreesCoat* offers a sustainable clothing solution made from recycled materials – automobile tires and recycled cotton and wool nonwoven fabrics. This guarantees a high-quality product made from waste materials.

By turning waste into a new wearable product, this business would reduce waste over time, as well as inspire other companies to find creative solutions to create products without using new materials. Also, there is an eco-social impact on society, because sustainability would be perceived as a major factor in deciding to buy a product. Additionally, new technologies would be developed to decrease the production cost of recycled materials, because the market would prove that this business model is efficient. The biggest challenge is still the recycling. Even if the product is made from recycled materials, it is difficult to trace the end of life, because the sorting of waste has still not reached the maximum efficiency.

Reborn Threads

This eco-design business idea proposes to revive old clothes from second-hand collections or from clothing companies' cutting waste, and make new fashionable clothes or accessories. The idea combines recycled and used clothes with sustainability and unique, trendy fashion. In *Reborn Threads*, pre-loved garments from second-hand stores will be collected and creatively transformed into stylish, one-of-a-kind pieces. Each item will be made with techniques like tailoring, dyeing, patchwork, embroidery, and reassembly, giving discarded clothes a fresh start. The main goal is to reach like-minded people who want to create and make an impact in saving the world by reducing the amount of waste generated by fast fashion. This business idea is for people who are interested in global well-being and love unique fashion.

There are many similar products or small sustainable fashion brands that are made by individuals. Commonly recycled fabrics include denim scraps, cotton, wool, cashmere, polyester, nylon, and recycled leather. All *Reborn Threads* materials are recycled or recovered from clothing manufacturers, significantly reducing the need for non-renewable resources. Newly produced products will be one-of-a-kind. Therefore, customers will always have a unique garment in their wardrobe. All materials will be carefully selected to ensure that they align with the core values: eco-consciousness, waste reduction.

The process of making the new products from end-of-life items is:

- Collection of old clothing from thrift shops, donations, vintage markets or cut-waste from clothing manufacturers.
- Washed and quality checking of each clothing piece as well as sorting them by raw material.
- Designing of a new piece from the prepared materials.
- Construction of a new clothing or accessory form sourced materials by sewing them together, dyeing, tailoring and restructuring.
- Quality checking of each item and preparation for sale.

Reborn Threads stands out by being a fresh, authentic, and eco-forward brand. Every *Reborn Threads* piece is one-of-a-kind, offering customers clothing and accessories that no one else in the world owns. Customers can feel good knowing their purchase supports environmental responsibility and reduces waste. Potential customer is everybody who cares about sustainability, ethical consumption, and personal style, and individuals who love standing out with one-of-a-kind clothing rather than mass-produced fast fashion.

Collecting and delivering second-hand garments, especially if sourced from distant locations, can generate CO_2 emissions. The use of sewing machines, lighting, and heating in a studio contributes to electricity use. Improperly disposed of packaging, even recyclable, can contribute to litter or contamination in recycling streams. Thus, by transforming waste into new unique products, *Reborn Threads* fights overproduction and reduces resource, energy consumption as well as additional pollution.

4. Conclusion

The innovation in eco-design in textile and fashion is focused on finding new and creative ways to reduce the environmental impact of this industry. This includes the development of new sustainable or biodegradable materials, exploring new production methods, or turning waste into raw materials for new products.

Supporting young researchers and entrepreneurs who question outdated business practices opens the door to innovative, sustainable solutions – from new materials to smarter technologies – shaping a better future for us all.

References

1. MIKUCIONIENE, D., HALAVSKA, L., MELNYK, L. et al. Classification, Structure and Construction of Functional Orthopaedic Compression Knits for Medical Application: A Review. *Applied Sciences*, 2024, 14(11): 4486. https://doi.org/10.3390/app14114486
2. TRIPA, S., INDRIE, L., GARCIA, P.D. et al. Solutions to reduce the environmental pressure exerted by technical textiles: a review. *Industria Textila,* 2024, 73(1): 66-74.
3. MIKUCIONIENE, D., MINGUEZ-GARCIA, D., REPON, M.R., et al. Understanding and addressing the water footprint in the textile sector: A review. *Autex Research Journal*, 2024, 24(1): 20240004. https://www.degruyterbrill.com/document/doi/10.1515/aut-2024-0004/html
4. AHMAD, S., WONG, K.Y., TSENG, M.L., and W.P. WONG. Sustainable product design and development: A review of tools, applications and research prospects. *Resources Conservation and Recycling,* 2018, 132: 49-61. https://doi.org/10.3390/polym14235309
5. DE ABREU, M.C.S., FERREIRA, F.N.H., PROENCA, J.F. and D. CEGLIA. Collaboration in achieving sustainable solutions in the textile industry. *Journal of Business & Industrial Marketing*, 2020, 36(9): 1614-1626. https://www.emerald.com/insight/content/doi/10.1108/jbim-01-2020-0041/full/html

INDUSTRIAL DESIGN AND ENGINEERING

Design and Simulation of Torp Prosthesis in the Case of Injured Stapes

Anthony FRAT[1], Virginija GYLIENĖ[2]*, Paulius VAIČIULIS[3]

[1] *University of Lorraine, Metz, France*

[2] *Kaunas University of Technology, Kaunas, Lithuania*

[3] *Kauno klinikos, Kaunas, Lithuania*

* *virginija.gyliene@ktu.lt*

Abstract
The study focuses on the design and simulation of TORP-type hearing prosthesis. The prosthesis of the middle ear was analysed by using computer-aided design (CAD) and computer-engineering techniques. Geometrical modelling was combined with the Finite Element (FE) method to set various assemblies of a TORP prosthesis, stapes footplate and the tympanic membrane. The design process included the development of 3D numerical models, taking into account the idea to increase the stability of the hearing prosthesis.

Keywords: Hearing, prosthesis, modal analysis,

1. Introduction

The human auditory system has a role in converting pressure variations from sound wave propagation into bioelectrical signals. The ossicular chain, comprising the malleus, incus, and stapes, transmits acoustic vibrations from the tympanic membrane to the cochlea via the oval window. The integrity and mobility of these bones are essential for proper sound conduction. Damage to this chain from infection, chronic otitis, trauma, or tympanosclerosis may result in conductive hearing loss requiring surgical reconstruction.

Two types of prosthesis are used for middle ear reconstruction: the first one is the application of the total ossicular chain replacement prosthesis (TORP) technique, and the second one is the partial ossicular replacement prosthesis (PORP) technique. TORP is typically used when both the incus and the stapes superstructure are absent, such as in advanced cholesteatoma or severe ossicular erosion due to chronic otitis media. In contrast, PORP may suffice when the stapes remains intact and mobile. The choice of prosthesis is crucial for optimizing sound transmission and minimizing complications. The analysis of the literature represents a few topics in the field of the study of the reconstruction of the ossicular chain after the surgical intervention, as it is presented in Figure 1. Figure 1 was generated using software VOSviewer 1.6.20 (Copyright © 2009-2023 Nees Jan van Eck and Ludo Waltman). As it is presented in Figure 1 middle ear surgery, namely the ossiculoplasty and tympanoplasty, are the techniques for the reconstruction of the ossicular chain by adapting an appropriate TORP or PORP prosthesis. Clinically, postoperative hearing outcomes depend not only on prosthesis design but also on its integration with the middle ear structures. Poor prosthesis positioning or mobility can lead to extrusion, persistent conductive hearing loss, or the need for revision surgery. When a prosthesis is introduced, it is important to assure the stability of the prosthesis, because bad contact and poor osseointegration affect the sound transmission after the ossiculoplasty [1], [2]. Therefore, stable coupling between the hearing prosthesis and the elements of middle ear is essential for hearing results [1], [2]. For example, in order to improve the stability of the prosthesis after the ear surgery, adjusted-angle ear prosthesis was proposed [3].

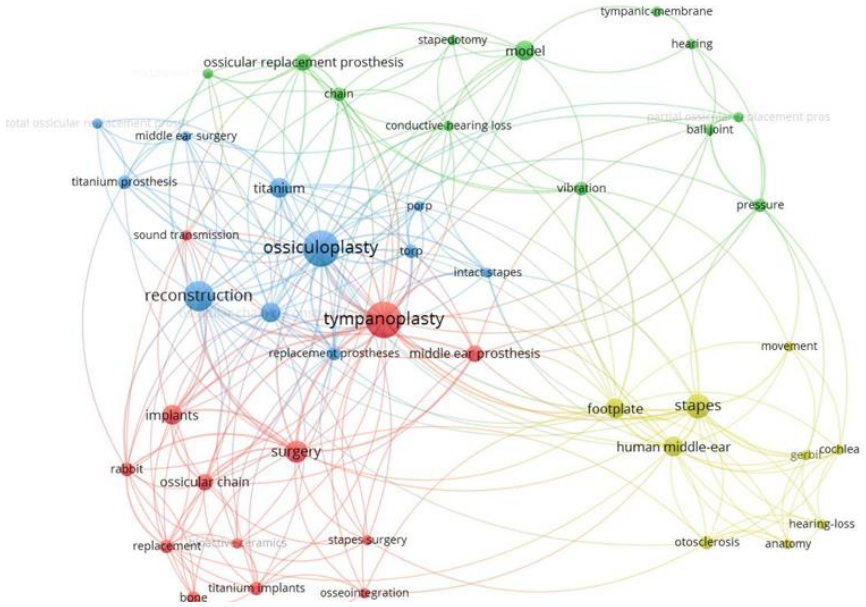

Fig. 1 Main research fields of the reconstruction of the ossicular chain

This article focuses on TORP prosthesis, when the stapes, one bone of the three ossicular bones, is partially or fully damaged.

2. Methods

At the first stage, the 3D CAD models of the stapes were created. As the dimensions of the stapes are variable, 3D models were prepared according to the maximum and minimum dimensions found in the literature [4], [5], [6]. Figure 2 represents the stapes 3D model, according to minimum dimensions. Additionally, schematically, it is represented how the chronic otitis can injure the crus of the stapes.

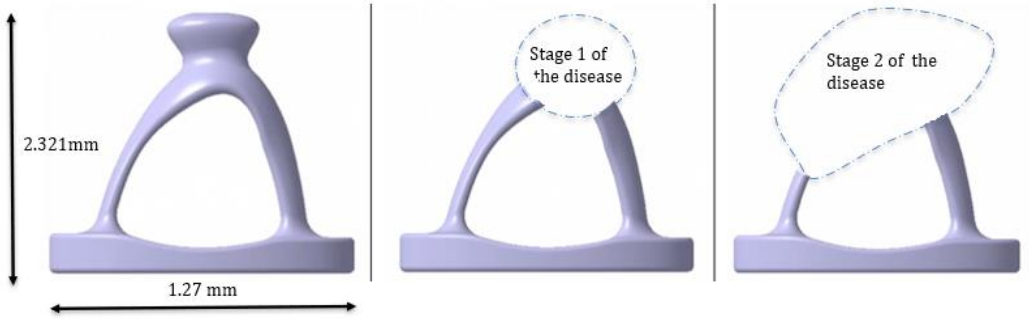

Fig. 2 General view of stapes with minimum dimensions and the stages of injury of crus after the chronic otitis

As it can be seen from Figure 2, the state of the injured stapes can be affected differently, according to the disease, and for example, the crusses can be injured totally. Thus, the state of the stapes after the chronic otitis will demand an appropriate hearing prosthesis.

3. Results

According to the assumption that stapes can be partially or fully damaged, different new hearing prostheses were modelled, aiming to "use" the geometry of the footplate and the crusses of stapes. According to this idea, new modelled prostheses were modelled and presented in Figure 3.

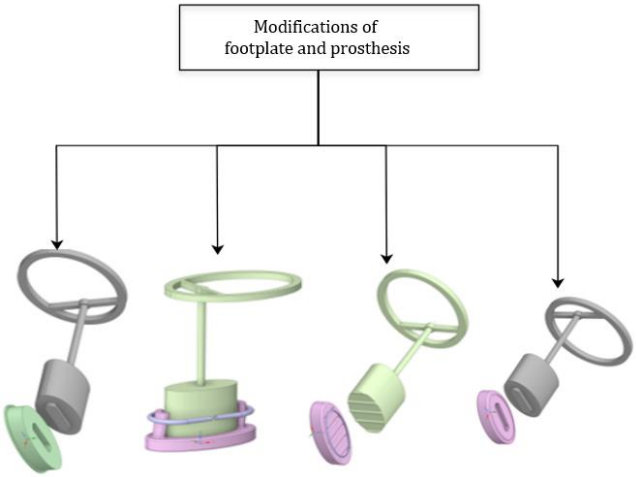

Fig. 3 General view of new modifications of TORP prosthesis

As it is presented in Figure 3, by performing the modifications of the footplate and the modifications of the standard TORP prosthesis, new geometries of the hearing prosthesis were created. However, for better osseointegration of the prosthesis, other techniques should be applied, particularly techniques of surface modification of titanium [7].

3. Conclusions

1. New 3D CAD models were created, aiming to save the remaining parts of the stapes in order to increase the stability of the hearing prosthesis.
2. The "scratch" technique, used in medicine, was applied for the creation of new 3D CAD geometries for multibody dynamic analysis, aiming to increase the stability of hearing prosthesis, in the case of injured stapes.

References

1. NEUDERT M., BERNER M., BORNITZ M., BELEITES T., NEY T., ZAHNERT T. Osseointegration of prostheses on the stapes footplate: Evaluation of the biomechanical feasibility by using a finite element model. *JARO*, vol. 8, no. 4, pp. 411–421, Dec. 2007, doi: 10.1007/s10162-007-0094-7.
2. NEUDERT M. *et al.* Osseointegration of Titanium Prostheses on the Stapes Footplate. *JARO*, vol. 11, no. 2, pp. 161–171, Jun. 2010, doi: 10.1007/s10162-009-0202-y.
3. GYLIENE V., EIDUKYNAS V., GYLYS G., MURUGESAN S. Numerical Analysis of Stapes Prosthesis Constraining in the Case of Otosclerosis. *Materials*, vol. 14, no. 24, p. 7747, Dec. 2021, doi: 10.3390/ma14247747.
4. SUN Q., GAN R. Z., CHANG K.-H., DORMER K. J. Computer-integrated finite element modeling of human middle ear. *Biomech. Model. Mechanobiol.*, vol. 1, no. 2, pp. 109–122, Oct. 2002, doi: 10.1007/s10237-002-0014-z.
5. KULKARNI S. V., YAMAGAR N. M., POL S. A., PATEL R, GILANI A. Study of Morphological and Anthropometric Features of Human Ear Ossicles. *Indian J. Otolaryngol. Head Neck Surg.*, vol. 76, no. 1, pp. 846–851, Feb. 2024, doi: 10.1007/s12070-023-04295-y.
6. SIM J. H., ROEOESLI C., CHATZIMICHALIS M., EIBER A., HUBER A. M. Characterization of Stapes Anatomy: Investigation of Human and Guinea Pig. *JARO*, vol. 14, no. 2, pp. 159–173, Apr. 2013, doi: 10.1007/s10162-012-0369-5.
7. ZHANG L.-C. and CHEN L.-Y. A Review on Biomedical Titanium Alloys: Recent Progress and Prospect. *Adv. Eng. Mater.*, vol. 21, no. 4, p. 1801215, Apr. 2019, doi: 10.1002/adem.201801215.

Modelling of Industrial Equipment Operator Decision-Making

Rokas VAITKUS*, Lina KAVALIAUSKIENĖ

Kaunas University of Technology, Kaunas, Lithuania

** rokas.vaitkus@ktu.edu*

Abstract

Europe is trailing in Industrial Revolution 4.0 tool use when compared to the USA and China. Here, Machine Learning is utilized to optimize set-value parameter data of an industrial film web processing machine. XGBoost, Logistic Regression, Naïve Bayes, and SVM modelling techniques are evaluated in binary machine state classification based on set-value parameters due to their prominence in recent works. XGBoost is found to be the most accurate, achieving an MCC score of 0.673 prior to hyperparameter tuning and 0.776 after tuning. PSO is used to find optimal parameter inputs based on model prediction probabilities, with the found parameter set suggesting a mean success probability of 0.784 for 35 different products. The input parameters are projected to improve the machine availability by 8.2%, resulting in an OEE increase of 7.3% points, which can be considered a major improvement.

Keywords: machine learning, industrial optimisation, modelling.

1. Introduction

The term Industry 4.0 (IR4) has been established more than ten years ago, but the adoption rates measured in various metrics have only reached above 40% in 2023 or 2024, depending on the country, according to a study by the global consultancy MHP (n = 856). Overall, the maturity level of Digital Twin technology for production facilities has reached 48%, autonomous systems have reached 46%, and Internet of Things (IoT) has reached 57% in 2024. It should be noted that the usage of IR4 technologies differs widely between economic powers. China and the USA lead the way in supply chain transparency, autonomous systems, Digital Twins, and IoT technology use. Germany, Austria, Switzerland, and the UK are significantly behind in comparison. Several roadblocks to the implementation of IR4 have been reported by the interviewees, with the shortage of skilled labour being the most repeated at 52%, followed by incompatibility with legacy systems and difficulties adapting to day-to-day business, both at 47%. The gap between Europe and other industrial blocks could be reduced with more training, standard establishment and collaboration between companies as part of the management strategy to enhance the positive impacts gained by adapting the IR4 technologies, with Machine Learning (ML) being considered one of the most prominent [1].

Machine Learning is a broad term under the Artificial Intelligence (AI) umbrella. While AI refers to the attempt to mimic human intelligence in machines, ML specifically uses algorithms to train and make predictions on data without step-by-step programming. The models can also be used to explore, transform, and classify the input data apart from prediction. In the context of industrial manufacturing, the main enabler of this approach is the large amount of sensor or system data from production equipment and material or spare parts movement. If the data flow is integrated, for example, by using a Supervisory Control and Data Acquisition (SCADA) system, it can be utilized not only in tracking changes over time but also in the making of robust ML models. These models can be used to control processes, improve quality outcomes, plan production schedules, and predict mechanical breakdown in production equipment, to give some examples. Overall, ML is a powerful tool with a myriad of applications in production optimisation [2].

This work aims to utilize the parameter data generated during the operation of industrial film web processing equipment to reduce the number of manual parameter searches needed during a changeover. Parameters such as pick and place coordinates, punch tool or sealing tool positions and movement are tracked, as these parameters are adjusted after a changeover most often. Currently, each changeover requires manual parameter search and station adjustments to produce quality products in a stable manner. The complex changeovers generate a large amount of scrap and result in downtimes due to poorly selected parameters. ML frameworks specializing in machine parameter optimizations and capable of working with high-dimensionality data are of relevance here. Moreover, the relationship between human decision-making and the utilization of ML in the context of manufacturing equipment optimization is also important. Overall, the ability to discern machine downtimes due to parameter choice and unrelated equipment breakdown is useful for PdM applications.

2. Methodology

Previous research has suggested specialized approaches to ML [3–5], the generalized process of ML framework creation can be summarized as shown in Fig. 1.

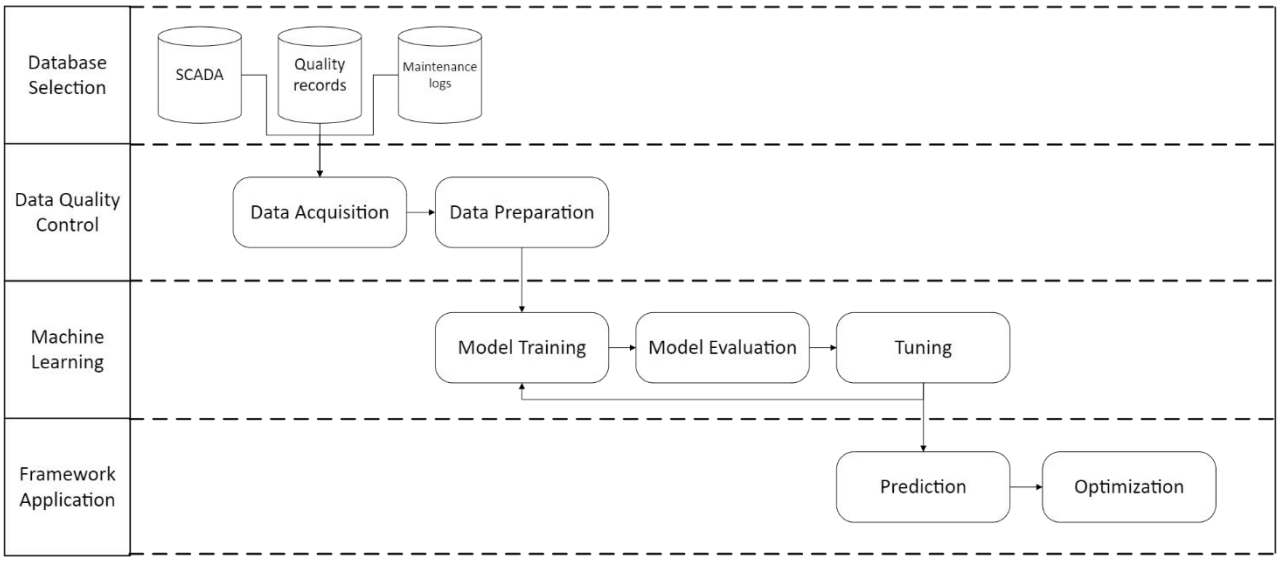

Fig. 1 General ML framework in manufacturing [6, 7]

When the data is prepared to be trained on, it is used to train the selected ML models. The choice of an ML model, however, is not straightforward. After the selected model is trained, the next step is to evaluate the performance and optimize it. Common measures of classification ML model accuracy include precision, recall, and specificity metrics, given in equations 1,2 and 3. Recall is also known as the True Positive Rate (TPR), and Specificity is the True Negative Rate (TNR) [8].

$$Precision = \frac{TP}{TP+FP}; \quad (1)$$

$$TPR = \frac{TP}{TP+FN}; \quad (2)$$

$$TNR = \frac{TN}{TN+FP}; \quad (3)$$

where: TP – True positives, FP – False positives, FN – False negatives.

Further useful measures are the AUC, F1 and MCC coefficients. The AUC is the Area Under Curve of the TPR and the False Positive Rate (FPR) plot with values of 0.50 to 0.60 indicating failure, and 0.90 to 1 being excellent. The F1 measure punishes models, which favour prediction extremes by

taking the harmonic mean of TPR and Precision, see equation 4. A more comprehensive evaluation is made by using the Matthews Correlation Coefficient (MCC), which evaluates TR, FP, FN, and the True Negatives (TN), given in equation 5 [3, 8].

$$F1 = 2 \times \frac{Precision \cdot TPR}{Precision + TPR}; \tag{4}$$

$$MCC = \frac{TP \times TN - FP \times FN}{\sqrt{(TP+FP)(TP+FN)(TN+FP)(TN+FN)}} . \tag{5}$$

Industrial film web processing equipment data is going to be analysed. The equipment is used in company X, which is not going to be disclosed due to a non-disclosure agreement and the possibility of revealing sensitive information. The equipment can produce six families of products, each with different features. The main processes employed in the equipment are film heat-sealing, film hole punching, picking and placing of raw materials on the film web, and in-process automated visual inspection. The equipment is complex and has over 40 stations, which means many parameter changes are needed every time a changeover to a different family or a different product within a family occurs.

The time series data of parameter values have been collected for 8 weeks. Here, the commonly adjusted parameters have been chosen for each product made during this period. The parameters include the fine positioning of stations, the servo motor extension distances, or the robot pick/place coordinates. The data is collected using a SCADA every time a parameter value changes, meaning that if the time stamp is considered, each value is unique. There have been various downtimes during the period, including mechanical breakdown, no demand, quality issues, no operators, engineering studies, and finally, difficulty selecting the right machine parameters. In other words, the parameters are expected to be only a fraction of downtime causes. With this knowledge in mind, a tailored approach can be constructed. First, the missing values are going to be removed from the data. Then, the data is resampled with 1 minute frequency. The values have been logged on a parameter change, meaning that missing values after resampling can be interpolated by repeating the last logged value. This allows for dismissing recipe change cases, where data points include mixed values. The time stamp feature is split into four more features to allow for learning: month, day of the week, hour, and minute. The data is then explored by ranking the features in terms of their information content. The features are going to be pruned to find if the accuracy of modelling without hyperparameter tuning can be improved. Several classification models are evaluated, including EXtreme Gradient Boosting (XGBoost), Logistic Regression, Naïve Bayes, and Support Vector Machine (SVM). The evaluation is made by calculating the AUC, F1, precision, recall, and MCC measures. The best approach is then optimised by tuning the hyperparameters using the RandomSearchCV algorithm by splitting into 5 cross-validation samples. The presented workflow is comparatively simplistic but likely to produce good results based on previously discussed research.

3. Results

The feature removal has not been included in the hyperparameter optimization step as no improvement is shown during initial testing. The Information Gain Ratio, Gini Decrease, and the χ^2 Criterion are considered when ranking the features concerning the target variable – the state of the machine. The evaluation criteria did not converge on the same variables, with the Information Gain Ratio agreeing well with the Gini Decrease coefficient but not the χ^2 Criterion. Reducing the number of parameters used in modelling shows a slight reduction in accuracy. The SVM model is not optimized due to poor performance during initial testing. RandomSearchCV with 5-fold cross-validation sampling is used to optimize the hyperparameters, selected based on the default options used in the initial testing. The model accuracy results are shown in Table 1. Hyperparameter optimization has substantially improved the performance of both XGBoost and

Logistic Regression. XGBoost shows an excellent AUC score of 0.942, a high Recall score of 0.952 and a relatively high MCC score of 0.766.

Table 1. Results prior to and after hyperparameter tuning

	Model	AUC	F1	Precision	Recall	MCC
Prior tuning	Gradient Boosting	0.889	0.833	0.851	0.835	0.685
	Logistic Regression	0.46	0.352	0.267	0.516	0
	Naive Bayes	0.734	0.659	0.669	0.661	0.331
	SVM	0.5	0.365	0.726	0.522	0.074
After tuning	Gradient Boosting	0.942	0.895	0.844	0.952	0.776
	Logistic Regression	0.805	0.755	0.733	0.778	0.480
	Naive Bayes	0.734	0.719	0.692	0.748	0.398

Running the PSO algorithm for 100 iterations with 40 time samples and 70 particles results in a parameter set with a predicted mean success probability of 78.4% across 37 different products. This is considerably higher than the mean machine availability of 52.6% during the analysed period. This suggests that there is likely some value to be gained by reducing the variation in these parameters. It should be noted that there are many other causes of downtime other than parameter settings, and a probability of 1.0 would be unexpected.

The optimal parameter search has been performed with bounds set within the minimum and maximum ± 5 % of each parameter in the original dataset. See the values of the most interesting parameters, found in Figure 2–3.

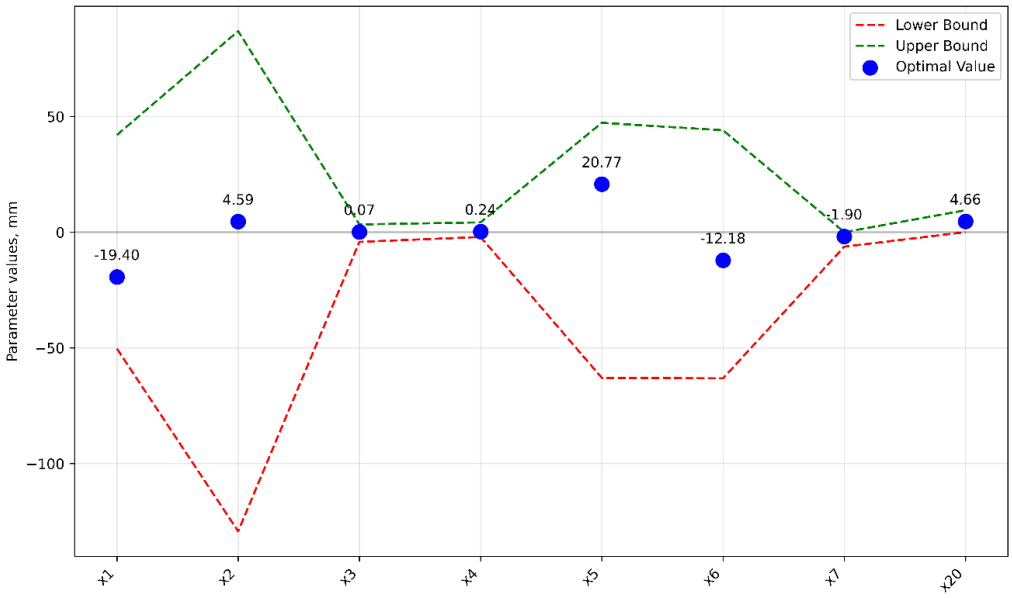

Fig. 2 Optimal station position parameters

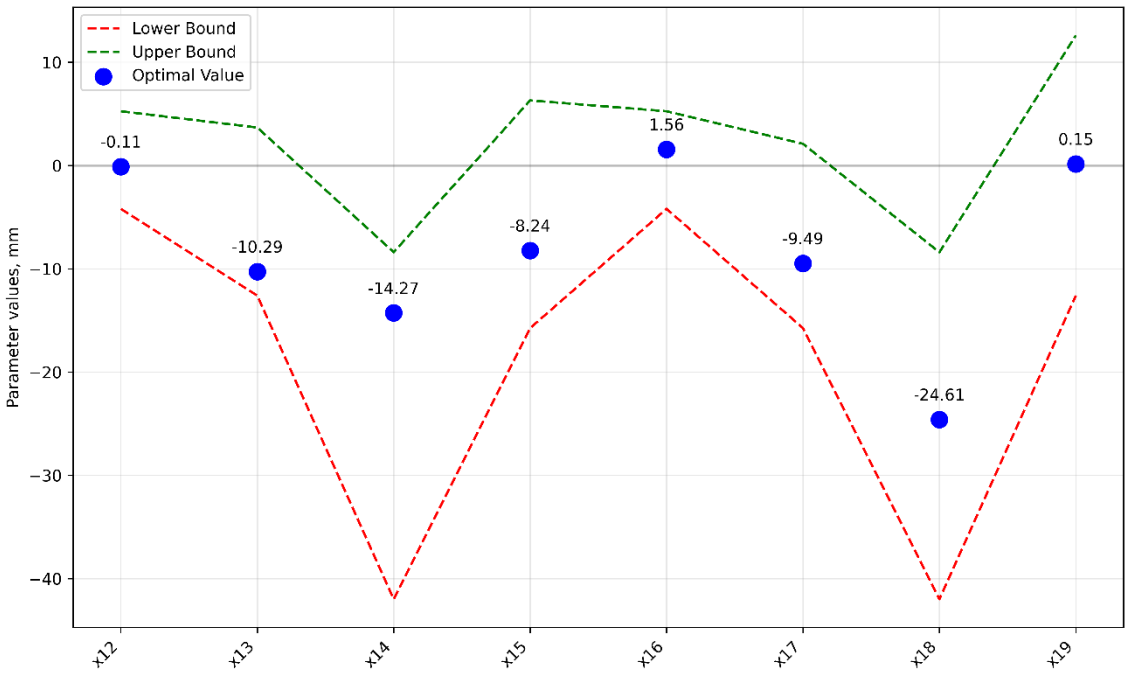

Fig. 3 Optimal pick and place position parameters

The plot in 2 shows multiple station position adjustment parameters. The parameters denoted *x1* to *x7*, and *x20* are the equipment parameter inputs, which determine the product feature positions, e. g. the seal positions, or hole punch positions on the film. The plot in Fig. 3 shows the parameters of two parallel pick and place robots with the parameters being the positions in 3D space. The parameters *x12* and *x16* are the z-axis pick positions, determining the reliability of gripping an object to be sealed to the film from the infeed conveyor belt. The *x13*, *x14*, *x15* with *x16*, *x17*, *x18* are the x-axis, y-axis, and z-axis robot place positions respectively, determining the positioning of the object on the film.

The mean success probability, according to the model, is 0.784, and using the MCC score of 0.776, the worst-case hypothetical availability of 60.8% can be calculated. Compared to the historical availability of 52.6%, this means that 8.2% points of availability and 7.3% points of OEE can be gained with this change, with a multiple of performance and quality at 89.2%. The actions necessary for the proposed improvement would require the testing of the parameters throughout several changeovers, training of operators and changing the format recipes to the best performing parameters.

Generally, the applicability of ML modelling and optimization of model inputs is intended to be applicable to various equipment with minor changes to the algorithm. However, several preconditions are required to enable this approach. First, the equipment should have sufficient accuracy in process control via input parameters. In case of the analysed film processing equipment, the station positions are controlled using servo motors or digital position indicators, enabling high precision and stability of the finished good quality. Secondly, the equipment should allow real-time tracking of the input parameters, the machine state, and be integrated with a SCADA or similar system to allow the storage of the data.

4. Conclusions

1. Gradient Boosting, Logistic Regression, Naïve Bayes classifier, and SVM techniques have been utilized to model the data. Some parameters do not have a statistically significant relationship to the target variable as measured by the χ^2 Criterion. Culling the statistically insignificant parameter columns results in worse prediction quality, meaning most parameters did have information to be extracted, as evaluated by the Information Gain and Gini ratios. SVM did not

perform well during the initial testing, with an AUC score of 0.5 and has been rejected. Hyperparameter tuning using the RandomSearchCV algorithm has been used for the remaining models. Gradient Boosting performed the best, scoring 0.776 in MCC, while Naïve Bayes performed the worst at 0.398 in MCC.

2. A single set of optimal machine parameters has been found using PSO by evaluating the prediction probability of the XGBoost ML model over random time samples. The mean success probability of the machine running across all formats with a single set of machine parameters is 78.4%. If the parameter set is applied in the machine, OEE is estimated to improve by 7.3% points.

References

1. Industry 4.0 Barometer 2024. MHP Management- und IT-Beratung. Web site. Available from: https://www.mhp.com/en/insights/what-we-think/industry-40-barometer-2024. [Viewed 28 September 2024].
2. TERCAN, Hasan and MEISEN, Tobias. Machine learning and deep learning based predictive quality in manufacturing: a systematic review. Journal of Intelligent Manufacturing. 1 October 2022. Vol. 33, no. 7, p. 1879–1905. DOI 10.1007/s10845-022-01963-8.
3. MENDIA, Izaskun, GIL-LOPEZ, Sergio, GRAU, Iñaki and DEL SER, Javier. A novel approach for the detection of anomalous energy consumption patterns in industrial cyber-physical systems. Expert Systems. 2024. Vol. 41, no. 2, p. e12959. DOI 10.1111/exsy.12959.
4. MIETKIEWICZ, Joseph, ABBAS, Ammar N., AMAZU, Chidera W., BALDISSONE, Gabriele, MADSEN, Anders L., DEMICHELA, Micaela and LEVA, Maria Chiara. Enhancing Control Room Operator Decision Making. Processes. February 2024. Vol. 12, no. 2, p. 328. DOI 10.3390/pr12020328.
5. YAO, Yu and QIAN, Quan. Dynamic Industrial Optimization: A Framework Integrates Online Machine Learning for Processing Parameters Design. Future Internet. March 2024. Vol. 16, no. 3, p. 94. DOI 10.3390/fi16030094.
6. WEICHERT, Dorina, LINK, Patrick, STOLL, Anke, RÜPING, Stefan, IHLENFELDT, Steffen and WROBEL, Stefan. A review of machine learning for the optimization of production processes. The International Journal of Advanced Manufacturing Technology. 1 October 2019. Vol. 104, no. 5, p. 1889–1902. DOI 10.1007/s00170-019-03988-5.
7. CHEN, Tingting, SAMPATH, Vignesh, MAY, Marvin Carl, SHAN, Shuo, JORG, Oliver Jonas, AGUILAR MARTÍN, Juan José, STAMER, Florian, FANTONI, Gualtiero, TOSELLO, Guido and CALAON, Matteo. Machine Learning in Manufacturing towards Industry 4.0: From 'For Now' to 'Four-Know.' Applied Sciences. January 2023. Vol. 13, no. 3, p. 1903. DOI 10.3390/app13031903.
8. CHICCO, Davide and JURMAN, Giuseppe. The Matthews correlation coefficient (MCC) should replace the ROC AUC as the standard metric for assessing binary classification. BioData Mining. 17 February 2023. Vol. 16, no. 1, p. 4. DOI 10.1186/s13040-023-00322-4.

Waste Valorization – Recycling of Kombucha's Bacterial Cellulose for Industrial Use

Manojkumar MURUGAN*, Jurgita DOMSKIENE

Kaunas University of Technology, Kaunas, Lithuania

** manojkumar.murugan@ktu.edu*

Abstract

Kombucha is a traditionally fermented tea drink consumed worldwide. Its consumption is rapidly increasing due to its health benefits. During fermentation, a byproduct called Bacterial Cellulose (BC) is produced, which has excellent physical properties. As a result, it has numerous applications in fields such as textiles, biomedicine, electronics, the paper industry, and the food industry. To utilize the BC film for other applications, it must undergo a purification process, such as washing and drying. The process of converting waste into a valuable product is known as waste valorization. According to the analysis, waste valorization in the Kombucha industry is not well-established due to limitations, such as the lack of standard recycling methods or machines available for large-scale Kombucha industries to recycle this valuable waste. The purification process of BC is currently performed only in laboratories using lab equipment for washing and drying, which is not suitable for large-scale recycling. However, opportunities to adopt recycling methods and machines from the plastic industry exist, as their recycling processes also include washing and drying, resembling the purification processes used for BC. This article explores the implementation of waste valorization in the Kombucha industry and the possibility of adopting recycling methods from the plastic industry for Kombucha's BC.

Keywords: Kombucha tea, Bacterial Cellulose, Circular Economy, Waste Valorization, Recycling.

1. Introduction

The Kombucha fermentation process involves making sweetened tea and then adding a Symbiotic Culture of Bacteria and Yeast (SCOBY) to the tea solution [1]. The SCOBY, a cellulose film also known as Kombucha Mother, is responsible for fermenting the tea solution. This fermentation produces byproducts such as a Bacterial Cellulose film seen on the surface of the tea solution. The produced Bacterial Cellulose (BC) is referred to as the daughter SCOBY [2]. The tea originated in ancient China in 220 B.C. and made its way into Europe during the Second World War [3]. The consumption of this tea is rapidly increasing due to its health benefits, like boosting the immune system. This tea contains probiotics that are good for gut health. Like the drink, the produced byproduct BC also has numerous benefits and potential applications in different industries like textile, biomedical, electronics, and food [4].

The BC provides excellent mechanical properties, higher purity, and higher crystallinity, which makes it suitable for industrial uses [4]. The BC can also be produced separately by following static or agitated/shaking cultivation. The static cultivation method is the same as the kombucha fermentation technique, where the bacteria responsible for producing the BC are introduced into the growing medium. The growing medium is also known as HS (Hestrin Schramm) medium, which contains nutrients such as glucose, peptone, and yeast extract, which are essential for the bacteria to produce BC [5]. In the agitated/shaking fermentation method, the solution is stirred constantly, which results in producing BC in the form of spheres or pellets. The BC produced from agitation/shaking shows low yield and low crystallinity compared to the BC produced from the static cultivation method. Hence static cultivation method is widely chosen for producing BC [6].

Even though BC has various industrial applications, the production cost makes it very hard to commercially produce BC. Hence, BC producers are looking for alternative ways to produce BC, like using agricultural waste, such as fruit waste, as a medium to produce BC [4]. Using a Kombucha fermentation medium is also considered an alternative method to produce BC. The BC produced from kombucha fermentation also shows excellent physical properties. Hence, the waste BC produced during kombucha fermentation from the kombucha factories is also a way to commercially produce the BC films for industrial uses.

The process of converting waste into a valuable product is known as waste valorization. Waste valorization techniques are employed across various industries to transform waste into valuable products, including using that waste as raw material for different sectors. In the food industry, waste valorization can be applied to repurpose food waste as biofuels, biopolymers, adsorbents, and more [7, 8]. In the kombucha sector, waste valorization involves reusing spent tea leaves as a composite and utilizing the produced BC as animal feed. The BC films, which possess excellent mechanical properties, have the potential to serve as an alternative to textiles used as animal feed.

2. Industrial Production of Kombucha Drink

The technique used in the preparation of Kombucha drinks in the Kombucha industry resembles the traditional kombucha fermentation process. For large-scale production, such as preparing 1000 litres of Kombucha tea, brewing equipment known as a kombucha fermenter is utilized. As shown in Fig. 1, the brewing process begins by preparing a starter liquid, where 10 kg of tea leaves are added to 150 litres of water, and the temperature of the tea solution is maintained at 85°C throughout the process. The tea solution is recirculated inside the mixing tank using a pump for 30 to 45 minutes. The second step is the fermentation process, which starts by transferring the tea solution to another mixing tank, while the tea leaves are filtered out using a mesh filter. Next, 60 kg of sugar is added and stirred for ten minutes until it dissolves. The next step involves adding 900 litres of cold water into the mixing tank. Once the temperature of the solution drops below 28°C, the starter liquid (previously made kombucha tea) and SCOBY are added. The temperature must be below 28°C, or it may kill the bacteria in the starter culture. The tea solution is left to ferment for 4-6 weeks [9]. During the fermentation process, a daughter SCOBY is produced on the surface of the tea solution, while the mother SCOBY sinks to the bottom [10]. After the fermentation, the newly produced SCOBY is removed from the tea solution, and the solution is pumped into another mixing tank where flavours are added before being bottled for sale [9].

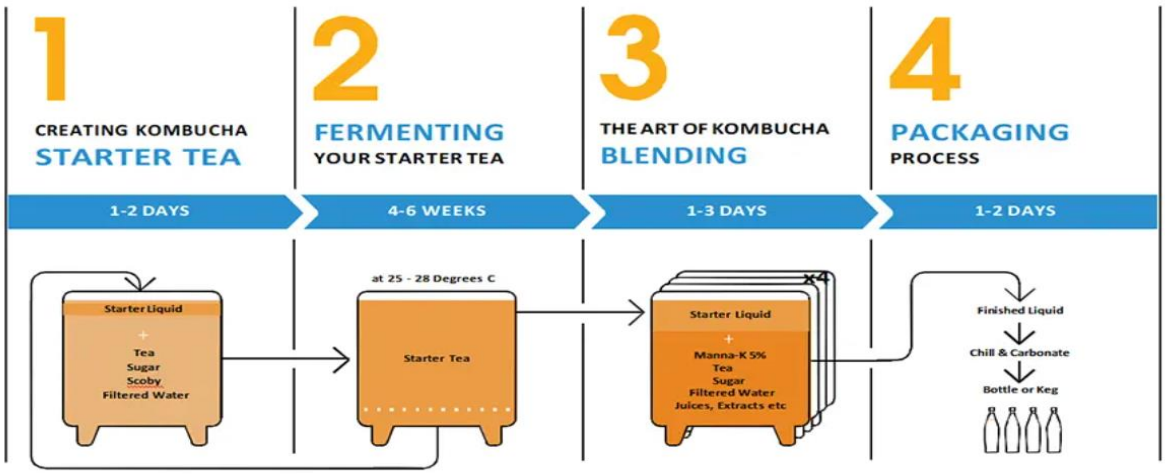

Fig.1. Steps involved in the large-scale production of Kombucha tea [9]

In the kombucha sector, waste valorization involves reusing spent tea leaves and BC as a

composite [8]. The BC films, which possess excellent mechanical properties, have the potential to serve as an alternative to textiles [4, 5] used as animal feed.

3. Downstream Process of BC

To use the BC for other applications, downstream or purification is necessary. The purification process involves washing and drying to remove impurities present in the BC films. NaOH (sodium hydroxide) is utilized as a washing agent, and NaOCl (sodium hypochlorite) is used as a bleaching agent [11]. After washing, the BC films are dried in the oven at a certain temperature to eliminate the water content. The drying hours of the films vary according to the temperature. If the films are decided to dry at 25℃, then it takes 24 hours to dry the BC films. The washing of BC takes place in a shaking water bath, a laboratory device designed for washing samples. This instrument includes a thermostat that maintains the water temperature consistently throughout the washing process [12]. The equipment used for washing and drying the BC films is not intended for industrial use. The BC produced from the kombucha industry is larger as the diameter of the kombucha fermenter is larger, and it requires machines that are large enough to wash the BC. Hence, recycling methods used in other industries that involve washing and drying are analyzed to be able to be used in the Kombucha industry.

One of the recycling methods that involves washing and drying is known as mechanical recycling, and it is used in the plastic industry. In the plastic recycling method, the plastic wastes are washed with NaOH solution and then dried [13]. The machine used for plastic recycling is shown in Fig. 2.

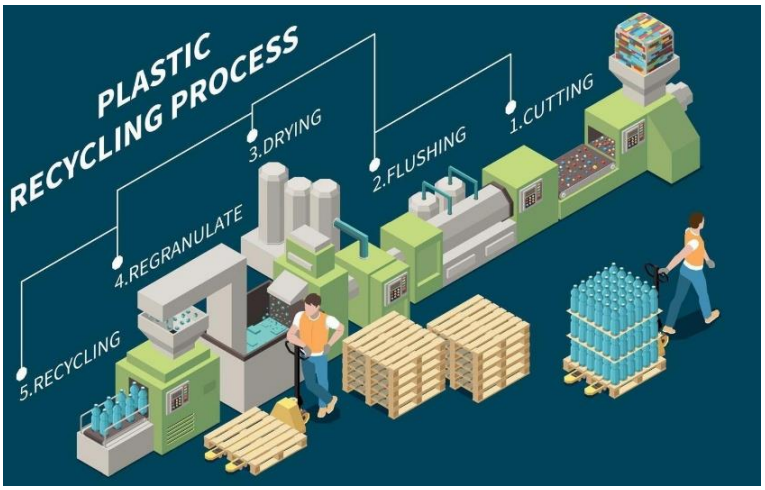

Fig. 2. Assembly line for plastic recycling [14]

The assembly line for plastic recycling includes cutting, which shreds the plastic waste, flushing/washing, which washes the plastic waste with NaOH solution, drying, which dries the plastic until 0.1% moisture is left, and a regranulation extruder, which melts the plastic and then moulds it into plastic water bottles. The recycling assembly includes a washing and drying unit for the waste plastic. The different types of washing units that are used for washing the plastic waste such as water baths, washing lines, and friction washers. Among those water baths are suitable for BC washing. In this type, the waste plastics are soaked in hot water for a few hours [15]. For drying, centrifugal dryers are used. Centrifugal dryers are effective in separating the plastic waste from residual water. Using a centrifugal dryer in BC recycling is not an ideal solution. The centrifugal dryer uses spinning to remove the water from the plastic waste [16]. Here, in the case of BC purification, the water is absorbed by the BC film due to its hydrophilic properties. Hence, it is harder to separate the water from BC by spinning, which may lead to damage to the BC film. The ideal solution would be to use an industrial drying chamber to dry the BC film.

4. Recycling of Kombucha's BC

As shown in Figure 3, Recycling of Kombucha's BC begins with washing the wet BC film obtained from Kombucha fermentation using a 1% NaOH solution. After washing with the NaOH solution, the BC films are rinsed with NaOCl for 2 hours. The solution of temperature must be maintained at 90°C. The amount of the NaOH solution used for washing may vary depending on the size of the BC film. For laboratory-produced BC, which weighs approximately 80g, one litre of 1% NaOH solution (10g of NaOH and 990 mL of water) is needed to wash the BC film. In an industrial setup, let's assume 10 kg of BC needs to be washed, hence, the amount of NaOH and the water level will be increased. To wash 10 kg of BC, a water tank that has a volume of 1000 litres is used for washing; therefore, the 1% NaOH solution should contain 10kg of NaOH in 990 litres of water. The same applies to the NaOCl washing. An industrial stirrer will be connected to the washing tanks to mix the solution, facilitating faster removal of impurities. The stirrer's rpm is set to 100, as a higher rpm may damage the BC films. An immersion heater is fixed at the bottom of the water tank to maintain the temperature throughout the whole process. After the washing process, the films need to be dried. A tray dryer, which is used in the food and pharmaceutical industry to dry the material, can be used for drying. The ambient temperature would be 25°C, and the time duration for the whole drying process will be 24 hours. After drying, the BC films will lose most of their weight and look like a thin film, as described in Fig. 3, which is now suitable for other applications.

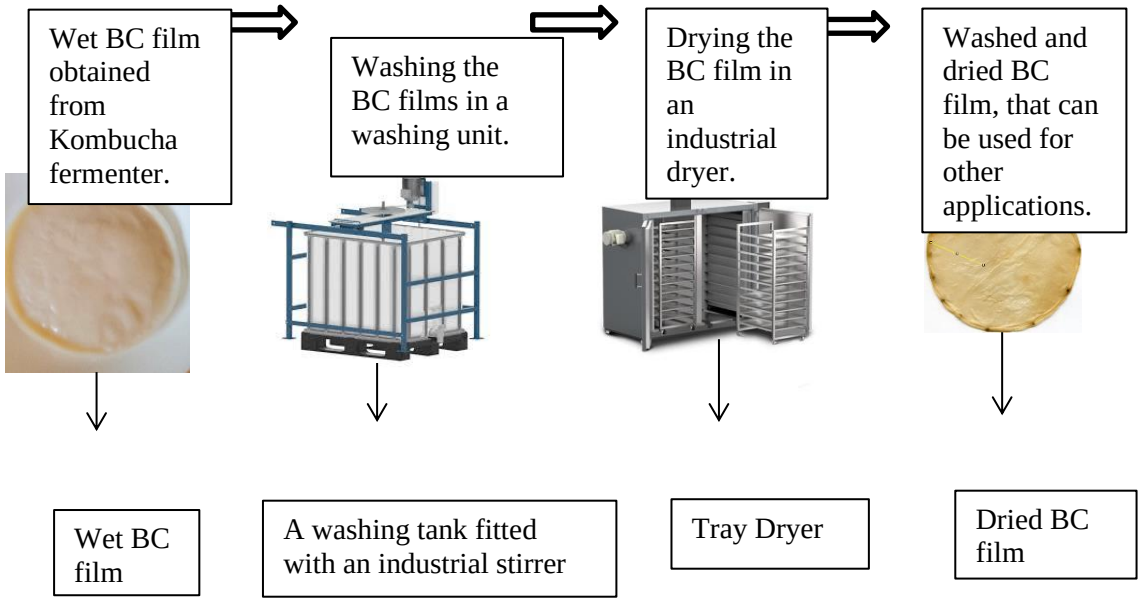

Fig. 3. Principle of the BC recycling line and the possible machines that can be used for BC recycling

5. Conclusions

1. The recycling methods and machines used in the plastic industry are analyzed to assess the feasibility of utilizing them in Kombucha's BC recycling. Plastic recycling includes more processes than BC purification, but washing and drying used in plastic recycling are similar to BC purification.
2. Hence, the washing and drying unit of the plastic recycling line is analyzed, and it is found that the washing unit can be used for BC washing, but the drying unit cannot be used, as it employs centrifugal drying instead. An industrial drying chamber can be used for drying the BC films.
3. The principal units of Kombucha's BC recycling are discussed, and the BC recycling process is developed, indicating the main parameters of each step.

4. As the world is moving towards more sustainability, the implementation of waste valorization in the Kombucha industry by reusing the BC as a raw material for other industries could be a potential game changer. Also, it opens a new line of business for Kombucha manufacturers.

References

1. LAUREYS, D., BRITTON, S.J. and DE CLIPPELEER, J. Kombucha Tea Fermentation: A Review. *Journal of the American Society of Brewing Chemists*, July 2, 2020, vol. 78, no. 3 [viewed Apr 14, 2025]. pp. 165–174.
2. COELHO, R.M.D., et al. Kombucha: Review. *International Journal of Gastronomy and Food Science*, -12-01, 2020, vol. 22 [viewed Apr 14, 2025]. pp. 100272.
3. NYHAN, L.M., LYNCH, K.M., SAHIN, A.W. and ARENDT, E.K. Advances in Kombucha Tea Fermentation: A Review. *Applied Microbiology*, /3, 2022, vol. 2, no. 1 [viewed Apr 14, 2025]. pp. 73–103.
4. CUBAS, A.L.V., et al. Advances in the Production of Biomaterials through Kombucha using Food Waste: Concepts, Challenges, and Potential. *Polymers*, -03-29, 2023, vol. 15, no. 7 DOI 10.3390/polym15071701.
5. SINGHANIA, R.R., et al. Developments in Bioprocess for Bacterial Cellulose Production. *Bioresource Technology*, -01-01, 2022, vol. 344 [viewed Mar 10, 2025]. pp. 126343.
6. MORENO-DÍAZ, C., GONZÁLEZ-ARRANZ, S. and MARTÍNEZ-CEREZO, C. Bacterial Cellulose Production within a Circular Economy Framework: Utilizing Organic Waste. *Polymers*, -09-27, 2024, vol. 16, no. 19 DOI 10.3390/polym16192735.
7. RABBI, M.F. and AMIN, M.B. Circular Economy and Sustainable Practices in the Food Industry: A Comprehensive Bibliometric Analysis. *Cleaner and Responsible Consumption*, -09-01, 2024, vol. 14 [viewed Mar 16, 2025]. pp. 100206.
8. NAYAK, A. and BHUSHAN, B. An Overview of the Recent Trends on the Waste Valorization Techniques for Food Wastes. *Journal of Environmental Management*, -03-01, 2019, vol. 233 [viewed Mar 17, 2025]. pp. 352–370.
9. What is the process for preparing kombucha tea? - Micet Group. -02-28, 2023 [viewed Apr 15, 2025]. Available from: https://www.micetgroup.com/what-is-the-process-for-preparing-kombucha-tea/.
10. DUTTA, H. and PAUL, S.K. Production and Management of Beverages A.M. GRUMEZESCU and A.M. HOLBAN eds., Woodhead Publishing, -01-01, 2019 [cited Apr 15, 2025]. *Kombucha Drink: Production, Quality, and Safety Aspects*, pp. 259–288. Available from: https://www.sciencedirect.com/science/article/pii/B9780128152607000080 ISBN 9780128152607.
11. GEA, S., et al. Investigation into the Structural, Morphological, Mechanical, and Thermal Behaviour of Bacterial Cellulose After a Two-Step Purification Process. *Bioresource Technology*, -10-01, 2011, vol. 102, no. 19 [viewed Apr 7, 2025]. pp. 9105–9110.
12. SUTRISNO, T.A., et al. The Effect of Chemical Pretreatment Process on Mechanical Properties and Porosity of Bacterial Cellulose Film. *Journal of Mechanical Engineering Science and Technology*, 2019, vol. 3, no. 1. pp. 8–17.
13. SHEN, L. and WORRELL, E. Handbook of Recycling (Second Edition) C. MESKERS, E. WORRELL and M.A. REUTER eds., Elsevier, -01-01, 2024 [cited Apr 7, 2025]. *Chapter 31 - Plastic Recycling*, pp. 497–510.
14. Plastic-Recycling-Composition-Vector.Jpg (1540×980) [viewed Apr 14, 2025]. Available from: https://static.vecteezy.com/system/resources/previews/006/846/981/non_2x/plastic-recycling-composition-vector.jpg.
15. *How Plastic Recycling Washing Machines Work*-02-19, 2020 [viewed Apr 14, 2025]. Available from:https://www.accextrusion.com/news/how-plastic-recycling-washing-machines-work/.
16. How Centrifugal Dryers Enhance Plastic Recycling Efficiency. -12-04, 2024 [viewed Apr 14, 2025]. Available from: https://www.energycle.com/how-centrifugal-dryers-enhance-plastic-recycling-efficiency/.

Impact of Automated Guided Vehicles on Logistics Operations in Manufacturing Enterprise

Hajar El MASTOR*, Laura GEGECKIENĖ, Ingrida VENYTĖ

Kaunas University of Technology, Kaunas, Lithuania

** hajar.el@ktu.edu*

Abstract

While Automated Guided Vehicles (AGVs) have transformed simple order picking tasks by reducing manual labor and optimizing processes, the literature leaves significant opportunities for further exploration. As highlighted by several research papers, literature often focuses on technical aspects of technology such as navigation, path optimization and hardware. There is, however, a notable lack of studies addressing the implementation of AGV fleets in the industrial warehouse for higher operational efficiency, particularly in relation to throughput. The choice of type of AGV is based on activities to be automated, and the setup of AGV environment based on future plans of expansion and change in infrastructure, as well as future automation endeavours, is detrimental to the ease of configuration of future implementations that are bound to be needed.

Keywords: Automated Guided Vehicles (AGVs), warehouse automation, material handling automation.

1. Introduction

Amid the shift towards smart manufacturing, attention has turned to the supply chain and its importance in the capability of industrial operations. Due to the rising environmental and operational challenges, a warehouse is now no longer just a storage area for inventory but rather a crucial tool for fulfilling customization in customer demands, increasing operational efficiency and protecting organizations from volatile markets. With future warehouses shifting to innovative technologies, the concept of a smart warehouse has emerged. Technologies such as robotics, big data analytics and artificial intelligence are all transformative technologies in today's smart warehouse and consequently today's automated supply chain [1]. In tune with industrial goals, the model of a smart warehouse is ideal with its focus on the highest levels of operational efficiency that can only be reached with high levels of autonomy and low levels of reliance on manual workload and paper-based applications [2]. The introduction of barcodes in the 1960s was the foundation of warehouse automation, allowing inventory management to incorporate real-time data processing within modern warehouse management systems (WMS). Barcode scanning opened doors for technologies such as radio-frequency identification (RFID) supported by the Internet of Things (IoT) systems, enabling the concept of automated warehouse operations [3]. IoT integration allows for a constant flow of real-time data from distributors, carriers, suppliers and customers, improving planning and control of supply chain factors. Within this technological framework, Automated Guided Vehicles (AGVs) are pivotal tools for smart warehouse operations, providing efficient material handling systems that reduce operational expenses and increase productivity.

The novelty of the work lies in a methodological approach based on analysis of actual AGV implementation, including automated processes, data collection methods and performance of AGVs deployed.

2. Functionality and types of AGVs

In an example from the automotive industry discussed in the literature, with the underrun AGVs replacement of manual tugger trains, the vehicles not only replicate the tasks performed by the driver but also ergonomically eliminate the strain in pushing and pulling trolleys that often weigh beyond the health and safety requirements.

Fig. 1 Examples of various types of an Underrun AGV [4]

Fig. 2 shows four common types of automated warehouse layouts as presented by Hang et.al. Traditional layouts are often in symmetrical straight lines with shelves on both sides and routes in the middle. The fishbone layout shown in Figure 2d is the new layout adapted for increasing storage locations. However, this layout increases the chances of deadlock when more than one AGV is used and is therefore ineffective for material handling and transport operated by an AGV fleet. Deadlock refers to a situation where two or more robots are unable to proceed as they block each other's paths [5].

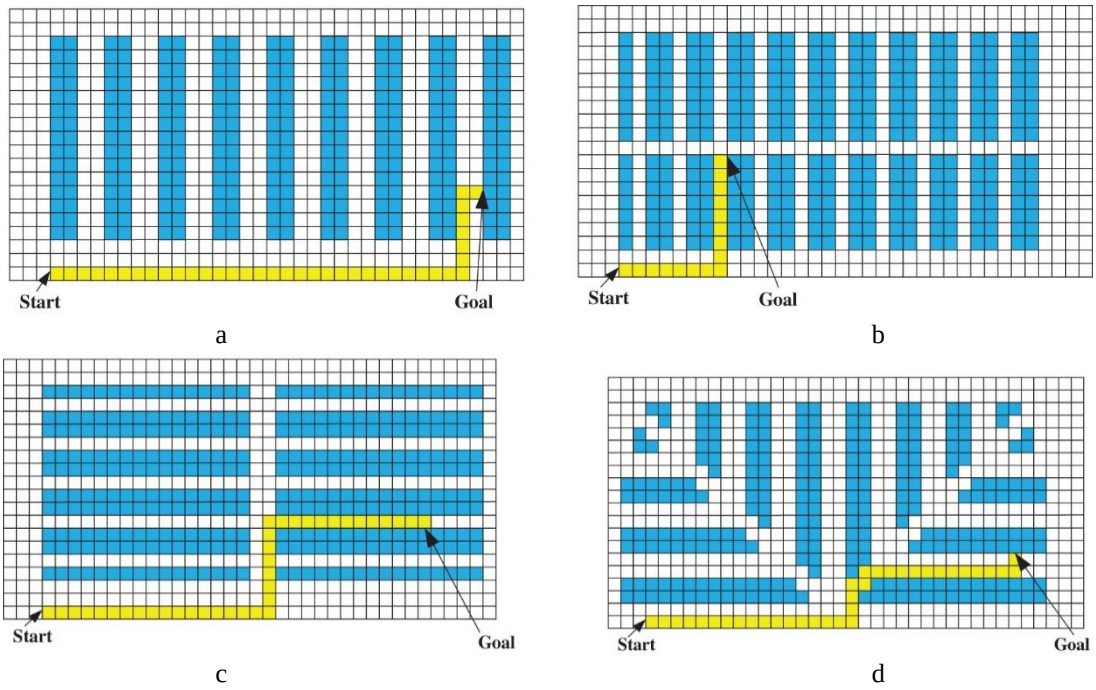

Fig. 2 Four common warehouse schemes: a – traditional parallel layout; b – traditional vertical layout; c – traditional horizontal layout; d – fishbone layout [5]

One of the factors that affects AGVs' performance is the layout of its environment. Many research papers highlight the importance of warehouse layout choice based on the number and type of AGVs used. Rubio et al. highlights that an AGV environment is made from pathways and lanes as well as stations, machines, walls, warehouse shelves and much more. The lanes can be designed

to be one-way or multiple lanes depending on how much traffic is needed in that particular area. The design of the pathways is done taking into account deadlock avoiding when multiple AGVs are used and the optimization of routes to ensure that AGVs are travelling through the shortest and fastest between the source and the sink points [6].

3. Implementation of AGVs in an Industrial Warehouse Environment

In this work, a mixed-methods approach will be adopted to assess the impact of AGVs on real-life warehouse operational efficiency by integrating qualitative process analysis and quantitative study of operational performance metrics. First, a documentation of warehouse operational workflows will be presented establishing baseline expectations for the system. Second, the implementation of AGV technology will be analysed and the methods of performance tracking and data collection will be presented.
The baseline expectation of the AGV implementation in the first phase was to set up the vehicles physically to the warehouse and production area with the major requirement being to stabilize the physical execution of automated transportation with AGVs. The overarching goal is to ensure a smooth integration of processes through an Enterprise Resource Planning (ERP) system, Manufacturing Execution System (MES), AGV connector, Fleet management and the AGV as shown in the illustration in Fig. 3.

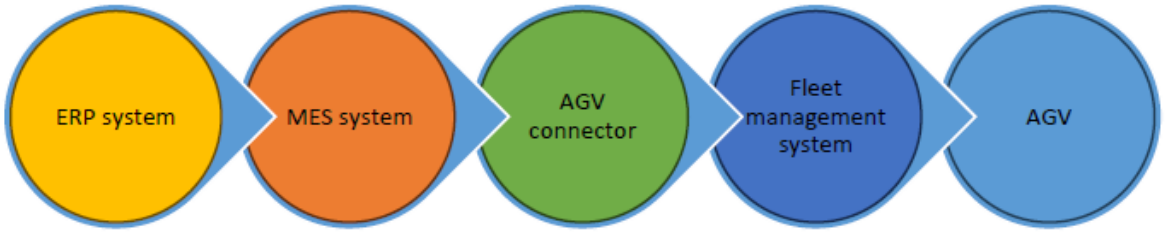

Fig. 3 Overview of flow processes

Before to AGV implementation, the initial situation for this particular use case is that operators used to move purchased raw components and finished goods between storage locations and production lines. Material requests were generated manually through the ERP system, and warehouse coordinators communicated instructions to tugger train operators. Warehouse coordinators are the responsible employees in the warehouse with access to operational data within the ERP system allowing them to control material flow and transport tasks. The coordinators directed tugger train drivers (otherwise called line feeders) to locate and transport the material.
The Active Shuttle by Rexroth AGV (shown in Fig. 4) was the chosen robot for this task of transport of items from production to warehouse. The choice was made based on the ease of the set-up of the system and low investment with a short ROI of maximum two years.

Fig. 4 Picture of Active Shuttle by Rexroth AGV [7]

The AGV can transport items from a specified handover location to a designated drop-off location. There are two types of AGV handover locations: the unit and the flow lane. Flow lanes can accommodate multiple dollies depending on the allocated length of the lane. They have one input position and one output position. The AGV transports the trolley from the input position to the end of the flow lane or to the last AGV already situated in the flow lane. The flow lanes maintain the FIFO (First In, First Out) principle. The unit handover location is a single point that can only manage one trolley. The input and output positions are the same for this option. The type of handover location is chosen based on operational requirements such as throughput needs, spatial constraints, and material flow characteristics. This varies depending on the type of transport item.

Table 1. Material groups that will be transported using AGVs in this phase of the implementation

Item	**Description**
Purchased parts	Components to build the finished product. Components are stored in supplier empty packaging(box/tray) on trolleys.
Supplier empty packaging	Packaging without purchased parts from suppliers. The empty packaging is also transported on trolleys.
Finished goods	Finished produced parts. These parts are stored in customer empty packaging (boxes/trays) on trolleys.
Customer empty packaging	Packaging without finished goods. The empty customer packaging is also transported on trolleys.

4. Conclusions

1. Efficient material handling systems that reduce operational expenses and increase productivity were analysed to establish a basic understanding of the AGV processes and to draw attention to weaknesses of the existing manual internal transport system.
2. Four common types of automated warehouse layouts were analysed. Where established that traditional layouts are often in symmetrical straight lines with shelves on both sides and routes in the middle. The fishbone layout is the new layout adapted for increasing storage locations.
3. In this work, a mixed-methods approach was adopted to assess the impact of AGVs on real-life warehouse operational efficiency. The overarching goal was to ensure a smooth integration of processes through an Enterprise Resource Planning (ERP) system, Manufacturing Execution System (MES), AGV connector, Fleet management and the AGV.

References

1. TIWARI, S. Smart Warehouse: A Bibliometric Analysis and Future Research Direction. Sustainable Manufacturing and Service Economics, 2023, vol. 2, 100014. ISSN 2667-3444. Available from: https://www.sciencedirect.com/science/article/pii/S2667344423000063.
2. LIU, X., CAO, J., YANG, Y. and JIANG, S. CPS-Based Smart Warehouse for Industry 4.0: A Survey of the Underlying Technologies. Computers, vol. 7 (2018), no. 1, 13. Available from: https://doi.org/10.3390/computers7010013.
3. VAN GEEST, M., TEKINERDOGAN, B. and CATAL, C. Smart Warehouses: Rationale, Challenges and Solution Directions. Applied Sciences, vol. 12 (2022), no. 1, 219. Available from: https://doi.org/10.3390/app12010219.
4. ULLRICH, G., ALBRECHT, T. Automated Guided Vehicle Systems. A Guide – With Practical Applications – About The Technology – For Planning. Online. 2nd Edition. Springer Fachmedien Wiesbaden GmbH, part of Springer Nature 2023. Available from: https://link.springer.com/content/pdf/10.1007/978-3-658-35387-2.pdf. [viewed 18 December 2024].
5. ZHANG, Z., CHEN, J., GUO, Q. Application of Automated Guided Vehicles in Smart Automated Warehouse Systems: A Survey, CMES - Computer Modeling in Engineering and Sciences, vol. 134 (2022), no. 3, p.p. 1529-1563. ISSN 1526-1492. Available from: https://www.techscience.com/CMES/v134n3/49756.
6. RUBIO, F., LLOPIS-ALBERT, C. and VALERO, F. Multi-Objective Optimization of Costs and Energy Efficiency Associated with Autonomous Industrial Processes for Sustainable Growth. Technological Forecasting and Social Change, vol. 173 (2021), 121115. Available from: https://www.sciencedirect.com/science/article/pii/S0040162521005485 ISSN 0040-1625.
7. Bosch Rexroth. Active Shuttle page. Online. Available from: https://www.boschrexroth.com/en/de/products/product-groups/mobile-robotics/active-shuttle/. [viewed 18 December 2024].

MATERIALS SCIENCE AND ENGINEERING

Experimental Investigation of 3d-Printed Thermoplastic Copolyester and Graphene Composite Sheet Structures

Mangirdas PENKAUSKAS[1]*, Darius EIDUKYNAS[1], Gopi KOMPELLI[2]

[1]*Kaunas University of Technology, Faculty of Mechanical Engineering and Design, Kaunas, Lithuania*

[2]*Kaunas University of Technology, Institute of Mechatronics, Kaunas, Lithuania*

[*]*mangirdas.penkauskas@ktu.lt*

Abstract

This study analyses the mechanical and functional properties of thermoplastic composites composed of thermoplastic copolyester (TPC) and varying contents (4% and 8%) of graphene powder. To evaluate the influence of graphene content on composite behaviour and to determine the rational content for various industrial applications, tensile and cupping tests were conducted by ISO 527-3 and ISO 20482 standards. The obtained results revealed that a 4% graphene content significantly improved the tensile mechanical properties of the composite: the tensile stress increased by 32,2% compared to the pure polymer, and Young's modulus increased from 102,9 MPa to 265,7 MPa. However, this content was insufficient to ensure electrical conductivity. In addition, a considerable reduction in plasticity was observed, as the relative strain at break reached only 32,2% compared to 268% for the pure polymer. Increasing the graphene content to 8% improved tensile stress to 21,7 MPa (~75%) and Young's modulus to 581,9 MPa, but the relative strain dropped to 11,8%. Electrical conductivity was achieved, with the tensile specimens showing a resistance ranging from 86,5 to 500 Ω. The resistance increased with deformation, indicating changes in the conductive graphene network within the polymer matrix. Cupping tests confirmed these trends: pure TPC remained the most ductile (23,9 mm), while TPC/Gr-4% showed increased strength (799,2 N) and moderate ductility (12,3 mm). The TPC/Gr-8% composite was the most brittle, failing at 139,8 N with deformation of only 2,2 mm. Obtained results revealed the possibility to identify the graphene content influence on the parameters of composite structures, which are relevant to functional thermoplastic materials used in industrial applications, including automotive, electronics and biomedical sectors.

Keywords: thermoplastic copolyester, graphene, mechanical properties, 3D printed composite.

1. Introduction

Thermoplastic composites are increasingly important due to their advantageous mechanical and technological properties. These include low density, flexibility, and resistance to chemical and mechanical impacts, which meet the rapidly growing demand in advanced technology sectors. These materials are widely used in high-tech sectors such as aerospace [1], automotive [2], electronics [3] and biomedicine [4], where both mechanical reliability and specific functional characteristics are required [5]. However, the mechanical and functional properties of unfilled thermoplastic materials are often limited, which has led to the increasing application of functional fillers for property enhancement [6]. One of the most promising solutions involves the incorporation of nanostructured materials such as graphene [7-8]. Due to its exceptional mechanical and electrical properties, graphene can significantly improve composite performance; however, its effectiveness strongly depends on the appropriate selection of filler concentration [9]. Scientific literature indicates that excessive graphene content may reduce the material's ductility, increase brittleness, and limit the applicability of the composite [10]. However, limited

research exists on the incremental forming applicability of graphene-enhanced thermoplastic copolyester (TPC), and it remains unclear whether such composites have suitable formability and mechanical stability for incremental forming processes.

It is still unclear how the addition of graphene affects its mechanical and functional properties, especially when aiming to combine good conductivity with sufficient mechanical performance. Therefore, further research is needed to clarify these effects and to optimise the composition for functional applications.

The aim of this study is to evaluate the effect of graphene content on the mechanical and electrical properties of TPC composites, seeking an optimal balance between conductivity and mechanical performance. This research focuses on the development of electrically conductive, 3D-printable TPC–graphene composites, which have not been previously studied in the literature.

2. Research Methodology and Experimental Investigation

Composite material specimens based on TPC infilled with different concentrations of graphene powder (4% and 8%) were fabricated. In this study, 4% and 8% graphene concentrations were selected based on preliminary insights into the influence of graphene on the electrical and mechanical properties of composites. A 4% concentration was chosen as the minimum level at which the onset of electrical conductivity is commonly observed in the literature, while maintaining good elasticity and deformation resistance of the polymer. An 8% concentration was selected to evaluate the effect of increased filler content on structural strength, considering the potential risk of increased brittleness, particularly under compressive or bending loads. This selection allows for the assessment of both the conductivity threshold and mechanical property changes at higher filler contents. The material strands were fabricated using a powder extrusion method to ensure a homogeneous composite structure. TPC pellets and graphene powder were precisely weighed, mechanically mixed into a uniform blend, and extruded using a Noztek Touch HT extruder, which enables precise control of both the heating temperature and the diameter of the extruded filament (1,75 ± 0,01 mm in this study). Throughout the extrusion process, the temperature was maintained at approximately 200–210 °C to ensure optimal mixture homogeneity and a consistent filament diameter.

The prepared filament strands were used to fabricate specimens for mechanical properties and conductivity testing using 3D printing technology with a Prusa Slicer MK3s printer. During the printing process, parameters including environmental temperature (23°C), printing speed (20 mm/s), and layer thickness (0,1 mm) were controlled to ensure specimen homogeneity and dimensional accuracy. For experimental investigations, a series consisting of four standard-sized specimens was fabricated by standards ISO 527-3 (Fig. 1, a) and ISO 20482 (Fig. 1, b). The mechanical properties of the fabricated materials were evaluated using tensile and cupping test methods.

Tensile tests were carried out using a Tinius Olsen H10KT testing machine. The specimens were stretched at a constant rate of 50 mm/min until failure, while load and deformation data were recorded using the integrated data acquisition system of the testing machine. Based on the collected data, the key mechanical parameters were calculated, including tensile strength, Young's modulus, maximum stress, and strain at break. Cupping tests were performed using a dedicated test rig equipped with a punch. The specimens were compressed at a constant speed of 50 mm/min, while the increasing load and central deformation of the specimens were recorded. In addition, the electrical conductivity of the composites was evaluated to determine their potential as electrically conductive materials. The aim was to assess whether the addition of graphene enables the formation of a conductive network within the polymer matrix. Electrical conductivity

measurements were performed by applying silver paste to the surfaces of tensile specimens to ensure electrical contact, and resistance changes during deformation were recorded using a Fluke 3000 FC multimeter.

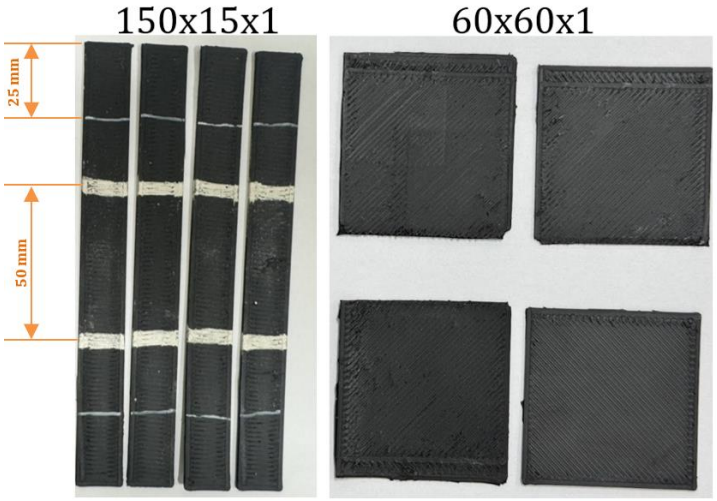

a b

Fig. 1. Fabricated specimens of composite material: a – for tensile testing, b – for cupping testing

Figure 2 presents the experimental setup view during specimen conductivity and tensile testing.

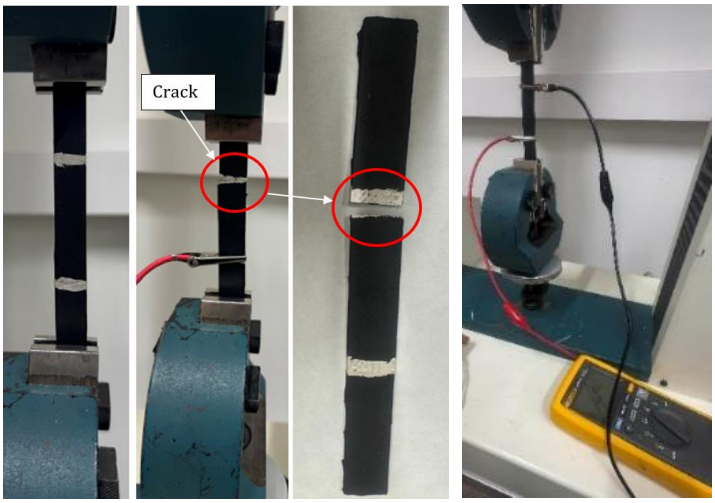

a b

Fig. 2. Experimental setup of the tensile test: a – structural fractures, b – conductivity measurement

3. Results

The TPC/Gr-4% composite materials specimens showed notable ductility, with a strain at break of 32.2% and an average tensile stress of 16.4 MPa (see Fig. 3). The Young's modulus was approximately 265,7 MPa (see Fig. 4), which indicates structural flexibility and lower stiffness. No electrical conductivity was detected with specimens containing 4% graphene.

During experimental tests with specimens containing 8% graphene, the average tensile stress exceeded 21.7 MPa (see Fig. 3) and the modulus reached approximately 581,9 MPa (see Fig. 4). However, the average strain at break decreased by 11,8%, indicating increased brittleness. Specimens containing 8% graphene showed measurable electrical conductivity, with average resistance values ranging between 86,5 and 500 Ω during the entire tensile test. During the tensile test, the resistance of the specimens increased proportionally with deformation, indicating a decrease in electrical conductivity.

For comparison, pure TPC showed an average tensile stress of only 12.4 MPa (see Fig. 3), while due to it is high plasticity, the relative strain was significantly higher at 268.6% and the Young's modulus was 102.9 MPa (see Fig. 4). All results are presented as average values.

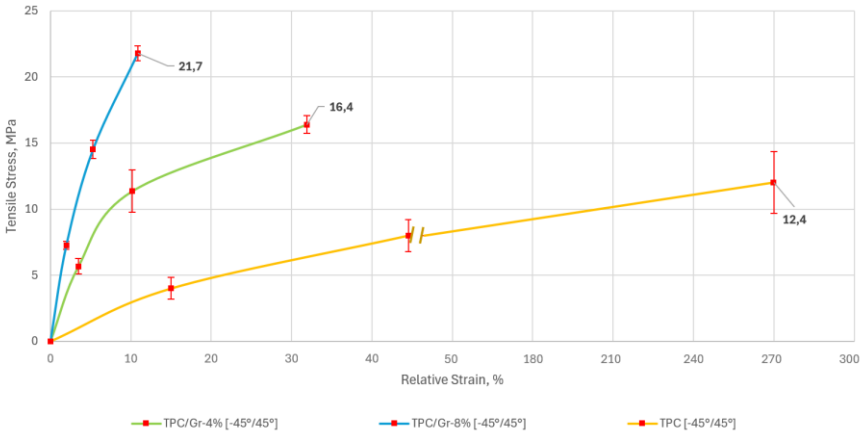

Fig. 3. Stress vs. Strain curves of the composite structures with varying graphene content

Figure 4 presents the experimentally determined Young's modulus values for different material contents.

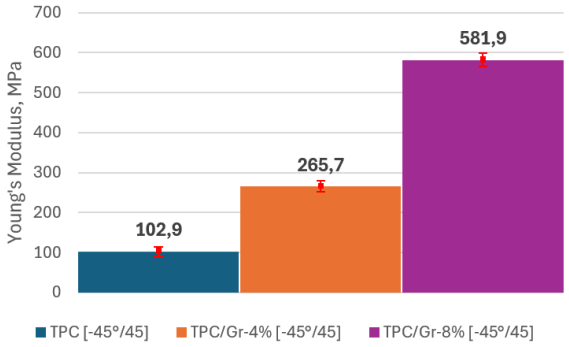

Fig. 4. Young's modulus of the composite structures with varying graphene contents

The pure TPC specimens showed relatively high ductility and moderate mechanical strength during cupping tests. Average load was 511.4 N, and average strain at failure 23.9 mm (see Fig. 5).

The TPC/Gr-4% composite material specimens showed relatively high mechanical strength and ductility during cupping tests. Average load was 799.2 N and average strain at failure 12.3 mm (see Fig. 5).

The TPC/Gr-8% specimens showed pronounced brittleness during cupping tests. Average load reached 139,8 N and average strain at failure 2,2 mm (see Fig. 5).

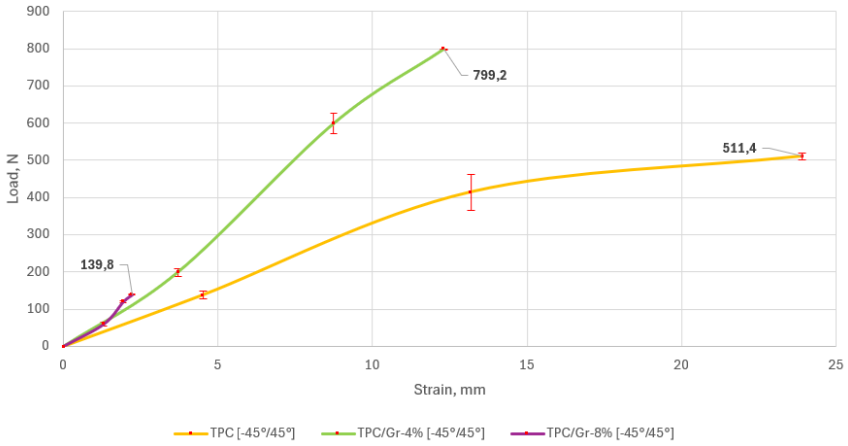

Fig. 5. Load vs. Strain curves of the composite structures with varying graphene content

Visual observations revealed that TPC/Gr-4% specimens showed greater deformation prior to fracture, with a more plastic and bulging fracture morphology. In contrast, the TPC/Gr-8% structures showed a clear brittle failure, lower deformation and straight cracks without a visible plastic deformation zone (Fig. 6).

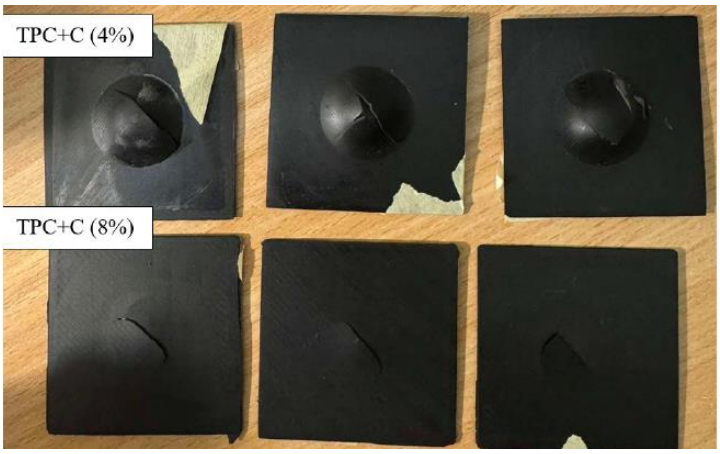

Fig. 6. Specimen appearance after cupping test

4. Conclusions

1. Tensile test results showed that a 4% content of graphene powder in the TPC matrix significantly improves the tensile mechanical properties of the composite. Pure TPC had an average tensile stress of 12,4 MPa and a strain at break of 268%. With 4% graphene content, the tensile stress increased to 16,4 MPa (~32%) and Young's modulus increased from 102,9 MPa to 265,7 MPa (~158 %). The strain at break decreased to 32,2%. When the graphene content was increased to 8%, the tensile stress reached 21,7 MPa (~75%), while the strain at break dropped to only 11,8%. Young's modulus increased further to 581,9 MPa, indicating higher stiffness and brittleness.
2. Electrical conductivity tests showed that 4% graphene content was not sufficient to ensure conductivity, while 8% resulted in measurable conductivity, with resistance ranging from 86,5 to 500 Ω. The resistance increased with deformation, indicating changes in the conductive graphene network within the polymer matrix.
3. Cupping test results showed that pure TPC was the most ductile, with an average failure load of 511,4 N and a strain at failure of 23,9 mm. The TPC/Gr-4% composite showed higher strength, with an average failure load of 799,2 N and a reduced strain of 12,3 mm. The TPC/Gr-8% composite was the most brittle, with an average strain of only 2,2 mm and a failure load of 139,8 N.

Acknowledgement

This project has received funding from the Research Council of Lithuania (LMTLT), agreement No. S-MIP-24-39.

References

1. SHI, H., FERNÁNDEZ VILLEGAS, I. and BERSEE, H.E.N. Exploring ultrasonic and resistance welding for thermoplastic composites in aerospace applications. *Composites Part A: Applied Science and Manufacturing*, 2024, p. 107-269
2. PANNEERSELVAM, K., ARAVINDAN, S. and HAQ, A.N. Advances in lightweight composite materials in automotive engineering: State-of-the-art review. *Alexandria Engineering Journal*, 2024, p. 137–150.
3. SEIDEL, G.D. and LAGOUDAS, D.C. A review of thermoplastic composites in wind turbine blade electronics: Current trends and prospects. *Composites Part B: Engineering,* 2024, p. 108-820.
4. SERVADEI, F., ZOLI, L., GALIZIA, P., MELANDRI, C. and SCITI, D. Synthesis and use of thermoplastic polymers for tissue engineering applications: A comprehensive review. *Materials Today Bio*, 2024, p. 100-258.
5. VALENTE, M., ROSSITTI, I. and SAMBUCCI, M. Different production processes for thermoplastic composite materials: sustainability versus mechanical properties and processes parameter. *Polymers*, 2023, p. 1–25.
6. KIEFER, B. and LAGOUDAS, D.C. Developments and future prospects of welding technology for thermoplastic composites. *Composites Part A: Applied Science and Manufacturing,* 2024, p. 107-270.
7. SEIDEL, G.D. and LAGOUDAS, D.C. Graphene-enhanced polymer composites: A state-of-the-art review. *FlatChem*, 2024, p. 100-411.
8. WEBB, G.V., LAGOUDAS, D.C. and KURDILA, A.J. Graphene at different scales to synergistically optimize the thermal and mechanical properties of thermoplastic composites. *Composites Part A: Applied Science and Manufacturing*, 2024, p. 107-271.
9. KWON, D.J., KIM, H.J., KIM, Y.S. and JANG, J.H. Impacts of thermoplastics content on mechanical properties of continuous fiber-reinforced thermoplastic composites. *Composites Part B: Engineering*, 2021, p. 108-859.
10. DAVARPANAH, M.J., BANSAL, S. and MALHOTRA, R. Influence of single point incremental forming on mechanical properties and chain orientation in thermoplastic polymers. *Journal of Manufacturing Science and Engineering*, 2016, p. 139.

Polyetherimide Hollow Fiber Membranes incorporating clays for CO_2 Separation

Tayyib MURTAZA[1], Naveed RAMZAN[2], Asif JAMIL[1]*

1 Department of Chemical, Polymer and Composite Materials Engineering, University of Engineering and Technology Lahore (New Campus), Pakistan

2 Department of Chemical Engineering, University of Engineering and Technology Lahore, Pakistan

** majamil@uet.edu.pk*

Abstract

The goal of this study is to develop mixed matrix hollow fiber membranes (HFMs) with improved CO_2/CH_4 separation performance by incorporating montmorillonite (MMT) nanofillers into a polyetherimide (PEI) matrix. Two types of MMT—unmodified (hydrophilic) and surface-modified (hydrophobic)—were used to investigate the impact of filler characteristics on membrane morphology and gas separation behaviour. The membranes were fabricated using the dry-wet spinning method and characterized by field emission scanning electron microscopy (FESEM) to assess structural morphology. Gas permeation experiments were conducted with pure CO_2 and CH_4 at 6 bar and ambient temperature. The PEI membrane containing modified MMT showed the best performance, achieving the highest CO_2/CH_4 selectivity of 1.7, which is higher than neat PEI and PEI-Na-MMT by 12.5 % and 28.57 %, respectively, due to improved polymer–filler compatibility and reduced non-selective voids. These findings demonstrate the potential of surface-modified nanofillers to enhance gas separation efficiency in PEI-based HFMs.

Keywords: Polyetherimide (PEI), Hollow Fiber membranes (HFMs), CO_2 Separation, Montmorillonite, Cation Exchange.

I. Introduction

Toyota Central Research Laboratories introduced the first and foremost commercial applications of polymer clay composite in the automotive industry in 1990 [1]. Since then, clay minerals have gained tremendous response both from academia and industry because of their economic viability and potential to enhance mechanical, chemical, thermal, and barrier properties of polymer clay composites [2]. To date, various clay minerals have been incorporated in polymer matrices for the development of flat sheet membranes, and its effect on morphology has been investigated. However, the effect of clay loading and dispersion conditions on the morphology and mechanical properties of clay filled polymer hollow fibre membranes (HFMs) have not investigated much, despite of the fact that HFMs are preferred over flat sheet membranes (FSMs) for large scale applications because of its higher surface area [3]. The development of HFMs is a far more complicated phenomenon than FSMs, as the dope viscosity ranges from a few hundred centipoises to later parts and a few thousand for its counterpart [4]. The morphology and structural properties of mixed matrix membrane (MMM) is dependent on the physical properties of both polymer and clay, along with the distribution of fillers. Generally, hydrophobic polymers like PVDF (polyvinylidene fluoride), PE (polyethylene), and PTFE (polytetrafluoroethylene) are used to develop membranes, however, it has certain limitations in terms of separation ability and mechanical properties [5]. Polyetherimide (PEI), despite of its hydrophobic nature, possesses a high glass transition temperature, which makes it chemically and thermally resistant. Natural montmorillonite (MMT), a type of clay with exchangeable cations, can be converted from

hydrophilic to hydrophobic by replacing inorganic cations with organic cations such as quaternary ammonium salts [6].
MMT consists of negatively charged silicate layers, which are balanced by exchangeable interlayer cations such as Na^+ and Ca^{2+}. This ionic structure renders MMT hydrophilic, leading to water absorption and swelling, which ultimately results in poor compatibility with hydrophobic polymer matrices. The aforementioned inorganic cations can be exchanged with long-chain organic cations, which increase the interlayer spacing of MMT and facilitate its exfoliation and uniform dispersion within the polymer matrix [7]. Moreover, the incorporation of MMT clay fillers can alter the membrane's skin layer thickness, surface porosity, and hydrophobicity. Zulhairun and Ismail [8] fabricated mixed matrix membranes (MMMs) using commercially modified Cloisite 15A, which is modified with Bis (hydrogenated tallow alkyl) dimethyl ammonium. They observed that increasing the filler loading resulted in diffusion pathway blockage. Consequently, even at a low filler content of 0.5 wt%, the membrane's permeability decreased, while CO_2/CH_4 selectivity significantly increased by 144%.

In this study, Na-Montmorillonite, a layered silicate, is used to exchange cations with ω-amino acid to introduce organophilic and compatibility towards organic polymers. Moreover, the objective of this research work is to observe Na-MMT and organo-modified clay (*f*-MMT) on PEI hollow fibre membrane morphology and CO_2/CH_4 separation performance.

2. Experimental Methodology

2.1. Materials

A variant of Na-MMT with a cation exchange capacity of 100 meq/100 g, KUNIPIA-F, has been provided by Kunimine Ind. Co., Japan. The following compounds were provided by Sigma Aldrich: polyetherimide (PEI; melt index: 9 g/10 min),), N-methyl-2-pyrrolidone (NMP, purity 99.5% , and 12-aminolauric acid (purity, 95%). On the other hand, HCl was supplied by Merck. The interlayer modification of Na-MMT was was performed as mentioned elsewhere[9].
The dope solutions consist of 23% PEI and 77% NMP, with 3% solid polymer derived from Na-MMT and *f*-MMT. To achieve the desired dopant composition, the designated quantities of Na-MMT and *f*-MMT were combined in NMP solvent and subsequently sonicated for one hour at 40 °C to guarantee homogeneous mixing. Subsequently, for priming, include 10 weight percent PEI into the solution and continuously mix for three hours at 70 °C. The residual PEI was subsequently introduced to the solution in a gradual, continuous flow until it fully dissolved. Following a 12-hour stirring of the solution, it was let to cool to room temperature to eliminate any gas and air bubbles. The viscosity of a dope was assessed at 30 rpm utilizing a Fungilab Rotational Viscometer (Model Alphas L).

Table 3. Dope solution composition

Dope solution	PEI (wt.%)	Na/*f*-MMT Wt.% of PEI	Viscosity (cp)
Neat PEI	23	0	5.617
PEI-Na-MMT	23	3	9.014
PEI-*f*-MMT	23	3	14.110

2.2. Hollow fibre membrane fabrication

The phase inversion method was used to spin HF membrane at ambient conditions through HF spinning experimental set up. Tube in orifice spinneret was used for dope extrusion with outer/inner diameter ratio as 0.8 mm/0.4 mm. Lab scale hollow fibre spinning experimental set up was utilized to develop HF membranes at ambient conditions. A constant nitrogen gas pressure of 100 kPa is supplied in order to create inert environment and dope solution is pumped

continuously at a particular flow rate and syringe pump maintained the bore fluid flow rate. The air gap distance was fixed at 15 cm and tap water was used both as external and internal coagulant. The solvent exchange start from lumen side however after passing through spinneret the fibre transported to a solvent-exchange coagulation bath. After spinning, the HF were immersed in water for 3 days for complete removal of residual solvent with daily water changed followed be drying at room temperature. Table 2 described the spinning conditions for both PEI-Na-MMT and PEI-*f*-MMT HF membranes.

Table 4. Spinning conditions for hollow fibre membranes

Spinning Conditions	**Values**
OD/ID (mm)	0.8/0.4
T (°C)	25
Coagulant	Water
AG (cm)	15
Dope rate (mL/min)	0.8
Bore rate (mL/min)	1
Take up	Free fall

2.3. Characterizations

FTIR spectroscopy (Perkin Elmer 1650) is used to confirm the attachment of ω-aminolauric acid in the interlayer gallery of MMT. Thermo gravimetric Analyzer (TGA, Perkin Elmer, STA 6000)TGA is used to check the content of amino acid attached. Small angle XRD (SAX, BRUKER, XRD/D8) is used with CoKα radiation (0.154 nm) to measure the interlayer distance of layered silicate. Morphological structure of spun HF membrane are studied by using FESEM. The HF membrane are break in liquid nitrogen and then analyze through Field Emission Scanning Electron Microscope (FESEM, Zeiss Supra55 VP).

2.4. Gas Separation Test

A gas permeation test was performed at 6 bar pressure and ambient temperature using gases that were 99% pure, namely CO_2 and CH_4. An injection of a 2-fiber pile was introduced into the module; one end of the pile was covered with epoxy glue to inhibit gas passage, while the other end may be exposed to the selected intake gases. The desired gas was injected into the hollow fibers via their shell side to facilitate penetration. The total effective fiber area was approximately 7.54 cm^2. A digital flow meter is employed to measure the downstream gas flow rate. The equation was employed to ascertain the permeance (1).

$$P_i/l = \frac{Q}{A\Delta P}\left(273.15/T\right) \quad (1)$$

Here, P_i represents the gas permeability of species *i* (e.g., CO_2 or CH_4), expressed in Gas Permeation Units (GPU). The variable, *l,* denotes the membrane thickness, while *Q* refers to the volumetric gas flow rate. *A* is the effective membrane area, and *ΔP* indicates the pressure difference across the membrane, measured in cm.Hg. The permeation temperature is denoted by *T*, expressed in Kelvin (K).

α_{ij} represents ideal selectivity of gas i to j, and was calculated using the equation (2).

$$\alpha_{ij} = \frac{\left(P_i/l\right)}{\left(P_j/l\right)} \quad (2)$$

Whereas P_i/l, P_j/l represents permeation of gas i and j, respectively.

3. Results and Discussion

FTIR technique is utilized to investigate the presence of ω-aminolauric acid in the interlayer gallery of Na-MMT. A typical structure of montmorillonite shows peaks as shown in figure 1 (a). The peaks are shown in figure 1(a) at wave number 521, 1041, 1637, 3467 which represents Al-O-Si deformation, Si-O stretching and H-O-H bending and Al-O stretching respectively. In amino functionalized MMT, the new peaks appear around 1713, 2850, 3236 and 3617 and are the characteristic peaks of carbonyl group, C-H bond stretching, NH stretching and OH stretching of structural hydroxyl group [10,11]. All-important bands and assignments of functional groups can be seen in Table 2.

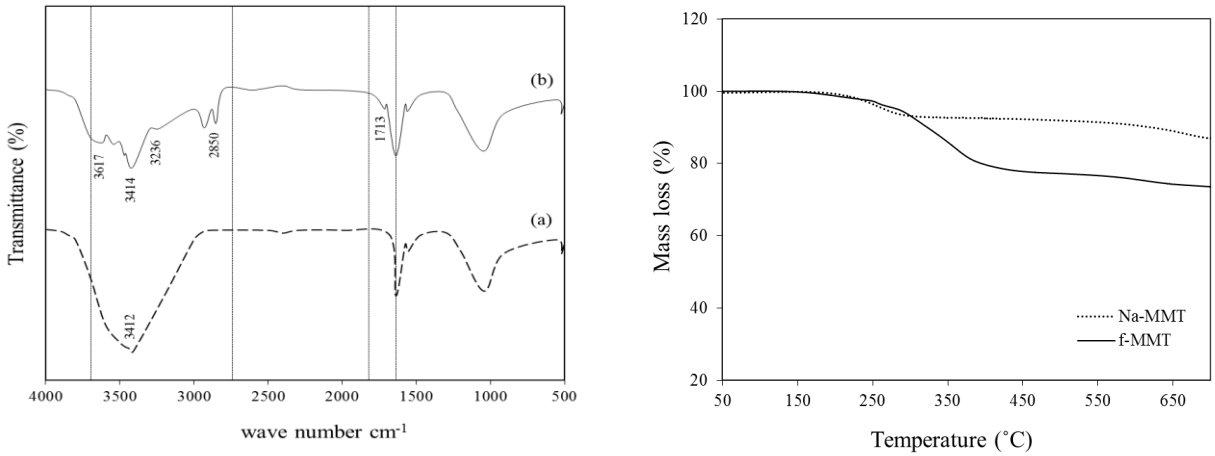

a b

Fig. 7. a – FTIR, b – TGA analysis of clays

Table 5. FTIR peaks and bonds assigned

SN	Wave Number (cm^{-1})		Bond Assigned	Theoretical Range
	Na-MMT	*f*-MMT		cm^{-1}
1	521	521	Al-O-Si deformation	-
2	1041	1048	Si-O stretch	1030-1045
3	1637	1638	H-O-H bending	1610-1650
4		1713	Carbonyl group	1690-1760
5		2850	C-H stretching	2850-2960
6		3236	N-H stretch	-
7	3412	3414	H-O-H stretch	3410-3445
8		3617	Structural OH stretch	3597-3645

According to thermal analysis performed by TGA, the attached amino acid chains are stable up to 280 ^{o}C after that it start to disintegrate from the interlayer gallery space, it can be evident in Figure 1 (b). Also, the extent of attachment can be estimated from TGA analysis, the difference between weight decreases in MMT and modified MMT is approximately 21 %. The content of organic compounds in modified MMT was calculated by the weight loss MMT by heating from 25 to 700 ^{o}C. The weight loss from 120 to 700^{o}C considered to be the contents of organic and structurally absorbed water in MMT. The weight loss for MMT is 7% from 210 to 300^{o}C whereas a significant

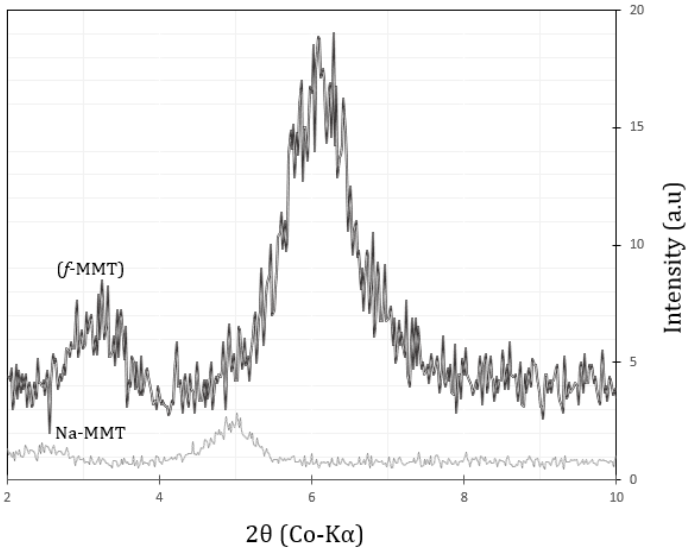

Fig. 8. XRD pattern for pure and Func. MMT

weight loss is observed for modified clay from 240 to 460 °C i.e. 22%. The absorbed water content believed to be 7 % and organic content is approximately 21 % which is quite a significant amount. The presence of organic compound in basal spacing of MMT is confirmed by FTIR and TGA. The interlayer distance can be estimated by XRD. Figure 2 depicts the XRD pattern of MMT and modified MMT. We can observe the few additional peaks in modified MMT which suggests the spatial change inside layers. In MMT spectra, peak observed was around 2-theta value of 5 degree whereas it was shifted to 6.2 degree for modified MMT, which suggests the increase in inter layer distance. The interlayer distance counted for modified MMT is approximately 14.26 Å, which is consistent with literature [12, 13].

Cross sectional morphology of spun hollow fiber membranes have been depicted in Figure 3. It is observed that porous morphology is obtained due to the adoption of phase inversion method. The finger like pores are the dominant morphology in all the developed HFMs with thin top skin layer.

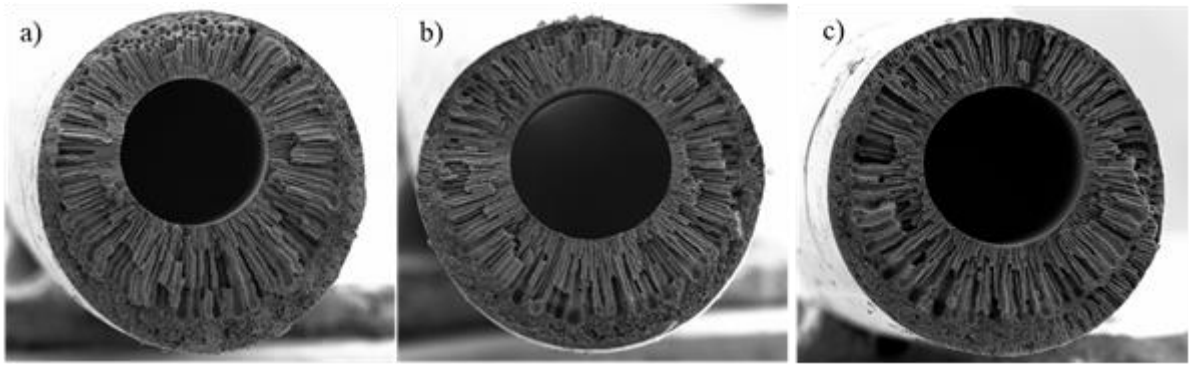

Fig. 9. FESEM micrographs of developed HF membranes at magnification of 100 μm

The phase inversion process influences the shape, mechanical properties, and gas separation performance of the membranes throughout development. The macromolecular architecture of spun membranes can be influenced by many thermodynamic and kinetic parameters associated with the phase inversion process. These parameters encompass interactions among polymers and solvents, between solvents and coagulants, and the viscosity of the dope [14]. The solvent/coagulant interactions are responsible for the pore structure and distributions. The favorable interaction leads to instant solvent exchange which creates long finger like pores. Dope

solution contained NMP as a solvent and water is used as non-solvent. The interactions of PEI-NMP is weak in comparison to NMP- water interactions. During membrane development process, NMP leached out of the nascent membrane and water replaced it inside the newly spun hollow fiber membranes, as a result finger like pores are formed. Upon contact with the external coagulant, the membrane surface solidifies, resulting in the formation of a thick outer skin layer, which signifies the conclusion of pore development [15].

In addition, the viscosity of the dope solution is another factor that governed the morphological structure. The viscosity of PEI-*f*-MMT dope solution is higher as compared to other dope solutions as depicted in Table 1. Due to higher viscosity, the pore forming process slowed down and thicket outer skin layer is formed [16]. The outer skin is thicker for neat PEI and PEI-*f*-MMT membranes in comparison to PEI-Na-MMT HF membrane. Due to hydrophilic nature of Na-MMT, the water interactions increases which result in thinner skin layer formation. The thinner skin enhance the gas permeance however the selectivity has to compromise [17].

Figure 4 shows the CO_2 permeance of all three developed hollow fiber membranes at 600 kPa pressure. CO_2, CH_4 permeance can be seen in Figure 4(a) whereas Figure 4(b) represent the selectivity. PEI-Na-MMT showed the highest permeation for CO_2 and CH_4. The poor polymer filler interactions create surface voids and leads to Knudsen diffusion which is responsible for higher gas permeance [18]. The Na-MMT in PEI-Na-MMT is hydrophilic in nature as compared to hydrophobic PEI, as a result poor polymer filler interactions are responsible for higher gas permeation and also the thin skin layer formation for this membrane leads to lower CO_2/CH_4 selectivity as observed in figure 4 (b).

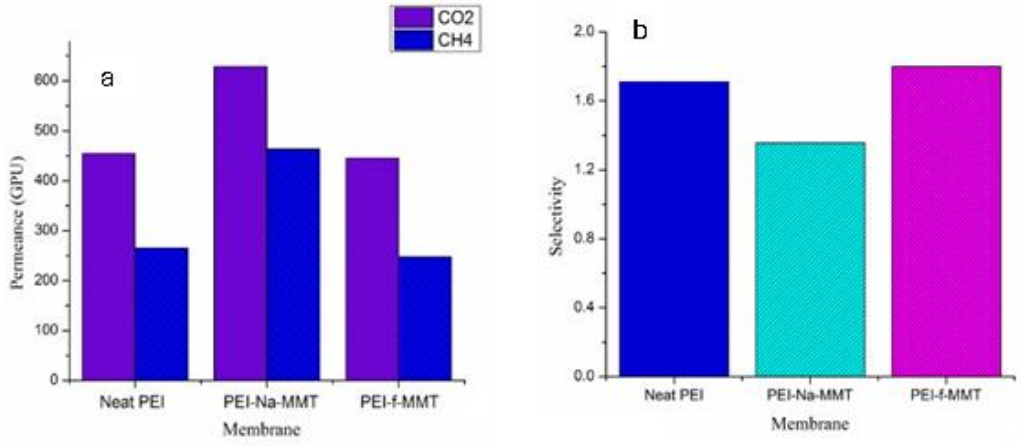

Fig. 10. The permeance (CO_2, CH_4) and selectivity of spun hollow fibre membranes

The hydrophobic MMT is compatible with host PEI, as a result form evenly distributed morphology and showed highest gas permeance for CO_2 gas. In addition, the higher aspect ratio of the functionalized clay plays an important role in increasing the exfoliated morphology, even distribution and enhancement in tortuous path [19]. All the phenomena support the selectivity enhancement for mixed matrix membrane. Due to higher aspect ratio for functionalized clays, the interlayer interactions are weak, and clay layers separated from each other during dope preparations and evenly distribution in polymer matrix. This uniform distribution of clay increases the tortuous path for the incident gas, which creates more hindrance for the gas passage particular for the gas molecules with higher kinematic diameter. Due to this reason, for PEI-*f*-MMT the CH_4 transportation is lowest. Due to this reason the selectivity is highest as compared to both neat PEI and PEI-Na-MMT. The results are consistent with the previous literature [20, 21]. Hashemifard et al. embedded hydrophobic and hydrophilic MMT in PEI matrix to cast flat sheet membrane [21]. The CO_2 permeance for hydrophilic MMT (1 wt.%) is 74 % higher than neat PEI whereas it is 48% higher in the case of hydrophobic MMT. However, relative selectivity is higher for hydrophilic MMT due to the void's creation in the skin layer of FSMs.

4. Conclusion

Na-Montmorillonite is layered structure containing Na^+ as interlayer cation, and organophilic in nature. Na-MMT was successfully modified with ω-amino acid and the intercalation of organic compound inside gallery of layered structure is confirmed by FTIR, and the content of attached compound of amino acid is approximately 15 %, with basal spacing of 14.26 Å. Mixed matrix HFMs with Na-MMT and *f*-MMT were developed via phase inversion method to study the effect on its morphology and CO_2/CH_4 separation. For modified clay, the inorganic cation of Na-MMT was replaced with organic cation of aminolauric acid to induce hydrophobicity. FESEM images suggested the uniform finger like pore generation for both types of MMT, which ultimately support the CO_2, CH_4 permeation as evident from gas separation test. The PEI-*f*-MMT showed lower CO_2, CH_4 permeance as compared to neat PEI and PEI-Na-MMT HFMs owing to improved filler distribution, however showed improved selectivity by 28.57 %.

Acknowledgement

The work is supported by the National Research Program for Universities (NRPU), Higher Education Commission Pakistan, No. 20-15709/NRPU/R&D/HEC/2021.

References

1. NGUYEN, Q.T., BAIRD, D.G. Preparation of polymer–clay nanocomposites and their properties. *Advances in Polymer Technology: Journal of the Polymer Processing Institute*. 2006 Dec;25(4):270-85.
2. ANADO, P., et al., Polysulphone/montmorillonite nanocomposite membranes: Effect of clay addition and polysulphone molecular weight on the membrane properties. *Journal of Membrane Science*. 455: p. 187-199.
3. MITTAL, V., Polymer layered silicate nanocomposites: a review. *Materials,* 2009. 2(3): p. 992-1057.
4. JAMIL, A., CHING, O.P., SHARIFF, A.M. Mixed matrix hollow fibre membrane comprising polyetherimide and modified montmorillonite with improved filler dispersion and CO2/CH4 separation performance. *Applied Clay Science.* 2017 Jul 1;143:115-24.
5. JAMIL, A., CHING, O.P., SHARIFF, A.B. Current status and future prospect of polymer-layered silicate mixed-matrix membranes for CO2/CH4 separation. *Chemical Engineering & Technology.* 2016 Aug;39(8):1393-405.
6. PAVLIDOU, S., PAPASPYRIDES, C.D. A review on polymer–layered silicate nanocomposites. *Progress in polymer science*. 2008 Dec 1;33(12):1119-98.
7. KIM, G.M., LEE, D.H., HOFFMANN, B., KRESSLER, J., STÖPPELMANN, G. Influence of nanofillers on the deformation process in layered silicate/polyamide-12 nanocomposites. *Polymer.* 2001 Feb 1;42(3):1095-100.
8. ZULHAIRUN, A.K., ISMAIL, A.F. The role of layered silicate loadings and their dispersion states on the gas separation performance of mixed matrix membranes. *Journal of Membrane Science*. 2014 Oct 15;468:20-30.
9. OKADA, A., USUKI, A. The chemistry of polymer-clay hybrids. *Materials Science and Engineering*: C. 1995 Nov 1;3(2):109-15.
10. NAVRATILOVA, Z., WOJTOWICZ, P., VACULIKOVA, L. and V. SUGARKOVA, "Sorption of alkylammonium cations on montmorillonite," *Acta Geodynamica et Geomaterialia,* vol. 4, p. 59, 2007.
11. SAIKIA, B.J. and G. PARTHASARATHY. Fourier transform infrared spectroscopic characterization of kaolinite from Assam and Meghalaya, Northeastern India. *Journal of Modern Physics,* vol. 1, p. 206, 2010.
12. L. ZHOU, H. CHEN, X. JIANG, F. LU, Y. ZHOU, W. YIN, *et al.* Modification of montmorillonite surfaces using a novel class of cationic gemini surfactants. *Journal of colloid and interface science,* vol. 332, pp. 16-21, 2009.
13. N.M. ISMAIL, A.F. ISMAIL, A. MUSTAFA, T. MATSUURA, T. SOGA, K. NAGATA, T. Asaka Qualitative and quantitative analysis of intercalated and exfoliated silicate layers in asymmetric polyethersulfone/cloisite15A mixed matrix membrane for CO2/CH4 separation.Chem. *Eng. J.,* 2015, 268 , 371–383.

14. JAMIL, A., CHING, O.P. AND SHARIFF, A.M. Macrovoids suppression in Polyetherimide (PEI) hollow fibre membranes by optimizing the air gap. *International Journal of Applied Engineering Research*, 2016, 11.19, 9684-9688.
15. REZAEI, M., ISMAIL, A.F., HASHEMIFARD, S.A. AND MATSUURA, T. Preparation and characterization of PVDF-montmorillonite mixed matrix hollow fiber membrane for gas–liquid contacting process. *Chemical Engineering Research and Design*, 2014, 92, 2449-2460.
16. HUSAIN, S. AND KOROS, W.J., Macrovoids in hybrid organic/inorganic hollow fiber membranes. *Industrial & Engineering Chemistry Research*, 2009, 48, 2372-2379.
17. ZULHAIRUN, A.K., ISMAIL, A.F., MATSUURA, T., ABDULLAH, M.S. AND MUSTAFA, A., Asymmetric mixed matrix membrane incorporating organically modified clay particle for gas separation. *Chemical Engineering Journal*, 2014, 241, 495-503.
18. KIM, W.G., LEE, J.S., BUCKNALL, D.G., KOROS, W.J. AND NAIR, S. Nanoporous layered silicate AMH-3/cellulose acetate nanocomposite membranes for gas separations. *Journal of membrane science*, 2013, 441, 129-136.
19. JAMIL, A., ZULFIQAR, M., ARSHAD, U., MAHMOOD, S., IQBAL, T., RAFIQ, S., IQBAL, M.Z. Development and Performance Evaluation of Cellulose Acetate-Bentonite Mixed Matrix Membranes for CO2 Separation. *Advances in Polymer Technology*. 2020, 1:8855577.
20. Hashemifard, S.A., Ahmad, F. I. and T. Matsuura. Effects of montmorillonite nano-clay fillers on PEI mixed matrix membrane for CO2 removal. *Chem. Engg. J.*, 2011, 170.1, 316-325.

Development of Highly Porous Bioactive 3d-Printed Polylactic Acid/Hydroxyapatite Scaffolds for Bone Tissue Engineering

Jokūbas LUKOŠIŪNAS*, Gabrielė ŠARAPAJEVAITĖ, Lidija TURILINAITĖ, Kamilė DARGYTĖ, Odeta BANIUKAITIENĖ

Kaunas University of Technology, Kaunas, Lithuania

** jokubas.lukosiunas@ktu.lt*

Abstract

The development of biomimetic scaffolds is essential for advancing bone tissue engineering. This study aimed to fabricate and evaluate polylactic acid and hydroxyapatite (PLA-HAP) composite scaffolds using 3d printing technology. Three scaffold geometries, mimicking cancellous bone, were designed and fabricated. PLA filaments were prepared by incorporating 5%, 10%, 20%, and 30% HAP. Filaments containing up to 20% HAP exhibited good extrusion stability, uniform morphology, and consistent printability. In contrast, the 30% HAP filament was brittle and failed during extrusion. SEM analysis revealed more uniform HAP distribution at lower concentrations. The printed scaffolds demonstrated 60–80% porosity with interconnected pores. These results highlight the importance of optimizing HAP content to ensure scaffold quality and functionality for tissue engineering applications.

Keywords: polylactic acid, hydroxyapatite, composite, scaffolds.

1. Introduction

Every year, human cell, tissue, and organ transplantation saves lives, treats diseases, and alleviates trauma worldwide. In recent decades, these procedures have become more frequent and successful due to advancements in donor transplant exchange programs. Despite these developments, challenges such as graft quality, shortages, and immune rejection responses persist [1].

one tissue damage caused by various injuries or degenerative diseases remains one of the most commonly encountered clinical issues [2]. Worldwide, researchers are increasingly focused on developing innovative biomaterials that can replace donor grafts, thereby addressing the persistent challenges associated with transplantation [3]. In this regard, 3d porous scaffolds are being developed for bone tissue regeneration in defect areas. These scaffolds are fabricated using various synthetic and natural polymers, inorganic materials, or their combinations [4].

3d printing technology has emerged as a promising tool for fabricating scaffolds with precise control over structure, porosity, and mechanical properties, making it highly suitable for tissue engineering applications [5].

The objective of this study is to develop and evaluate highly porous 3d-printed scaffolds made of PLA and HAP composites for bone tissue engineering.

2. Materials and methods

Three distinct scaffold geometries with varying internal architectures were designed using Z-SUITE software (Zortrax, Poland). Each model was configured as a 20 × 20 × 20 mm cube, with

the internal structures tailored to mimic the morphology of cancellous bone. The finalized 3d models are presented in Figure 1.

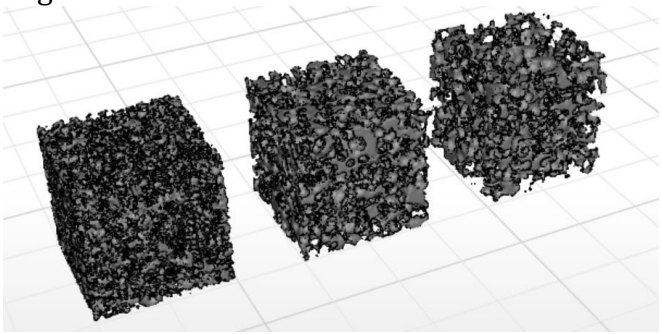

Fig. 1 3d models of the designed composite scaffolds

Poly(lactic acid) (PLA) and hydroxyapatite (HAP) were selected as the primary materials for scaffold fabrication. Four different composite filaments were prepared with HAP concentrations of 5%, 10%, 20%, and 30%. The composite scaffolds were then fabricated using a Zortrax M200 Plus 3d printer.
Fourier-transform infrared (FT-IR) spectra were recorded using a Perkin Elmer Spectrum GX spectrometer. The morphology of the materials was examined using a high-resolution S-3400N scanning electron microscope (SEM, Hitachi S-3400N, Japan).

3. Results and discussion

In this work, PLA and HAP were successfully used as primary materials for the fabrication of composite scaffolds. Four different composite filaments were prepared, incorporating HAP concentrations of 5%, 10%, 20%, and 30% by weight, with a filament diameter of 1.75 ± 0.05 mm. The filaments with 5%, 10%, and 20% HAP content were successfully extruded, maintaining consistent diameter and mechanical integrity throughout the process. However, the composite filament containing 30% HAP exhibited significant brittleness and poor flowability, leading to extrusion failure and the inability to produce a functional filament. SEM analysis confirmed that in the PLA filament containing 30% HAP, the HAP was unevenly distributed, the filament diameter was inconsistent, and the surface appeared rough.
The composite scaffolds were subsequently fabricated using 3d printing technology. Scaffolds containing up to 20% HAP were successfully printed, exhibiting consistent pore geometry and surface quality. In contrast, the composite with 30% HAP failed during filament extrusion due to brittleness and poor flow characteristics, preventing the fabrication of scaffolds from this material. "It was determined that filaments containing 5–20% HAP are suitable for fabricating 3d scaffolds with porosity ranging from 60% to 80%.
The FT-IR spectrum of the PLA-HAP scaffold sample retains the characteristic peaks of both components, indicating successful incorporation of HAP into the PLA without significant chemical alteration.

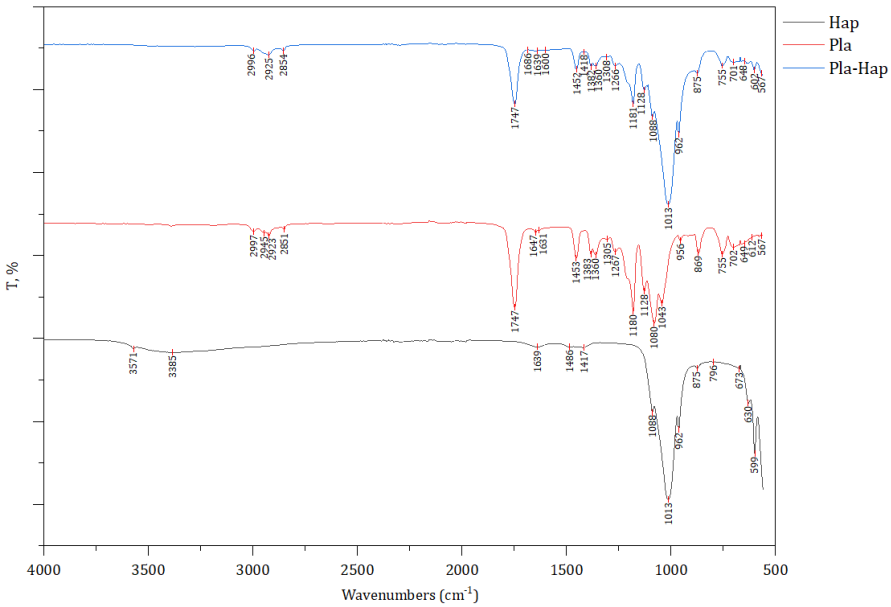

Fig. 2 FTIR spectra comparing Pla, Hap and Pla-Hap composite

The FT-IR spectrum of the PLA-HAP scaffold sample retains the characteristic peaks of both components, indicating successful incorporation of HAP into the PLA without significant chemical alteration.

4. Conclusions

1. The composition of the filaments and the applied technological parameters significantly influenced the stability of the 3d printing process, layer adhesion, and scaffold morphology. Polylactic acid filaments containing 5–20% hydroxyapatite demonstrated good processability and structural integrity, indicating their suitability for tissue engineering applications.
2. A reduction in hydroxyapatite content within the filament led to improved printing stability, enhanced interlayer adhesion, and a more uniform scaffold morphology, emphasizing the importance of optimizing hydroxyapatite concentration to achieve desirable scaffold properties.

References

1. MACHAIRAS, Nikolaos and SOTIROPOULOS, Georgios. Living donor liver transplantation could solve shortage of liver grafts in Greece. Hellenic Journal of Surgery. 2025. DOI 10.59869/24041.
2. PAI, Varsha, SINGH, Bhisham Narayan and SINGH, Abhishek Kumar. Insights into advances and applications of biomaterials for nerve tissue injuries and neurodegenerative disorders. Macromolecular Bioscience. 2024. p. e2400150. DOI 10.1002/mabi.202400150.
3. PHAM, John-Paul A. and CORONEL, María M. Unlocking transplant tolerance with biomaterials. Advanced Healthcare Materials. 2024. p. e2400965. DOI 10.1002/adhm.202400965.
4. DENG, Qingzha, LI, Xu-Ran, LIU, Po-Lin, HE, Shu-Hang, GAO, Yuan, HAN, Ziyue, SHEN, Zhi-Han, WEI, Zhan-Ying, ZHANG, Chang, WANG, Fei, DAWES, H., ZHU, Tong-He, GUO, Shang-Chun and TAO, Shi-Cong. 3D Cryo-Printed Hierarchical Porous Scaffolds Harmonized with Hybrid Nanozymes for Combinatorial Mitochondrial Therapy: Enhanced Diabetic Bone Regeneration via Micromilieu Remodeling. Advanced Functional Materials. 2024. DOI 10.1002/adfm.202403145.
5. CHAN, Shareen S. L., BLACK, Jay R., FRANKS, George V. and HEATH, Daniel E. Hierarchically porous 3D-printed ceramic scaffolds for bone tissue engineering. Biomaterials Advances. 2024. Vol. 169, p. 214149. DOI 10.1016/j.bioadv.2024.214149.

Biofuel ash treatment with water to extract useful elements

Nojus GRIGALIŪNAS*, Egidijus PUIDA

Kaunas University of Technology, Kaunas, Lietuva,

** nojus.grigaliunas@ktu.edu*

Abstract

Biofuel ash from industrial biomass boilers is often considered waste, yet it holds considerable potential for reuse in circular systems. After collecting ash from the industrial wood-fueled boiler, the finer material was separated from slag using a manual sifting process. The fine ash was then mixed with distilled water to extract water-soluble compounds, mainly consisting of alkali salts and certain trace elements. The ash–water suspension was filtered using filters, and the resulting liquid was dried to leave behind solid residues. These residues were weighed to determine the extractable portion of the ash. The process highlights a simple, low-energy method to reclaim useful materials and reduce waste, supporting more sustainable practices in bioenergy [1].

Keywords: biomass ash, wood ash, AWE(s).

1. Introduction

The development of renewable energy technologies is essential to reduce reliance on fossil fuels and minimize environmental pollution. Among these technologies, bioenergy—particularly from woody biomass—offers a carbon-neutral option for generating heat and power. However, while the energy output and emission reduction benefits are well recognized, the solid by-products from combustion, such as wood ash, are often disregarded in conversations about sustainability [2].

Emerging attention has been drawn to the role of ash in circular systems, highlighting it as an overlooked component with material recovery potential. Studies have shown that wood ash contains not only nutrients but also alkali compounds and trace elements that may be suitable for reuse rather than disposal. Discarding this ash contributes to unnecessary waste generation and missed opportunities for resource conservation [3].

In this work, a simple water-based method was explored to recover useful substances from wood ash produced in a biofuel boiler system. By separating fine ash and suspending it in water, water-soluble components can be extracted, including alkali salts, particularly potassium and calcium compounds, along with trace metal ions and organic residues. These extractions result in a lye-like solution that can be dried to isolate reusable residues.

To further support this approach, lab results from external analytical sources were reviewed (Table 1) to verify the chemical composition and solubility of selected ash samples.
This data helps validate the presence of key water-soluble components such as potassium, calcium, magnesium, and trace minerals across similar ash types. Comparative analysis supports the broader applicability of the findings beyond a single sample source.

This water-based ash extract falls within a broader category of Agro-Waste Extracts (AWEs)–liquids derived from agricultural or biomass residues using low-tech, low-energy processes, often rich in alkalis, nutrients, or trace minerals. AWEs are increasingly recognized as viable

alternatives to commercial chemicals in eco-conscious applications, ranging from natural fertilizers and biodegradable cleaning agents to soap-making bases and textile treatments.
The integration of AWE use into biomass energy systems contributes to both waste valorization and sustainable chemical sourcing, reinforcing the principles of circular bioenergy and practical environmental stewardship [4].

2. Digital Experimental Details

Wood ash was collected from the discharge system of an industrial biofuel boiler fueled by chips of biomass. Ash was sifted using a stainless-steel sieve (OKO mesh 0.80 mm, wire 0.5 mm) to separate fine ash from slag and unburnt residues. From ~1.4 kg of raw ash, ~1 kg of fine ash was stored in sealed glass containers to prevent moisture uptake.

For extraction, 20 g of fine ash was mixed with 200–1400 mL of distilled water in a 2000 mL container. Stirring was performed at ~100 rpm and ~22 °C using a Heidolph RZR 2020 overhead stirrer. Two mixing durations were tested:
• 15 minutes
• 30 minutes
Post-mixing, using filters ash are derived from the solution, and it was done immediately to reduce atmospheric CO_2 interaction. Filtrates were collected in pre-weighed flasks, then dried at 60–80 °C in a fume cupboard oven until water evaporates and there is only useful elements left (12–18 h). Final weights were measured using a Shimadzu AY220 balance (±0.001 g) to determine extracted solids. All processes are shown below (Figure 1).

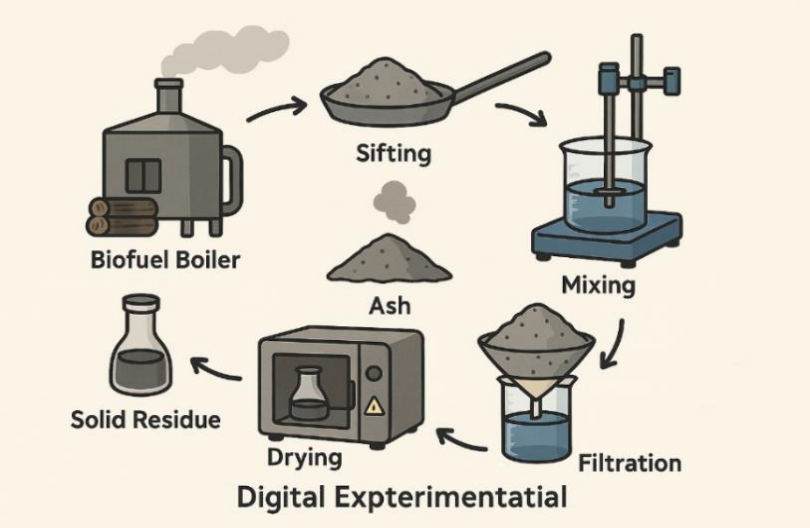

Fig. 1. Illustration of ash processing: sifting, mixing, filtering, and evaporating with an electric furnace setup.

Solubility Observations (Table 1)
Soluble in water:
• Potassium (K), Calcium (Ca), Magnesium (Mg)
• Boron (B), Phosphorus (P), light organic residues
• Trace elements: Vanadium (V), Zinc (Zn), Copper (Cu)
Insoluble or poorly soluble:
• Heavy metals (Pb, Cr, Ni, As, Cd, Hg)
• Hydrophobic organics like benzopyrene
These results confirm that the extract – an alkaline lye – is rich in soluble mineral salts and fits within the category of Agro-Waste Extracts (AWEs) for sustainable reuse in detergents, composting.

Table 1. Results of the study of elements contained in biofuel ash. Research methods and results:

Research parameter	Research results		Research methods (label)
pH	12,5	12,4	ISO 10390:2021
In dry matter:			
Organic carbon %	1,34	1,06	LST EN 15936:2022
Phosphorus (P) mg/kg	13116	13625	LST EN 13657:2003, LST EN ISO 6878:2004
Potassium (K) mg/kg	76250	62917	LST EN 13657:2003, LST ISO 9964-3:1993
Calcium (Ca) mg/kg	229083	146000	LST EN 13657:2003, LST ISO 7980:2000
Magnesium (Mg) mg/kg	21000	17583	
Arsenic (As) mg/kg	<0,5*	<1,5**	LST EN 13657:2003, LST EN ISO 11885:2009
Cadmium (Cd) mg/kg	<1,5	<0,5	
Lead (Pb) mg/kg	<2,5	<2,5	
Nickel (Ni) mg/kg	5,33	3,80	
Vanadium (V) mg/kg	3,87	6,80	
Boron (B) mg/kg	161	123	
Chromium (Cr) mg/kg	15,9	13,2	
Zinc (Zn) mg/kg	128	72,7	
Copper (Cu) mg/kg	102	51,6	
Mercury (Hg) mg/kg	<0,02	<0,02	LST EN 13657:2003, LST EN 12846:2012
Benzapyrene µg/kg	<0,5	<0,5	LST EN 17503:2022

*<0.5 - detection limit.
**<1.5 - detection limit.

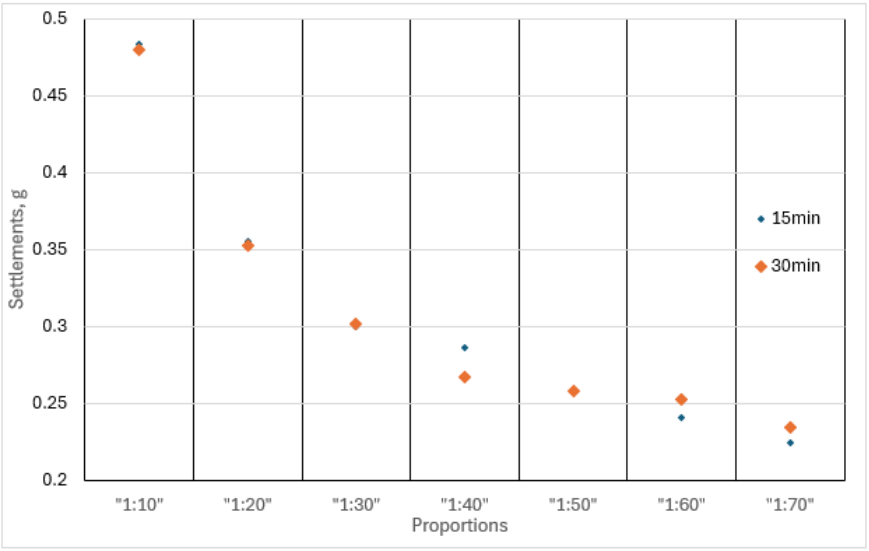

Fig. 2. The useful substances obtained from the ash between 100 g of solution of different proportions ash to water, 15 minutes and 30 minutes of ash and water contact time.

As shown in Figure 2, the concentration of useful substances obtained from wood ash, measured per 100 g of solution, across different ash-to-water ratios (1:10 to 1:70). The results compare 15-minute and 30-minute mixing durations. As the ash-to-water ratio becomes more diluted, the concentration of extractable compounds per 100 g of solution decreases, demonstrating a typical dilution effect. However, this decrease in concentration is offset by an increase in total extracted mass across the entire solution volume, indicating improved overall extraction efficiency. Additionally, the minimal difference observed between the 15-minute and 30-minute mixing times suggests that extending the contact duration provides limited benefit, making the shorter mixing period more practical and efficient.

Table 2. Concentration and total yield of useful substances from wood ash at various ash-to-water ratios after 90 minutes of contact.

Proportions	100g of solution settlements, g	Whole solution settlements, g	Ash, g	Distilled water, g
"1:10"	0.514	1.029	20	200
"1:30"	0.287	1.722	20	600
"1:50"	0.251	2.508	20	1000
"1:70"	0.294	4.113	20	1400

As shown in Table 2, extending contact time to 90 minutes yields only a slight increase in extracted material compared to Figure 2. The declining concentration per 100 g reflects dilution, not reduced recovery. Since total recovered mass still rises, longer mixing offers minimal benefit. A 15-minute mixing time remains optimal for efficiency.

3. Calculation methodology

Numerical evaluation was used to determine the concentration of solid residues obtained from the aqueous extraction of wood ash. This was achieved through a series of standardized mass calculations. Each dried sample was weighed in a flask, and the mass of extractable solid residue was calculated by subtracting the empty flask weight:

$$m_{residue} = m_{flask+\,residue} - m_{flask} \quad (1)$$

The mass of the liquid solution in each trial was also determined by subtracting the empty flask mass from the flask containing the liquid extract:

$$m_{solution} = m_{flask+\,solution} - m_{flask} \quad (2)$$

The concentration of extractable solids per gram of solution was calculated by dividing the mass of residue by the mass of solution:

$$C_{solid} = \frac{m_{residue}}{m_{solution}} \quad (3)$$

To express the concentration in grams of solids per 100 grams of solution (as shown in the results chart), the value was multiplied by 100:

$$C_{solid(per\ 100g)} = \left(\frac{m_{residue}}{m_{solution}}\right) \times 100 \quad (4)$$

These formulas were applied to all sample sets under both 15-minute and 30-minute mixing conditions to ensure comparability across tests.
Boundary conditions applied throughout all experimental runs:
• Initial ash mass: 20.00 g
• Water volumes: 200 ml to 1400 ml (in 200 ml increments)
• Mixing duration: 15 minutes and 30 minutes
• Stirring speed: ~100 rpm (Heidolph RZR 2020 overhead stirrer)
• Drying temperature: 60–80 °C (in a fume cupboard oven)
• Flask weights: Individually pre-measured prior to each trial
This consistent calculation framework enabled reproducible results and supported quantitative comparisons regarding how dilution and mixing time affected the extraction of water-soluble components from wood ash.

4. Results and Discussion

Water extraction of fine wood ash showed consistent results across samples. Seven 20 g batches were mixed with 200–1400 mL distilled water (in 200 mL steps), stirred at ~100 rpm, filtered, and evaporated to isolate solids. As water volume increased, residue per flask decreased due to dilution, but total mass recovery rose, indicating more complete mineral leaching. Minimal differences between 15- and 30-minute mixing suggest most soluble compounds dissolve within 15 minutes, supporting efficient processing.

Dried residues were light and fine-grained, consistent with compounds like potassium carbonate, calcium hydroxide, and magnesium salts – aligned with solubility data for alkali, alkaline earth metals, borates, and phosphates. These findings highlight wood ash's value as a source of Agro-Waste Extracts (AWEs)[5].

5. Conclusions

1. Aqueous extraction of 20g of wood ash with increasing water volumes (200g to 1400g) shows that higher dilution leads to lower concentration of residue in solution.
2. Comparing mixing times of 15 and 30 minutes under identical conditions reveals minimal difference in extracted useful materials, indicating that longer mixing offers no significant improvement for extracting useful materials from ash.
3. These results support the conclusion that a 15-minute mixing period is sufficient for practical extraction under the tested conditions, optimizing time and energy use in similar future procedures.
4. It's not very cost-effective to increase the ratio beyond 1:70, as the dissolution becomes negligible past this point, and further increases are no longer economically viable due to the mass and concentration involved, mainly because moving large quantities of material with diminished value becomes increasingly challenging.

References

1. SARMAH, Debasish; BORAH, Kamala Kanta ir BORA, Utpal. Aqueous extracts of biomass ash as an alternative class of Green Solvents for organic transformations: A review update. *Sustainable Chemistry and Pharmacy*, vol. 24 (2021), pp. 100551. Prieiga per: https://www.sciencedirect.com/science/article/pii/S2352554121001789..
2. WANG, Lili ir PANG, Jun. Assessing the impact of climate mitigation technology and environmental tax on renewable energy development: A dynamic threshold approach. *Renewable Energy*, vol. 244 (2025), pp. 122683. Prieiga per: https://www.sciencedirect.com/science/article/pii/S0960148125003453..
3. PETTERSSON, M.; BJÖRNSSON, L. ir BÖRJESSON, P. Recycling of ash from co-incineration of waste wood and forest fuels: An overlooked challenge in a circular bioenergy system. *Biomass and Bioenergy*, vol. 142 (2020), pp. 105713. Prieiga per: https://www.sciencedirect.com/science/article/pii/S0961953420302476.
4. DANISH, Aamar; KARADAG, Omer; BILIR, Turhan ir OZBAKKALOGLU, Togay. Valorization of biomass ashes in the production of cementitious composites: A comprehensive review of properties and performance. *Construction and Building Materials*, vol. 405 (2023), pp. 133244. Prieiga per: https://www.sciencedirect.com/science/article/pii/S0950061823029616..
5. STEENARI, B-M; KARLSSON, L. G. ir LINDQVIST, O. Evaluation of the leaching characteristics of wood ash and the influence of ash agglomeration. *Biomass and Bioenergy*, vol. 16 (1999), nr. 2, pp. 119–136. Prieiga per: https://www.sciencedirect.com/science/article/pii/S0961953498000701.

Influence of Silica Aerogel and Preheat Temperature on Thermomechanical Properties of Polyurethane

Muneeba RASHID[1], M. Hassan ATIQUE[1], Muhammad FAKHIR[1], M. Haseeb IQBAL[1], Kashif SOHAIL[2*], Asif JAMIL[1*]

1 Department of Chemical, Polymer and Composite Materials Engineering, University of Engineering and Technology, Lahore (New Campus), Pakistan

2 Ahmed Medix Pvt Limited, Lahore, Pakistan

** majamil@uet.edu.pk*

Abstract

This research investigates how the addition of silica aerogel and pre-heating temperature affect the thermos-mechanical behavior of Polyurethane (PU) foams. Conventional PU foams, despite their widespread applications, face limitations in their mechanical strength and thermal insulation. In this study, 3% by weight silica aerogel, known for its exceptional thermal insulation and lightweight nature, was incorporated into the PU formulation. Pre-heating temperatures of 30℃, 40℃ and 50℃ were employed to study their impact on the foam characteristics. The results have shown that preheat temperatures significantly affect mechanical durability and thermal insulation without compromising flexibility. These findings support the development of high-performance PU foams, tailored to the application in automotive, medical, and construction sectors.

Keywords: polyurethane foam, silica aerogel, thermal properties, mechanical properties, preheat temperature.

1. Introduction

Polyurethane (PU) foams are a versatile material widely used in various industrial applications due to their remarkable properties, including thermal properties, mechanical strength, and lightweight structure. Rigid and flexible PU foams are predominantly used in construction and furniture, and automobile cushioning applications because of their thermal insulation, comfort and durability. However, traditional PU foams often suffer brittleness, thermal degradation and poor mechanical strength, which limits their demanding durability and consistent performance under varying conditions for different applications [1].

To address these limitations, researchers have explored the incorporation of functional fillers, such as cellulose, rubber, latex, and starch, to enhance the thermal and mechanical performance of PU foams. Along with many other materials, silica aerogels also attracted the attention of scientists as they exhibit low thermal conductivity, low density, high porosity and superior mechanical reinforcement capabilities [2]. Research indicates that the integration of silica aerogel enhances the cell nucleation and delays the foam formation. Silica aerogel incorporation in PU foams has demonstrated that it enhances the insulation abilities of foams, particularly in applications where energy efficiency is the primary concern [3]. Several studies have indicated that adding silica aerogel 1-3% by weight in PU foams can significantly reduce the thermal conductivity while maintaining or enhancing the mechanical characteristics [3–5]. However, beyond this loading, opposite trends emerged due to disrupted hydrogen bonding, altered stoichiometry, increased viscosity-induced nanoparticle agglomeration, and poor nanoparticle distribution.

Other than adding the fillers, if we focus on the temperature, it is also an important factor that influences the properties of the PU foams. The study reveals that the preheating of polyol and isocyanate before mixing effects the foaming time, reaction kinetics and structural characteristics. According to the research, increasing the preheat temperature accelerates the foaming process, decreases foaming time, and increases the porosity. However, this may also result in a decrease in the mechanical strength of PU foams. Because higher temperatures can lead to lower density and a weak cell wall [6, 7]. Therefore, pre-heating temperature plays an important role in the formation and properties of the PU foams, but it is also important to control the preheat temperature to ensure that the foaming time is optimized, and final foam characteristics are not compromised.

Although studies have been done on the individual effect of these factors, i.e. preheat temperature and silica aerogel concentration on properties of PU Foams. However, the combined impact of these parameters on PU foams remains largely unexplored. Moreover, the excessive amount of aerogel can cause poor mechanical strength of PU foams [Kim et al,2021]. To achieve the desired balance between thermal and mechanical properties depends on the concentration of silica aerogel incorporated. The pre-heating temperature should also be controlled to get the desired properties. This study intends to explore the combined effect of 3% by weight silica aerogel incorporation and preheat temperature (30 ℃, 40 ℃, 50 ℃) on PU foams' thermal and mechanical properties.

2. Experimental Methodology

2.1. Materials

The materials used in this study were polyol (viscosity @ 25℃: 260 ± 40 cPs, density: 1.15 - 1.16 g/cm^3); diphenylmethane diisocyanate (brown liquid, viscosity @ 25℃: 170-250 mPa.S) and silica aerogel. The materials used in this work were of commercial grades and provided by Ahmed Medix (Pvt) Limited, Lahore, Pakistan.

2.2. Synthesis of Polyurethane Foam

This research focuses on the controlled temperature synthesis of silica-aerogel-modified PU, which requires the precise mixing of reactants and temperature control. The synthesis process began with the accurate measurement of chemical compounds, silica aerogel was later added to the isocyanate compound, 3% by weight of the solution, as depicted in Figure 1. The reactants are then heated by using a water bath up to the desired preheat temperature (30 ℃, 40 ℃, 50 ℃). This temperature is continuously monitored and maintained throughout the process.
After the component approaches the desired temperature, a homogeneous mixture is prepared by mixing the preheated components using an electronic mixer. This mixture was then poured into the mould (sizing 27000 cm^3) and allowed to be cured at room temperature for 2 hours. The wet Tare test was used to maintain quality control. It also helped to monitor the evaporation of isocyanate. This test includes the transferring of isocyanate in a beaker over multiple cycles and measuring weight loss. This test ensures the minimization of any inconvenience during the chemical process.

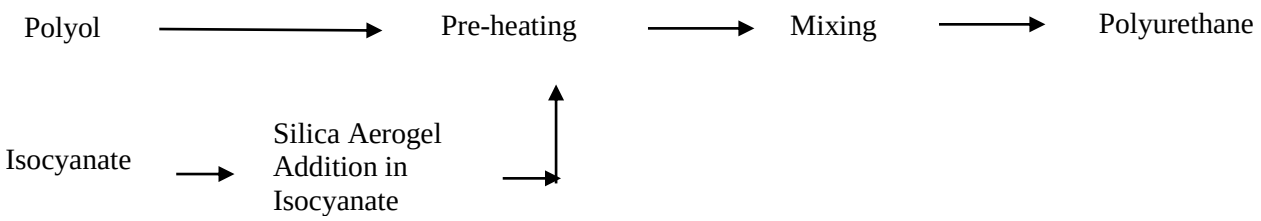

Fig.1. Block Flow diagram for the production of silica aerogel modified PU

The calculation for the required components for the production of silica-aerogel-modified PU was based on the desired volume of mixture and isocyanate to polyol ratio of 1.25: 1. The volume of the mold used was 27000m^3, using the isocyanate to polyol ratio of 55:45% for reaction as it is the best ratio that gives us the high mechanical strength [6]. Silica aerogel was incorporated 3% by weight of the solution.

Table 1. Mass composition of materials used

Component	**Total mass (%)**
Polyol	45.45
Isocyanate	55.56
Total Mixture	100
Silica Aerogel	3

2.3 Characterization of Polyurethane Foam

2.3.1. Free Rise Density

The free rise density of the PU foam is measured by ASTM D 7487. It is the ratio of foam weight to the cup volume. The sample foam was in the cubic shape, having dimensions 30*30*30 cm^3 and its weight was measured by a digital balance.

2.3.2. Thermal Conductivity

The thermal conductivity of silica-aerogel-modified PU foam was measured by ASTM D 5334 using a thermal conductivity meter by the needle probe method. The needle probe of the thermal conductivity meter was inserted into the sample, and electrical power was supplied for a specific time. The thermal conductivity of the sample was measured by thermal conductivity-time and temperature-time curve.

2.3.3 Mechanical properties testing

The compression force deflection test was carried out using a Universal Testing Machine (UTM). The sample had a surface area of 2500 mm^2 and was deflected up to 50% of its original thickness. The maximum stress and load were noted for each sample.

3. Results and Discussion

3.1 Free Rise Density of PU foam

Density is the most important parameter in the physical, mechanical and thermal properties of PU foams and has a vital influence on its applications. It is also significantly influenced by the temperature during processing. The results obtained are shown in Table 2 and reveal that with the increased preheat temperature, the density of the PU foams decreased. This variation in density is explained by how temperature affects the chemical reactions that take place during the foaming process [6]. Figure 2 states the chemical reaction involved in the process. Elevated temperature is expected to fasten the reaction processes, which could result in more CO_2 production and foam expansion, which would reduce the density [Juan Wang et al,2022].

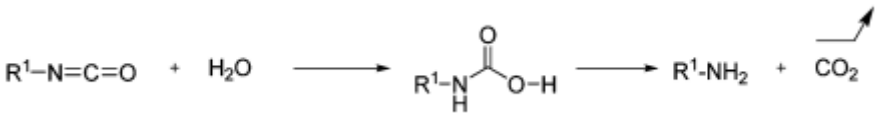

Fig. 2. Reaction of polyurethane [8]

The other factor that effects the foam density is the increased viscosity of the mixture at higher temperatures, which causes voids [7]. These factors affect the foaming process and the density of the PU foam.

Table 2. Free Rise density table

Temperature (□)	Foam weight (W_{foam})(g)	Volume of Cup (litre)	Density(kg/m³)
30	542	27	20.07
40	510	27	18.88
50	500	27	18.51

3.2 Thermal Conductivity of PU foams

PU foams are widely used in construction and panel production due to their thermal insulation property. That is why ensuring better thermal insulation silica aerogel integration at different pre-heat temperatures is noted, because it has high porosity and low density. The thermal conductivity results of PU foam are shown in Figure 3, and it was observed that upon increasing the pre-heat temperature, the thermal conductivity of the PU foams decreases, as the higher temperature ensures the better dispersion of silica aerogel, which decreases the thermal conductivity. Nastaran et al revealed that upon addition of silica aerogel, the thermal conductivity of the cyclopentane blown PU reduced from 0.0314 to 0.0268 W/(m K). Kim et al also observed the reduction in thermal conductivity of PU upon the addition of silica aerogel, comparable to the original PU. Kin et al also tell in their study that upon the addition of 3% silica aerogel, 0.03109 W/(m K) thermal conductivity was observed.

According to different studies, it can be considered to occur due to various factors, including the pre-heating temperature. Pre-heating temperature affects the cell structure, increases the porosity and decreases the density of the PU foam, which greatly influences the thermal conductivity [6]. This decline in thermal conductivity makes these foams effective thermal insulators for use in insulation and heat retention applications.

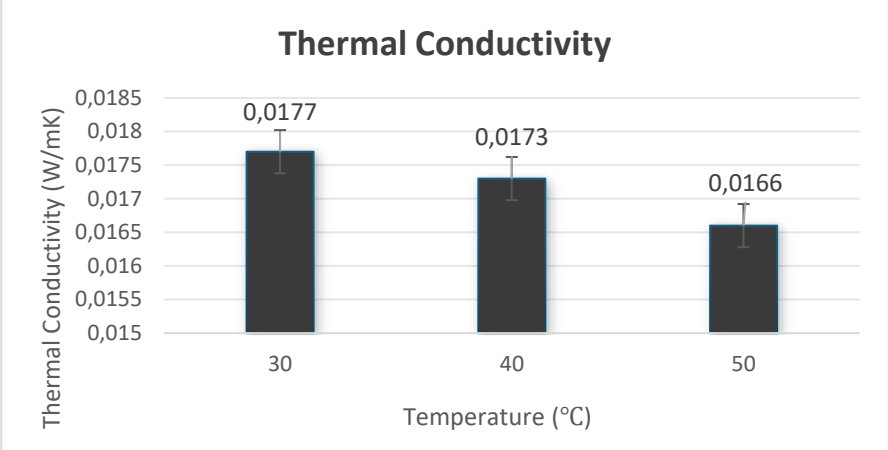

Fig.3. Thermal Conductivity of Silica aerogel modified PU (PU) foam

3.3 Compression Strength of PU foam

Compressive strength is the other most significant parameter in the PU foam selection, as it is used under different conditions and environments. It is analyzed by testing 3 different samples of each pre-heat temperature by up to 50% thickness deflection to determine the stress-strain relationship of the PU foams. The results of compression tests at different preheat temperatures are given in Figure 4. The higher mechanical properties were achieved by the addition of silica aerogel. Upon increasing the pre-heat temperature and isocyanate ratio, mechanical properties

such as tensile stress and compressive stress decrease up to a certain temperature and then increase. Results show that at lower pre-heat temperature, the compressive stress is maximum, whereas it decreases as the temperature increases [6]. The decrease in compressive stress is explained by the change in cell structure of the PU foam when the pre-heating temperature increases [7]. The dispersion and the pore generation also become the reason for decreased compressive strength with an increase in preheat temperature [4].

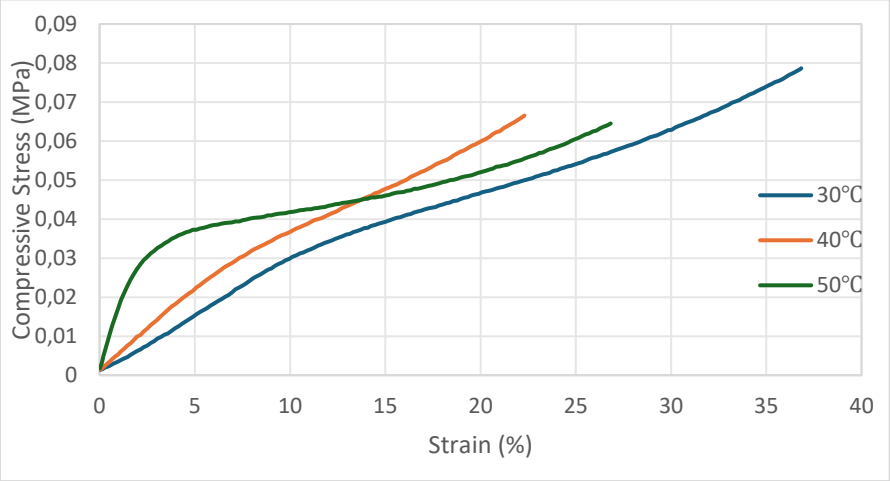

Fig.4. Compressive Stress of Silica aerogel modified PU foam

4. Conclusion

In this study, the effect of pre-heat temperature (30 °C, 40 °C, 50 °C) on density, thermal conductivity and compressive strength of the PU is investigated by integrating 3% silica aerogel. It was observed that upon increasing the preheat temperature, the density of the PU foam decreases due to rapid chemical reaction, which increases the foam expansion. The thermal insulation of the PU foams also increases with the increase in pre-heating temperature because of their cell structure and the addition of silica aerogel. The compressive strength of the PU tends to decrease with the increase in pre-heating temperature because of the pore formation and cell morphology at the higher temperature, and the presence of silica aerogel.

Acknowledgement: The author thanks Ahmed Medix (Pvt) Limited, Lahore for the financial and technical support for this study. The work is also supported by the National Research Program for Universities (NRPU), HEC Pakistan, No. 20-15709/NRPU/R&D/HEC/2021.

References

1. ATES, M., KARADAG, S., EKER, A. A., & EKER, B. Polyurethane foam materials and their industrial applications. *Polymer International*, 71(10) (2022), 1157-1163. https://doi.org/10.1002/pi.6421.
2. LEI, J., ZHENG, S., HAN, Z., NIU, Y., PAN, D., LIU, H., ... & SHEN, C. A brief review on the preparation and application of silica aerogel. *Engineered Science*, 30 (2024), 1214. https://doi.org/10.30919/es8c512.
3. NAZERAN, N., & MOGHADDAS, J. Synthesis and characterization of silica aerogel reinforced rigid polyurethane foam for thermal insulation application. *Journal of Non-Crystalline Solids*, 461 (2017), 1-11. https://doi.org/10.1016/j.jnoncrysol.2016.12.006.
4. KIM, J. H., AHN, J. H., KIM, J. D., LEE, D. H., KIM, S. K., & LEE, J. M. Influence of silica-aerogel on mechanical characteristics of polyurethane-based composites: Thermal conductivity and strength. *Materials*, 14(7) (2021), 1790. https://doi.org/10.3390/ma14071790.
5. BOZOGLU, D., DELIGOZ, H., ULUTAS, K., YAKUT, S., & DEGER, D. Structural and dielectrical characterization of low-k polyurethane composite films with silica aerogel. *Journal of Physics and Chemistry of Solids*, 130 (2019), 46-57. https://doi.org/10.1016/j.jpcs.2019.01.017.

6. OPPON, C., HACKNEY, P. M., SHYHA, I., & BIRKETT, M. Effect of Varying Mixing Ratios and Pre-Heat Temperature on the Mechanical Properties of Polyurethane (PU) Foam. *Procedia Engineering*, 132 (2015), 701-708. https://doi.org/10.1016/j.proeng.2015.12.510.
7. WANG, J., ZHANG, C., DENG, Y., & ZHANG, P. A Review of Research on the Effect of Temperature on the Properties of Polyurethane Foams. *Polymers*, 14(21) (2022), 4586. https://doi.org/10.3390/polym14214586.
8. DELEBECQ, E., PASCAULT, J. P., BOUTEVIN, B., & GANACHAUD, F. On the versatility of urethane/urea bonds: reversibility, blocked isocyanate, and non-isocyanate polyurethane. *Chemical Reviews*, 113(1) (2013), 80-118. https://doi.org/10.1021/cr3000873.
9. NICULESCU, A. G., TUDORACHE, D. I., BOCIOAGĂ, M., MIHAIESCU, D. E., HADIBARATA, T., & GRUMEZESCU, A. M. An updated overview of silica aerogel-based nanomaterials. *Nanomaterials*, 14(5) (2024), 469. https://doi.org/10.3390/nano14050469.
10. RIGACCI, A., MARECHAL, J. C., REPOUX, M., MORENO, M., & ACHARD, P. Preparation of polyurethane-based aerogels and xerogels for thermal superinsulation. *Journal of Non-Crystalline Solids*, 350 (2004), 372-378. https://doi.org/10.1016/j.jnoncrysol.2004.02.020.

Thermal Characterisation of Binder Constituents and Wax-Based Aluminium Metal Injection Moulding Feedstock for Micro-Metal Parts

Aliyu Alhaji ABDULLAHI[1,3]*, Imtiaz Ahmed CHOUDHURY[2,3], Azuddin MAMAT[3]

1 Department of Mechanical Engineering, Federal University of Technology, Minna, Nigeria

2 Department of Mechanical and Production Engineering, Ahsanullah University of Science and Technology, Dhaka, Bangladesh

3 Department of Mechanical Engineering, University of Malaya, Kuala Lumpur, Malaysia

** aliuaabdullah@futminna.edu.ng*

Abstract

Thermal decomposition behaviours of the binder constituents have been identified to influenced the quality of metal injection moulding (MIM) feedstock and sintered parts. This research investigates the thermal characterisation of the binder constituents and wax-based aluminium MIM feedstock. The binder system is composed of paraffin wax (PW) – 65 wt.%, high density polyethene (HDPE) – 30 wt.% and Stearic acid (SA) – 5 wt.%. While, the wax-based aluminium MIM feedstock is formulated with the proportions of the binder constituents and 99.999% pure aluminium powder at solid loading of 62 vol.%. Thermal characterisation technique employed for the evaluation of the binder constituents and wax-based aluminium MIM feedstock were differential scanning calorimetry and thermogravimetric analysis (TGA). Significant changes were observed for the binder constituents at various temperatures 45 ˚C and 60 ˚C (PW), 135 ˚C (HDPE), 75 ˚C (SA) and 45 ˚C, 60 ˚C, 135 ˚C (Wax-based aluminium MIM feedstock) on the DSC profiles. While TGA results revealed that binder constituents can be removed completely around 580 ˚C from the wax-based aluminium MIM feedstock. Thermal behaviour of the binder system established will be useful for setting suitable injection moulding temperature, development of the thermal profile(s) for debinding and sintering processes of the aluminium MIM micropart production.

Keywords: aluminium, metal injection moulding, paraffin wax, thermal characterisation, wax-based feedstock.

1. Introduction

Metal injection moulding (MIM) is an advanced powder metallurgy technique which integrate plastic injection moulding with powder injection moulding, originally developed for processing ceramic parts. This microfabrication technique has been utilized for various metal powder processing ranging from ferrous and non-ferrous metals [1–3]. However, aluminium MIM is still reported as empirical findings and industrial aluminium MIM feedstock is yet to be established as obtained for ferrous metals. This may be attributed to quite a number of issues which include: formation of thin oxide layer, low melting point, highly reactivity, difficulty in achieving full densification during sintering [4]. Despite these challenges encountered, processing of aluminium and aluminium alloys [4–8] by MIM technique is explored.

Formulation and mixing of powder-binder constituents is the first process of the technique, then follow by injection moulding, debinding and sintering processes. Therefore, success of the MIM for production of defect-free and high-quality sintered part; strongly depends on binder system. Binder systems developed for various metal powder injection moulding can be categorised as

follow: petroleum, green and/or water soluble [9–15]. The petroleum-based are further grouped into wax-based [7] and polymer-based [12] binder systems. Though a binder system usually contains two or more components that are carefully chosen for specific task. For instance, the polymer provides stability and strength required, stearic acid usually used as dispersant and wax is added to enhance flowability. The wax-based binder systems were found to be suitable for powder injection moulding technique [2]. Meanwhile, thermal behaviour of a binder system is investigated in order to determine suitable injection moulding temperature. In addition, it is used for development of suitable thermal profiles for debinding and sintering processes of the MIM feedstock. Therefore, this study examines thermal characterisation of binder constituents and wax-based aluminium MIM feedstock.

2. Materials and methods

The composition of the binder system and proportions of the constituents is as follows: paraffin wax (PW) – 65 wt.%, high density polyethene (HDPE) – 30 wt.% and stearic acid (SA) – 5 wt.%. Aluminium powder with 99.999% purity was used for the formulation of the feedstock. The wax-based aluminium MIM feedstock is formulated with the proportions of the binder constituents at solid loading of 62 vol.%. [2, 7]. Samples of the aluminium powder and binder constituents as received from the supplier are shown in Fig. 1, prepared samples of aluminium MIM feedstock are shown in Fig. 2. Physical properties of the binder constituents and aluminium powder are shown in Table 1. Density of the aluminium MIM feedstock is theoretically evaluated to be 2.0284 g/cm^3 at 62 vol.% solid loading.

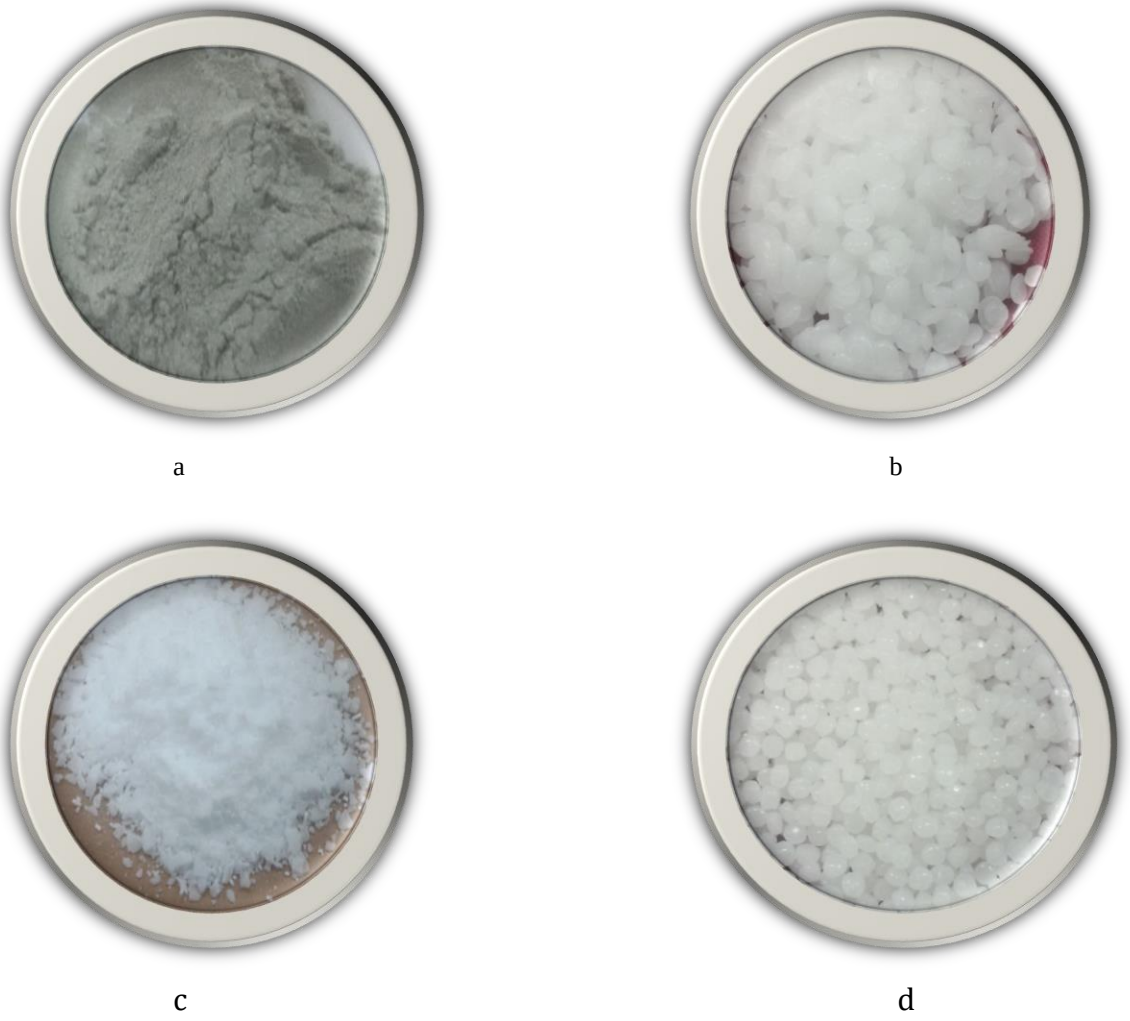

Fig. 11. Samples of the powder used and binder constituents as received: a – Al; b – PW; c – SA; d – HDPE

a b c

Fig. 2. Samples of the wax-based aluminium MIM feedstock as prepared: a – 3 mm pelletise; b – granulated; c – 8 mm extruded

Table 1. Physical properties of wax-based binder constituents and aluminium powder

S/N	Binder constituents/ powder	Density, g/cm^3	Chemical structural/ symbol
1	PW	0.92	C_nH_{2n+2}
2	HDPE	0.96	$(C_2H_4)_n$
3	SA	0.94	$CH_3(CH_2)_{16}COOH$ or $C_{18}H_{36}O_2$
4	Aluminium	2.70	Al

Thermal characterisation of the binder constituents and wax-based aluminium MIM feedstock samples was investigated using thermogravimetric analysis (TGA) and differential scanning calorimetry (DSC) [11, 15]. The DSC is used for the determination of the melting point of the binder constituents and aluminium MIM feedstock samples. About 15 mg of the samples were carefully weighed and sealed in aluminium crucibles of 40 µl, placed in the DSC chamber and set at 10 ˚C/min of heating rate, and readings were recorded from 30 ˚C to 210 ˚C for various samples of the binder constituents and aluminium MIM feedstock.

Furthermore, the thermal stability and decomposition rate of the binder constituents and aluminium MIM feedstock samples were investigated using TGA. About 20 mg of the samples each was carefully weighed and loaded into the TGA machine and the analysis was conducted under vacuum atmospheric conditions. The tests were conducted from 25 ˚C to 600 ˚C at a scanning rate of 10 ˚C/min.

3. Results and discussion

Results of the thermal characterisation of the binder constituents and aluminium MIM feedstock samples investigated are shown in Figs. 3 and 4. The DSC spectrum of the wax-based aluminium MIM feedstock shown in Fig. 3 reveal the homogeneity of the of powder-binder mixture as various peaks depict the presence of binder constituents (PW, HDPE and SA).

Similarly, the TGA of the binder constituents and aluminium MIM feedstock samples were investigated, results obtained are shown in Figure 4. It was observed that no residue of PW and SA were obtained at 575 ˚C. This indicates the suitability of multi-step debinding; involving solvent extraction to be followed by thermal debinding. In addition, it is evident from the TGA spectra that the wax-based aluminium MIM feedstock gain more weight from 525 ˚C; this phenomenon characterising unalloyed aluminium was reported by Schaffer and Hall [16]. Furthermore, some notable thermal characteristics of the binder constituents and aluminium MIM feedstock is hereby summarised in Table 2, based on DSC and TGA respectively.

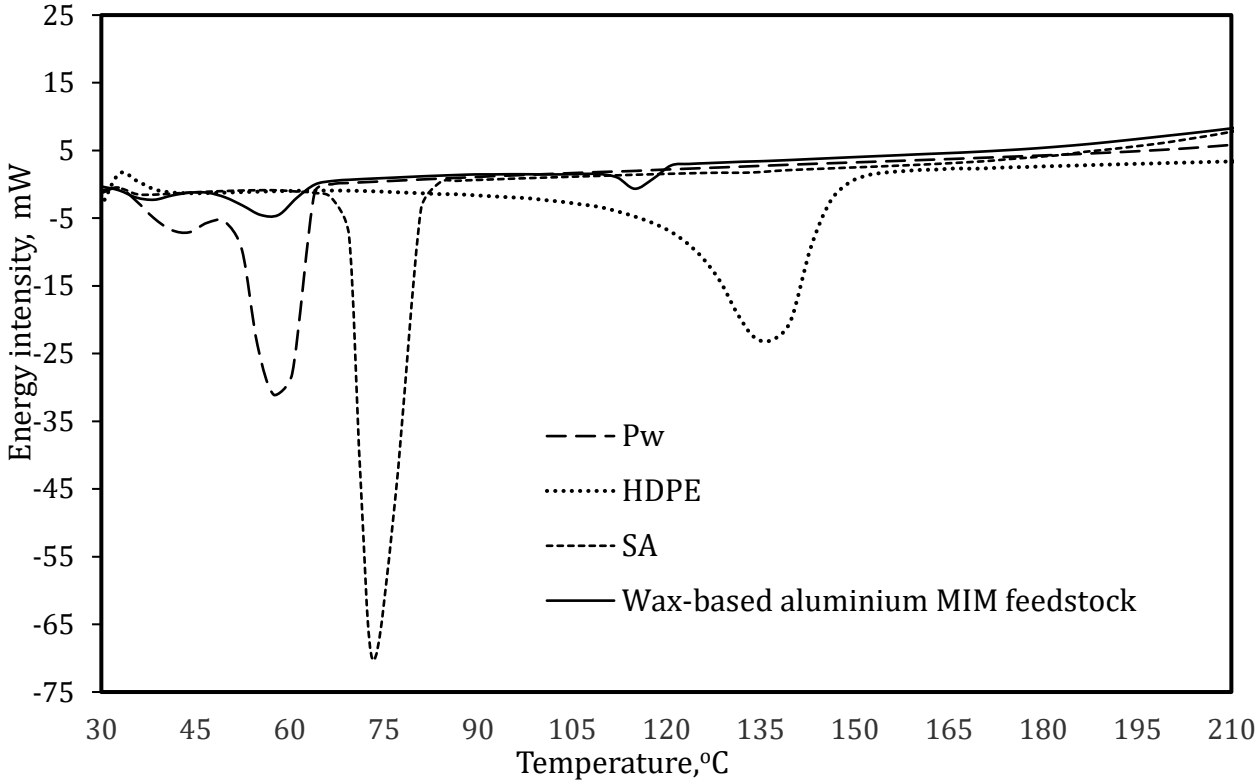

Fig. 3 DSC thermogram of the binder constituents and wax-based aluminium MIM feedstock

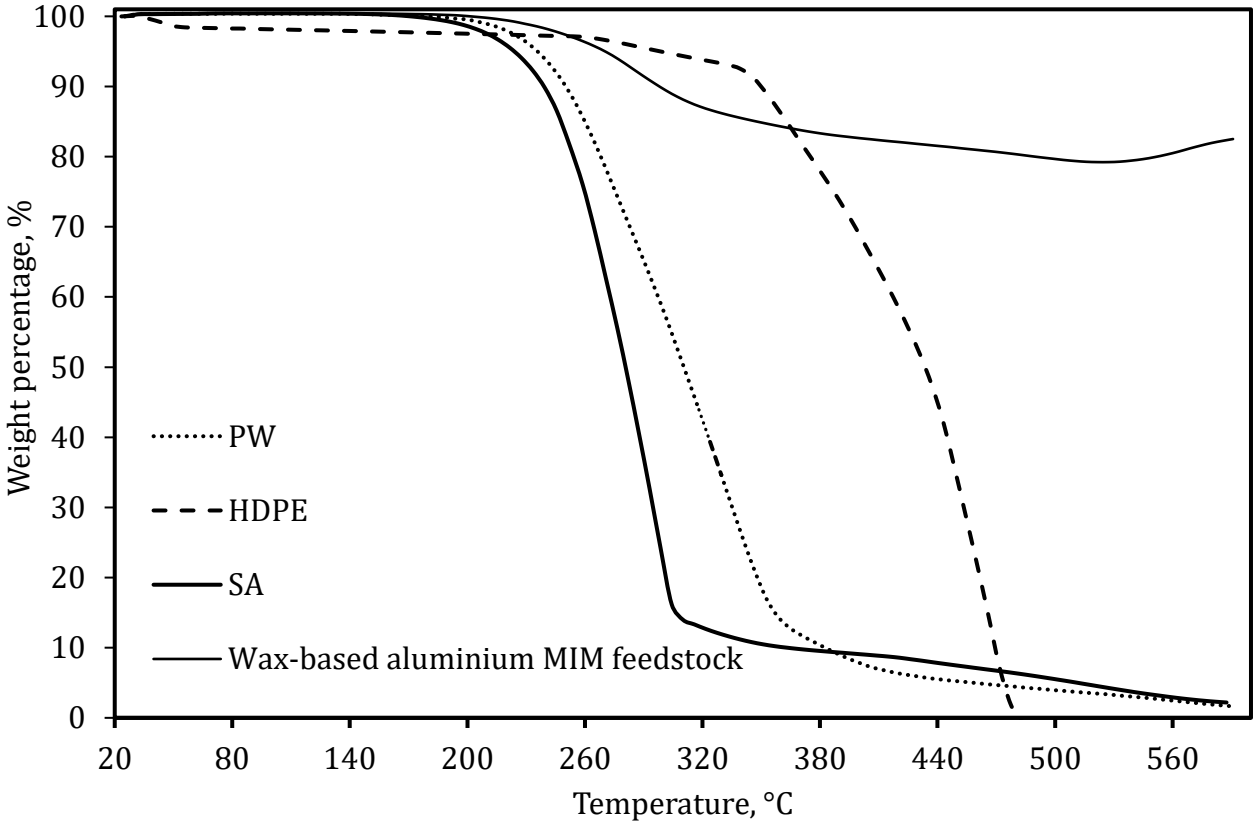

Fig. 4. TGA of the binder constituents and wax-based aluminium MIM feedstock

Table 2. Thermal characteristics of the binder constituents and wax-based aluminium MIM feedstock

S/N	Binder constituents/ feedstock	Melting Point, °C	Weight loss start temperature, °C	Rapid weight loss temperature, °C	Weight loss end temperature, °C
1	PW	58	182	242	481
2	HDPE	139	181	346	477
3	SA	72	180	233	580
4	Aluminium MIM feedstock	660	188	277	525

Comparative analysis of the results shown in Table 2, weight loss of the binder constituents began from 180 ˚C. Therefore, injection moulding temperature can conveniently be set slightly below this temperature within the range 150–179 ˚C. Furthermore, development of the combine or separate thermal profile(s) for debinding and sintering must consider at least a soaking/ holding time at 346–480˚C to burn-off the polymer constituents in order to produce carbon free parts.

4. Conclusions

The following conclusions are drawn:

1. Melting and degradation temperature range of the binder constituents were established.
2. Significant changes were observed for the wax-based aluminium MIM feedstock at various degradation temperatures of the binder constituents, indicating homogenous mixture of powder-binder.
3. The degradation temperature determined for the binder constituents and wax-based aluminium MIM feedstock will be useful in setting injection moulding temperature, development of the thermal profiles for debinding and sintering processes using this binder system.

References

1. GERMAN, R. M. Powder injection molding. New Jersey, USA, Metal powder industries federation, 1990. ISBN-13 978-0918404954.
2. GERMAN, R. M. Powder injection molding-Design and applications. Innovative materials solutions, USA, 2003. ISBN 0-9727642-0-8.
3. GERMAN, R. M. Progress in titanium metal powder injection molding. *Materials,* vol. 6 (2013), no. 8, pp. 3641-3662.
4. LIU, Z. Y., SERCOMBE, T. B., SCHAFFER, G. B. Metal injection moulding of aluminium alloy 6061 with tin. *Powder Metallurgy*, vol. 51 (2008), no. 1, pp. 78-83.
5. PINWILL, I. E., EDIRISINGHE, M. J., BEVIS, M. J. Fabrication of aluminium components by injection moulding: Role of carbon residue caused by removal of the organic vehicle. *Journal of Materials Science Letters*, vol. 10 (1991) no. 18, pp. 1107-1110.
6. JOYS, J., KASLER, R., RAMSEY, C. Aluminum MIM: New advanced powders and feedstock achieve higher densities. *Powder Injection Moulding International,* vol. 8 (2014), no. 2, pp. 75-79.
7. ABDOOS, H., KHORSAND, H., YOUSEFI, A. A. Torque rheometry and rheological analysis of powder-polymer mixture for aluminum powder injection molding. *Iranian Polymer Journal*, vol. 23 (2014), no. 10, pp. 745-755.
8. KATOU, K., MATSUMOTO, A. Application of Metal Injection Molding to Al Powder. *Journal of the Japan Society of Powder and Powder Metallurgy,* vol. 63 (2016), no. 7, pp. 468-472.
9. WEN, G., CAO, P., GABBITAS, B., ZHANG, D., EDMONDS, N. Development and design of binder systems for titanium metal injection molding: An overview. *Metallurgical and Materials Transactions a-Physical Metallurgy and Materials Science A,* vol. 44 (2013), no. 3, pp. 1530-1547.
10. LADO-Touriño, I. MERODIO-PEREA, R. G. Molecular Dynamics Simulations of Sustainable Green Binders for Metal Injection Molding. *Sustainability*, vol. 17 (2025), no. 5, pp. 2263-2279.
11. MOMENI, V., SHAHROODI, Z., GONZALEZ-GUTIERREZ, J., HENTSCHEL, L., DURETEK, I. SCHUSCHNIGG,

S., KUKLA, C., HOLZER, C. Effects of Different Polypropylene (PP)-Backbones in Aluminium Feedstock for Fused Filament Fabrication (FFF). *Polymers*, vol. 15 (2023), no. 14, pp. 3007-3025.
12. HANEMANN, T., WEBER, O. Polymethylmethacrylate/polyethyleneglycol-based partially water soluble binder system for micro ceramic injection moulding. *Microsystem Technologies-Micro-and Nanosystems-Information Storage and Processing Systems,* vol. 20 (2014), no, 1, pp. 51-58.
13. AGGARWAL, G., PARK, S. J., SMID, I., GERMAN, R. M. Master decomposition curve for binders used in powder injection molding. *Metallurgical and Materials Transactions a-Physical Metallurgy and Materials Science*, vol. 38 (2007), no. 3, pp. 606-614.
14. ZOU, H., CHEN, M., FU, Y., XIONG, H., ZHANG, l., ZHOU, K. Microstructure and mechanical properties of complex-shaped 7075 aluminium alloy prepared using modified polyoxymethylene-based feedstock. *Trans. Nonferrous Met. Soc. China*, vol. 34 (2024), no. 11, pp. 3862−3875.
15. LIM, K., HAYAT, M. D., JENA, K. D., ZHANG, W., Li, L. CAO, P. Interactions of polymeric components in a POM-based binder system for titanium metal injection moulding feedstocks. *Powder Metallurgy*, vol. 66 (2023), no. 4, pp. 355-364.
16. SCHAFFER, G. B., HALL, B. J. The influence of the atmosphere on the sintering of aluminum. *Metallurgical and Materials Transactions A*, vol. 33 (2002), no. 10, pp. 3279-3284.

Properties of Polyhydroxyalkanoate Copolymer and Shungite Composites

Domas GRIGALIŪNAS[1]*, Malik Daniyal ZAHEER[2], Deividas UMBRASAS[3], Rolandas DAUKŠEVIČIUS[2], Virginija JANKAUSKAITĖ[1]

1 Kaunas University of Technology, Faculty of Mechanical Engineering and Design, Kaunas, Lithuania

2 Kaunas University of Technology, Institute of Mechatronics, Kaunas, Lithuania

3 MB Matteraxis, Kaunas, Lithuania

** do.grigaliunas@ktu.edu*

Abstract

In this study, the effects of shungite as a functional filler on the thermal stability, electrical conductivity, and mechanical performance of bio-based poly(3-hydroxybutyrate-co-3-hydroxyhexanoate) are investigated. For this reason, the polymer was filled with 5–30 wt.% of shungite. The morphology of the shungite was studied by scanning electron microscopy. The influence of the filler on the thermal stability of the obtained compositions was evaluated using thermogravimetry. Moreover, the electrical and mechanical properties of the polymer with the addition of shungite were determined. Obtained results show that the presence of shungite significantly influences mechanical properties as well as electrical conductivity.

Keywords: poly(3-hydroxybutyrate-co-3-hydroxyhexanoate), shungite, electrical properties, thermal properties, mechanical behaviour.

1. Introduction

Finding sustainable bio-based alternatives to petroleum-based plastics has become a major global priority. Among these alternatives, polyhydroxyalkanoates (PHAs) have attracted a lot of interest because of their ability to biodegrade in the natural environment. To improve properties such as flexibility, impact resistance, and ease of processing, researchers have explored copolymers of poly(3-hydroxybutyrate) (PHB) with other PHA-type monomers. The most notable examples are poly(3-hydroxybutyrate-co-3-hydroxyvalerate) (PHBV) and poly(3-hydroxybutyrate-co-3-hydroxyhexanoate) (PHBH) (Fig. 1). PHBH in particular has better thermal stability, a wider processing range, and better mechanical properties due to its ability to combine rigid 3HB units and flexible 3HH components [1].

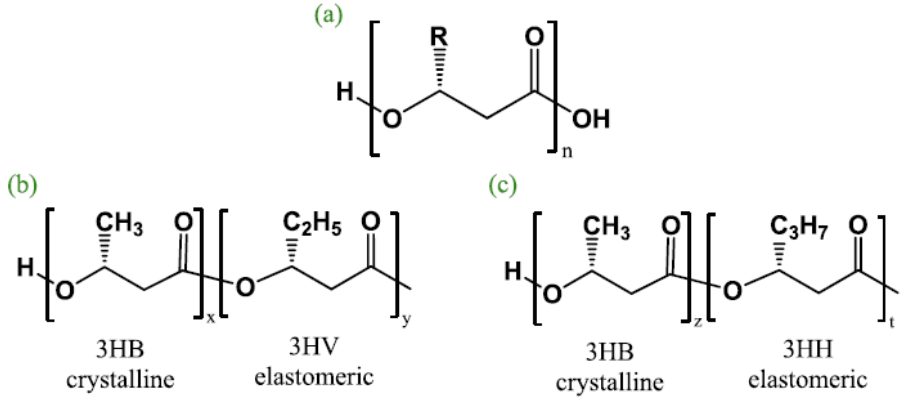

Fig. 1. Chemical structure of a general PHA (a), PHBV (b), and PHBH (c) [1]

PHBH is also gaining attention for its potential in electrical and electronic applications. It can achieve desirable thermal and dielectric properties, making it suitable for components like insulating layers, casings, and biodegradable electronic packaging. Its balance of rigidity and flexibility, combined with improved thermal stability, allows it to meet some of the functional requirements in the electronics sector, especially where environmental sustainability is a key consideration.

Carbon-based materials can be used to modify the electrical properties of PHBH. Shungite is a naturally occurring carbon-rich mineral primarily composed of amorphous carbon, with a unique structure that includes fullerenes – spherical carbon molecules [2]. It is predominantly found in the Karelia region of Russia and is classified based on its carbon content, ranging from low carbon shungite to elite shungite, which contains over 90% carbon. Shungite exhibits notable electrical conductivity, thermal stability, and adsorption properties, making it of interest for applications in water purification, electromagnetic shielding, and advanced composite materials. Shungite after fine grinding can be used as a filler for polymeric composites [3]. The aim of this study is to investigate the effects of shungite as a functional filler on the thermal stability, electrical conductivity, and mechanical performance of bio-based poly(3-hydroxybutyrate-co-3-hydroxyhexanoate).

2. Experimental

Fully biobased, water/soil-degradable and home-compostable semi-crystalline PHA copolymer poly(3-hydroxybutyrate-co-3-hydroxyhexanoate) (PHBH) Bluepha BP350 as powder feedstock (from Bluepha Co., Ltd, China) was used. Main properties of PHBH are $T_m \sim 133$ °C, $T_g = -2$ °C, $\rho = 1.2$ g/cm^3 and MFI = 10–15 g/10 min (at 165 °C and load 5 kg). Shungite (ShC) was kindly provided by UAB Matteraxis.

The PHBH compositions with shungite (PHBH/ShC) samples were prepared by extrusion using Noztek Touch single-screw extruder. The extrusion process of the same composition was repeated twice to obtain a homogeneous distribution of ShC. PHBH samples in the shape of filaments with a diameter of 1.8 ± 0.05 mm were moulded. The process parameters are listed in Table 1.

Table 1. Main parameters of the PHBH filament extrusion process

Extrusion parameter	1st extrusion	2nd extrusion
Extrusion zone (nozzle) temperature	135 °C	130 °C
Mixing zone temperature	130 °C	130 °C
Nozzle diameter	1.75 mm stainless steel	
Motor speed	8 RPM	6 RPM
Cooling type	Air cooling off (at filament exit)	

The electrical resistance of all the filament samples (L = 100 mm) was measured at room temperature using a current/voltage source and measurement unit (SMU) Keithley SourceMeter 2614B. Silver paint was applied in a 2-3 mm section at both ends of each filament, where the probes were connected to measure resistance. The filaments were dried at room temperature for at least 2 h before measurement. The silver painted areas were connected to probes of the Keithley SMU, using a four-point (Kelvin) method, with an applied voltage of 1 V for the resistance measurement. The four-point method eliminates the effect of parasitic contact resistance during measurement, providing accurate values of filament resistance. The resistivity of the filament was

calculated using equation: $\rho = R\frac{A}{L}$ (ρ is electrical resistivity, R is resistance, A is the cross-sectional area, and L is the length of the filament).
Scanning electron microscope (SEM) S-3400N (Hitachi, Japan) was used to analyze the ShC particles morphology. Thermogravimetric analysis (TGA) was performed using a Perkin Elmer instrument (TGA 4000) in a nitrogen atmosphere in the temperature range of 25 °C to 1000 °C at a heating rate of 10 °C/min. Tensile testing was carried out using an H10KT universal testing machine (Tynius Olsen, England) with a load cell of 250 N and a crosshead speed of 50 mm/min. The mechanical properties of the PHBH filament samples (l = 120 mm, ∅ = 1,8 ± 0.05 mm), such as yield strength, tensile strength, ultimate strength, elongation at break, were measured at room temperature using a self-tightening grip.

3. Results and Discussions

The SEM image of ShC particles and their size distribution is shown in Fig. 2. As can be seen particles exhibit irregular, angular to sub-angular morphologies, which is typical of mechanically ground materials. A broad size distribution of ShC particles is observed with size ranges from less than 0.5 μm to approximately 3–4 μm. Most particles fall in the 1–2 μm range and the calculated mean size is approx. 0.63 μm. Some areas suggest agglomeration, where smaller particles cluster around larger ones, probably due to van der Waals forces.

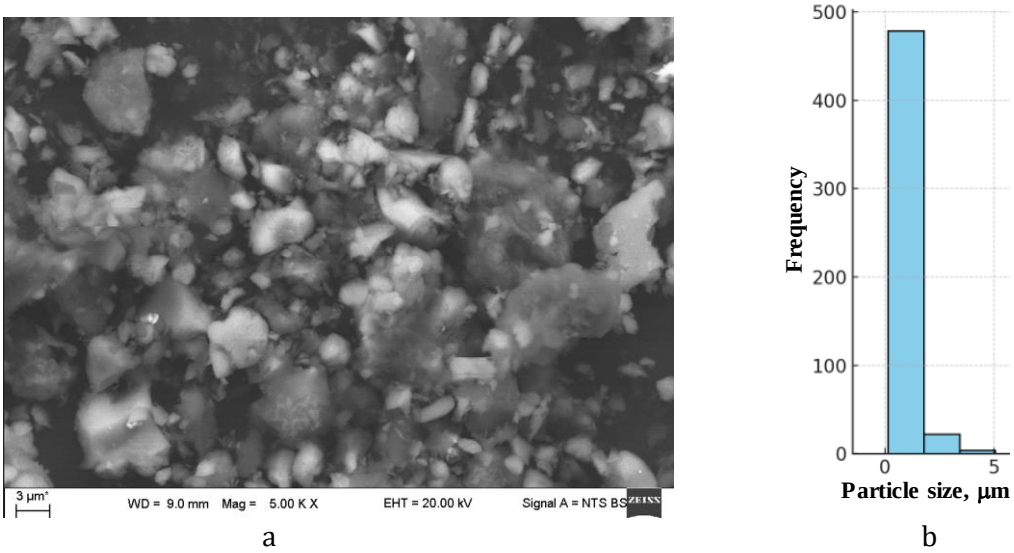

a b

Fig. 2. a – SEM image of ShC particles; b – their size distribution based on this image

The TGA curves show the relative mass change of PHBH samples of different composition as they are heated up to 1000 °C (Fig. 3). All samples exhibit a sharp and significant mass loss in the temperature range 250–310 °C, which corresponds to the thermal decomposition of the polymer. Only slightly higher resistance to thermal degradation can be observed in this case of PHBH+ShC(30%) composition. For example, a 30% mass loss occurs at 295 °C for this composition, compared to 285 °C for pure PHBH. The residue at 1000 °C increases with increasing ShC content. Only minimal mass remains in the case of pure PHBH, indicating complete decomposition and the absence of a thermally stable residue. This behaviour is characteristic of biodegradable PHBH, which breaks down into volatile products at relatively low temperatures (>300 °C). The highest residue is obtained in the case of PHBH+ShC(30%), reflecting the presence of thermally stable ShC.

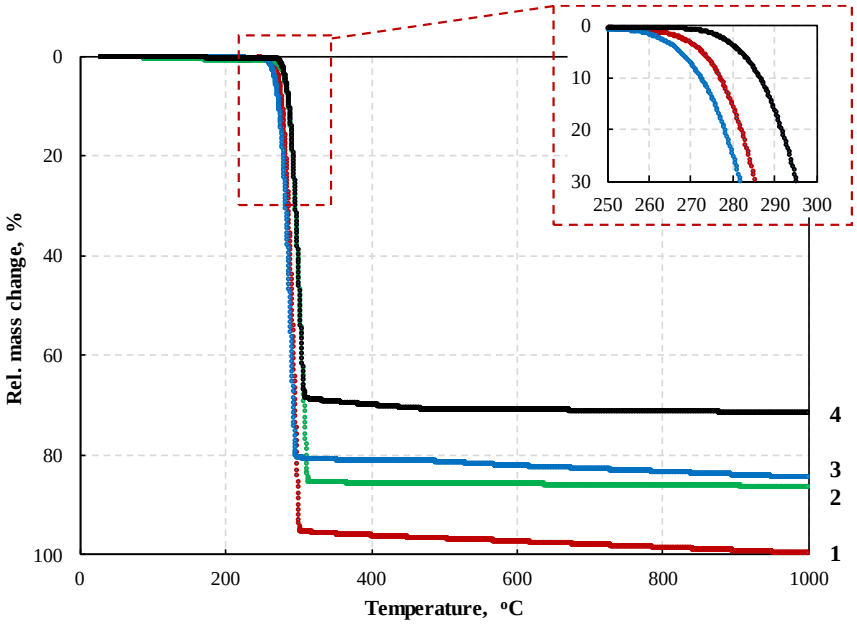

Sample	Residue, %
PHBH	0.3
PHBH/ShC(5%)	13.7
PHBH/ShC(15%)	15.5
PHBH/ShC(30%)	28.5

Fig. 3. TGA curves and residue of PHBH compositions after heating up to 1000 °C : 1 – pure PHBH; 2 – PHBH/ShC(5%); 3 – PHBH/ShC(15%); 4 – PHBH/ShC(30%)

Pure PHBH behaves like a typical insulating biopolymer (Table 2). The addition of ShC significantly reduces both resistance and resistivity. For example, at ShC(30%), the resistivity decreases by over 60% compared to pure PHBH. ShC, being a carbon-rich material, exhibits good electrical conductivity due to its graphitic and fullerene-like structures**.** However, even at 30% ShC filler loading, the PHBH composition achieves a conductivity of only $\sim 10^{-5}$ S/m, which remains several orders of magnitude lower than that of conductive polymers (10^{-2} – 10^{0} S/m) or metals ($\sim 10^{7}$ S/m).

Table 2. Electrical resistance and resistivity of PHBH compositions

Specimen	Resistance, GΩ	Resistivity, 10^5 Ω·m
PHBH	7.5	1.89
PHBH/ShC(5%)	7.2	1.83
PHBH/ShC(15%)	4.2	1.07
PHBH/ShC(30%)	2.8	0.71

Incorporating ShC into polymer matrix can modify mechanical properties, often reducing tensile strength while increasing flexibility [4]. As illustrated in Fig. 4a, the mechanical behaviour of PHBH changes markedly by incorporation of ShC used. While PHBH has a high ultimate tensile strength (~45 MPa) and high ductility at strains close to 70 %, PHBH/ShC composites fail at much lower strains (~5-10 %), indicating a loss of ductility. The stiffness of PHBH/ShC composites appears increased, especially for higher ShC content. The stress-strain curve for PHBH shows a distinct strain-hardening region after yielding, while for PHBH/ShC there is no evident strain-hardening behaviour, indicating a brittle failure.Even a low content of ShC(5%) decreases ultimate strength and strength at break of the PHBH composite in 30-40 % (Fig. 4b). However, the intensity of the change in strength with further increases in ShC content is not as significant.

The PHBH elongation at ultimate stress decreases twice (from 7.8 % to 3.9 %) when 30% of the ShC filler is loaded. Meanwhile, the elongation at break is reduced from 81 % to 12 % when 5 % ShC is added (Fig. 4c). Such mechanical behaviour of PHBH may be due to the relatively large size of ShC particles, their aggregation and poor distribution in the PHBH matrix, and defects formation, which may lead to the formation of defects.

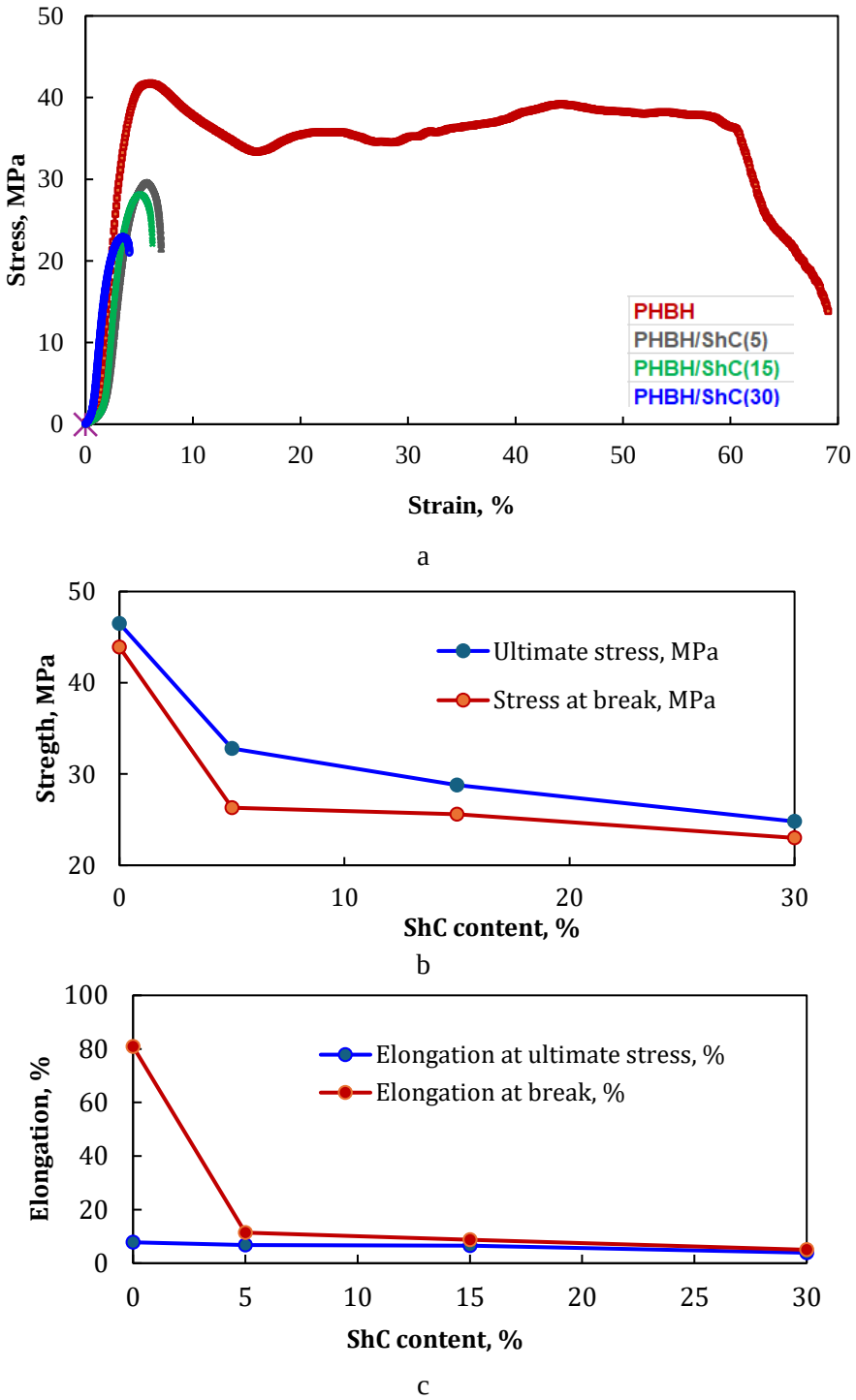

Fig. 4. Influence of the ShC content on the stress-strain behaviour (a), strength properties (b), and deformability (c) of PHBH

Thus, not only physicochemical peculiarities predetermine ShC filler behaviour in polymeric matrixes but also structural properties as particle size and polydispersity.

4. Conclusions

1. Shungite particles exhibit irregular, angular to sub-angular morphologies with average diameter of 1–2 μm.
2. PHA copolymer poly(3-hydroxybutyrate-co-3-hydroxyhexanoate) break down into volatile products at temperature higher than 250 °C and complete decomposes at ~300 °C.
3. Shungite, due to its graphite and fullerene structure, significantly reduces the resistivity and resistance of poly(3-hydroxybutyrate-co-3-hydroxyhexanoate). However, even at shungite content of 30%, the polymer composite exhibits low conductivity.
4. The addition of shungite reduces poly(3-hydroxybutyrate-co-3-hydroxyhexanoate) ductility and tensile strength, but slightly increases stiffness. The reduced mechanical properties are most likely due to the poor dispersion and aggregation of filler particles, and potential defect formation in the polymer matrix.

References

1. ERASLAN, Kerim *et al*. Poly(3-hydroxybutyrate-co-3-hydroxyhexanoate) (PHBH): Synthesis, Properties, and Applications – A Review. *European Polymer Journal*, 167 (2022), 111044; https://doi.org/10.1016/j.eurpolymj.2022.111044
2. OLEWNIK-KRUSZKOWSKA, Ewa *et al.* Comparison of How Graphite and Shungite Affect Thermal, Mechanical, and Dielectric Properties of Dielectric Elastomer-Based Composites. *Energies*, 15, (2022), 152; https://doi.org/10.3390/en15010152
3. ROZHKOVA, Natalia N. Shungite - a Carbon-Mineral Filler for Polymeric Composite Materials. *Composite Interfaces* 8 (2001), 3-4, 307–312. https://doi.org/10.1163/15685540152594767
4. BEKNAZAROV, Kanat *et al*. Influence of Kazakhstan's Shungites on the Physical–Mechanical Properties of Nitrile Butadiene Rubber Composites, *Polymers,* 16 (2024), 3370; https://doi.org/10.3390/polym16233370

Investigation of the Suitability of Compositions of Polyvinylpyrrolidone and Hyaluronic Acid Derivatives for Forming by Electrospinning

Ugnė ZASČIURINSKAITĖ*, Ingrida VENYTĖ, Laura GEGECKIENĖ, Virginija JANKAUSKAITĖ, Erika ADOMAVIČIŪTĖ

Kaunas University of Technology, Lithuania

** ugne.zasciurinskaite@ktu.edu*

Abstract

In this study, the effect of sodium hyaluronate (Na-HA) on the spinnability of the polyvinylpyrrolidone (PVP) solution was investigated. PVP-ethyl alcohol and aqueous Na-HA solutions were prepared by stirring at room temperature. Scanning electron microscopy was used to analyze the morphology of the electrospun mats, and the diameter distribution of the resulting nano- and microfibers was calculated. It was determined that Na-HA-modified PVP fibres exhibit a uniform, smooth, and free-of-distress structure.

Keywords: nano/microfibers, electrospinning, polyvinylpyrrolidone, sodium hyaluronate.

1. Introduction

The skin is the largest human organ, composed of three layers: the epidermis, the upper external part of the skin; the dermis, a middle layer that is formed from connective tissue and fibroblasts; and the hypodermis, which is composed of fatty connective tissue [1]. Skin is often damaged because of its size and exposure to the external environment, such as contact with chemicals, heat sources, mechanical tools, etc. Skin injuries vary from small epidermis abrasions to large wounds that can affect muscles, bones, or even nerves. Depending on the severity of the wound, it can be categorised as acute or chronic wounds, acute wounds tend to heal normally, while chronic wounds do not recover fast and remain in a stagnant healing phase [1]. Wound healing is a complex process that has four stages: haemostasis, inflammation, proliferation, and remodelling. Each stage is crucial as it prevents the patient from blood loss, infection, promotes skin regeneration, and the formation of a new tissue [2]. Disruption of these stages can lead to longer healing times or scarring; furthermore, untreated wounds can lead to infection, an increased risk of amputation, or the development of chronic wounds.

To obtain an optimal skin healing process, it is important to provide a moist wound healing environment, allow vapour exchange, and provide wound protection from external factors and bacterial contamination [2]. Conventional wound dressings do not provide a conductive environment for skin healing. Therefore, innovative wound-healing bands and technologies are explored. One of them is electrospinning, which enables the development of innovative non-woven medical materials [1]. Nanofibres obtained by electrospinning from biodegradable polymers display properties such as gas exchange and hydration, fluid absorption, and high biocompatibility [1]. Nanofibers resemble the extracellular matrix of healthy skin, supporting the adhesion and migration of fibroblasts and keratinocytes and promoting faster cell regeneration [2].

Polyvinylpyrrolidone (PVP) is a synthetic polymer known for its non-toxicity, biocompatibility, physicochemical stability, and surface activity properties. These characteristics make PVP widely utilized in the pharmaceutical industry, while electrospun PVP nanofibers have significant applications in drug delivery systems and tissue engineering, where they provide controlled release profiles and enhance cell attachment [3].

The addition of bioactive materials to the polymeric solution can provide beneficial properties to nanofibers for wound dressings. Biocompatible and non-toxic hyaluronic acid (HA) is a main component of the extracellular matrix of the skin. Because of its anti-inflammatory, antiproliferative, regenerative and moisturising properties, HA is widely applied in tissue engineering, wound healing and anti-cancerous treatment [4].

The aim of this study is to investigate the possibility of incorporating hyaluronic acid derivative, sodium hyaluronate, into polyvinylpyrrolidone-ethyl alcohol solution and to determine its effect on the polymer's spinnability.

2. Methods

The 10 wt% concentration of polyvinylpyrrolidone (PVP) solution was prepared by dissolving polymer powder (Mw=1,300 kDa) in ethyl alcohol (EtOH). The solution was mixed using a magnetic stirrer (MSH BASIC Heat Stirrer) at room temperature for 2 h.
Sodium hyaluronate (Na-HA) with a molecular weight ranging from 1,200 to 1,800 kDa was utilized in this study. A 0.5 wt% Na-HA solution was prepared by dissolving its powder in distilled water under continuous stirring for 30 min at room temperature. The prepared solutions were stored at 4 ° C until use. Before electrospinning, aqueous Na-HA solution was mixed with PVP solution in EtOH by magnetic stirring for 30 min. The compositions used for electrospinning are provided in Table 1.

Table 1. PVP compositions for electrospinning

Code of sample	Composition
PVP	10 g PVP + 90 g EtOH
PVP/Na-HA(0.55 wt%)	9 g PVP + 81 g EtOH + 0.05 g Na-HA + 9.95 g H_2O
PVP/Na-HA(1.25 wt%)	8 g PVP + 72 g EtOH + 0.1 g Na-HA + 19.9 g H_2O

Nonwoven mats from the solutions were created by using a rotating roller electrospinning machine “NanospiderTM“ (Elmarco, Czech Republic). The duration of the electrospinning process for each specimen was 5 min at an operating voltage 60 kV.
A scanning electron microscope (SEM) S-3400N (Hitachi, Japan) was used to describe the electrospun mats' morphology. The diameter of nano/microfibers (50 measurements) was calculated from SEM images (×10000) using the “Image J” software.

3. Results and Discussions

SEM images of electrospun mats from PVP nanofibers with and without the addition of Na-HA are shown in Fig. 1. It is visible that in all cases, the PVP nanofibers are randomly distributed without clear orientation. Surfaces of the nanofibers are smooth and uniform, with no visible defects such as breaks, tears, beads or droplets. This indicates that the nano-mats were formed during a stable electrospinning process, with appropriately selected parameters and suitable compositions.

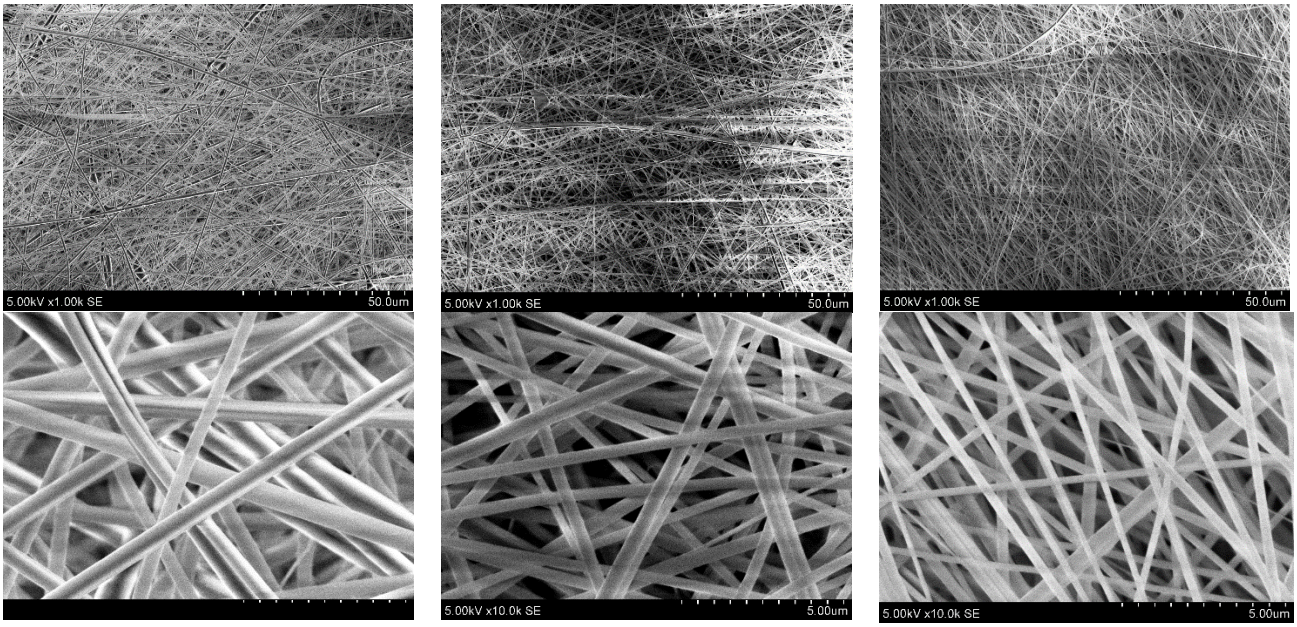

a b c

Fig. 1 SEM images of electrospun PVP mats with varying compositions: a – pure PVP; b – PVP/Na-HA(0.55 wt%); c – PVP/Na-HA(1.25 wt%). Images were captured at magnifications of ×1,000 and ×10,000

From Figure 2, it is evident that the majority of both pure PVP and PVP/Na-HA fibers fall within a relatively narrow diameter range of 100-200 nm. In the case of pure PVP the majority of fibers fall into the 151–200 nm range. The addition of Na-HA leads to a reduction in fiber diameter, shifting the distribution toward finer fibers. The predominant diameter range of PVP/Na-HA fibers is 101–150 nm; however, a significant proportion also falls within the 51–100 nm range, which is well within the nanometre scale. No significant effect of Na-HA content (0.55 % or 1.25 %) on the nano/microfibers diameter distribution was observed.

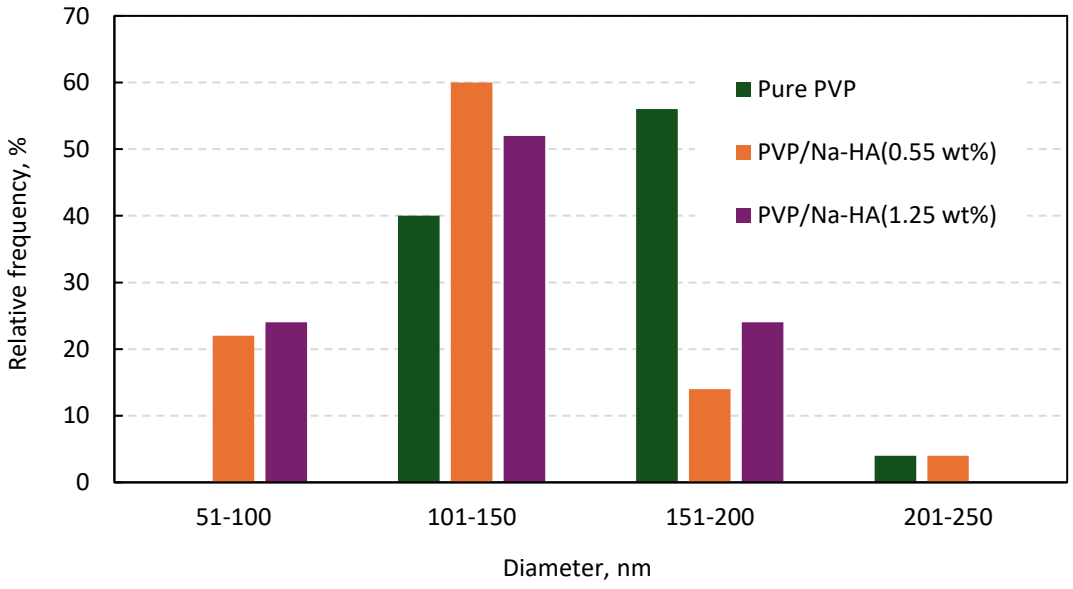

Fig. 2 Composition dependence of PVP nano/microfibers diameter distribution

The influence of Na-HA on fibers diameter may be attributed to changes in solution viscosity, conductivity, or surface tension, influencing the electrospinning process. On the other hand, the

electrospun PVP fibres of all samples remained uniformly thin and smooth, with no observable defects. Such a finely structured and densely packed surface is likely to enhance cell adhesion and proliferation, thereby contributing to improved biocompatibility of the polymer with skin.

4. Conclusions

1. Low content of sodium hyaluronate can be effectively incorporated into polyvinylpyrrolidone electrospinning solution.
2. The incorporation of sodium hyaluronate into polyvinylpyrrolidone resulted a decrease in nanofiber diameter, while the fibers remained smooth, uniform, and free of defects, indicating a stable electrospinning process.

References

1. BOMBIN, Adrian D. Juncos; DUNNE, Nicholas J.; MCCARTHY, Helen O. Electrospinning of natural polymers for the production of nanofibres for wound healing applications. Materials Science and Engineering: C, 2020, 114: 110994.
2. AKHMETOVA, Alma; HEINZ, Andrea. Electrospinning proteins for wound healing purposes: opportunities and challenges. *Pharmaceutics*, 2020, 13.1: 4.
3. LUO, Yu, et al. Multifunctional role of polyvinylpyrrolidone in pharmaceutical formulations. AAPS PharmSciTech, 2021, 22: 1-16.
4. YASIN, Aqeela, et al. Advances in hyaluronic acid for biomedical applications. Frontiers in Bioengineering and Biotechnology, 2022, 10: 910290.

PRODUCTION TECHNOLOGIES AND ENGINEERING

Study of Surface Quality in Additive Manufacturing

Rahul Siddharth WASE*, Inga SKIEDRAITĖ

Kaunas University of Technology, Kaunas, Lithuania

** rahul.wase@ktu.edu*

Abstract

Surface roughness tends to have a significant influence on the mechanical performance, functionality and aesthetics of components produced by additive manufacturing (AM). Although there is an extensive amount of research on process parameters' effects on surface quality, far fewer studies address how a component's geometry interacts with these parameters across different additive manufacturing processes. This paper investigates the correlation between surface roughness, geometry and process parameters on selected additive manufacturing technologies such as fused deposition modelling (FDM), stereolithography (SLA), and selective laser sintering (SLS). Through a systematic review and analysis of published experimental data in various studies, this study is trying to identify the parameter-geometry correlations and their influence on surface finish. Key findings reveal that geometric orientation has significant effects on the surface quality in FDM and SLS due to layer-stepping and balling phenomena, while SLA shows a greater consistency due to its photopolymerization mechanism. This paper shows that geometry-dependent process optimisation is critical for achieving targeted surface quality. It also highlights the need for optimised design stage considerations, where geometry and parameters are not treated separately but optimised together with each other for functional surface performance. These findings provide strong insights into the foundation for future work in predictive modelling and closed-loop control systems, enabling more accurate surface finish control in AM applications. This research supports general AM practitioners in making geometry-aware, parameter-optimised decisions to reduce post-processing needs and improve part quality directly from the build process.

Keywords: additive manufacturing, process parameters, surface quality, geometry, non-metal additive manufacturing.

1. Introduction

Additive Manufacturing (AM) has transformed the approach to production and prototyping of components in major sectors such as aerospace, medical, automotive, and consumer industries. This has been due to the ability to produce complex structures, thus providing flexibility and freedom in the design of new products. However, there are still certain issues with this technology which make it difficult to adopt widely and replace traditional manufacturing. One of the critical factors influencing the acceptance of this technology is surface quality, which directly impacts the functionality, mechanical performance, aesthetic quality, part performance and even influences the production cost, which adds up due to post-processing. High surface roughness can result in premature mechanical failures, reduced aerodynamic efficiency, or poor biocompatibility [1]. Although considerable research has been done investigating the influence of various AM process parameters on surface roughness, most studies focus narrowly on single-technology, parameter-specific, or flat geometry scenarios. However, in practical applications, diverse geometric features, such as curved, angled or intricate details, are observed. Each feature is influenced by

process parameters in its own way [2]. Thus, a lack of understanding about how geometry influences the parameter roughness relationship remains a significant gap.

Addressing this knowledge gap, this paper examines the correlation between surface roughness, geometry and influential process parameters across the three most used polymer-based AM methods - fused deposition modelling (FDM), stereolithography (SLA), and selective laser sintering (SLS). Using secondary data sourced and cited from existing experimental studies, the analysis tries to identify critical geometric influences and parameter sensitivities, aiming to establish foundational knowledge to enhance the predictability of surface roughness of an AM-produced part. This study integrates geometry-dependent observations with parameter optimisation, aiming to provide valuable guidance for general additive manufacturing (AM) practitioners seeking improved control of surface finish during the design and manufacturing stages. Furthermore, the insights can serve as the basis of future research into predictive modelling and closed-loop control strategies for surface roughness in AM.

2. Research Methodology

2.1. Research Approach

This study uses a secondary data analysis approach, sourcing data exclusively from peer-reviewed publications and reputable experimental studies available in scientific databases. By systematically reviewing and extracting data, this method ensures the validity and reliability of the findings while avoiding unsubstantiated claims. Data was collected in a systematic literature review (SLR) using targeted keyword searches ("surface roughness," "geometry effects," "additive manufacturing process parameters," "FDM," "SLA," "SLS") across reputable databases such as Science Direct, Research Gate, Google Scholar, IEEE Xplore, MDPI, Web of Science etc. Only studies providing clear and detailed experimental conditions and numeric roughness values (*Ra*) were considered. Data was organised according to process, geometry and parameter variations.
The criteria for the selection of the study include:

1. report of *Ra* values for specific geometry and process settings;
2. involve non-metal polymer materials (e.g., PLA, PA12, PA11, resin);
3. at least one of the selected process parameters;
4. must clearly describe geometry (flat, angled, or curved).

2.2. AM Process and Material Selection

Out of the several AM techniques, fused deposition modelling (FDM), stereolithography (SLA), and selective laser sintering (SLS) are the most adopted in the industry and display unique mechanisms of surface formation [1]. These three processes utilise different methods to fabricate individual layers of a part: FDM processes thermoplastic filament through a heated nozzle; SLA uses ultraviolet light to cure layers of photopolymer resin; and SLS utilises a laser to sinter powdered polymers. All these methods operate using different forms of materials and methods in which energy is given to the material, thus rendering different levels of surface roughness. The technologies were chosen based on their high utilisation in industries, thus paying special attention to the influence of process parameters, geometry, and surface quality [2].

2.3. Geometric Considerations

Recognising that geometry significantly affects AM surface roughness, this study specifically investigates three geometric orientations commonly encountered:

- *Flat surfaces (horizontal and vertical)*: baseline roughness measurement, least affected by stair-stepping anomalies.
- *Angled surfaces* (45° and 90° inclinations): typically exhibit pronounced stair-step effects, especially in FDM and SLS.
- *Curved geometries*: used to analyse complexity-driven roughness variation, critical in functional or aesthetic components.

These categories allow a comprehensive understanding of geometry's influence on parameter-roughness relationships [3].

2.4. Process Parameters Selection

Surface roughness for additive manufacturing (AM) differs in each printing technology, including fusion deposition modelling (FDM), stereolithography (SLA), and selective laser sintering (SLS). In the case of fused deposition modelling (FDM), some of the important parameters are layer height, nozzle temperature and print speed. Thicker layers tend to produce rougher surfaces thanks to more noticeable stair-stepping effects, while thinner layers produce smoother finishes at the cost of longer print times. The temperature of the nozzle affects the thermoplastic filament's flow and adhesion; higher temperatures are typically better for layer fusion and surface quality. In the same manner, slower print speeds allow better mixing and can lower surface roughness due to better control of filament deposition [5]. Smoothness in stereolithography (SLA) is defined by the layer thickness, exposure time and resin viscosity. Thinner layers provide better vertical resolution and smoother surfaces, and exposing each layer for the correct amount of time is a must, too little light and layers won't cure, too much and rough or over-cured textures are observed. The viscosity of the resin is also a factor; lower viscosity aids flow and uniform polymer curing, and therefore, better surface finish [6]. In selective laser sintering (SLS), surface roughness is mainly determined by three factors, namely, laser power, scan speed, and particle size of the powder. Proper settings achieve sintering without too much energy density that can damage or overheat the surface. Generally, finer powders produce smoother parts because they pack more densely and behave differently during melting, but they need exacting handling to prevent partial sintering (the unwanted bonding of particles) or powder balling [7]. Experimental studies consistently identify these parameters as influential factors on the resulting surface roughness and quality of finished surfaces across all three technologies. The following Table 1 shows the rationale for the selected parameters, based on the studied literature.

Table 1. Rationale for Parameter Selection based on Literature [5-7]

AM Process	Parameter	Justification
FDM	Layer Height	Dominant stair-step effect
FDM	Nozzle Temp.	Influence on filament flow and bonding
FDM	Print Speed	Controls cooling rates and surface consistency
SLA	Layer Thickness	Directly related to surface step height
SLA	Exposure Time	Controls the resin curing depth
SLA	Resin Viscosity	Influence on uniformity of flow
SLS	Laser Power	Determines sintering completeness
SLS	Scan Speed	Controls energy absorption
SLS	Powder Size	Influences powder bed packing

2.5. Surface Roughness Metrics and Measurement

In general, surface roughness is expressed as the average roughness value *Ra*, which is a commonly utilised means by which the texture of a manufactured surface can be assessed. The measurements for this study were obtained from previously published experimental studies

utilising standard measurement techniques. Out of these, contact profilometry is one of the most popular methods, because of its precision and applications in measuring linear roughness on flat and angled surfaces. It works by mechanically following the profile of the surface with a stylus and gives accurate *Ra* values [7]. Optical profilometry and microscopy are used for more complex geometries, especially for curved or detailed surfaces. They are, therefore, non-contact and allow for high-resolution surface mapping on surfaces that cannot be physically disturbed, such as delicate or fine-featured parts [8]. These widely accepted procedures used in several studies provide a uniform basis for comparative surface roughness analysis.

3. Discussions

3.1. Geometric Influence on Surface Roughness

The reviewed literature demonstrates a clear relationship between part geometry and surface roughness across FDM, SLA, and SLS. During cross comparison, it is observed that the surface roughness *Ra* increases significantly as the geometric orientation diverges from the vertical or horizontal plane; the stair step phenomenon is the result of this deviation. This can be theoretically quantified using the stair-step height formula [4]:

$$h_s = L \times \sin(\theta) \tag{1}$$

where: h_s - stair step height; L - layer thickness; Θ - surface angle relative to the horizontal plane
Conversely, surface roughness in all three AM processes is significantly affected by geometric orientation. In FDM, roughness varies from 7.95 μm (flat) to 12.94 μm (curved), with 10.5 μm found at 45° due to the stair-stepping phenomenon, which occurs due to material deposition [3]. The increase in layer thickness with SLA is more gradual as it transitions from 0.81 μm (horizontal) to 1.2 μm (vertical) based on the incidence of light and depth of local resin curing affected by photo-polymerisation homogeneity [6]. In SLS, *Ra* values vary from 6.3 μm (flat) to 7.8 μm (curved), due to anisotropic melting of the powder and energy dispersion on slopes [7]. These differences prove that orientation on a single face has a substantial impact on Ra and should be taken into account when the process is customised as per geometry [4].

3.2. Influence of Key Process Parameters

Fused deposition modelling (FDM). The main key process parameters that closely influence surface roughness in FDM are layer height L_h, nozzle temperature T, and print speed S. This is reflected as it can be described from research introducing an empirical model to estimate the surface roughness in extrusion-based processes, which is written as [3]:

$$Ra = k \cdot (L_h)^a \cdot (S)^b \cdot e^{(c/T)} \tag{2}$$

where *k, a, b*, and *c* are experimentally determined constants.

This theory was experimentally confirmed by a study that reported *Ra* values decreasing nearly 50% from this trend, with a reduction in layer height. From the data obtained in a 2020 study, the best theoretical temperature for the nozzle for the PLA material, which maintains the optimal viscosity with the least roughness while maintaining the most tasteless filament flow with good layer adhesion, is 205 °C [9]. Fused deposition modelling (FDM) exhibited the most sensitivity to the geometry and orientation of the samples, owing predominantly to the stair-stepping phenomenon induced by the layer-by-layer extrusion and deposition process fundamental to FDM. In FDM, layer height had the most effect, with reduced parameter values greatly improving *Ra* but also affecting cost and time of production [5].

Stereolithography (SLA). In SLA, both layer thickness and exposure time E_t have a major influence on surface roughness. The cure depth C_d in SLA obeys the Beer-Lambert law according to Jacobs [10]:

$$C_d = D_p \cdot In\ (E_{max}/E_c) \tag{3}$$

where: C_d - depth of cured resin; D_p - penetration depth of the resin; E_{max} - peak exposure energy provided; E_c - critical exposure energy for resin curing.

This model reveals how overexposure ($E_{max}>E_c$) may lead to overcuring of resin, which increases roughness. Underexposure leads to incomplete polymerisation, which increases roughness as well. The 2023 experimental study highlighted the necessity for value optimisation of the operating parameters for energy exposure responsible for obtaining the appropriate part surface quality, as well as the required cure depth of the SLA printed parts [6]. Although SLA was not affected by a broad orientation of the specimen, SLA still consistently showed the lowest Ra due to the photopolymerization mechanism affecting its geometry. In SLA, the balance between exposure energy and resin penetration is essential to avoid overcuring or undercuring of resin, reducing the stair-stepping effect [10].

Selective laser sintering (SLS). The parameters like laser power P, scan speed V, hatch spacing h, layer thickness t, etc, mainly affect the surface finish in polymer-based SLS. A vital factor is the energy density E_d deposited in the powder bed, and follows the relationship [11]:

$$E_d = \frac{P}{V \times h \times t} \tag{4}$$

Since the surface finish in SLS determines the functionality, laser power, scan speed, layer thickness, and hatch spacing must be controlled precisely for an optimal surface finish. The correlation between proper power and scan speed is crucial - the right amount leads to the desirable effects of fusion and smoothness, whilst too much can result in polymer degradation or warping, whilst too little leads to a lack of complete sintering. Thinner layers reduce the average Ra values, but raise the build time per part, while thicker ones do the opposite by increasing the stair step effect but allowing for much faster print speeds. When hatch spacing is not ideal, it may cause surface defects or weak bonds of the scan lines. A well-balanced array of these parameters ensures the complete melting without overheating, yielding a better surface quality for the polymer SLS parts. Surface quality in SLS was moderate, affecting the real roughness by powder features and energy density in the area [7].

3.3. Comparative Analysis of AM Processes

Surface smoothness achieved through SLA is the smallest among the three AM processes studied, owing to its photopolymerization mechanism and limited mechanical interactions, which results in Ra values varying from 0.8 to 1.2 μm [6]. The finish with FDM is the roughest, with a *Ra* between 7.9 and 12.9 μm, because of the layer-by-layer extrusion process and the stair-stepping of slopes [5]. Considering SLS, surface roughness indicates an intermediate value, usually in the range of 6.3 to 7.8 μm, in correspondence with the powder fusion quality, type and size of the microphone and laser parameters [7]. These differences are very important things to consider when choosing an AM process, according to the surface finish, such as the particulate size allowed for the final application. Table 2 and Figure 1 show a graph of surface roughness by geometry and AM processes.

Table 2. Surface Roughness by Geometry and AM Process

AM Process	Geometry	Surface Roughness (Ra, µm)	Material
FDM	Flat	7.95	PLA
FDM	Angled	10.5	PLA
FDM	Curved	12.94	PLA
SLA	Flat	0.81	Resin
SLA	Angled	1.2	Resin
SLA	Curved	0.98	Resin
SLS	Flat	6.3	PA11
SLS	Angled	7.0	PA11
SLS	Curved	7.8	PA11

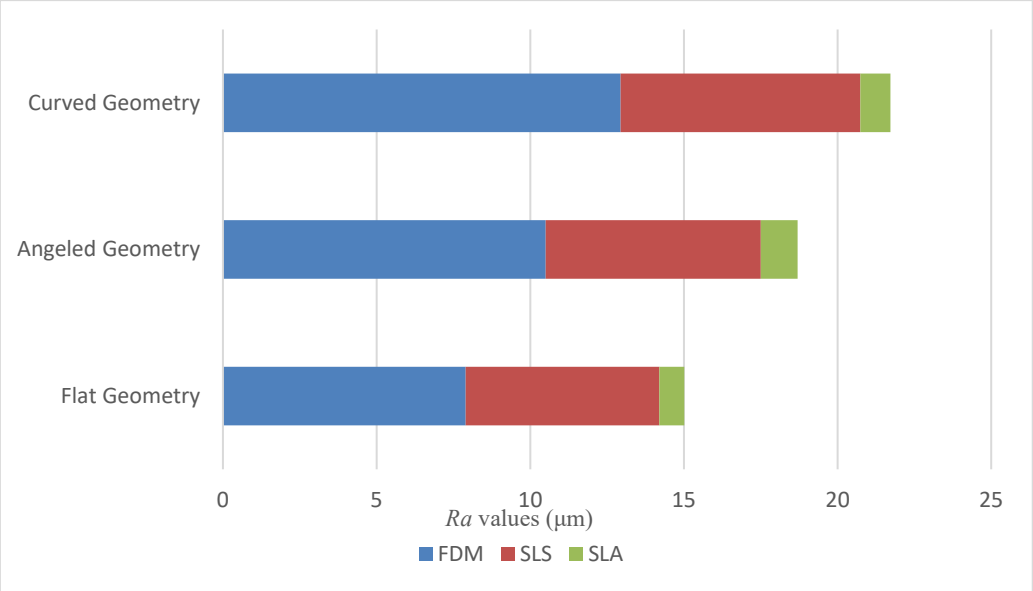

Fig. 1. Surface roughness by geometry and AM processes

4. Conclusions

1. The roughness of the surface in the AM is geometry-dependent, and it increases especially on angled or curved surfaces for FDM, SLA, and SLS processes.
2. FDM exhibits the most variable roughness due to the stair-stepping effect, while SLA has the lowest roughness, both on average and peak roughness, while SLS manages to give an acceptable range of surface roughness with values lying between FDM and SLA.
3. In the FDM process, layer height has the most significant effect on *Ra*, while the exposure time and layer thickness dominate the surface quality in SLA, and the laser power, scan speed, and powder size are the main factors for SLS.
4. Lower layer height in FDM, exposure parameters optimisation for SLA and fine powders with balanced energy density in SLS are successful approaches to reducing the *Ra*.
5. Stair-stepping is recognised as the dominant surface roughness factor for all non-flat geometries in all AM methods, implying that part orientations should be considered in design.
6. Accurate predictions of the AM surface roughness rely on a simultaneous consideration of process and geometry parameters, providing a solid foundation for further developments in predictive models and control strategies.

References

1. SYRLYBAYEV, Daniyar; SEISEKULOVA, Aidana; TALAMONA, Didier and PERVEEN, Asma. The Post-Processing of Additive Manufactured Polymeric and Metallic Parts. *Journal of Manufacturing and Materials Processing*, vol. 6 (2022), no. 5. ISSN 2504-4494. Available from: https://doi.org/10.3390/jmmp6050116
2. NGO, Tuan D.; KASHANI, Alireza; IMBALZANO, Gabriele; NGUYEN, Kate T. Q. and HUI, David. Additive manufacturing (3D printing): A review of materials, methods, applications and challenges. *Composites Part B: Engineering*, vol. 143 (2018), pp. 172–196. ISSN 1359-8368. Available from: https://www.sciencedirect.com/science/article/pii/S1359836817342944..
3. BUJ-CORRAL, Irene; DOMÍNGUEZ-FERNÁNDEZ, Alejandro and DURÁN-LLUCIÀ, Ramón. Influence of Print Orientation on Surface Roughness in Fused Deposition Modelling (FDM) Processes. *Materials*, vol. 12 (2019), no. 23. ISSN 1996-1944. Available from: https://doi.org/10.3390/ma12233834
4. IAN GIBSON, David R., Brent Stucker. *Additive Manufacturing Technologies: 3D Printing, Rapid Prototyping, and Direct Digital Manufacturing.* 2nd Edition, 2015. ISBN 978-1-4939-2113-3. .
5. BAKHTIARI, Hamed; NIKZAD, Mostafa and TOLOUEI-RAD, Majid. Influence of Three-Dimensional Printing Parameters on Compressive Properties and Surface Smoothness of Polylactic Acid Specimens. *Polymers*, vol. 15 (2023), no. 18. ISSN 2073-4360. Available from: https://doi.org/10.3390/polym15183827
6. MUKHANGALIYEVA, Aishabibi; DAIRABAYEVA, Damira; PERVEEN, Asma and TALAMONA, Didier. Optimisation of Dimensional Accuracy and Surface Roughness of SLA Patterns and SLA-Based IC Components. *Polymers*, vol. 15 (2023), no. 20. ISSN 2073-4360. Available from: https://doi.org/10.3390/polym15204038
7. TONELLO, Riccardo; CONRADSEN, Knut; PEDERSEN, David B. and FRISVAD, Jeppe R. Surface Roughness and Grain Size Variation When 3D Printing Polyamide 11 Parts Using Selective Laser Sintering. *Polymers*, vol. 15 (2023), no. 13. ISSN 2073-4360. Available from: https://doi.org/10.3390/polym15132967
8. ALZYOD, Hussein and FICZERE, Peter. Neosanding postprocessing for improving surface roughness of extrusion-based 3D printing of PLA parts: a comparative analysis of stylus profilometer and confocal profilometry methods. *Journal of the Brazilian Society of Mechanical Sciences and Engineering*, vol. 46 (2024), no. 4, pp. 238. ISSN 1806-3691. Available from: https://doi.org/10.1007/s40430-024-04817-x.
9. KANDANANOND, Karin. Optimisation of fused filament fabrication system by response surface method. *Int.J.Metrol.Qual.Eng.*, vol. 11 (2020). Available from: https://doi.org/10.1051/ijmqe/2020002.
10. JACOBS, Paul F. *Stereolithography and other RP&M technologies: from rapid prototyping to rapid tooling.* ASME Press, 1996. ISBN 9780872634671. .
11. BOURELL, David; COHOLICH, Jeremiah; CHALANCON, Antoine and BHAT, Abhimanyu. Evaluation of energy density measures and validation for powder bed fusion of polyamide. *CIRP Annals*, vol. 66 (2017), no. 1, pp. 217–220. ISSN 0007-8506. Available from: https://www.sciencedirect.com/science/article/pii/S0007850617301282.

Overview of Additive Manufacturing Application for Sensors Production

Paulina GRIGUTYTĖ*, Tomas KUNCIUS

Kaunas University of Technology, Kaunas, Lithuania

** paulina.grigutyte@ktu.edu*

Abstract

Sensors are crucial across various sectors as they detect environmental changes and convert them into measurable signals. Additive manufacturing (AM), particularly filament-based material extrusion (FBME) technology, has emerged as a powerful method for rapid prototyping and customization of sensor components due to its accessibility, cost-efficiency and compatibility with functional materials. This study explores the use of FBME in producing sensor elements and the impact of material combinations. Several commercially available and custom composite filaments were evaluated for their mechanical performance in applications for sensing elements. Interlayer tensile strength tests were conducted on specimens fabricated with combinations of PLA, PETG, CB/PLA, and Fe/PLA, according to ISO 527:2012-1BA standard. Results showed that combinations with PETG have significantly lower interlayer tensile strength, while PLA+CB/PLA combination showed the highest value among the combination groups. The weakest adhesion was observed between pure PLA and PETG, confirming poor inter-material compatibility. The findings highlight the potential of functional composites in sensor fabrication and the importance of material pairings optimization for improved mechanical reliability.

Keywords: sensors, additive manufacturing, adhesion, composites, filaments.

1. Introduction

Sensors are crucial in various fields, ranging from environmental monitoring to healthcare. Their main functionality is to detect and measure environmental changes and to convert them into measurable signals. Rapid prototyping and customization have been improved with the use of additive manufacturing (AM). The ISO/ASTM 52,900 standard defines AM, as the "process of joining materials to make parts from 3D model data, usually layer upon layer, as opposed to subtractive manufacturing methodologies" [1]. Traditional manufacturing methods are costly and time-consuming for the production of complex shapes, whereas AM allows the direct creation of complex nonplanar structures. Although many researchers focus on functional AM materials fabrication by incorporating additives, their transition to real-world applications is slow-paced. While there are several commercially available composite filaments, they tend to lack variety in their composition and filler percentage, thus, researchers are creating and testing custom-made filaments for their required applications [2, 3]. The article focuses on the role of filament-based material extrusion (FBME) technology in sensor production, highlighting the materials and their applications in sensing elements production. The FBME method was chosen due to its high commercial availability, cost-effectiveness, and compatibility with various functional materials.

2. Filament-based material extrusion

Filament-based material extrusion is the most popular AM technology due to its lower price and easier access. It uses thermoplastic polymers that can be melted by heating and solidified when

cooling several times [3]. This method consists of three stages: pre-processing, printing, and post-processing.
The pre-processing stage covers the 3D model and toolpath code creation. The model is created using computer-aided design (CAD) software, which is uploaded to a slicing software to set the printing parameters (printing orientation, layer height, temperature, infill, printing speed, etc.). The toolpath with other set parameters is saved as a G-code, which can be uploaded to the printer's controller. The printing process covers material extrusion according to the G-code. The filament is directed from its spool to the extrusion head, where it is melted and extruded through the nozzle onto the build platform layer by layer. These technology machines are most commonly based on cartesian coordinates system. During post-processing stage the supporting structures are removed, if they were required by the geometry. Removal of supports can reduce surface quality which can be improved either with mechanical (machining, sanding, abrasive, vibratory, barrel finishing) or chemical (painting, coating, heating, vapor deposition process) methods [4].

3. Additive Manufacturing Materials in Sensors Production

The main components of sensors are a sensor housing and a sensing element. For the former, mechanical properties are usually the top priority, and for the latter, the materials must be able to detect and respond to an environmental change with a measurable signal [2]. Common pure polymers used for sensor housing are Polylactic Acid (PLA), Acrylonitrile Butadiene Styrene (ABS), Thermoplastic Polyurethane (TPU), Polyethylene Terephthalate Glycol (PETG) and Polycarbonate (PC). These materials require extrusion temperatures in range of 190-310°C. A distinctive feature of TPU is high flexibility and elasticity, while PLA and PETG are safe and easy to print, ABS and PC have higher strength, however, their printing releases toxic fumes.
Pure polymers used in FBME are low-cost and have a low melting point, however, they may lack the required functionality of a sensing element. Proper mechanical, thermal, and electrical properties are acquired by use of composites where the base polymer is combined with other materials (fillers) [5]. The properties and brittleness of composites depend on the filler type, concentration, dispersion quality, and in the case of nanotubes, on the alignment of the tubes. The choice of base polymer also highly affects the mechanical properties, as PLA and ABS provide rigid structure, however, TPU offers greater flexibility. Composites compatible with FBME can be electrically conductive, show magnetic or piezoelectric properties. Common composite additives for sensing element production are introduced in Table 1.

Table 1. Common composites

Additive	Possible matrix	Properties	Application	Commercial suppliers
Graphene [4]	PLA, ABS, and PC	Flexibility, low resistivity, high electron mobility, electrical and thermal conductivity	Resistive, capacitive, and piezoresistive sensors	Angstron Materials, Graphene 3D Labs, Black Magic 3D, Filabot
Carbon Black (CB) [4]	Polycaprolactone (PCL), PLA, and ABS	Low cost and chemical stability, piezoresistive properties, semiconductor-like electrical conductivity		Proto-Pasta
Multi-walled carbon nanotubes (CNTs) [4]	ABS, PLA, and PETG	High electrical conductivity, axial thermal conductivity, lateral insulation, and high tensile strength and stiffness		3DXTech, Functionalize F-Electric, Filabot, Cheap Tubes Inc., Nanocyl

Magnetic materials (Maraging steel, Iron) [3, 6]	PLA, PETG	Maraging steel is a soft magnet; lower viscosity and lower extrusion temperature due to metal particles	Magnetic field detection or proximity sensors	Proto-Pasta, PrusaResearch
Barium Titanate nanowires [7]	Polyvinylidene Fluoride, PLA	Barium Titanate is a piezoelectric ceramic, however, on its own, it is brittle	Force, vibration, or pressure sensors	-

4. Additively Manufactured Sensors Applications

Although, FBME can be used for the outer sensor part and/or sensing element fabrication, here, more focus is put on physical, electrochemical and biosensors where the sensing element is manufactured using the ME method. Physical sensors detect and measure physical parameters. Electrochemical sensors convert chemical information into an electrical signal through electrochemical reactions. Biosensors measure biological or chemical reactions by generating signals proportional to the concentration of an analyte in the reaction [8]. However, electrochemical sensors and biosensors elements often require post-processing (chemical treatments, coatings).

One instance of stain or piezoresistive sensor production using composites combines TPU filament containing 3 wt% (percentage by weight) CNTs and pure TPU filaments to create a bidirectional and stretchable piezoresistive sensor. The sensor behaviour response depends on the sensor pattern and good cyclic repeatability was reported for both electrical and mechanical performance. In addition to that, a glove prototype for measuring finger flexure was created. This example shows that mentioned composite can be printed with other commercial filaments [9].
Another example of ME application for strain sensing element production is the use of CB/CNT/TPU composite. The effect of CB was analysed, and it showed that the inclusion of CB improved the strain-sensing property of the material as CB filled vacant conductive paths in the CNTs network. The sensing properties of the composites were used to monitor human activity (mouth, finger, knee, and elbow motion) [10].

Commercially available conductive filament use for sensors production example is a bendable, coplanar capacitive sensor for liquid-level measurement. Here, TPU 95A and conductive AlfaOhm (PLA/CNT) filaments were used. The sensor was tested with sunflower oil and showed good sensitivity and linearity, in addition to that, its capacitance was unaffected by bending. This proves an opportunity for rapid prototyping and low-cost production [11].
An example of an electrochemical sensor is a low-cost, portable system for on-site detection of soil pH and potassium levels. The system employs additively manufactured miniaturized ion-selective electrodes fabricated using commercially available conductive CB/PLA filament [12]. ME method application for medical field biosensors, and this method's advantages during a crisis is the development of Au-modified additively manufactured biosensors using a commercial G-PLA filament for detecting SARS-CoV-2 and a potential disease biomarker [13].

5. Experimental Methodology

The specimens for tensile testing were modelled according to the ISO 527:2012 standard 1BA requirements for small specimens [14]. To accommodate the use of different materials, the model was divided into separate parts using PrusaSlicer software. A sketch of the specimen is presented in Figure 1.

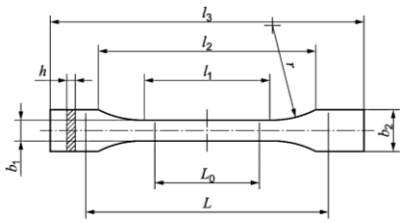

l_3	75 mm
l_1	30 mm
r	30 mm
l_2	58 mm
b_2	10 mm
b_1	5 mm
h	2 mm
L_0	25 mm
L	60 mm

Fig. 1 Sketch of a small specimen for tensile testing [15]

For adhesion testing two polymers PLA and PETG from Prusa Research and two composites Electrically Conductive Composite PLA (PLA >67%, CB <20%, other polymers <13%) and Iron-Filled Metal Composite PLA (PLA >54%, Iron <45%, other polymers <1%) from ProtoPasta were used [6]. The combinations group has six material combinations, each containing five specimens: PLA with CB/PLA, PETG with CB/PLA, PLA with Fe/PLA, PETG with Fe/PLA, CB/PLA with Fe/PLA, and PLA with PETG. In contrast, the control group consists of four subgroups, each made up of a single material: PLA, PETG, C/PLA, and Fe/PLA. CB/PLA filament required extensive purging, causing high material waste, thus, it was printed as the top part of the specimens in required combinations. Specimens made with TPU filaments failed due to excessive base vibrations and the rubber-like nature of TPU.

The specimens were printed with Prusa MK3.5 MMU3 printer using 0.4 mm diameter nozzle, 0.2 mm layer height and 100% infill. Extrusion temperature for specimens with PLA was 215°C and with PETG 240°C. The bed temperature was set to 60°C and 80°C, respectively. Printing orientation was vertical to ensure failure between the layers (Fig. 2). To minimize vibrational distortion, the printing speed was later reduced manually.

For measurements of specimens "Teng Tools" caliper with a measurement length of 150 mm and a division value of 0.01 mm was used. The adhesion testing was carried out using a universal tensile-flexural machine Tinius Olsen H25 KT. According to the standard, tensile tests were carried out using 2 mm/s speed with 1kN force sensor.

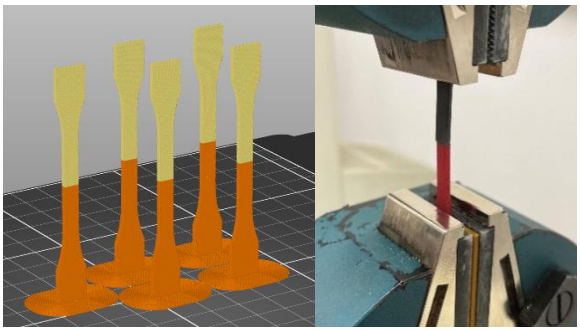

a b

Fig. 2. Testing specimens: a – specimens printing orientation and placement of the printing bed; b – specimen fixture in universal tensile-flexural machine

6. Results and discussion

After post-processing operations specimens' centre part was measured at three different points. It was observed that PETG experienced shrinkage in width (b_1), whereas other materials showed an increase in width and thickness (h) compared to the original 3D model. Summarized and averaged measurement results are presented in Table 2.

Table 2. Average measuring results of specimens

Combinations group				**Control group**			
Materials	b_1, mm	h, mm	Cross-sectional area, mm²	Materials	b_1, mm	h, mm	Cross-sectional area, mm²
PLA + CB/PLA	5.06	2	10.11	PLA	5	2.05	10.24
PETG + CB/PLA	5.07	1.99	10.1	PETG	4.86	2.06	10
PLA + Fe/PLA	5.08	2.03	10.31	Fe/PLA	5.02	2.09	10.48
PETG + Fe/PLA	5.1	2.02	10.28	CB/PLA	5.01	2.03	10.15
CB/PLA + Fe/PLA	5.04	2.02	10.15				
PLA + PETG	5.11	2.03	10.37				

Specimens' behaviour during tensile testing is illustrated in Figure 3. All specimens separated within a displacement range of 0.8-1.5 mm during tensile testing. The weakest adhesion was observed between pure PLA and PETG, suggesting poor compatibility. However, PLA composites with CB and Fe showed slightly improved adhesion with PETG. Control group results show that composite materials are inherently more susceptible to tensile stress.

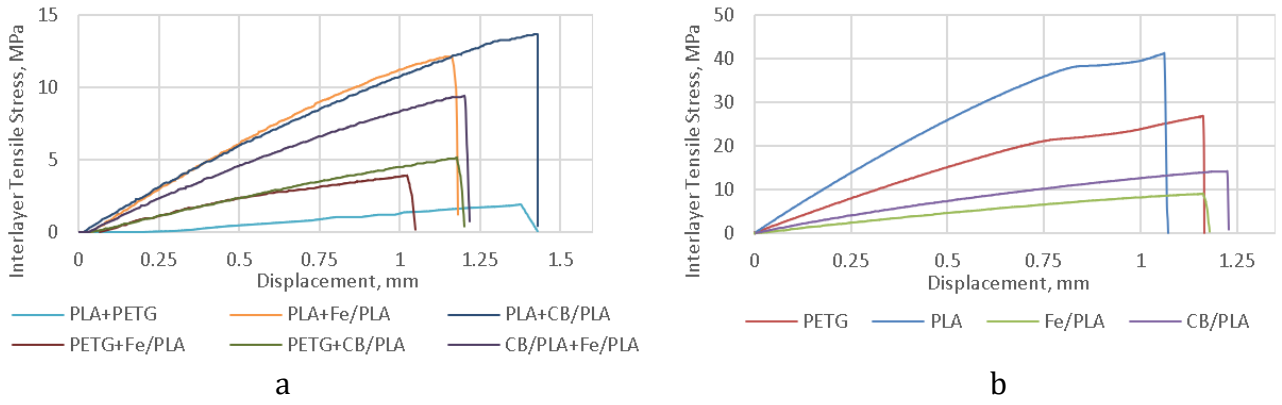

a b

Fig. 3 Interlayer Tensile Stress-Displacement curves: a – combinations group, b – control group

The average interlayer tensile strength of the tested specimens, along with the results dispersion, is illustrated in Figure 4. Overall, the control group demonstrated higher interlayer tensile strength compared to the combination group. Among the control materials, PLA exhibited the highest strength – 38.62 MPa, while Fe/PLA had the lowest value – 10.35 MPa. In the combinations group, PLA+CB/PLA specimens showed the highest strength – 12.7 MPa), followed by PLA+Fe/PLA and CB/PLA+Fe/PLA. Several PETG combination' specimens failed during clamping, indicating that PETG had the weakest interlayer adhesion with the tested materials. Compared to pure PLA, its composites showed a 62–73% decrease in interlayer tensile strength, and in the combinations group, PLA+CB/PLA and PLA+Fe/PLA experienced a 67–70% interlayer tensile strength decrease in comparison to pure PLA. The most consistent results were observed in CB/PLA and PLA+Fe/PLA, while the highest variability occurred in PLA and PLA+CB/PLA specimen groups. Based on the tested combinations, PLA is recommended as the preferred material for further prototyping, while PETG should be avoided unless low interlayer tensile strength is required.

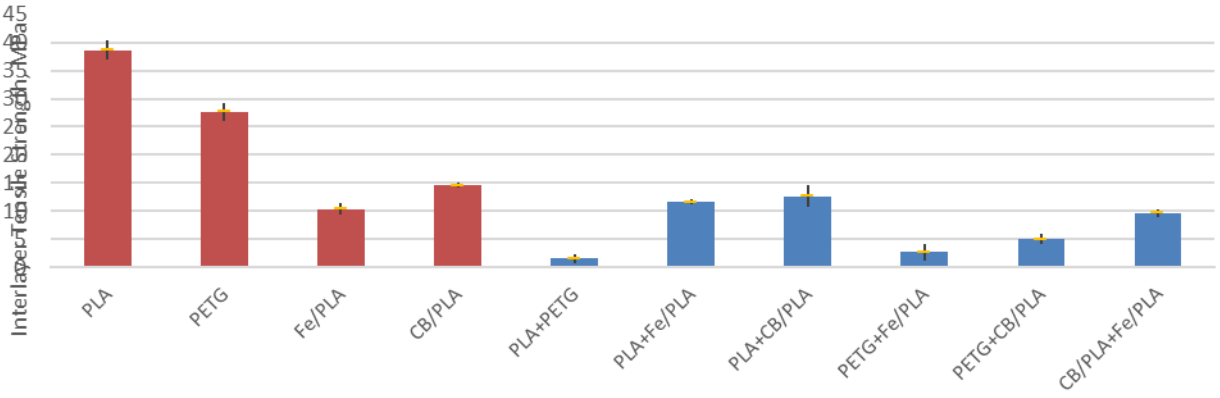

Fig. 4. Interlayer Tensile Strength: red – control group, blue – combinations group

7. Conclusions

1. Common polymer additives used to achieve electrical conductivity, magnetic or piezoelectric properties are such: graphene, carbon black, carbon nanotubes, magnetic materials (maraging steel, iron), barium titanate nanowires.
2. Measurements showed that PETG experienced shrinkage in width by 0.14 mm, while other materials exhibited slight increases in width and thickness. TPU specimens were excluded due to print failure caused by excessive vibrations and its rubber-like properties.
3. The combinations group specimens showed lower interlayer tensile strength compared to pure PLA – 62–73% reduction. PLA+CB/PLA showed the highest interlayer tensile strength among combinations – 12.7 MPa, while PETG combinations showed the weakest adhesion, often failing during clamping, which shows poor material compatibility.

References

1. ISO/ASTM. *ISO/ASTM 52900:2021. Additive manufacturing — General principles — Fundamentals and vocabulary*. Online. Available from: https://www.iso.org/obp/ui/#iso:std:iso-astm:52900:ed-2:v1:en [viewed 2025-04-06].
2. HOSSAIN, Md Jarir, TABATABAEI, Bahareh Tavousi, KIKI, Mazen and CHOI, Jae-Won. Additive manufacturing of sensors: a comprehensive review. *International Journal of Precision Engineering and Manufacturing-Green Technology*, 12 (2024), no. 1, pp. 277. ISSN 2288-6206.
3. DÍAZ-GARCÍA, Álvaro, LAW, Jia Yan, FELIX, Manuel, GUERRERO, Antonio and FRANCO, Victorino. Functional, thermal and rheological properties of polymer-based magnetic composite filaments for additive manufacturing. *Materials & Design*, 219 (2022). ISSN 0264-1275.
4. BERBER, Mohamed R. and HAZZAA HAFEZ, Inas. *Carbon Nanotubes: Current Progress of Their Polymer Composites*. Online. London: IntechOpen, 2016. ISBN 978-953-51-2470-2. Available from: https://www.intechopen.com/books/5167 [viewed 2025-03-10].
5. RAJAN, Kumaresan, SAMYKANO, Mahendran, KADIRGAMA, Kumaran, HARUN, Wan Sharuzi Wan and RAHMAN, Md Mustafizur. Fused deposition modeling: process, materials, parameters, properties, and applications. *The International Journal of Advanced Manufacturing Technology*, 120 (2022), no. 3–4, pp. 1531. ISSN 0268-3768.
6. PROTO-PLANT. *Material Data Table*. Online. Available from: https://proto-pasta.com/pages/material-data-table [viewed 2025-03-18].
7. MALAKOOTI, Mohammad H., JULÉ, Florian and SODANO, Henry A. Printed nanocomposite energy harvesters with controlled alignment of barium titanate nanowires. *ACS Applied Materials & Interfaces*, 10 (2018), no. 44, pp. 38359. ISSN 1944-8244.
8. BHALLA, Nikhil, JOLLY, Pawan, FORMISANO, Nello and ESTRELA, Pedro. Introduction to biosensors. *Essays in Biochemistry*, 60 (2016), no. 1, pp. 1. ISSN 0071-1365.

9. CHRIST, Josef F.; ALIHEIDARI, Nahal; PÖTSCHKE, Petra and AMELI, Amir. Bidirectional and Stretchable Piezoresistive Sensors Enabled by Multimaterial 3D Printing of Carbon Nanotube/Thermoplastic Polyurethane Nanocomposites. *Polymers*, vol. 11 (2018), no. 1. https://doi.org/10.3390/polym11010011 [viewed 2025-03-10].
10. ZHANG, Zixi, XIANG, Dong, WU, Yuanpeng, ZHANG, Jie, LI, Yaxin et al. Effect of carbon black on the strain sensing property of 3D printed conductive polymer composites. *Applied Composite Materials*, 29 (2022), no. 3, pp. 1235. ISSN 0929-189X.
11. RAGOLIA, Mattia Alessandro; LANZOLLA, Anna M. L.; PERCOCO, Gianluca; STANO, Gianni; DI NISIO, Attilio. Thermal Characterization of New 3D-Printed Bendable, Coplanar Capacitive Sensors. *Sensors*, 21(19), 6324. https://doi.org/10.3390/s21196324 [viewed 2025-04-16].
12. MCCOLE, Matthew, BRADLEY, Martin, MCCAUL, Margaret and MCCRUDDEN, Denis. A low-cost portable system for on-site detection of soil pH and potassium levels using 3D printed sensors. *Results in Engineering*, 20 (2023). ISSN 2590-1230.
13. SILVA, Luiz R. G.; STEFANO, Jéssica S.; ORZARI, Luiz O.; BRAZACA, Laís C.; CARRILHO, Emanuel et al. *Electrochemical Biosensor for SARS-CoV-2 cDNA Detection using AuPs-Modified 3D-Printed Graphene Electrodes.* MDPI AG, -08-10, 2022.
14. BRITISH STANDARDS INSTITUTION. *BS EN ISO 527-2:2012 – Plastics – Determination of tensile properties – Part 2: Test conditions for moulding and extrusion plastics*. Online. Available from: https://bpb-eu-w2.wpmucdn.com/blogs.brighton.ac.uk/dist/0/9491/files/2021/11/BS-EN-ISO-527-2-2012-tensile-test-specimens.pdf [viewed 2025-03-18].

Investigation of the Effect of Abrasive Water Jet Machining Parameters on Basalt Fiber Reinforced Epoxy Composites

Sachinkumar MANCHERY SAJAN*, Kristina ŽUKIENĖ

Kaunas University of Technology, Kaunas, Lithuania

** sachinkumar.manchery@ktu.edu*

Abstract

Nowadays, the use of composites is very common in every industry. The reason behind this is the better properties of composites compared to traditional materials. Abrasive water jet machining (AWJM) is widely used in industry for composite materials. However, AWJM faces certain challenges when cutting composite materials, including delamination, fiber pull-out, matrix erosion, and the tapering of the cutting kerf. This paper presents an investigation of the effect of AWJM parameters on basalt fiber reinforced epoxy composites. The influence of the feed rate on the cutting quality of the samples was investigated. The responses of the machining process, such as kerf and roughness parameters, are measured and studied.

Keywords: Abrasive water jet, Composite, Cutting, Kerf, Roughness.

1. Introduction

Nowadays, the use of composites is very common in every industry. This is because composites have better properties than traditional materials, such as high strength-to-weight ratios, corrosion resistance, structural flexibility, low thermal conductivity, etc. [1]. There are two types of composites available on the market, synthetic and natural. The basalt fiber reinforced polymer composite is an example of a composite derived from a mineral source [2]. Basalt fibers are made from basalt rock by melting it and converting it into fiber [3]. The eco-friendly nature of this composite makes it a more sustainable option than many other composites [3]. Due to the wide use of composites, the machining of these materials is also becoming increasingly important these days [4]. There are numerous methods available in the market for cutting and other machining operations of composites. Among them, abrasive water jet machining (AWJM) has a higher priority due to the many advantages of this method [4]. In this paper, the use of AWJM is highlighted for the cutting of composite materials. To analyse the cutting quality, the kerf characteristics and roughness characteristics are measured and studied. This study aims to investigate the effect of AWJM parameters on basalt fiber reinforced epoxy composites.

2. Materials and methods

The basalt composite was produced by cutting 10 basalt fibres plies (Basaltex NV, Wevelgem, Belgium) with dimensions of 100 × 100 mm. A 7:3 mix of epoxy resin and hardener (R&G Faserverbundwerkstoffe GmbH, Epoxy Resin L, Hardener S) was used to prepare the composite. The epoxy resin is cold cured with a cure time of 24 hours. The composite was produced using a hand-lay-up technique with the support of the vacuum bagging technique. Composite samples with a dimension of 30 × 30 mm were cut using a Wazer desktop AWJM. 80-mesh alluvial garnet was used as the abrasive particle in the AWJM cutting operation. The abrasive rate was 0.15 kg/min. Two types of cuts were made: coarse (feed rate was 22 mm/min) and fine (feed rate was 10 mm/min). A cutting path is shown in Figure 1.

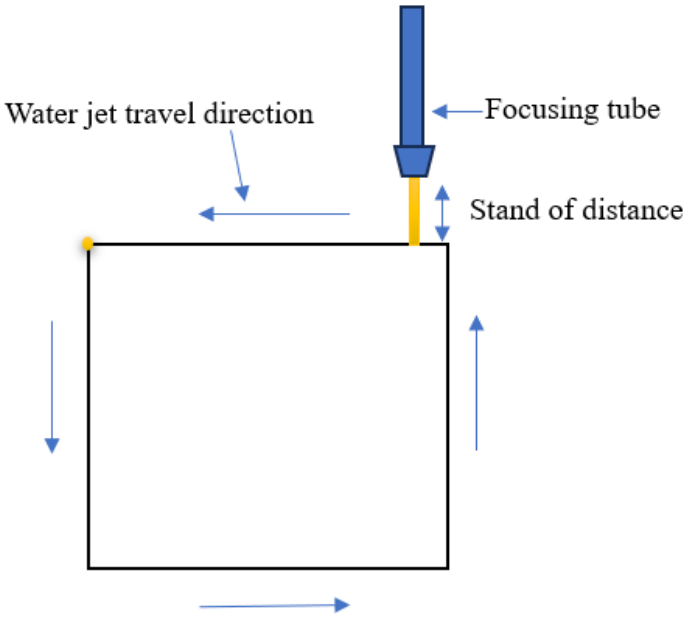

Fig. 1 Schematic of the cutting path

To investigate the quality of the cut, the samples were examined after cutting using a Nikon ECLIPSE LV100ND optical microscope. The images captured by this microscope were used to calculate the values of the roughness parameters of the cut surfaces. The roughness parameters calculated in this work are the arithmetic mean roughness (R_a) and the root mean square roughness (R_q). Parameters were calculated using ImageJ software. At least three cross-sectional profiles of the optical microscope images were used for the calculations and were extracted using ImageJ software. The system analyses the intensity of the grey variation on the cut surface along a selected line. The x-axis shows the length of the horizontal scan in pixels, and the y-axis shows the intensity of the grey. Peaks in the profile indicate high grey values, and valleys are low grey values.

Kerf angles were measured using the optical microscope "Moticam 1000 1.3M Pixel" and "Motic Images plus 2.0" software. The Kerf angles were calculated from four measurements. Using the same microscope, a qualitative study of the delamination images was carried out to investigate the presence of delamination after the cutting process.

3. Results and discussion

As can be seen in Figure 2, AWJM provided a high-quality surface finish on the samples, reducing or eliminating the need for secondary processes. The photographs in Figure 2 show the results of the coarse and fine cutting of the basalt fibre reinforced epoxy composite. Although the examples show that both cuts produce a high-quality cut, the main problem encountered in machining composites is the delamination that occurs during the cutting process [5].

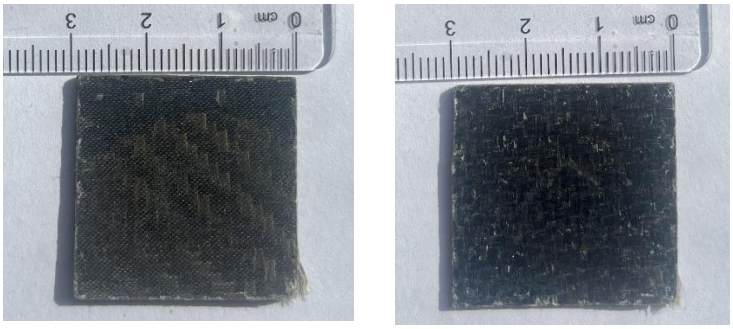

a b

Fig. 2. Images of BFRPC samples: a - coarse cut and b - fine cut

The microscopic view of delamination of the samples is shown in Figure 3: coarse cutting (Fig. 3 a), and fine cutting (Fig. 3 c). It can be seen that the delamination occurred on the edge from which the cutting process started. The investigations of Shanmugam et al. [5] show that the delamination is caused by a shock wave caused by a water jet and the abrasive particles used in the cutting process. In addition, composites without good adhesion between the matrix and the reinforcing fibre are prone to defects such as cracks and delamination.

The cross-sectional surface images obtained from the optical microscope make it easy to identify the individual layers of the plays and the interface between them. Optical microscope images show that coarse cutting produces fractures and misalignments in the fibres (Fig. 3 b). The dark areas with small granular structures are the matrix region, which looks rough and uneven. There is also a visible gap between the fiber and the matrix (Fig. 3 b). In the case of fine cutting (Fig. 3d), less fiber breakage is visible compared to coarse cutting. The matrix region is also more compacted. Fine cutting samples show low fiber pull-out and more fiber matrix bonding. The alignment of the fibers is also more parallel and cleaner. In coarse cutting, microcracks are more present than in fine cutting.

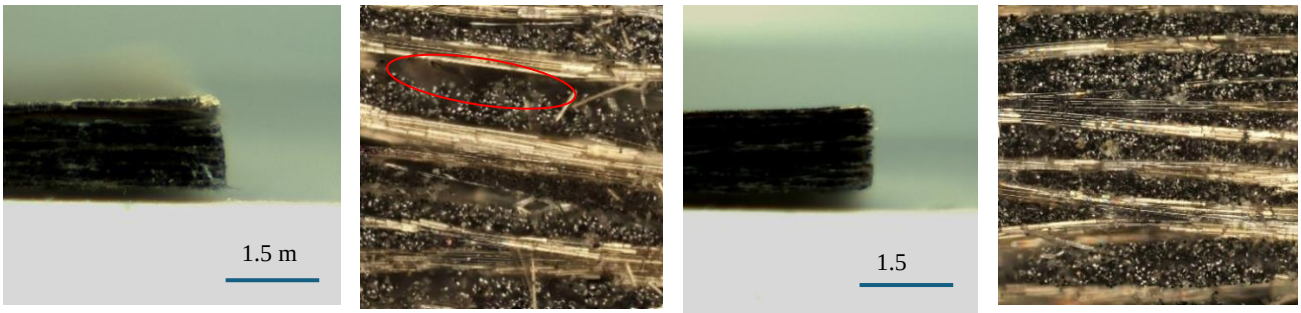

a b c d

Fig. 3 Optical microscope images of BFRPC samples delamination: a- coarse cutting, c - fine cutting and images of BFRPC cross-sections at magnification ×10: b - coarse cutting)., b - fine cutting

The cross-sectional profiles presented in Figure 4 illustrate the surface profile of BFRPC after the coarse and fine cutting processes. In the coarse cutting profile, a very large difference between the peaks and valleys is clearly visible in some regions. This indicates that the surface is less smooth and rougher after coarse cutting. Sharp peaks and deep valleys are visible in the profile, which may be due to the effect of fiber pull-out or delamination during the cutting process. The increase in feed rate compared to fine cutting can be the reason for a more aggressive cutting action. The fine cutting profile shows high fluctuation, which means strong irregularities in the cut profile.

Fine cutting with a feed rate of 10 mm/min is supposed to be normal cutting with minimal damage, but the profilogram shows a result of a higher level of irregularities for a low feed rate.

From the details given in Table 1 on the roughness values. Normally, the values of R_a and Rq were expected to be lower for fine cutting compared to coarse cutting, but in this situation, the results were the opposite of what was expected.

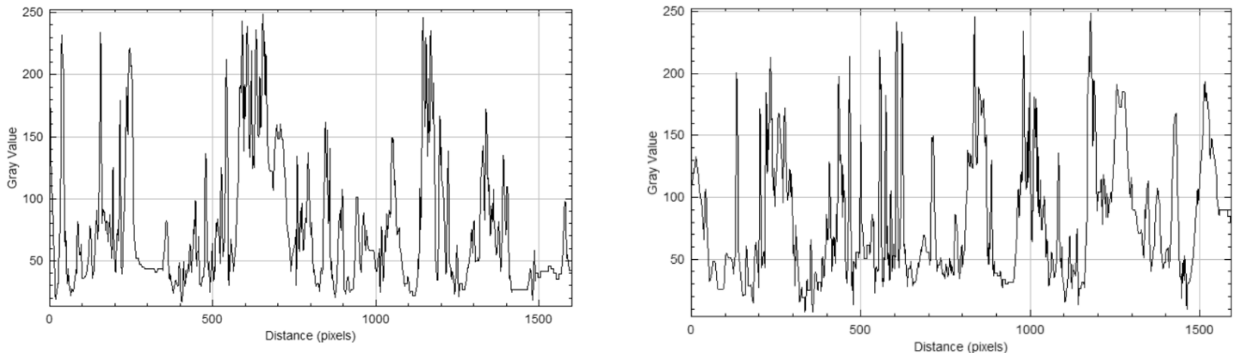

a b

Fig. 4 Cross-sectional profile of BFRPC samples: a - coarse cutting; b – fine cutting

Table 1. Surface roughness values of coarse and fine cutting samples

Cutting type	R_q (µm)	R_a (µm)
Coarse (22 mm/min)	57.240	30.63
Fine (10 mm/min)	59.372	32.95

However, the kerf angle values of both cuts show that the value of the kerf angle increased more than twice, then the feed rate increases from 10 mm/min to 22 mm/min (Fig. 5). During the cutting, the enrgy distibuted from the water jet varies from top to bottom of the specimen. On top, the energy will be higher, which causes more material removal, and at the bottom, the energy distribution decreases gradually, resulting in taper angles. At higher feed rates, the jet nozzle moves faster, reducing the interaction time and the chances of cutting through the material completely, especially at the bottom, resulting in a wider cut at the top and a narrower cut at the bottom [6]. Studies by other researchers showed that a cone profile is formed at high feed rates and a reverse cone at low feed rates. The Kerf profile can be uniform and parallel at the optimum feed rate [7].

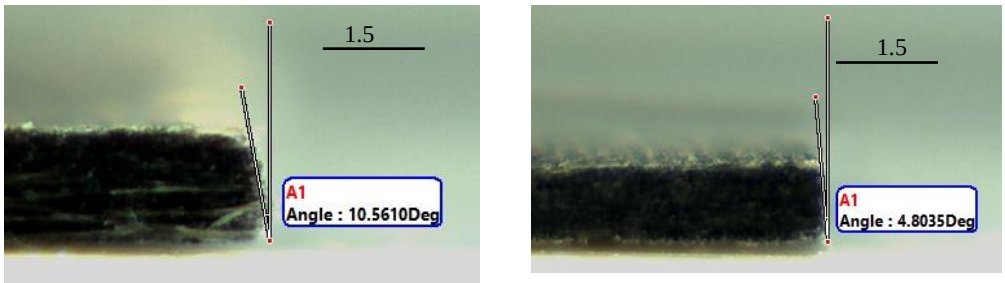

a b

Fig. 5 The kerf angles of BFRPC: a - coarse cutting; b - fine cutting

4. Conclusions

The results obtained clearly demonstrate that AWM is an appropriate method for the machining of BFRPC.

1. Analysis of the roughness parameters showed that a low feed rate of 10 mm/min resulted in slightly higher roughness values compared to a feed rate of 22 mm/min.
2. The delamination of the cut surfaces was not affected by increasing the feed rate from 22 mm/min to 10 mm/min. The presence of delamination was obtained at the starting point of the composite cut due to the shock wave caused by a water jet and the abrasive particles used in the cutting process and the insufficient interfacial adhesion between the epoxy matrix and the basalt fibres.
3. The analysis of the angles showed that the low feed rate of 10 mm/min resulted in smaller angles and fewer defects compared to the feed rate of 22 mm/min, indicating that improved cut quality is achieved with lower feed rates.

References

1. BHONG, M., et al. Review of Composite Materials and Applications. *Materials Today: Proceedings*, 2023.
2. DHAND, V., et al. A Short Review on Basalt Fiber Reinforced Polymer Composites. *Composites Part B: Engineering*, 2015, vol. 73, pp. 166–180.
3. BINAZ, V., DEEPAK, K. and SINGH, I. Comparative Assessment of Cutting Processes in the Mechanical Behavior of Basalt Fiber/Poly (Lactic Acid) Matrix Composites. *Express Polymer Letters*, 2023, vol. 17, no. 2, pp. 152–168.
4. NATARAJAN, Y., MURUGESAN, P.K., MOHAN, M. and KHAN, S.A.L.A. Abrasive Water Jet Machining Process: A State of Art of Review. *Journal of Manufacturing Processes*, 2020, vol. 49, pp. 271–322.
5. SHANMUGAM, D.K., NGUYEN, T. and WANG, J. A Study of Delamination on Graphite/Epoxy Composites in Abrasive Waterjet Machining. *Composites Part A: Applied Science and Manufacturing*, 2008, vol. 39, no. 6, pp. 923–929.
6. KARKALOS, N.E., DEKSTER, L., KUDELSKI, R. and KARMIRIS-OBRATAŃSKI, P. A Statistical and Optimization Study on the Influence of Different Abrasive Types on Kerf Quality and Productivity during Abrasive Waterjet (AWJ) Milling of Ti-4Al-6V. *Materials*, 2023, vol. 17, no. 1, pp. 11.
7. KHAN, M.A., SONI, H., MASHININI, P.M. and UTHAYAKUMAR, M. Abrasive Water Jet Cutting Process Form Machining Metals and Composites for Engineering Applications: A Review. *Engineering Research Express*, 2021, vol. 3, no. 2, pp. 022004.

Application of Innovative Teaching Methods in the Study Process

Laura GEGECKIENĖ*, Ingrida VENYTĖ, Darius PAULIUKAITIS

Kaunas University of Technology, Kaunas, Lithuania

** laura.gegeckiene@ktu.lt*

Abstract

The rapidly changing digital technology environment encourages higher education institutions to adapt and implement innovative solutions. The study module "Digital Media Technologies and Design" is one example in which students develop practical skills through real, complex project tasks.
Didactic innovations in the module include project-based learning, technology integration, the formation of students' digital identity, and the principle of reflexive learning.

Keywords: didactic innovations, study process, teaching methods.

1. Introduction

Given the challenges of modern higher education, especially in the fields of technology and creative industries, the need to implement didactic innovations is becoming increasingly relevant. Didactic innovations are innovative, purposefully applied teaching (learning) solutions that improve the quality of learning, promote student engagement and adapt learning content to changing technologies and student needs. These innovations include both teaching methods, assessment strategies, and the use of technologies in the study process [1–2]. One of the modules that implements these principles in practice is “Digital Media Technologies and Design”, during which students acquire interdisciplinary competencies that include graphic design, website development, 3d modelling and information visualisation.

The educational innovation process consists of five phases (see Fig. 1).

Fig. 1 The educational innovation process [3]

The first two phases are aimed at getting a thorough understanding of the context in which a certain innovation initiative takes place. Phase 2 relates to the overall educational aspects, such as the vision for education and the intended learning outcomes. After completing the first two phases, the (re)design itself defines the third phase. During the fourth phase, all the above is brought together in building the design. In the fifth and final phase, measurements are set up to see if the aims have been met [3].

University lecturers play a significant role in developing and implementing teaching innovations. They contribute to the development of the study content, define teaching objectives and didactic provisions, select didactic methods and media, taking into account their learning groups [4-5]. The aim of this paper is to show how innovative teaching methods are applied in the module "Digital Media Technologies and Design" and to substantiate the importance of didactic innovations.

2. Creation of a digital portfolio

The main task of the project is to demonstrate the competencies acquired during the study module: to create an individual website that presents the results of the student's semester work. This task promotes computer literacy skills, communication skills, reflection, and visual thinking.

The project task includes the following stages:

1. Creation of a website, implementing the intended technical and design requirements;

2. Structuring the website content according to the evaluation criteria;

3. Submission of a project report, uploading a link to the website to the Moodle virtual learning environment Moodle.

The innovations applied in the module are reflected in the tools and work methodology used. Students are actively encouraged to use open-source and professional design programmes (e.g. Krita, Autodesk 3ds Max), which allow them to get acquainted with relevant technologies used in practice. The following innovative elements are integrated into the project:

- A vector logo created using Krita or another graphic design programme develops students' imagination and understanding of branding;
- A three-dimensional model with adapted lighting and overview animation, created using 3ds Max, illustrates the form, functionality and aesthetics;
- A project description in text format, which provides information about the product's technical characteristics, design solutions, and creative process;
- Quality of information presentation – the website must clearly and consistently display information about the materials used, functionality, target audience, etc.;
- The section "About the author" provides a brief introduction of the student, helping to form a personal digital identity.

Clearly defined assessment criteria help students to achieve results that are focused on quality, functionality, and aesthetics. They also encourage independence and develop the ability to plan work and properly document and present it.

3. Didactic innovations in the module

Application of technologies: students learn to work with modern design and modelling tools: Krita, Autodesk 3ds Max; digital competencies are developed.

Project-based learning: students independently plan, create, test, and publish a website; the task covers the entire product life cycle from idea to presentation.

Reflective learning: The "About the author" page encourages reflection and the ability to review one's experience and development during the study module.

Interdisciplinary integration: graphic design, programming, 3d modelling and communication disciplines are combined.

According to the 2024 internal module evaluation survey:

• 87% of the students said that the website design assignment improved their digital literacy;

• 91% confirmed that the project helped them better understand the integration of design and technology;

• 78% indicated that it was the most valuable assignment of the semester.

4. Conclusions

1. The didactic innovations applied in the study module "Digital Media Technologies and Design" are an essential condition for achieving relevant and high quality learning.
2. Didactic innovations in the module "Digital Media Technologies and Design" allow achieving higher-level learning goals by developing both technological and creative competencies. Such projects strengthen the connection between theory and practice, which is one of the most important goals of didactic innovations in higher education.
3. Didactic innovations help students master the most important digital media technologies and encourage them to reflect on their creative activities in the study process.

References

1. LAURILLARD, Diana. Teaching as a Design Science: Building Pedagogical Patterns for Learning and Technology. Teaching as a Design Science: Building Pedagogical Patterns for Learning and Technology. 2012, 1-258. 10.4324/9780203125083.
2. GARRISON, D. R., & VAUGHAN, N. D. Blended Learning in Higher Education: Framework, Principles, and Guidelines. San Francisco, CA: Jossey-Bass, 2008.
3. BUDKE, A., SANCHEZ-KIRSCH, N., QUINTERO-RIVAS, E. Long-term didactic innovations in higher education teaching caused by the coronavirus pandemic? Frontiers in Education, 2023, Volume 8. https://www.frontiersin.org/journals/education/articles/10.3389/feduc.
4. BRENNAN, J., BROEK, S., DURAZZI, N., KAMPHUIS, B., RANGA, M., and RYAN, S. Study on innovation in higher education. Publications Office of the European Union, Luxembourg. Available at: http://eprints.lse.ac.uk/55819/ (Accessed March 27, 2023).
5. GIESBERS, B, & DOEL, M. Blended co-design of education: Way of working report, 2020.

Plastic Packaging Chemical Recycling: A Review

Erika GRIGAITYTĖ*, Ingrida VENYTĖ

Kaunas University of Technology, Kaunas, Lithuania

** erika.grigaityte@ktu.edu*

Abstract

By today's trends, companies need to apply a circular economy model, which involves extending the life cycle of a product, thereby ensuring that manufacturing plants will continue to operate without interruptions. In this regard, plastic recycling technologies are an important tool for extending the cycle of plastic packaging. Although many companies have currently implemented models of mechanical recycling technologies, chemical recycling can be another excellent tool to recycle plastic packaging and efficiently manage packaging waste. This review examines chemical recycling technologies specifically applied to plastic packaging materials and provides an overview of the current situation, challenges and future directions.

Keywords: chemical recycling, plastic packaging, packaging waste management.

1. Introduction

Modern society is a consumer community; therefore, with each passing day, not only does the volume of production increase, but also the amount of waste. It is estimated that in 2022, about 58.7 million tons of plastic products were produced in Europe, of which about 39% were packaging [1]. A large proportion of plastic products are still made from fossil-fuels; it is calculated that less than 10% are made from recyclates [1]. The majority of recycling facilities are using mechanical recycling technology, but plastic waste can also be recycled by chemical technologies. Besides, chemical recycling technologies are attractive, because they disrupt the structure of plastics and thus produce monomers or other chemicals, while mechanical recycling focuses on the physical processing of plastic and does not change its chemical structure [2]. Furthermore, recycled plastic achieved from mechanical recycling has lower quality: it might have impurities, reduced strength and can vary in colours [2], at the same time these problems can be avoided by chemical recycling.

This article reviews the chemical recycling technologies, that could be used to recycle plastic packaging. The advantages and limits of the systems are reviewed, to understand what future prospect does chemical recycling have, that would help to achieve sustainable plastic waste management.

2. Variety of plastic packaging waste

Polymers for packaging are chosen for various properties, such as toughness, resistance, impermeability and other various features. However, each plastic packaging is different from one other, because not only different polymers are used, but additives such as paper, organic materials, halogens, metals can be added [3]. So, nowadays, packaging must meet design requirements for recycling. Often it means, that design should be sustainable, so when package goes to recycle stream, it lessens plastics emissions and enhance the recovery [4]. Furthermore, there are key elements, for recycling-focused design, which includes to choose materials with good recycling properties and proper labelling, which ensures easy disassembly if needed, understanding real-time conditions of the recycling market [4]. Polymer complexity, contamination levels, for example, labels, adhesives, additives, inks, often are reasons why

mechanical recycling is unable to recycle plastic packaging waste into high-quality recyclates, and for that reason, interest in chemical recycling emerges [3, 4].

3. Chemical recycling technologies

As mentioned above, chemical recycling is a process where plastic waste is fractured into other chemical components, and it could be high-quality monomers, oligomers, oils, fuels and much more. Since it can obtain high-quality materials, those feedstocks can be used in new production streams. There are several chemical recycling methods, which are presented in Table 1., nonetheless all of them fall into these 2 main categories: thermolysis and solvolysis.

Table 1. Chemical recycling methods for types of plastic packaging [5–8]

Recycling technology	**The type of plastic that can be recycled by this method**	**Main reaction of the technology**	**Main products from the reaction**
Pyrolysis	Polyolefins, such as polyethylene (PE), polypropylene (PP), polystyrene (PS), as well as mixtures of plastics	Thermal decomposition is carried out in an inert environment at temperatures between 450–800°C, if needed a catalyst is used	Various organic compounds, including fuels, waxes, oils and monomers
Hydrocracking	Polyolefins, such as polyethylene (PE), polypropylene (PP), polystyrene (PS), as well as mixtures of plastics	Hydrogen and catalysts used to break down plastics, environment is 350–525°C	Fuels and other high-value chemicals
Gasification	Mixtures of plastics and non-recyclable plastics	Reaction takes place at temperatures above 700°C using oxygen or steam	Various synthetic gases
Hydrothermal liquefaction	Polyolefins, such as polyethylene (PE), polypropylene (PP), polystyrene (PS), as well as mixtures of plastics	The reaction is carried out at high temperatures of 290–450°C under pressure	Plastics break down into crude oil-type products
Catalytic cracking	Polyolefins, such as polyethylene (PE), polypropylene (PP), polystyrene (PS), as well as mixtures of plastics	The reaction is similar to pyrolysis, but catalysts are used, so it is carried out at lower temperatures	Chemical components and fuels
Glycolysis	Polyethylene terephthalate (PET), other polyesters, polyurethane (PU)	Depolymerization of plastics by applying glycols such as ethylene glycol	Monomers and oligomers
Hydrolysis	Polyethylene terephthalate (PET), polyamides (PA)	Depending on the type of hydrolysis, water, aqueous concentrated acids ($H_2SO_{4(aq)}$), as well as aqueous bases ($NaOH_{(aq)}$) are used for depolymerization	Monomers
Alcoholysis	Polyethylene terephthalate (PET),	Alcohols such as methanol or ethanol are used for depolymerization	Monomers and other chemical materials

Recycling technology	**The type of plastic that can be recycled by this method**	**Main reaction of the technology**	**Main products from the reaction**
	other polyesters, polycarbonates (PC)		
Aminolysis and ammonolysis	Polyethylene terephthalate (PET), polyurethane (PU)	Depolymerization using amines or, in the second case, ammonia (NH_3)	Amine structure monomers

The names of the categories explain themselves, as in thermolysis main reaction is carried out in high temperatures, or in solvolysis, the reaction could not be done without a solvent. From table 1, one can understand, that chemical recycling can be used to recycle not only thermoplastics, but also thermosets, like polyurethane, unlike mechanical recycling. Several of the mentioned technologies are applied to an industrial level, like pyrolysis in companies such as *BASF* [9]*, Plastic Energy* [10], or methanolysis at *Eastman* [11], or glycolysis of PET in company *Loop Industries* [12].

4. Challenges, limitations and prospects

Although there are 9 chemical processing technologies mentioned, the broad adoption of chemical recycling is hampered by issues with scalability and economic feasibility [2]. At the moment, these procedures are less financially appealing than conventional recycling techniques since they need larger expenses such as high energy consumption, the cost of catalysts or other chemical reagents, and so on [2,13]. Furthermore, packaging waste comes very heterogenous and in high contamination, so it might affect effectiveness of catalysts, so it is very hard to transition technologies from laboratory to full-scale without capital investments [2]. Despite the fact, that chemical recycling is presented to a circular economy and decrease dependence on virgin fossil-based materials [13], some chemical recycling reactions can generate hazardous by-product or secondary emissions [2]. Needless to say, that higher energy consumption often means more environmental gas, meanwhile used chemicals from reaction, if not reusable, more disposable waste.

Nevertheless, additional researching to develop more favourable catalysts, for their properties like acidity, pore structures, surface area, promoters, metal composition and dispersion, and the metal-support interaction [13], could advance chemical recycling prospects. After solving main problems of chemical recycling technologies, it could be main system for recycling, as for high-quality produced product, which would help to close the loop in circular economy.
Since the European Commission has set very yearning circularity goals for plastics, like that the amount of recycled plastic in plastic products would be at least 30% by 2030 and by 2035 10% of waste could be landfilled [14], it made great support for advancement of chemical recycling. According to Plastics Europe [15], significant investments are being dedicated for developing chemical recycling technology, with projected expenditures increasing from EUR 2.6 billion in 2025 to EUR 8 billion by 2030.

5. Conclusions

1. Chemical recycling, specifically thermolysis processes such as pyrolysis, hydrocracking, gasification, catalytic cracking and hydrothermal liquefaction, could be used as a technology to handle mixed or contaminated plastic packaging waste streams, unlike mechanical recycling, where the plastic waste stream is principally sorted and cleaned several times before recycling.

2. Many different products could be produced from using chemical recycling technologies, for instance, from PET waste, which is depolymerized by the glycolysis process, is obtained high-quality raw material is obtained, which could be used to make food-grade PET plastic, and from mixed plastic packaging waste - by hydrocracking - liquid fuels.
3. Further research is needed to implement and develop chemical recycling technologies in industry, as there are challenges, which include high energy consumption, various expensive catalysts, creation of secondary emissions and chemical wastes.

References

1. *Plastics -the Fast Facts 2023.* Plastics Europe. Available from: https://plasticseurope.org/knowledge-hub/plastics-the-fast-facts-2023/. [viewed 2025-03-18].
2. HARASYMCHUK, Ivanna; KOČÍ, Vladimír and VITVAROVÁ, Monika. Chemical recycling: comprehensive overview of methods and technologies. *International journal of sustainable engineering*, vol. 17 (2024), nr. 1, pp. 124–148. ISSN 1939-7038.
3. ROOSEN, Martijn; MYS, Nicolas; KUSENBERG, Marvin; BILLEN, Pieter; DUMOULIN, Ann and kt. Detailed Analysis of the Composition of Selected Plastic Packaging Waste Products and Its Implications for Mechanical and Thermochemical Recycling. *Environmental science & technology*, vol. 54 (2020), nr. 20, pp. 13282–13293. ISSN 0013-936X.
4. DING, Qian and ZHU, Heping. The Key to Solving Plastic Packaging Wastes: Design for Recycling and Recycling Technology. *Polymers*, vol. 15 (2023), nr. 6, pp. 1485. ISSN 2073-4360.
5. LIU, Yanbing; SHI, Jinwen; JIN, Hui and GUO, Liejin. Chemical recycling methods for managing waste plastics: a review. *Environmental chemistry letters*, vol. 22 (2024), nr. 1, pp. 149–169. ISSN 1610-3653.
6. LI, Houqian; AGUIRRE-VILLEGAS, Horacio A.; ALLEN, Robert D.; BAI, Xianglan; BENSON, Craig H. et al. Expanding plastics recycling technologies: chemical aspects, technology status and challenges. *Green Chemistry*, vol. 24 (2022), nr. 23, pp. 8899–9002. ISSN 1463-9262, 1463-9270.
7. THIOUNN, Timmy ir SMITH, Rhett C. Advances and approaches for chemical recycling of plastic waste. *Journal of polymer science* (2020), vol. 58 (2020), nr. 10, pp. 1347–1364. ISSN 2642-4150.
8. MUNIR, Dureem; IRFAN, Muhammad F. and USMAN, Muhammad R. Hydrocracking of virgin and waste plastics: A detailed review. *Renewable & sustainable energy reviews*, vol. 90 (2018), pp. 490–515. ISSN 1364-0321.
9. *BASF*. BASF Global Sustainability. Website. Available from: https://www.basf.com/global/en/who-we-are/sustainability/our-contributions-to-enabling-the-green-transformation/circular-economy/circular-feedstocks/chemcycling. [viewed 2025-04-04].
10. *Plastic Energy.* Plastic Energy Technology. Website. Available from: https://plasticenergy.com/technology/. [viewed 2025-04-04].
11. *Eastman.* Eastman Sustainability. Website. Available from: https://www.eastman.com/en/sustainability/environmental/circularity/resources/publications. [viewed 2025-04-04].
12. *Loop Industries.* Loop Industries Technology. Website. Available from: https://www.loopindustries.com/en/technology. [viewed 2025-04-04].
13. HUANG, J. et al. Chemical recycling of plastic waste for sustainable material management: A prospective review on catalysts and processes. In *Renewable and Sustainable Energy Reviews*. 2022. Vol. 154, p. 111866.
14. EUROPEAN PARLIAMENT AND COUNCIL. 2025. Regulation (EU) 2025/802 of 11 April 2025 on requirements for recycled plastic in products and amending certain regulations. Official Journal of the European Union, L 40, 12 April 2025, Available from: https://eur-lex.europa.eu/legal-content/EN/TXT/?uri=OJ:L_202500040. [viewed 2025-04-14].
15. *Plastics Europe.* Plastics Europe Chemical Recycling. Website. Available from: https://plasticseurope.org/sustainability/circularity/recycling/chemical-recycling/. [viewed 2025-04-14].

SUSTAINABLE CONSUMPTION AND BUSINESS MANAGEMENT

AHP-Based Decision Support System (DSS) for Reducing Energy Consumption in Data Centers

Keshmin SENARATNA[1]*, Jūratė ŠLIOGERIENĖ[2]

1 Riga Technical University, Latvia
2 Vilnius Gediminas Technical University, Lithuania
** keshmin.senaratna@edu.rtu.lv*

Abstract

Data centers comprise important IT infrastructure but represent major energy users, particularly in tropical climates where cooling needs are high. This research presents an Analytic Hierarchy Process (AHP)-based Decision Support System (DSS) to systematically prioritize solutions for lowering data center energy usage. By describing the issue as a goal, criteria, and alternatives, and gathering expert evaluations using Saaty's 9-point scale, the AHP framework statistically ranks each alternative's potential effect. A case study at Sri Lanka Telecom Data Center reveals that high-density modular configurations obtain the greatest priority weight, followed closely by green data center designs. The results underline the necessity to improve cooling and hardware infrastructure, considering the close connection between these elements and overall energy use. This DSS provides a transparent, data-driven decision-making strategy that is repeatable across comparable tropical conditions. Future studies may expand this technology to real-time energy monitoring and hybrid MCDM models.

Keywords: decision support system, multiple criteria decision making, AHP, energy efficiency infrastructure.

1. Introduction

Data centers have swiftly transformed into vital infrastructure, enabling the expansion of cloud computing, big data analytics, and different corporate applications globally [1]. However, these facilities are also regarded as substantial energy users, with a growing requirement for both processing power and cooling capacity. Recent estimates imply that around the world, data center operations account for a considerable amount of the world's electrical power consumption, prompting urgent requests for more efficient designs and operations [2]. Against this background, attempts to install greener technology and manage power use in high-density locations have become a strategic priority for organizations aiming to reconcile operational performance with sustainability objectives [3, 4].

This research tackles the critical issue of excessive energy usage in data centers operating in tropical, high-humidity environments, concentrating on approaches to minimize cooling loads while maintaining optimum infrastructure performance. The primary aim is to present a systematic and transparent means of analyzing alternative data center architectures to find the most energy-efficient alternative, utilizing the Analytic Hierarchy Process (AHP) methodology as a rigorous Multiple Criteria Decision Making (MCDM) tool [5]. By deconstructing the main purpose into hierarchical layers such as criteria, sub-criteria, and candidate alternatives, AHP offers measurable measurements of relative significance, thereby aiding infrastructure planners and managers in making balanced, data-driven decisions [6]. Expert opinion, acquired via paired

comparisons, provides the foundation of this weighted analysis, guaranteeing that the proposed technique is both contextually grounded and mathematically coherent.

To date, a considerable body of significant research has studied approaches to boost energy efficiency in data centers, spanning from enhanced cooling systems to renewable power integration and resource virtualization [7, 8]. While much research focuses on particular strategies, such as free-cooling or liquid cooling, fewer have utilized a systematic MCDM framework that holistically assesses numerous options on technical, environmental, and financial aspects. This gap underlines the necessity for a structured, transparent decision support system that synthesizes expert contributions and quantifies trade-offs among potentially conflicting factors, an area where AHP is especially well-suited. A recent research by Özkan et al. [9] examined and contrasted Asia Pacific Accreditation Cooperation (APAC) countries' risk profiles that influence data centers' (DCs) efficacy. They proposed a systematic assessment process employing two MCDM methodologies, namely spherical fuzzy AHP (SF-AHP) and EDAS (evaluation based on distance from average solution). While SF-AHP is favored to prioritize the main and sub-criteria in an imperfect decision-making environment, EDAS is employed to rank the countries' DC profiles, embedding the derived criterion weights. Erdem and Özdemir [10] assessed the eight major criteria and the forty-five sub-criteria for picking the most suitable site for the data center while considering the fifty various economies in different business areas. This was done by employing the continuous intuitionistic fuzzy sets (CIFS)-based AHP to specify the weights of each criterion and sub-criterion. Then, the CIFS-based approach for order of preference by similarity to the ideal solution (TOPSIS) is created to rank the fifty economies integrated with the weights from the CIFS-based AHP. Another study in a European environment likewise preferred MCDM-driven techniques, demonstrating that data centers containing virtualized systems could retain performance while drastically cutting their power use [11]. Relying on current literature, this study proposes an AHP-based decision-making method specific for a Data Center in Sri Lanka, intending to obtain compelling evidence on which modernization plan corresponds most closely with its sustainability goals.

Methodologically, the article used the AHP to acquire expert opinions, followed by consistency tests to confirm each comparison matrix. The final recommendations are then generated by calculating local and global priority weights for options, ending in a rating that indicates the option most likely to produce large energy savings. The key results suggest that high-density modular architecture and greener infrastructure technologies lead the way in minimizing the large cooling needs seen in tropical areas. Ultimately, this work adds to a greater body of knowledge on data center architecture, offering a reproducible blueprint for energy efficiency and decision-making excellence in this vital sector.

2. Methodology

This research used the AHP as an MCDM framework to systematically evaluate and prioritize options for minimizing energy usage in data centres. AHP enables decision-makers to organize intricate issues into a hierarchical framework, deconstructing the problem into a goal, criteria, sub-criteria, and alternatives. Expert ratings were collected via pairwise comparisons to ascertain the relative significance of each criterion and option. The research used Saaty's 9-point scale [12] to quantify expert assessments, facilitating a systematic analysis of decision-making elements. A case study methodology was used to implement the AHP concept in a practical context. The study focused on the Sri Lanka Telecom Data Center, a prominent data center in Sri Lanka. This selection was taken under many considerations, including industrial relevance, energy consumption concerns, and access to expert expertise. This analysis confirms that the AHP framework offers practical, data-informed suggestions applicable to similar data centers in tropical climatic regions.

The decision hierarchy was developed (see Fig. 1) based on the identified criteria and corresponding sub-criteria that greatly affect the energy efficiency in a data center. Three alternatives were considered as potential alternatives to transform the condition of the current data center to an energy-efficient data center. Each decision is evaluated in terms of impact criteria, and AHP is used to determine the priority ranking of these alternatives. This method guarantees an objective and mathematically rigorous approach to identifying data centers' optimal energy reduction strategy. A case study methodology was used to implement the AHP concept in a practical context. The study focused on the Sri Lanka Telecom Data Center, a prominent data center in Sri Lanka. The selection was justified due to the data center's operation in a high-temperature, high-humidity environment, necessitating substantial cooling measures. As a premier telecom operator, enhancing energy efficiency in its data centers directly influences operational efficacy and sustainability.

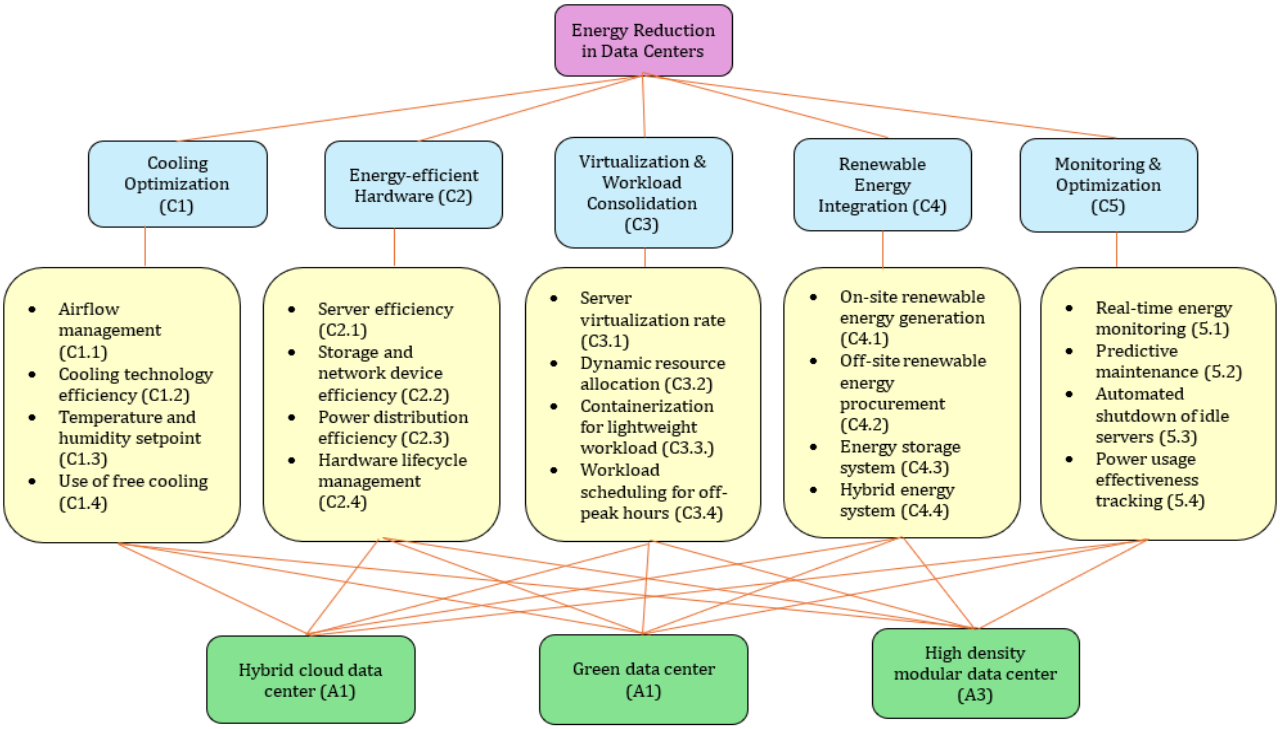

Fig. 2. AHP decision hierarchy for selecting the best energy-efficient data center category

Data gathering included expert surveys to acquire pairwise comparison evaluations. Four specialists with extensive data center operations and energy management expertise were chosen as detailed in Table 1.

Table 7. Industry experts participated in the pairwise comparison of criteria

ID	Occupation	Years of experience	Highest qualification
E1	Operational Manager	18 years	M.Sc. in Electrical Engineering
E2	Network Engineer	11 years	M.Sc. in Information Technology
E3	Data Center Technician	8 years	B.Sc. in Electrical and Electronic Engineering
E4	Professor	21 years	Ph.D. in Computer Science

The pairwise comparison matrix (PCM) was derived using a decision tree, assessing the weight of I_{Ti} relative to I_{Tj}. The matrix ranks components at each hierarchical level, using a standardized nine-point scale (see Table 2) introduced by Saaty to indicate preference.

Decision-makers offer judgments comparing criteria pairwise using the standard scale Table 2. These comparisons generate a reciprocal matrix. After that, the following steps are performed.
Step 1: The relative weights of the criteria are calculated by calculating the dominant eigenvector of the matrix. The weights are then normalized such that their total equals one. This technique facilitates the quantitative examination of subjective preferences [13].

Table 2. Saaty's nine-point scale for pairwise comparison [12]

Intensity of Importance	Definition	Explanation
1	Equally importance	Each of the two actions contributes equally to the objective
3	Moderate importance	Experience and judgment marginally favor one activity over another
5	Strong importance	Strong preference is given to one aspect over another
7	Demonstrated importance	The practical demonstration of an element's dominance
9	Extreme importance	An element's complete domination is confirmed at the highest level
2,4,6,8	Intermediate values	used to balance opposing opinions when analysing data

Step 2: The Consistency Ratio (CR) is computed to guarantee accurate judgments (see Table 3). If the CR is below 0.1, the matrix is deemed consistent. Otherwise, inputs should be corrected. This prevents against contradicting preferences and promotes decision robustness.

Table 3. Random indexes for the consistency ratio check [12]

n	1	2	3	4	5	6	7	8	9	10
RI	0	0	0.52	0.89	1.11	1.25	1.35	1.40	1.45	1.49

Step 3: Each choice is evaluated by multiplying its performance scores under each criterion by the relevant weight and totaling the results. The option with the greatest score is rated as the most favorable.

3. Results

Experts evaluated the five primary criteria for their impact on decreasing energy usage in data centers. Cooling optimization (C1) and energy-efficient hardware (C2) are often prioritized because of their immediate energy-saving effects. The normalized eigenvector obtained from the pairwise matrix establishes the relative significance of each primary criterion in attaining energy efficiency in data centers (see Table 4).

Table 4. Pairwise comparison of the goal and weights of the main criteria

Criteria	C1	C2	C3	C4	C5	Weight
C1	1	2	3	4	3	0.384
C2	1/2	1	2	3	2	0.239
C3	1/3	1/2	1	2	2	0.153
C4	1/4	1/3	1/2	1	2	0.126
C5	1/3	1/2	1/2	1/2	1	0.098

After calculation, the highest eigenvalue (λ_{max}) is determined to be 5.12, along with a consistency index (CI) of 0.03 and a random index (RI) of 1.12. The consistency ratio (CR) is calculated at 0.026, which is under the threshold of 0.1, indicating that the judgments of the decision-makers are consistent. Then, the experts evaluated the extent to which each alternative fulfils the primary criteria (see Fig. 2). Scores are local weights normalized under each criterion.

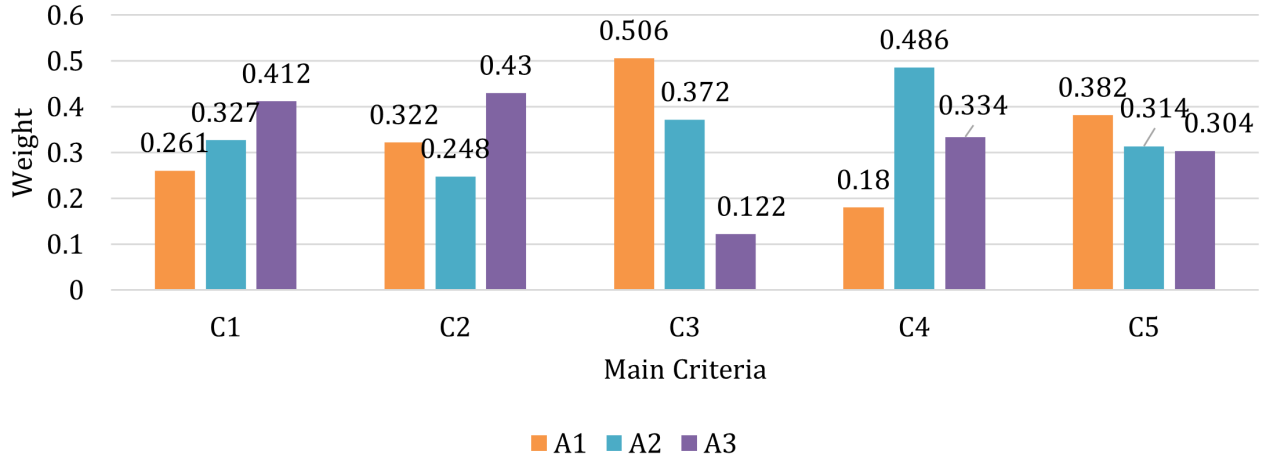

Fig. 4. Weights of alternatives against the main criteria

The total scores of the alternatives were obtained by synthesizing the local priority weights of each option under the five primary criteria with their corresponding global weights. This aggregate gives a complete assessment of how effectively each solution meets the purpose of energy savings in data centers. The final results reflect the relative efficacy of each data center plan based on expert judgments across major energy efficiency variables (see Fig. 3).

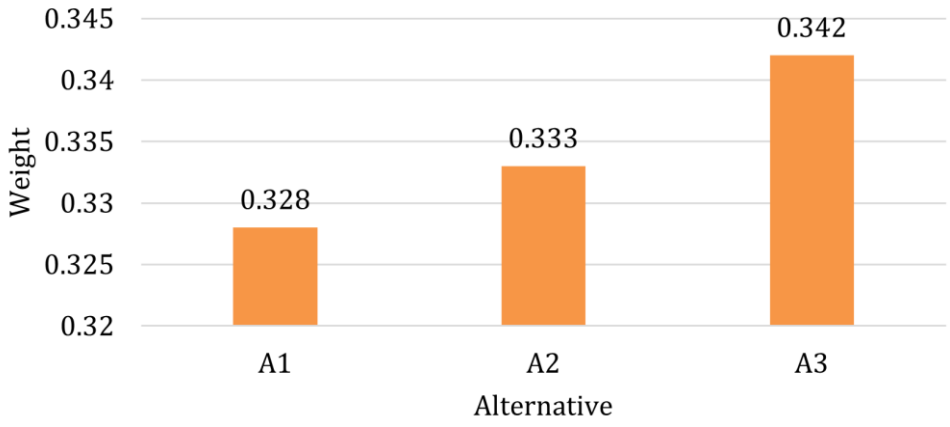

Fig. 6. Final weights of the alternatives

The results reveal that the High-Density Modular Data Center (A3) is the most suited solution for optimizing energy efficiency, followed closely by the Green Data Center (A2). The investigation reveals that emphasizing sophisticated cooling and hardware efficiency methods greatly helps to decrease energy consumption in data centers operating under tropical climatic conditions.

4. Conclusions

1. The research successfully developed an AHP-based DSS tailored for selecting the most energy-efficient data center design, especially addressing the operational issues of tropical climatic zones such as Sri Lanka.
2. Cooling Optimization (C1) and Energy-Efficient Hardware (C2) were identified as the most significant criteria, providing a combined weight of over 60% toward the aim of energy reduction, highlighting the vital need for infrastructure-level changes.

3. The High-Density Modular Data Center (A3) was selected as the most ideal solution, with a final weight of 0.342, because of its compatibility with sophisticated cooling systems and current hardware combinations.
4. The Green Data Center (A2) followed closely after, exhibiting significant alignment with renewable energy integration, whereas the Hybrid Cloud Data Center (A1) was more successful in virtualization-related elements but less influential in cooling and hardware domains.
5. This study indicates that MCDM methods like AHP offer an objective, transparent, and repeatable framework for complex infrastructure choices in the ICT industry, especially in energy-intensive contexts.
6. Future research should study hybrid MCDM models (AHP-TOPSIS or AHP-Fuzzy logic, etc.), include real-time energy data for dynamic decision-making, and expand the concept to cloud-native or edge data center architectures.

References

1. EWIM, Daniel Raphael Ejike, Nwakamma NINDUWEZUOR-EHIOBU, Ochuko Felix ORIKPETE, Blessed Afeyokalo EGBOKHAEBHO, Akeeb Adepoju FAWOLE, et al. Impact of Data Centers on Climate Change: A Review of Energy Efficient Strategies. The Journal of Engineering and Exact Sciences, vol. 9 (2023), no. 6, pp. 16397–01e. ISSN 2527-1075.
2. KOOT, Martijn, and Fons WIJNHOVEN. Usage impact on data center electricity needs: A system dynamic forecasting model. Online. Applied Energy, vol. 291 (2021), p. 116798. ISSN 0306-2619.
3. IKRAM, Muhammad, and Jinane Es SADKI. Resilient and sustainable green technology strategies: A study of Morocco's path toward sustainable development. Online. Sustainable Futures, vol. 8 (2024), p. 100327. ISSN 2666-1888.
4. ZHU, Hongyu, Dongdong ZHANG, Hui Hwang GOH, Shuyao WANG, Tanveer AHMAD, et al. Future Data Center Energy-Conservation and Emission-Reduction Technologies in the Context of Smart and Low-Carbon City Construction. Online. Sustainable Cities and Society, (2022), p. 104322. ISSN 2210-6707.
5. TOMCZEWSKI, Andrzej, Stanisław MIKULSKI, and Jan SZYMENDERSKI. Application of the Analytic Hierarchy Process Method to Select the Final Solution for Multi-Criteria Optimization of the Structure of a Hybrid Generation System with Energy Storage. Online. Energies, vol. 17 (2024), no. 24, p. 6435. ISSN 1996-1073.
6. KRISWARDHANA, Willy, Bladimir TOAZA, Domokos ESZTERGÁR-KISS, and Szabolcs DULEBA. Analytic hierarchy process in transportation decision-making: A two-staged review on the themes and trends of two decades. Online. Expert Systems with Applications, vol. 261 (2025), p. 125491. ISSN 0957-4174.
7. RAN, Yongyi, Han HU, Yonggang WEN, and Xin ZHOU. Optimizing Energy Efficiency for Data Center Via Parameterized Deep Reinforcement Learning. Online. IEEE Transactions on Services Computing, (2022), pp. 1–14. ISSN 1939-1374.
8. BEREZOVSKAYA, Yulia, Chen-Wei YANG, Arash MOUSAVI, Valeriy VYATKIN, and Tor Bjorn MINDE. Modular Model of a Data Centre as a Tool for Improving Its Energy Efficiency. Online. IEEE Access, vol. 8 (2020), pp. 46559–46573. ISSN 2169-3536.
9. ÖZKAN, Barış, Mehmet ERDEM, and Eren ÖZCEYLAN. Evaluation of Asian Countries using Data Center Security Index: A Spherical Fuzzy AHP-based EDAS Approach. Online. Computers & Security, (2022), p. 102900. ISSN 0167-4048.
10. ERDEM, Mehmet, and Akın ÖZDEMIR. Sustainability and risk assessment of data center locations under a fuzzy environment. Online. Journal of Cleaner Production, vol. 450 (2024), p. 141982. ISSN 0959-6526.
11. AVGERINOU, Maria, Paolo BERTOLDI, and Luca CASTELLAZZI. Trends in Data Centre Energy Consumption under the European Code of Conduct for Data Centre Energy Efficiency. Online. Energies, vol. 10 (2017), no. 10, p. 1470. ISSN 1996-1073.
12. SAATY, T. The analytic hierarchy process: Planning, priority setting, resource allocation. New York: McGraw-Hill International Book Co., 1980. ISBN 0070543712.
13. FORMAN, Ernest H., and Saul I. GASS. The Analytic Hierarchy Process–An Exposition. Operations Research. Vol. 49 (2001), no. 4, pp. 469–486. ISSN 1526-5463.

ESTE Framework: A Novel Approach to Construction Waste Management Through AHP-Based MCDM Model

Thilina Ganganath WEERAKOON*, Jūratė ŠLIOGERIENĖ

Vilnius Gediminas Technical University, Lithuania

** thilina-ganganath.weerakoon@vilniustech.lt*

Abstract

The construction industry greatly contributes to global waste generation, with construction and demolition waste (CDW) providing considerable environmental, economic, and operational difficulties. In many developing countries, traditional waste management systems fall short in encouraging sustainability, leading to wasteful resource usage and increased landfill dependency. This paper presents the ESTE Framework, an innovative method combining Economic, Social, Technological, and Environmental dimensions into an Analytic Hierarchy Process (AHP)-based Multi-Criteria Decision-Making (MCDM) model to improve Construction Waste Management (CWM) via circular economy (CE) principles, using Sri Lanka as a case study. Expert views were acquired via pairwise comparisons, indicating environmental elements as the most essential (41.6%), followed by economic (38.4%), technological (12.6%), and social (7.4%) concerns. On-site waste segregation was identified as the most effective option, with off-site treatment, prefabrication, and waste-to-energy conversion all considered. The research stresses the necessity for organized decision-making tools like the ESTE Framework and advises future integration of real-time data and artificial intelligence (AI) to better assist sustainable practices.

Keywords: multiple criteria decision making, AHP, construction industry, waste management.

1. Introduction

Globally, the construction industry substantially drives economic development, especially in emerging nations, nonetheless, this expansion has precipitated severe sustainability concerns with construction and demolition waste (CDW) [1]. Global annual CDW generation exceeds 3 billion tons, intensifying environmental challenges due to increased landfill use and resource exhaustion [2–4]. Conventional linear economic (LE) models (take-make-dispose) have shown their insufficiency, leading to the implementation of circular economy (CE) strategies that prioritize the recycling and reuse of resources within a closed-loop framework [5].

Integrating CE concepts into construction waste management (CWM) necessitates structured decision-making procedures owing to the complexities in choosing the optimum options. Multi-criteria decision-making (MCDM) approaches, especially the Analytic Hierarchy Process (AHP), have become essential instruments for methodically assessing several conflicting criteria, such as technological, social, economic, and environmental factors that impact sustainable waste management alternatives [6, 7]. Notwithstanding its potential, the present utilization of MCDM alongside CE principles in the construction industry is nonetheless constrained.

The current research addresses the highlighted gap by developing a complete, integrated framework that combines AHP-based MCDM methodologies with CE principles, designed to prioritize and optimize waste management strategies. The primary research inquiry is “What

ways can the incorporation of an AHP-based MCDM methodology improve the implementation of CE principles in CWM?"
The article introduces the ESTE (Environmental, Social, Technological, and Environmental) Framework, a systematic decision-making model built on an AHP-based MCDM methodology to tackle these difficulties. The ESTE Framework encompasses four fundamental elements for evaluating and selecting sustainable CWM options. The framework aims to improve the use of circular economy concepts in CWM procedures by methodically identifying trade-offs and interrelationships among these factors.

2. Theoretical Background of MCDM in CWM

MCDM methodologies have become vital in Construction Waste Management (CWM), given their potential to systematically analyze complicated and linked decision-making situations (Table 1). Among the most prominent MCDM methods utilized are the Analytic Hierarchy Process (AHP), Technique for Order of Preference by Similarity to Ideal Solution (TOPSIS), Decision-Making Trial and Evaluation Laboratory (DEMATEL), Analytic Network Process (ANP), Weighted Aggregated Sum Product Assessment (WASPAS), and Multi-Attributive Border Approximation Area Comparison (MABAC).

The AHP technique supports prioritizing by breaking complicated waste management solutions into hierarchical criteria, allowing stakeholders to analyze the relative value of alternative waste reduction options [8]. TOPSIS offers a systematic assessment of options by analyzing their proximity to an ideal solution, frequently utilizing fuzzy extensions to handle uncertainty and subjective data inputs, such as recycling rates and cost variations [9]. DEMATEL explicitly tackles interdependencies across crucial components, revealing key causal links and drivers in efficient CWM deployment, such as policy enforcement and technical availability. Additionally, ANP enhances the possibilities of AHP by supporting connected criteria rather than hierarchical structures alone, enabling flexibility in recording complicated decision networks [10]. Methods such as WASPAS and MABAC have lately been merged to handle thorough multi-criteria assessments, especially when paired with fuzzy logic or rough numbers, to successfully manage uncertainties inherent in construction projects [11]. These combined techniques increase robustness, precision, and transparency of CWM-related decisions.

Table 8. Summary of MCDM studies focused on CWM

Author(s)	Focus	Applied MCDM Method
Khoshand et al. [12]	Identify best CWM alternatives including landfilling, reusing, recycling, and reducing	Fuzzy AHP
Marzouk et al. [13]	Prioritizing waste management techniques by choosing the most sustainable disposable method	Fuzzy TOPSIS
Eghbali-Zarch et al. [14]	Ranks the feasible strategy solutions by the sustainable development criteria to enhance the performance of CWM	IDOCRIW+WASPAS
Shah. [15]	Optimal site selection of construction waste treatment options	AHP
Bin et al. [16]	Identify the most critical CWM factors	DEMATEL
Zhang et al. [17]	Develop a heterogeneous multi-criteria evaluation framework to assist decision-making in CDW utilization by selecting the most optimal waste management scheme from multiple alternatives	ANP+MABAC

Yi et al. [18]	CDW management by integrating Life Cycle Assessment (LCA) and Life Cycle Costing (LCC) into an MCDM framework	AHP+TOPSIS

However, despite their virtues, present MCDM applications confront constraints, including subjective biases in expert assessments, heavy data needs, dynamic cost swings, and the difficulty required in combining qualitative and quantitative data successfully. Overall, MCDM techniques greatly boost sustainable building processes by promoting transparent, informed, and methodical decision-making, so aligning closely with CE principles to promote resource recovery and waste reduction.

3. Methodology

This research employs the ESTE Framework, applying an AHP-based MCDM technique to thoroughly analyze CWM solutions. The AHP technique is chosen because of its organized approach, enabling complicated issues to be broken down hierarchically and appraised via pairwise comparisons. By evaluating four fundamental elements, the ESTE Framework offers a complete framework for choosing sustainable waste management choices. The technique is created primarily for poor nation environments, with Sri Lanka acting as a sample case study.

3.1. Research Design

The research's strategy makes use of the AHP methodological framework to make it simpler to discover elements impacting the CWM and suggest a new framework. The widely used AHP is an MCDM technique that allows for systematic comparisons and alternative ranking utilizing a hierarchical structure. Using AHP, decision-making modelling starts with the development of a decision tree. This decision tree (Fig. 1) contains the goal of the study, dimensions for CWM, and affecting factors within each dimension (Table 2).

Table 2. Dimensions and factors influencing CWM

Goal	Dimensions	Dimension Label	Influencing Factor
Selecting the ideal CWM strategy	Economic factors (EC)	EC1	Market demand for recycled materials
		EC2	Financial incentives
		EC3	Cost-effective practices
		EC4	Policies and regulations
	Social factors (S)	S1	Safety and health
		S2	Training and Education
		S3	Employment and labor regulations
		S4	Community involvement
		S5	Cultural attitudes towards waste management
	Technological factors (T)	T1	Waste tracking and monitoring
		T2	Development of modular construction
		T3	Waste segregation technologies
		T4	Waste recycling technologies
		T5	Product design
		T6	CWM infrastructure
	Environmental factors (EN)	EN1	Natural resource availability
		EN2	Ecosystem fragility
		EN3	Energy costs and sources
		EN4	Land availability for landfills

The review evaluates four waste management alternatives, including on-site segregation (A1), off-site treatment (A2), Waste-to-Energy (WTE) conversion (A3), and prefabrication and modular

Construction (A4). The Eigenvector Method is used to prioritize these options, providing an objective, mathematically rigorous approach.

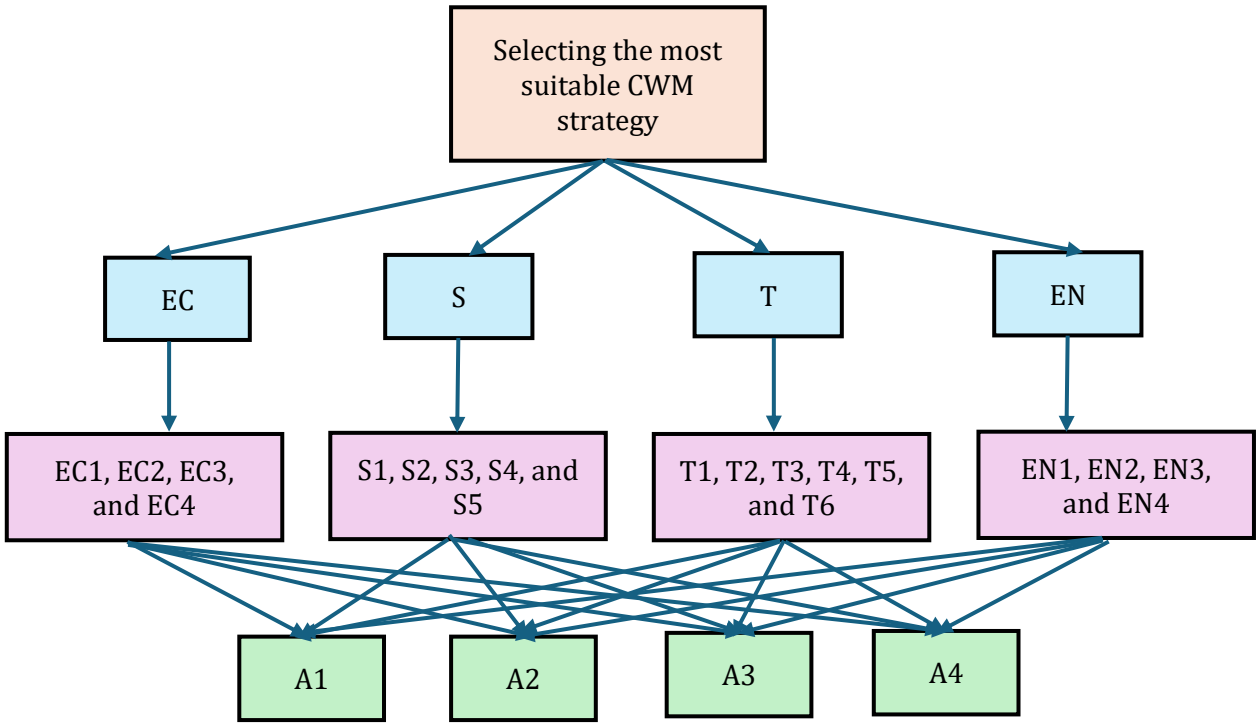

Fig. 1. AHP decision tree with goal, dimensions, and influencing factors for ESTE framework

This research examines developing countries, with Sri Lanka as a case study due to its significant urbanization and building sector expansion, insufficient recycling infrastructure, weak policy enforcement, and lack of circular economy integration. Despite these challenges, Sri Lanka has shown increased commitment to sustainability through legislative interventions, recycling efforts, and cooperation with foreign organizations. A structured survey was conducted among six industry professionals, ensuring a smaller, experienced panel for accurate and consistent decision-making, as MCDM approaches promote quality and depth of expert knowledge.

3.2. AHP Method

The pairwise comparison matrix (PCM). The matrix evaluates elements at each level of hierarchy with a predefined nine-point scale (Table 3) established by Saaty [19] for expressing preference of the experts.

Table 3. The nine-point scale used in the pairwise comparison of AHP [19]

Intensity of Importance	Definition	Explanation
1	Equally importance	Two activities contribute equally to the objective
3	Moderate importance	Experience and judgment slightly favor one activity over another
5	Strong importance	Experience and judgment strongly favor one activity over another
7	Very strong importance	An activity is favored very strongly over another
9	Extreme importance	The evidence favoring one activity over another is of the highest possible order of affirmation
2,4,6,8	Intermediate values	used to balance opposing opinions when analysing data

The Eigenvector Method, commonly known as the primary eigenvalue technique, is utilized in this study to estimate priority weights of criteria and rank alternatives in the AHP. It calculates the principal eigenvector of the pairwise comparison matrix. Once the comparison matrix is formed, the main eigenvector is derived by calculating the eigenvalue equation shown below (1):

$$A = \lambda_{max}\omega. \tag{1}$$

Where: λ_{max} is the greatest eigenvalue of matrix A, and w is the related eigenvector that specifies the priority weights of the criteria.
The eigenvector is normalized by formula (2) such that the sum of its constituents equals 1:

$$\omega_{ij} = \frac{\omega_i}{\sum_{j=1}^{n}\omega_j}. \tag{2}$$

One feature of the AHP method is the ability to verify the consistency of the responses. The consistency ratio (CR) is calculated using the formulas presented below (3) and (4):

$$IC = \frac{(\lambda_{max}-n)}{n-1}, \tag{3}$$

$$CR = \frac{IC}{RI}. \tag{4}$$

where: λ_{max} is the eigenvalue of each decision matrix, and n is the matrix order.

Each matrix's random index (RI) is determined by the number of criteria it contains. The RI values are displayed in Table 4 based on the matrix order (n).

Table 4. RI numbers used for computing CR [19]

n	1	2	3	4	5	6	7	8	9	10
RI	0	0	0.52	0.89	1.11	1.25	1.35	1.40	1.45	1.49

The CR value below 0.1 indicates acceptable consistency, while higher values suggest revision. Priority weights are computed, alternative levels compared, and final rankings obtained by the formula presented below (5):

$$S_j = \sum_{i=1}^{n} w_i a_{ij}, \tag{5}$$

where S_j is the final score of option j, w_i is the weight of criterion i, and a_{ij} indicates the relative performance of alternative j under criterion i.

3. Results

The experts used pairwise comparison and Saaty's scale to assess CWM alternatives. They normalized pairwise comparison matrices and determined priority weights for each criterion, ensuring direct comparisons. Environmental aspects were selected as the most essential feature, accounting for 41.4% of the total weight, showing the increased focus on resource conservation, land availability, and ecosystem preservation. Economic considerations followed with a weight of 38.6%, suggesting the considerable impact of market demand, financial incentives, and cost-effective procedures. Technological elements contributed 12.6%, stressing the impact of innovation in waste monitoring, recycling technology, and modular building. Social elements, although still vital, had the lowest weight at 7.4%, demonstrating that while community

engagement and labor standards are important, they are seen as secondary compared to environmental and economic concerns in construction waste management prioritizing.
The final scores were obtained by integrating these weights with the total relevance of the criteria. This method ensured consistency in decision-making by transforming subjective judgments into a measurable scale. The final ranking (Fig. 2) of CWM methods was obtained by combining weighted priority ratings across all assessment categories, ensuring the most sustainable and effective waste management solution is determined through a detailed, multi-criteria analysis.

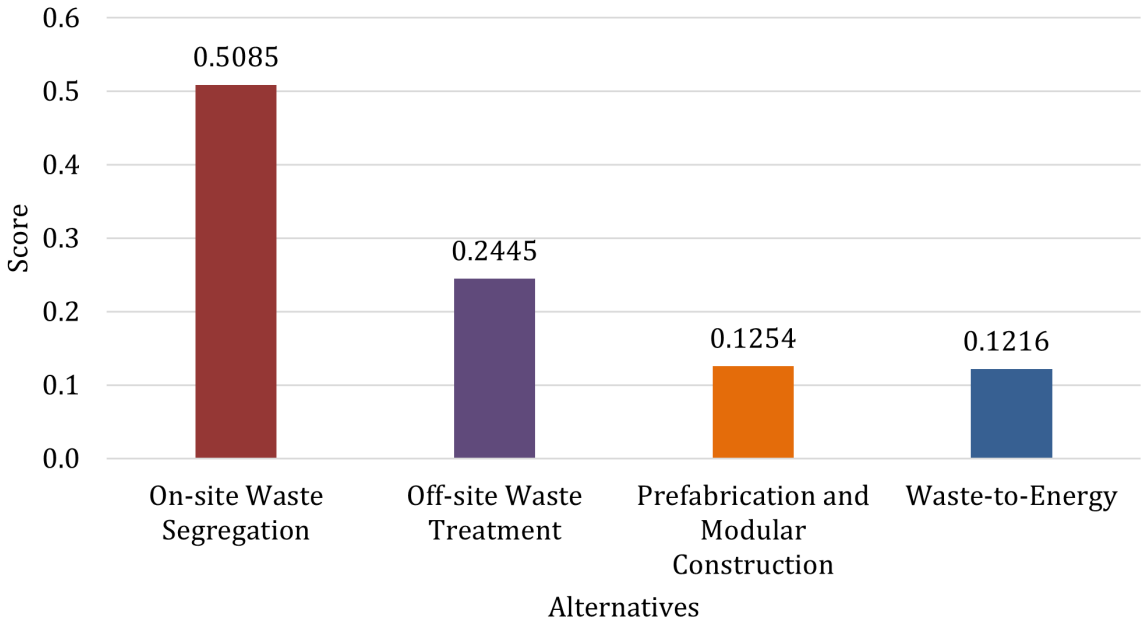

Fig. 2. Final weights of the alternatives

On-site Waste Segregation was the most recommended method, ranked at 0.5085 due to its economic feasibility, social acceptability, and technical efficacy. Off-site Waste Treatment followed with a score of 0.2445, showing potential for large-scale waste processing and recycling but needing additional logistical assistance. Prefabrication took third place with a score of 0.1254, benefiting from decreased material waste but facing cost and flexibility issues in Sri Lanka's current building scene. Waste-to-Energy Conversion ranked lowest at 0.1216, highlighting concerns about high initial costs, energy inefficiencies, and environmental limits. The study incorporated CE principles directly into the AHP-based MCDM framework for CWM, focusing on waste reduction, resource recovery, and recycling in the building environment. This comprehensive perspective connects well with the global focus on sustainability and provides practical insights for policy-makers and industry practitioners in developing sustainable waste management plans.

4. Conclusions

1. The proposed ESTE Framework, based on an AHP-based MCDM theory, offers an effective and systematic way an effective and systematic way to integrate CE concepts into CWM by incorporating environmental, economic, technical, and social elements.
2. On-site waste segregation and recycling (A1) was selected as the most successful CWM method, since it immediately decreases waste at the source, boosts material recovery, and promotes sustainability. It gives rapid advantages with very minimal technological complexity, making it extremely relevant in underdeveloped economies.

3. The framework enables stakeholders to understand and navigate the trade-offs involved in alternative waste management methods, such as off-site treatment, prefabrication, and waste-to-energy conversion, each of which offers distinct advantages and limitations, including cost, logistical challenges, and technology requirements.
4. This study presents a realistic and scalable decision-support tool for policymakers and industry practitioners in poor nations, where inadequate infrastructure and regulatory structures impede sustainable building methods.
5. Future studies ought to concentrate on improving the model's versatility through incorporation with real-time data analytics and AI, which could help overcome the static constraints of AHP and minimize subjectivity in expert judgments, leading to more dynamic and responsive decision-making systems.

References

1. HE, Qingsong, Min XU, Zike XU, Yanmei YE, Xianfan SHU, et al. Promotion incentives, infrastructure construction, and industrial landscapes in China. Land Use Policy, vol. 87 (2019), p. 104101. ISSN 0264-8377.
2. AKHTAR, Ali, and Ajit K. SARMAH. Construction and demolition waste generation and properties of recycled aggregate concrete: A global perspective. Journal of Cleaner Production, vol. 186 (2018), pp. 262–281. ISSN 0959-6526.
3. VILLORIA SÁEZ, Paola, and Mohamed OSMANI. A diagnosis of construction and demolition waste generation and recovery practice in the European Union. Journal of Cleaner Production, vol. 241 (2019), p. 118400. ISSN 0959-6526.
4. MENEGAKI, Maria, and Dimitris DAMIGOS. A review on current situation and challenges of construction and demolition waste management. Current Opinion in Green and Sustainable Chemistry, vol. 13 (2018), pp. 8–15. ISSN 2452-2236.
5. SHARMA, Nagendra Kumar, Kannan GOVINDAN, Kuei Kuei LAI, Wen Kuo CHEN, and Vimal KUMAR. The transition from linear economy to circular economy for sustainability among SMEs: A study on prospects, impediments, and prerequisites. Business Strategy and the Environment (2020). ISSN 1099-0836.
6. TORKAYESH, Ali Ebadi, Behnam MALMIR, and Mehdi RAJABI ASADABADI. Sustainable waste disposal technology selection: The stratified best-worst multi-criteria decision-making method. Waste Management, vol. 122 (2021), pp. 100–112. ISSN 0956-053X.
7. SOLTANI, Atousa, Kasun HEWAGE, Bahareh REZA, and Rehan SADIQ. Multiple stakeholders in multi-criteria decision-making in the context of Municipal Solid Waste Management: A review. Waste Management, vol. 35 (2015), pp. 318–328. ISSN 0956-053X.
8. BAFAIL, Omer A., and Reda MS ABDULAAL. New approach for selecting a suitable recycling collection program for recovered paper and pulp recyclables using AHP-TOPSIS techniques. Waste Management & Research: The Journal for a Sustainable Circular Economy, vol. 39 (2021), no. 2, pp. 1406-1413. ISSN 1096-3669.
9. SHAHBA, Sudabe, Reza ARJMANDI, Masoud MONAVARI, and Jamal GHODUSI. Application of multi-attribute decision-making methods in SWOT analysis of mine waste management (case study: Sirjan's Golgohar iron mine, Iran). Resources Policy, vol. 51 (2017), pp. 67–76. ISSN 0301-4207.
10. SAATY, Thomas L. Making and validating complex decisions with the AHP/ANP. Journal of Systems Science and Systems Engineering, vol. 14 (2005), no. 1, pp. 1–36. ISSN 1861-9576.
11. SALIMIAN, Sina, Seyed Meysam MOUSAVI, and Jurgita ANTUCHEVIČIENĖ. Evaluation of infrastructure projects by a decision model based on RPR, MABAC, and WASPAS methods with interval-valued intuitionistic fuzzy sets. International Journal of Strategic Property Management, vol. 26 (2022), no. 2, pp. 106–118. ISSN 1648-9179.
12. KHOSHAND, Afshin, Kimia KHANLARI, Hamidreza ABBASIANJAHROMI, and Milad ZOGHI. Construction and demolition waste management: Fuzzy Analytic Hierarchy Process approach. Waste Management & Research: The Journal for a Sustainable Circular Economy, vol. 38 (2020), no. 7, pp. 773–782. ISSN 1096-3669.

13. MARZOUK, Mohamed, and Mohamed Abd EL-RAZEK. Selecting Demolition Waste Materials Disposal Alternatives Using Fuzzy TOPSIS Technique. International Journal of Natural Computing Research, vol. 6 (2017), no. 2, pp. 38–57. ISSN 1947-9298.
14. EGHBALI-ZARCH, Maryam, Reza TAVAKKOLI-MOGHADDAM, Kazem DEHGHAN-SANEJ, and Amin KABOLI. Prioritizing the effective strategies for construction and demolition waste management using fuzzy IDOCRIW and WASPAS methods. Engineering, Construction and Architectural Management, ahead-of-print (2021), ahead-of-print. ISSN 0969-9988.
15. SHAH, Bhoomi. Sustainable landfill site selection for construction and demolition waste management using GIS and AHP. Lecture Notes in Civil Engineering, (2021), pp. 135–142.
16. BIN, Wei, Hongping YUAN, and Xiaozhi MA. An Empirical Analysis of Key Factors of Construction and Demolition Waste Management Using the DEMATEL Approach. Lecture Notes in Operations Research, (2023), pp. 164–172.
17. ZHANG, Fan, Yanbing JU, Ernesto D. R. SANTIBANEZ GONZALEZ, Aihua WANG, Peiwu DONG, et al. Evaluation of construction and demolition waste utilization schemes under uncertain environment: A fuzzy heterogeneous multi-criteria decision-making approach. Journal of Cleaner Production, vol. 313 (2021), p. 127907. ISSN 0959-6526.
18. YIA, Yanqing, Xunchang FEI, Andrea FEDELE, Maria Cristina LAVAGNOLO, and Alessandro MANZARDO. Decision support model for selecting construction and demolition waste management alternatives: A life cycle-based approach. Science of The Total Environment, (2024), p. 175408. ISSN 0048-9697.
19. SAATY, T. The analytic hierarchy process: Planning, priority setting, resource allocation. New York: McGraw-Hill International Book Co., 1980. ISBN 0070543712.

Construction Materials as A Source of Hazardous Substances in the Environment

Silvija SERAPINAITĖ[1]*, Jolita KRUOPIENĖ[2]

1 Kaunas University of Technology, Faculty of Mechanical Engineering and Design, Kaunas, Lithuania

2 Kaunas University of Technology, Institute of Environmental Engineering, Kaunas, Lithuania

**silvija.serapinaite@ktu.edu*

Abstract

Tris(2-chloro-1-methylethyl) phosphate (TCPP) is an organophosphorus flame retardant used in construction materials, mostly in polyurethane (PUR) foam insulation. Although effective in reducing fire risk, TCPP has raised increasing concern due to its persistence, chemical mobility, and toxicity. This paper represents an overview of the hazardous properties, regulatory developments and environmental occurrence related to TCPP in Europe. The paper highlights TCPP migration from construction products into indoor air, dust, and water systems such as stormwater and wastewater, based on various document analyses and scientific literature. Finally, the work introduces a conceptual model for TCPP flows in the construction sector, focusing on emission pathways.

Keywords: TCPP, flame retardants, construction materials, hazardous substances.

1. Introduction

Reducing the use of hazardous substances in the construction sector is increasingly recognised as a critical step towards protecting both the natural environment and human health, while promoting building sustainability. Flame retardants are chemical substances added to materials to reduce flammability and delay the spread of fire. One of the widely used flame retardants in the construction sector is TCPP, mostly applied in polyurethane (PUR) foam insulation. Although effective in fire prevention, TCPP has been connected with growing concerns due to its physical-chemical properties, including mobility, persistence in the environment and toxicity.

This paper focuses on TCPP used in construction materials and presents an overview of its hazard properties and regulatory, known environmental occurrence and implications for further analysis. The main objective is to summarise how this substance behaves in the built environment, based on published articles and screening evaluations carried out in the European Union (EU) countries. The study also introduces conceptual model for TCPP flows, by describing qualitative emission pathways, without quantitative estimates. The overall aim is to understand how TCPP are released from materials and transported through different environmental compartments.

2. Methods

The methodology applied in this paper is designed to systematically address the issue of TCPP in the construction sector and its environmental occurrence. Analysis was performed following the steps and methods indicated in Fig. 1.

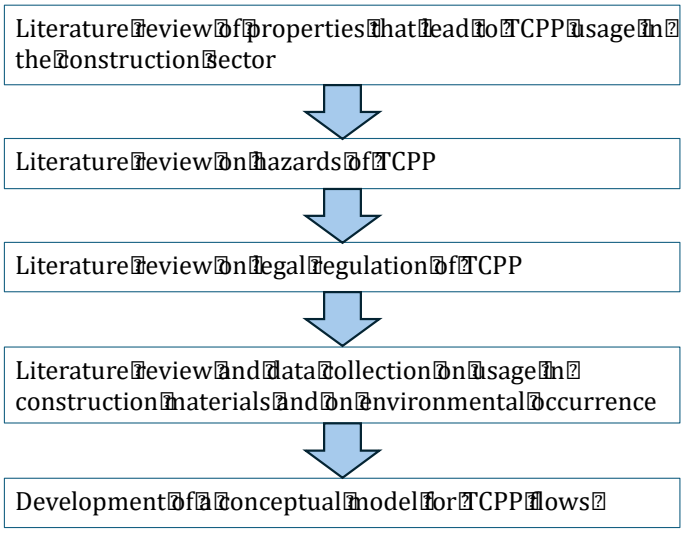

Fig. 1. Steps and research methods of the study

The methodology applied in this study combines literature review, data collection, and modelling to analyse the use and environmental pathways of TCPP in the construction sector. First, a literature review was conducted to identify the properties of TCPP that support its usage in construction materials. This was followed by a review of scientific literature and legal regulations associated with TCPP. Additionally, data were collected on the usage of TCPP in construction products and its occurrence in the environment. Based on the gathered information, a conceptual model was developed to illustrate the flows of TCPP within the construction sector and its transfer to the environment. Finally, conclusions were formulated.

3. Results and discussion

3.1. Use in construction

TCPP (CAS No. 13674-84-5, EC No. 237-158-7) is a liquid organophosphate flame retardant at room temperature. Its flame retardant performance is attributed to the presence of both phosphorus and chlorine atoms: phosphorus promotes char layer formation, while chlorine suppresses free radical generation during combustion [1]. According to the EU Risk Assessment Report [1], TCPP is primarily used in rigid polyurethane foams (PUR) found in construction insulation boards and sprayed foam systems. Typically, TCPP constitutes around 8–10% of PUR foam mass. Smaller quantities are used in flexible foams for furniture or automotive applications, electronics, coatings, adhesives, and paints. According to a report prepared within the NonHazCity 3 project [2], which includes an analysis of the Swedish Byggvarubedömningen (BVB) database, TCPP was identified in approximately 50 construction products, with concentrations ranging from 3% to 20%. BVB is an online Swedish database aimed at promoting the selection of environmentally preferable construction materials. Most of the materials were polyurethane- or foam-based materials such as insulation, sealing foams, and fire-resistant sealants.

According to the global market report of TCPP [3], in 2025 Europe accounted for over 30% of the global TCPP flame retardant market, valued at USD 113.07 million. Concerns over the toxicity and regulation of older brominated and chlorinated flame retardants have led to a shift toward less restricted alternatives such as TCPP, contributing to the growth of its market.

3.2. Hazard properties and regulatory framework

According to the classification provided by companies to European Chemicals Agency (ECHA) in CLP notifications [4], TCPP is classified as harmful if swallowed (H302), harmful to aquatic life with long lasting effect (H412), and suspected of causing cancer (H351) as well as suspected of damaging fertility and unborn child (H361). Despite these concerns, TCPP is not listed on the REACH Candidate List of Substances of Very High Concern, meaning its presence in construction materials does not need to be disclosed.
The EU Risk Assessment Report [1] initially concluded that no further risk reduction measures were necessary. However, a 2018 Screening Report [5] highlighted potential risks to children exposed to TCPP in flexible polyurethane foam products, leading ECHA to recommend a restriction similar to the one already applied to TCEP [6]. In 2019, the European Commission withdrew its proposal until the results of two carcinogenicity studies from the U.S. National Toxicology Program (NTP) became available [6].

ECHA has issued both an Assessment of Regulatory Needs (2022a) for a group of chlorinated trialkyl phosphate flame retardants - including TCPP - and a broader Regulatory Strategy for Flame Retardants (2023) [6]. These documents identified TCPP as potentially carcinogenic, reprotoxic, and endocrine-disrupting. The final proposed action was to introduce a restriction based on harmonised classification and labelling (CLH) for a group of flame retardants. However, it was recommended to wait for the full publication of two carcinogenicity studies prepared by the US National Toxicology Program (NTP).

In 2015, the inclusion of TCPP in the Community Rolling Action Plan (CoRAP) was first considered; however, the evaluation was postponed pending the results of the same two carcinogenicity studies conducted by the NTP. CoRAP is an initiative launched by ECHA aimed at assessing the risks of substances that raise concerns for human health or the environment. It is a continuously updated list of substances to be evaluated under the REACH Regulation. The plan covers substances that may pose risks such as carcinogenicity, endocrine disruption, or other hazards. Substances are prioritised for inclusion in CoRAP based on their potential risk, and they are evaluated within a defined timeframe to determine whether further actions, such as additional testing or, are needed. TCPP was officially included in CoRAP in 2022. The evaluation focused on the concerns outlined in the CoRAP justification document – namely, carcinogenicity, reproductive toxicity, and endocrine-disrupting properties. The assessment was based on data submitted in the registration dossier, full study reports, scientific literature, and the published results of the two NTP carcinogenicity studies. TCPP was also discussed during the 23rd meeting of ECHA's Endocrine Disruptor Expert Group, where experts concluded that sufficient evidence exists to establish a link between endocrine activity and adverse effects caused by the TCPP [6].
Based on the document prepared by Denmark [6] and its summary, it can also be concluded that TCPP may cause endocrine disruption and poses a risk to human health. The available information is considered sufficient for classification and labelling of the substance.

3.3. Environmental occurrence

According to a report prepared as part of the NonHazCity 3 project [2], TCPP has been increasingly detected in various environmental compartments, which is attributed to its high mobility and water solubility. A stormwater screening conducted in four cities (Stockholm, Västerås, Turku, and Helsinki) found TCPP in 37% of analysed samples. Detection frequencies varied by location: 55% in Turku, approximately 40% in both Helsinki and Stockholm, and 0% in Västerås. Concentrations were from below the limit of quantification (LOQ) up to 0.52 μg/L.

In research conducted in Stockholm during November–December 2023, stormwater samples were collected from seven urban sites representing various land use types, including residential, commercial, and light industrial areas. TCPP was detected in four locations: Hjulstadammen (0.15 µg/L), Sundbydammen (0.29 µg/L), Mårtensdal (0.44 µg/L), and Bergslagsdammen (0.25 µg/L).
The same analysis also provides data on wastewater systems. TCPP concentrations in residential wastewater reached 5.5 µg/L, while influent and effluent samples from a wastewater treatment plant (WWTP) showed concentrations of 3.6 µg/L and 1.5 µg/L, respectively. These results suggest that residential areas represent a primary source of TCPP entering wastewater infrastructure. Additionally, TCPP was the dominant substance among all analysed organophosphate esters (OPEs), occurring at the highest concentrations. Fig. 2 illustrates a comparison of TCPP concentrations in stormwater and wastewater across the cities.

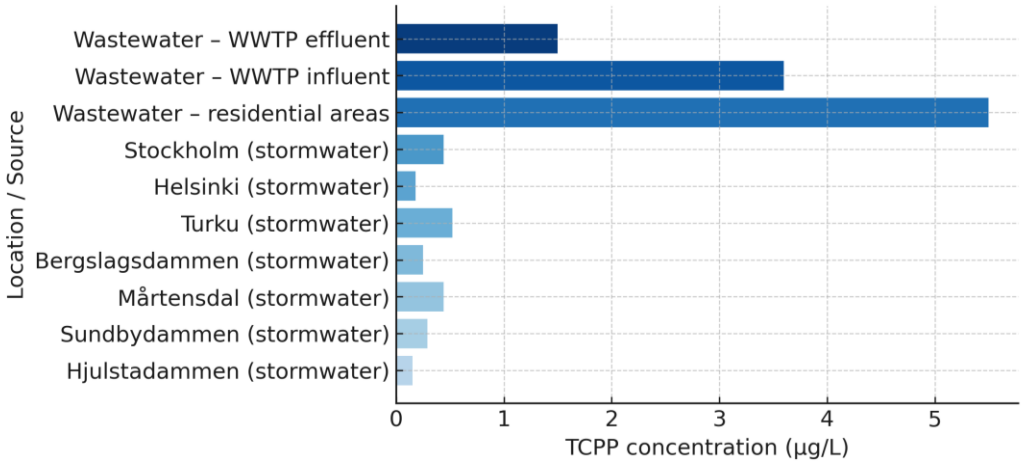

Fig. 2. TCPP concentrations in water sources. Compiled based on [2]

In the previously mentioned study, preschools in Västerås were investigated to assess the presence of TCPP in indoor dust. The average concentration of TCPP in dust samples was 0.665 µg/g. These results were compared to earlier studies:

1. In a 2015 study conducted in Stockholm, TCPP was not detected.
2. In a 2020 study, TCPP levels in dust ranged from 0.9 to 5.4 µg/g, while concentrations in the air ranged from below the detection limit to 30 ng/m^3.

These findings suggest that TCPP usage may be increasing and that its presence in indoor environments, particularly in facilities for children, is becoming more relevant.
One of the more comprehensive studies on the environmental occurrence and ecological risk of TCPP was conducted by Xie et al. [7]. The study compared two widely used chlorinated flame retardants, TCPP and TCEP, across various aquatic environments. In line with earlier sources, TCPP occurrence was attributed to its widespread use in construction materials, especially polyurethane foams, from which it can migrate into the environment via wastewater, surface runoff, or waste streams. The study analysed TCPP concentrations in WWTP effluent, rivers, lakes, and drinking water, and calculated ecological risk quotients (RQ). The highest concentrations (up to 10 µg/L) and the most significant ecological risk (RQ > 1) were observed in WWTP effluent in Japan (RQ = 4.47) and Sweden (RQ = 2.45). River water samples showed lower concentrations (up to 0.5 µg/L), although moderate risk levels were still observed in some locations (RQ up to 0.55). In contrast, TCPP levels in lakes and drinking water were very low (<0.1 µg/L), resulting in negligible ecological risk. Results are shown in Table 1 below.

Table 1. TCPP concentrations and ecological risk. Compiled based on [7]

Environment	TCPP concentration, µg/L	Ecological risk (RQ)
WWTP effluent	0.1 – 10.0	2.45 – 4.47
River water	0.001 – 0.5	up to 0.55
Lake water	0.001 – 0.1	< 0.1
Drinking water	<0.01	< 0.01

Another study about the migration of TCPP, more specifically, its isomer TCIPP (tris(1-chloro-2-propyl) phosphate), from construction materials was conducted by Brandsma et al. [8]. The study focused on the use of flame retardants in spray polyurethane foam insulation and their transfer to the environment, with particular attention to indoor dust, air, and potential migration into soil. The aim was to assess whether TCPP/TCIPP remains active and tends to migrate even during use. TCIPP was detected in significant concentrations in both indoor dust and air samples more than two years after the PUR insulation had been installed. This finding indicates that flame retardants continue to migrate actively from polyurethane foams into indoor environments over time.

The study also applied a hand wipe method: after a 10-second contact with the foam surface, samples were collected using sterile wipes and found to contain up to 2.7 µg of TCIPP. This confirmed that the flame retardant was still migrating from the material and could reach human skin through direct contact, even a long time after installation. Although the primary focus of the study was on indoor migration, the authors also highlighted the potential for TCIPP to migrate into soil. Spray foam insulation is often used beneath floors, especially in older buildings where the floor structure may be above unsealed ground. In such situations, TCIPP may leach into soil and groundwater. At the end of life, PUR insulation waste is difficult to recycle because it is strongly attached to construction materials such as concrete and bricks. As a result, this type of waste is often incinerated or sent to landfills. Studies have shown that TCIPP may leach from landfills into the environment, and inappropriate disposal of these materials could contribute to groundwater contamination.

3.4. Conceptual model

This section provides a qualitative overview of the potential flow pathways of TCPP used in construction materials. As an additive flame retardant, TCPP can migrate from products during use and at end-of-life stages. The conceptual model is presented in Fig. 3.

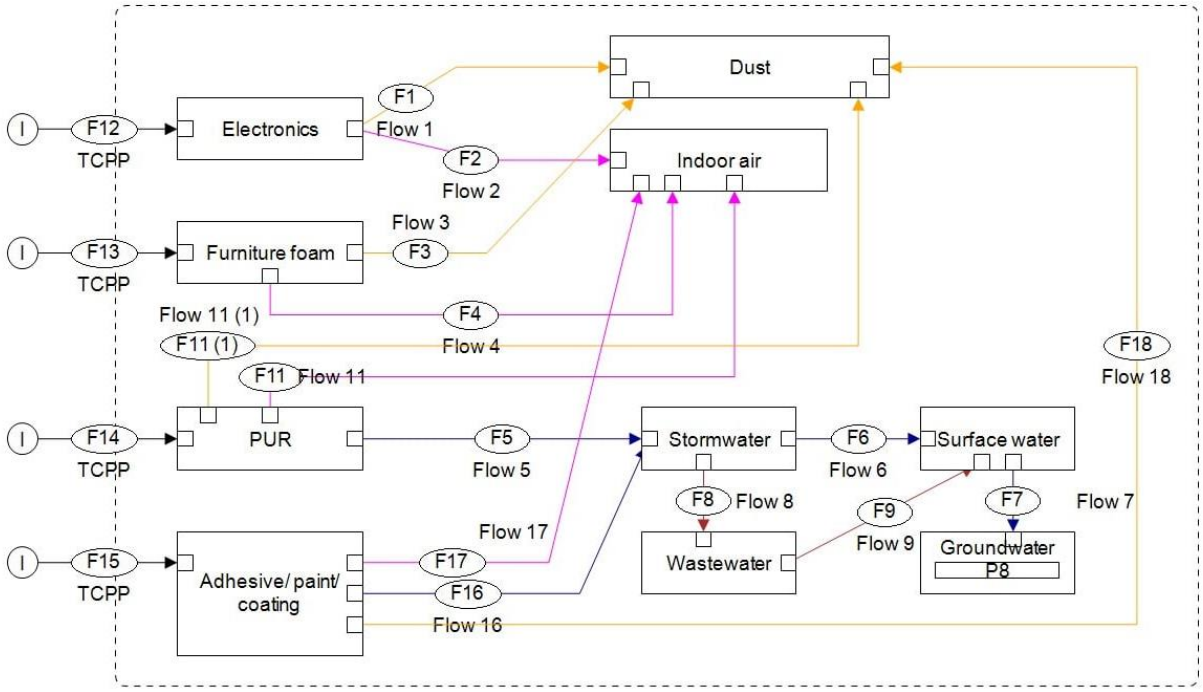

Fig. 3. Conceptual model of TCPP flows

The conceptual model aims to illustrate environmental compartments where TCPP is released, for further quantification of the volumes or fluxes involved. These pathways are relevant for understanding exposure risks and for identifying priority points for emission reduction and regulation.

4. Conclusions

1. TCPP continues to be commonly used in the construction sector, mainly in rigid polyurethane insulation.
2. Environmental monitoring confirms that TCPP is present in stormwater and wastewater, with the highest concentrations found in samples from residential areas.
3. Studies from indoor environments have also shown that dust and air contain TCPP, indicating long-term migration from building materials.
4. Among analysed organophosphate flame retardants, TCPP often dominates in terms of both frequency of detection and concentration levels.
5. The substance is currently under regulatory review in the EU, with concerns related to carcinogenicity, reproductive toxicity, and endocrine disruption forming the basis for proposed risk management measures.
6. The developed conceptual model of TCPP flows provides a structured basis for identifying key pathways and compartments and should be further extended into a quantitative flow analysis to assess substance loads, distribution, and potential environmental risks.

Acknowledgements: The work was partly performed within the Interreg Baltic Sea Region programme project #014 “Reducing hazardous substances in construction to safeguard the aquatic environment, protect human health and achieve more sustainable buildings” (NonHazCity 3).

References

1. EUROPEAN COMMISSION. European Union Risk Assessment Report: Tris(2-chloro-1-methylethyl) phosphate (TCPP). Luxembourg: Office for Official Publications of the European Communities, 2008. Available from: https://echa.europa.eu/documents/10162/17228/trd_rar_ireland_tccp_en.pdf [viewed 2025-03-14].
2. NONHAZCITY 3, 2024. Occurrence of Substances of Concern in Baltic Sea Region Buildings, Construction Materials and Sites. Report. INTERREG Baltic Sea Region Project NonHazCity 3. Available from: https://interreg-baltic.eu/project/nonhazcity-3/ [viewed 2025-03-10].
3. COGNITIVE MARKET RESEARCH, 2025. TCPP Flame Retardant Market Report [online]. Available from: https://www.cognitivemarketresearch.com/tcpp-flame-retardant-market-report [viewed 2025-03-20].
4. ECHA. Brief Profile: TCPP [online]. European Chemicals Agency. Available from: https://echa.europa.eu/brief-profile/-/briefprofile/100.033.766 [viewed 2025-03-10].
5. EUROPEAN CHEMICALS AGENCY (ECHA), 2018. Screening report: An assessment of whether the use of TCEP, TCPP and TDCP in articles should be restricted. Helsinki: ECHA. Available from: https://echa.europa.eu/documents/10162/13641/screening_report_tcep_tcpp_td-cp_en.pdf/e0960aa7-f703-499c-24ff-fba627060698 [viewed 2025-03-10].
6. DANISH ENVIRONMENTAL PROTECTION AGENCY, 2023. Substance Evaluation Conclusion and Evaluation Report for Reaction products of phosphoryl trichloride and 2-methyloxirane (EC No 807-935-0, formerly EC No 237-158-7). Odense: Danish EPA. 85 p. (Evaluating Member State: Denmark). Available from: https://echa.europa.eu/documents/10162/9f7c76ef-d3fb-ebc1-dce6-c88a6bae9d14 [viewed 2025-03-10].
7. XIE, Yi-Ge, et al. Toxicity comparison and risk assessment of two chlorinated organophosphate flame retardants (TCEP and TCPP) on Polypedates megacephalus tadpoles. Aquatic Toxicology, Vol. 272 (2024), p.106979. Available from: https://doi.org/10.1016/j.aquatox.2024.106979 [viewed 2025-03-18].
8. BRANDSMA, S. H., et al. Chlorinated paraffins and tris (1-chloro-2-propyl) phosphate in spray polyurethane foams – A source for indoor exposure? Journal of Hazardous Materials, Vol. 416 (2021), 125758. Available from: https://doi.org/10.1016/j.jhazmat.2021.125758 [viewed 2025-03-18].

Feasibility Study on Recycling-Reuse of Tetrapak Packaging

Eimantas PIKTURNA*, Regita BENDIKIENĖ

Kaunas Technology University, Kaunas, Lithuania

**eimantas.pikturna@ktu.edu*

Abstract

This study focuses on sustainability and commercial growth relating to the assessment of the environmental benefits, and economic impacts of recycling Tetrapak packaging materials. Tetrapak packaging is a multi-layered material composed of paper, plastic and aluminium ingredients, and it is popular as it provides excellent protective qualities. Tetrapak is very versatile, and it is most common useto develop packs for food and beverages there is an acceptance of Tetrapak across the supply chain and customers as it has less environmental impact than traditional packaging. Life cycle assessments illustrated environmental benefits of Tetrapak packaging, however, Tetrapak is composed of different elements, and the recycling capacity of Tetrapak is largely restricted to cellulose (paper). The remainder of the composite "PolyAl" (plastic and aluminum) is significantly limited so it is predominantly energy from waste or incinerated as separated, where appropriate it is difficult to obtain the layered material economically or practically.

Tetrapak packaging is a multi-component packaging made of paper, plastic, and aluminium. Its most widespread use is in the food and beverage industry because this packaging has good properties to protect the product, which is the essence of this packaging. Despite life cycle analyses showing environmental advantages over traditional packaging, recycling of this packaging is quite complicated. Simply put, only the cellulose part is currently recycled effectively, and, most often, the plastic and aluminium that remain after separation are incinerated. Modern hydrocellulose technologies of today partially allow the separation of materials, although full recycling is encountered in cases such as those related to "PolyAl" components. Many Tetrapak packages end up in mixed waste containers rather than in recycling, which indicates that the collection and recycling rates for this packaging are quite low. From this, we can conclude that it is necessary to increase both consumer awareness of this issue and the sorting and recycling infrastructure.

By implementing new solutions – nanotechnologies based on microfibrillated cellulose – we can achieve a higher level of sustainability, but in doing so, we face functional and economic challenges. Currently, we are increasingly seeing innovations being developed, such as artificial intelligence systems in sorting or chemical waste recycling methods but looking at it from the other side, the legal regulation is not so consistent. Recycling Tetrapak packaging has significant benefits, including reducing negative environmental impact, saving resources, and reducing carbon dioxide emissions. From an economic point of view, recycling Tetrapak packaging requires significant investments at the beginning, especially in sorting or separation technologies for this waste. However, taking all this into account, we see only growth, where new jobs are created, and opportunities are created to use secondary recycled materials and bring them to the market.

Keywords: recycling, Tetrapak, packaging, reuse.

1. Introduction

Tetrapak-type packaging, also known as beverage cartons, consists of layers of different materials: aluminum, paper, and plastic. Mostly used for the packaging of food products, especially milk and juice, due to their hygienic and barrier properties [1]. Although life cycle analysis data show that such packaging often outperforms plastic or glass in terms of renewable resource use and production efficiency, its recycling remains limited: usually only the cellulose fraction is recovered, while the plastic and aluminum parts are currently mostly incinerated [1]. Modern hydropulping technologies break down the packaging into components but do not address the issue of comprehensive recycling, and innovative ideas such as PolyAl recycling still face cost-effectiveness and logistical challenges [1].

Studies show that most of such packaging ends up in the mixed municipal waste stream rather than in specialized sorting containers, which significantly reduces the actual collection and recycling rate – for example, in Vienna, only about 19.6% of this packaging is collected separately [1]. This situation reveals the need to strengthen consumer information and modernize sorting and logistics systems. Furthermore, as people's awareness increases and environmental requirements are tightened, the beverage (liquid) industry is increasingly focussing on sustainable packaging solutions: using bioplastics or other recycled components [2]. Newly introduced nanotechnology-based packaging – microfibrillated cellulose (MFC) – improves the moisture and oxygen resistance of cardboard and paper packaging while reducing the need for plastic and improving their recyclability and compostability [3]. However, there is another side where the application of these technologies still faces challenges of functionality and economic sustainability, especially in industrial production [3].

This solution ensures that the shelf life of products without refrigeration or chemical preservatives is as long as possible, thereby reducing energy consumption and food waste [4]. This packaging is compatible with innovative, sustainable food processing technologies, such as HPP (high pressure processing), which allows the maintenance of the quality of the product significantly longer product quality maintenance [5]. Although these packagings have advantages, they pose several challenges during recycling – the cellulose fraction is easily separated and recycled, but the separation of the aluminum and plastic layers is difficult, and the recovery of these materials is limited [4]. Life cycle assessment (LCA) shows that we can reduce environmental and human health impacts mainly through recycling and reuse. Statistical data, according to the LCA meta-analysis, show that up to 1 day of healthy life (DALY) can be saved per ton of recycled plastic worldwide [6].

Furthermore, the efficiency of reuse depends on consumer habits – for example, if reusable plastic packaging were truly more environmentally friendly than single-use plastic, it would need to be reused at least 30 times [6]. Therefore, such data highlights the need to improve packaging recycling infrastructure, further develop circular economy solutions, and deepen public understanding of the importance of sustainable consumption.

Modern waste management systems pay increasing attention to the principles of the circular economy, and one of the priorities is the recycling and recovery of secondary raw materials [7]. This usually involves developing new ways and challenges to recycle plastic or other multi-layer packaging and separating it (plastic, aluminum, paper [8]. Single-use plastics used in industries such as food and beverage are usually partially recycled, while the rest of the packaging is incinerated or sent to a landfill (but this method is decreasing), which increases the negative impact on climate change [9]. Technological solutions such as the use of waste-derived fuel (RDF) in solid industry - cement production, show that this is progress in waste recycling, because at the same time renewable energy is used in the same production, which reduces CO_2 emissions [10]. Although active and smart packaging, such as those containing oxygen absorbers and gas

indicators, can also be recycled and contribute to a longer shelf life of the product and reduce food waste, due to its composition, recycling of this packaging is still very difficult [11].

With a focus on the separation challenges, increasing attention is being paid to the application of artificial intelligence and computer vision. Systems such as EcoMind use deep learning and local image datasets to improve the accuracy of waste classification and allow more efficient separation of materials in sorting lines [12]. This direction also includes the implementation of smart containers equipped with sensors and visual analysis, which increases the efficiency of sorting in both households and industries.

Tetra Pak-type packaging, as mentioned before, is widely used in the food and beverage industry and poses significant recycling challenges due to its multi-layer composition (paper, polyethylene, aluminium) – especially the difficult separation of plastic and aluminium layers [8]. In Lithuania, TetraPak packaging is not collected in the deposit system, although its management is regulated by the Packaging Waste Management Law; recycling is still carried out through the general waste stream, and there are no specific incentive mechanisms yet [13]. In the EU, the management of packaging waste is regulated by Directive 94/62/EC, but there is still a lack of unified solutions for Tetra Pak packaging – proposals for a standardized deposit system are currently being prepared [14]. Meanwhile, Sweden, Germany, and some Canadian provinces already apply integrated collection systems, which allow achieving high recycling rates [15]. Technological solutions such as optical sorting equipment, RDF technologies, or smart waste identification tools (EcoMind) provide the prerequisites for more efficient material recovery [10, 12]. However, clearer regulation, strengthening of infrastructure, and application of financial incentives to the recycling sector are necessary to accelerate Tetra Pak recycling.

2. Solutions

2.1. Opportunities and challenges for repurposing Tetrapak packaging

Tetrapak packaging is often considered a recycling challenge due to its complex multilayer structure, but recent studies reveal its potential as a source of raw materials in various industrial sectors, especially in the production of construction sector materials. Analyzed research studies show that recycled Tetrapak waste can be used as a filler or reinforcing material in wood-plastic composites (WPC), which are used in the production of building boards, furniture, packaging, and other durable structures (Ramli, 2024). WPCs, consisting of recycled plastics and wood or plant fibers, also allow for the effective use of agro-waste, such as sugarcane residues, rice husks, or fruit peels, while reducing manufacturing costs and carbon dioxide emissions [10]. In addition, such composites are characterized by moisture resistance, good mechanical properties, and durability, making them suitable not only for use in interior but also in exterior decoration [16].

Although we see many advantages, the reuse of Tetrapak packaging still poses a number of challenges. Firstly, their multilayer structure requires complex processing processes to effectively separate the materials and adapt them for further use [16]. Second, WPCs made from agricultural waste and Tetrapak components face variability - natural fibers are not uniform in their composition, which complicates quality control and standardization [16]. Furthermore, to ensure safety and compliance with the construction requirements of such materials, additional processing or reinforcement with additives is necessary, which increases the overall cost. Nevertheless, a growing number of projects show that the industrial recycling of Tetrapak into construction or creative materials – from wall panels to school furniture – is not only feasible but also contributes to the development of the circular economy and the reduction of waste [9].

2.2. Recycling/reuse costs, market demand for recycled materials, and potential economic benefits

The recycling of the aforementioned Tetrapak packages still poses a number of economic challenges due to their multilayer structure, as special equipment is required for the separation of aluminum, plastic and paper. The main factor that indicates low recycling efficiency is the high financial costs of sorting, collection and processing, especially if there are no deposit systems or separate collection points [17]. Analysis shows that with low collection rates, as in one of the articles in Australia, only about 41% of milk bottles are collected, this slows the development of the circular economy, leading to a less attractive investment attraction [18]. Additional financial costs arise from the need to ensure the properties of the chemicals used, especially when the packaging is intended for storing food products [19]. However, beyond the cost perspective, certain materials that are recycled, such as bioplastics, show a significantly growing market potential on a global scale. Investments in the production of biocomposite packaging are also growing, as these technologies allow the production of packaging with good properties, which is an alternative to conventional paper/plastic packaging, which allows managing plastic dependence [20]. At the same time, sustainable solutions, such as the compatibility of biomass-type waste use with energy recovery, only prove that such innovative solutions can not only reduce the cost of energy resources but also create new jobs and increase local and not only economic value [17]. Therefore, in short, from the economic perspective of recycling, it can be seen that it is directly related to newly developing technologies, from the regulatory perspective, through the environmental perspective, that more sustainable products need to be developed and used.

2.3. The opportunity to reduce waste, reduce carbon footprint, and conserve resources through recycling/reuse

Tetrapak packaging, despite the technological challenges of recycling, and considering the need to use circular economy goals, research analysis shows that recycled Tetrapak cellulose (called rCell), combined with a polybutylene succinate (called PBS)-based composite, can be used sustainably – in the construction sector, as a raw material from reusable materials [21]. The development of these materials significantly reduces dependence on primary resources, but at the same time helps to reduce or completely eliminate the disposal of cellulose in landfills, which does not decompose due to its structure (polymer). The analysis shows that they can be used because they have good composting conditions and are quite resistant to mechanical and thermodynamic damage [21].

Continuing on, by integrating recycled Tetrapak materials into the production stages, we can significantly reduce the number of resources and carbon dioxide emissions. For example, the production of a 1-liter Tetrapak package generates between 60 and 90 g of carbon dioxide, which is significantly less than the production of plastic packaging, which generates between 115 g and 200 g of CO_2, and the production of glass packaging up to 250 g of CO_2, so recycling Tetrapak packages only increases the ecological efficiency of such packaging [21]. Also, by performing an analysis (Life Cycle Analysis, abbreviated as LCA), we can more accurately assess the environmental impact of recycled materials throughout their entire life cycle, and with such data, we can reduce or completely avoid indirect impacts, such as unnecessary transportation or excess energy consumption [22]. Such assessments can lead to the conclusion that sustainable recycling practices can not only reduce waste and GHG emissions but also manage and control existing material flows, achieving an even higher level of sustainability.

3. Benefits and Recommendations

3.1. Environmental, economic, sustainability benefits, public awareness, and education, innovative solutions

First of all, it is worth repeating that recycling and reusing Tetrapak packages allows us to reduce the negative impact on the environment. As we know, these packages contain plastic, paper and aluminum. One solution is to use membrane technologies, which allow us to reduce both energy consumption in production and the generation of greenhouse gases (GHG) compared to traditional production methods, such as pasteurization or distillation [10]. At the same time, recycling, when we choose the principles of the circular economy, allows production to save on the cost of primary raw materials and create sustainable products with higher added value.

Equally important, from an economic perspective, recycling and reuse offer opportunities to reduce production costs, encourage innovation, and build new workplaces in sustainable sectors [23]. Public awareness and education are also essential components – raising awareness among consumers and producers about the benefits of sorting and recycling improves waste management outcomes. Research suggests that educational initiatives involving teachers and students can act as 'amplifiers', changing long-term habits and encouraging creative problem-solving [24]. These types of solutions, which include innovative technologies, the education sector, and legislators, are essential to ensure the long-term success of the circular economy in achieving sustainability.

3.2. Proposals for technological, policy and consumer engagement improvements to support Tetrapak recycling and reuse

For Tetrapak packaging recycling to be effective and economically viable, when advanced technologies are combined, legislators and consumers themselves, therefore, on the technological side, it is necessary to apply and develop smart sorting systems, as well as artificial intelligence functions that would allow identifying the type of waste and flows, to optimize recycling costs, as this would increase the accuracy of material separation [25]. From the legislator's side, deposit refund schemes should be further expanded, which would also include multi-layer packaging, Tetrapak. In short, on the economic side, it may be necessary to apply certain environmental taxes to Tetrapak packaging manufacturers and allocate certain subsidies to create an infrastructure to recycle this packaging [27]. Such mechanisms could incentivize producers and consumers to choose more sustainable alternatives and increase the scale of collection. Consumer engagement also remains a critical component – research shows that targeted education campaigns and details about the advantages of recycling significantly contribute to sorting activity, especially if information is presented transparently and with a clear social impact [26]. Therefore, only coordinated action at all levels – technological, institutional, and societal – creates the prerequisites for a more effective integration of Tetra Pak packaging into the circular economy.

In short, the analyzed topics of Tetrapak packaging recyclability and reuse still pose technological, economic and consumption habit challenges that still need to be worked on, which opens the way to a perspective towards a more sustainable path. Research shows that Tetrapak can be valued not only in the food industry but also in the hard sector, in the construction or energy sectors, which would allow them to reduce dependence on primary resources. To implement all this, we must use smart technologies, artificial intelligence, and innovative sorting solutions, as well as the necessary reforms in politics to allocate tools and funds for their implementation, from the expansion of deposit systems to financial grants for the implementation of sustainable solutions. Furthermore, society itself plays a crucial role, and it is necessary to strive for responsible consumption and consumers themselves, and only by using technological solutions, legislators

and social measures can good results be achieved by integrating Tetrapak packaging recycling into the circular economy.

4. Conclusions

1. Despite the environmental advantages, the recycling of Tetrapak packaging is hampered by multilayer materials, i.e. aluminum, and plastic, and advanced technological solutions are still required for these technologies.
2. To develop and integrate recycling effectively, more political regulatory involvement and more proposals for financial mechanisms are needed.

Consumer involvement and education are also very important, and these are some of the key factors that would determine the collection rates of the Tetrapak packaging itself.

References

1. GRITSCH, L., BRESLMAYER, G., & LEDERER, J. Comprehensive characterization of beverage cartons in urban waste: A case study from Austria. *Waste Management*, 2025, 201, 114781. Available from: https://doi.org/10.1016/j.wasman.2025.114781. [viewed 2024-04-04].
2. KUMAR, A., BARANWAL, J., BARSE, B., PIGA, I., CINCOTTI, A., & GATTO, G. *Sustainability of food packaging*. In Advances in Biopolymers for Food Science and Technology, 2024, (pp. 349–353). Elsevier. Available from: https://doi.org/10.1016/B978-0-443-19005-6.00014-1. [viewed 2024-04-03].
3. HÖFER, R. (2024). Nano-sized materials in paper and food packaging barrier coatings. In Reference Collection in Materials Science and Materials Engineering (pp. 1–8). Elsevier. Available from: https://doi.org/10.1016/B978-0-323-95486-0.00130-7. [viewed 2024-04-03].
4. RYAN, P. G., MOLONEY, C. L., & CONNAN, M. (2024). Recent changes in plastic bottles washing ashore on Inaccessible Island, Tristan da Cunha. Marine Pollution Bulletin, 209, 117292. Available from: https://doi.org/10.1016/j.marpolbul.2024.117292. [viewed 2024-04-02].
5. PÉREZ LAMELA, C. (2023). Green technologies for sustainable food production and preservation: High-pressure processing. In Sustainable Food Science: A Comprehensive Approach (Vol. 4, pp. 159–174). Elsevier. Available from: https://doi.org/10.1016/B978-0-12-823960-5.00094-9. [viewed 2024-04-02].
6. DEENEY, M., GREEN, R., YAN, X., DOOLEY, C., YATES, J., ROLKER, H. B., & KADIYALA, S. (2023). Human health effects of recycling and reusing food sector consumer plastics: A systematic review and meta-analysis of life cycle assessments. Journal of Cleaner Production, 397, 136567. Available from: https://doi.org/10.1016/j.jclepro.2023.136567. [viewed 2024-04-03].
7. KIRCHER, M., ARANDA, E., ATHANASIOS, P., RADOJCIC-REDNOVNIKOV, I., ROMANTSCHUK, M., RYBERG, M., SCHOCK, G., et al. (2023). Treatment and valorization of bio-waste in the EU. EFB Bioeconomy Journal, 3, 100051. Available from: https://doi.org/10.1016/j.bioeco.2023.100051. [viewed 2024-04-03].
8. REJEESH, C. R., & ANTO, T. (2023). Packaging of milk and dairy products: Approaches to sustainable packaging. Materials Today: Proceedings, 72, 2946–2951. Available from: https://doi.org/10.1016/j.matpr.2022.07.467. [viewed 2024-04-04].
9. ARIJENIWA, V. F., AKINSEMOLU, A. A., CHUKWUGOZIE, D. C., ONAWO, U. G., OCHULOR, C. E., NWAUZOMA, U. M., KAWINO, D. A., & ONYEAKA, H. (2024). Closing the loop: A framework for tackling single-use plastic waste in the food and beverage industry through circular economy—A review. Journal of Environmental Management, 359, 120816. Available from: https://doi.org/10.1016/j.jenvman.2024.120816. [viewed 2024-04-03].
10. SALARIPOOR, H., YOUSEFI, H., & ABDOOS, M. (2025). Life cycle environmental assessment of Refuse-Derived Fuel (RDF) as an alternative to fossil fuels in cement production: A sustainable approach for mitigating carbon emissions. Fuel Communications, 22, 100135. Available from: https://doi.org/10.1016/j.jfueco.2025.100135. [viewed 2024-04-02].
11. MISRA, S. K., & PATHAK, K. (2023). Legislation on active and intelligent packaging. In Green Sustainable

Process for Chemical and Environmental Engineering and Science (pp. 97–112). Elsevier. Available from: https://doi.org/10.1016/B978-0-323-95644-4.00012-7. [viewed 2024-04-02].
12. VALLEJO, P., CORREA, D., ARBELÁEZ, J. C., TABARES, M. S., RUIZ-ARENAS, S., RENDON-VELEZ, E., RÍOS-ZAPATA, D., & ALVARADO, J. (2024). EcoMind: Web-based waste labeling tool. SoftwareX, 26, 101684. Available from: https://doi.org/10.1016/j.softx.2024.101684. [viewed 2024-04-03].
13. Seimas of the Republic of Lithuania. (2001, September 25). Law on the Management of Packaging and Packaging Waste (No. IX-517). Available from: https://e-seimas.lrs.lt/portal/legalAct/lt/TAD/TAIS.161216?jfwid=. [viewed 2024-04-02].
14. Directive 94/62/EC. On packaging and packaging waste. European Parliament and Council. Available from: http://data.europa.eu/eli/dir/1994/62/oj:contentReference[oaicite:1]{index=1}. [viewed 2024-04-03].
15. Government of British Columbia. (2023). 2023 Recycle BC annual and assurance report. Ministry of Environment and Climate Change Strategy. Available from: https://www2.gov.bc.ca/assets/gov/environment/wastemanagement/recycling/recycle/paper-package/2023_recyclebc_annual_and_assurance_report.pdf. [viewed 2024-04-04].
16. ILIUSHINA, A., MAZANOV, G., NESTERUK, S., PIMENOV, A., STEPANOV, A., MIKHAYLOVA, N., BALDYCHEVA, A., & SOMOV, A. (2025). Data-centric approach for instance segmentation in optical waste sorting. Waste Management, 191, 70–80. Available from: https://doi.org/10.1016/j.wasman.2024.11.002. [viewed 2024-04-05].
17. VITALE, G., MOSNA, D., BOTTANI, E., MONTANARI, R., & VIGNALI, G. (2018). Environmental impact of a new industrial process for the recovery and valorisation of packaging materials derived from packaged food waste. Sustainable Production and Consumption, 14, 105–121. Available from: https://doi.org/10.1016/j.spc.2018.02.001. [viewed 2024-04-05].
18. MADDEN, B., JAZBEC, M., & FLORIN, N. (2023). Increasing packaging grade recovery rates of plastic milk bottles in Australia: A material flow analysis approach. Sustainable Production and Consumption, 37, 65–77. Available from: https://doi.org/10.1016/j.spc.2023.02.017. [viewed 2024-04-06].
19. GEUEKE, B., GROH, K., & MUNCKE, J. (2018). Food packaging in the circular economy: Overview of chemical safety aspects for commonly used materials. Journal of Cleaner Production, 193, 491–505. Available from: https://doi.org/10.1016/j.jclepro.2018.05.005. [viewed 2024-04-06].
20. TYAGI, P., SALEM, K. S., HUBBE, M. A., & PAL, L. (2021). Advances in barrier coatings and film technologies for achieving sustainable packaging of food products – A review. Trends in Food Science & Technology, 115, 461–485. Available from: https://doi.org/10.1016/j.tifs.2021.06.036. [viewed 2024-04-06].
21. PLATNIEKS, O., BARKANE, A., IJUDINA, N., GAIDUKOVA, G., THAKUR, V. K., & GAIDUKOVS, S. (2020). Sustainable Tetra Pak recycled cellulose/Poly (Butylene succinate) based woody-like composites for a circular economy. Journal of Cleaner Production, 270, 122321. Available from: https://doi.org/10.1016/j.jclepro.2020.122321. [viewed 2024-04-06].
22. FELICIANO, R. J., GUZMÁN-LUNA, P., BOUÉ, G., MAURICIO-IGLESIAS, M., HOSPIDO, A., & MEMBRÉ, J.-M. (2022). Strategies to mitigate food safety risk while minimizing environmental impacts in the era of climate change. Trends in Food Science & Technology, 126, 180–191. Available from: https://doi.org/10.1016/j.tifs.2022.02.027. [viewed 2024-04-08].
23. Editorial Team. (2023). A review of the key findings from the virtual special issue on sustainability of circular-based chemical processes. Journal of Cleaner Production, 416. Available from: https://doi.org/10.1016/j.jclepro.2023.137874. [viewed 2024-04-08].
24. KUMAR, A. T. V., ARADWAD, P., & YADAV, R. (2025). Packaging of green technology processed beverages: A development trend. In Emerging Green Processing Technologies for Beverages (pp. 309–324). Elsevier. Available from: https://doi.org/10.1016/B978-0-443-15732-5.00011-3. [viewed 2024-04-08].
25. SHELARE, S. D., BELKHODE, P. N., NIKAM, K. C., JATHAR, L. D., SHAHAPURKAR, K., SOUDAGAR, M. E. M., VEZA, I., KHAN, T. M. Y., KALAM, M. A., NIZAMI, A.-S., & REHAN, M. (2023). Biofuels for a sustainable future: Examining the role of nano-additives, economics, policy, internet of things, artificial intelligence and machine learning technology in biodiesel production. Energy, 282, 128874. Available from: https://doi.org/10.1016/j.energy.2023.128874. [viewed 2024-04-08].
26. ADEWALE, P., SHOKROLLAHI YANCHESHMEH, M., & LAM, E. (2022). Starch modification for non-food, industrial applications: Market intelligence and critical review. Carbohydrate Polymers, 291. Available

from: https://doi.org/10.1016/j.carbpol.2022.119590. [viewed 2024-04-08].
27. SEBASTIAN, R. M., & LOUIS, J. (2021). Understanding waste management at airports: A study on current practices and challenges based on literature review. *Renewable and Sustainable Energy Reviews, 147*, 111229. Available from: https://doi.org/10.1016/j.rser.2021.111229. [viewed 2024-04-08].

SUSTAINABLE ENERGY SYSTEMS

Investigation of Aerodynamic Performance of Hybrid Vertical Axis Wind Turbines Using CFD

Saad ASHRAF*, Antanas ČIUPLYS**

Kaunas University of Technology, Kaunas, Lithuania

** saaash@ktu.edu.lt*

*** antanas.ciuplys@ktu.lt*

Abstract

A sustainable transition requires window energy as the basic renewable energy source which prevents the use of fossil fuels for environmental protection. Hybrid Vertical Axis Wind Turbines including Savonius and Darrieus types prove their efficiency as wind technology solutions for diverse wind conditions. Hybrid VAWTs unite Savonius drag properties to capture low wind speeds with the Darrieus lift mechanism for achieving high wind power generation. Research investigates modern hybrid VAWT technology through evaluation of its present operational accomplishments and automated starting procedures. Results obtained by simulation work showed the improved performance is achieved by changes made in blade geometry and structural changes. Environmental turbine performance evaluations serve as the leading analytical measure to study temperature effects throughout this research. The research investigates operational parameters such as blade angle along with inlet velocity together with air density to evaluate their impact on hybrid VAWT performance via CFD simulation results. Research indicates that improved hybrid vertical axis wind turbine performance results from finding specific turbine configurations.

Keywords: hybrid vertical axis wind turbine, aerodynamic performance, computational fluid dynamics, lift and drag forces, Savonius Darrieus turbine.

1. Introduction

The world requires wind energy to aid its renewable energy transition, as it offers clean power and helps preserve nature differently to traditional fossil energy options. The most basic groups of wind turbines are Vertical Axis Wind Turbines (VAWTs) and Horizontal Axis Wind Turbines (HAWTs). At greater wing speed, Horizontal Axis Wind Turbines are as efficient at making electricity as other wind turbines with that design. Since the turbine spins on its axis, VAWTs function better in cities and crosswind areas and do not require yawing [1]. The current VAWT designs include the Savonius and Darrieus models. Savonius turbines function at low speeds mainly because of drag, but the performance drops as wind speed goes up. Efficiency in a Darrieus turbine is determined by lift principle, even though the torque at the start continues to be significant. Consequently, we wanted to develop a VAWT that combines the positive aspects of Savonius drag based action with Darrieus lift principles. With changing wind speeds, these turbines have become more efficient in both performance and work rate [2]. For this reason, further investigation into this area could greatly improve hybrid VAWTs, helping sustainable energy systems.

2. Recent Studies Conducted

Many researchers have shown intense interest in hybrid Vertical Axis Wind Turbines (VAWTs) through numerical investigations to boost their operational efficiency. The following research explores the most recent studies conducted in this field.

Hybrid VAWT Performance in Recent Research

Belal et al conducted a numerical evaluation which investigated how different internal rotor arc angles influence the working characteristics of a modified hybrid VAWT. Each rotor assisted in identifying optimal configuration through the developed numerical methodology which helped identify superior design choices to maximize efficiency [3].

Aerodynamic Performance of Hybrid Configurations

Research conducted through numerical simulation examined the usage of combined Darrieus and Savonius wind turbine systems in 2023. Multiple combination forms of turbines known as Hybrid T-II, T-III, and T-IV underwent aerodynamic performance testing through this research study. Particular combinations of hybrid systems showed better starting performance and total efficiency compared to separate conventional designs [5].

Numerical Advances in VAWT Design

Didane et al. simulated two vertically rotating blades and found that their VAWTs produced more torque and achieved greater operational efficiency [7, 9]. Experimental results show that Bianchini et al. achieved accurate predictions using 2D CFD for Darrieus turbines [10].

Hybrid VAWT Optimization

The focus of recent research has been on improving how well hybrid VAWTs start on their own and their aerodynamic performance. Optimizing the space and angles of a Savonius turbine with a Taguchi method led to an improvement of 19.69% in Cp at a TSR of 0.8 [11]. A second CFD investigation showed that improving the placement of the vortex cavity in H-type Darrieus rose Cp by 25%, however, the use of poor placement saw Cp fall by 54%. Installing a double deflector made the TSR able to go from 3.5 to 4.2, with the system's efficiency rising to 86% [12].

Innovation in Turbine Blades and Hybrid Configurations

Dynamic NACA-based flap settings helped lift-based turbines achieve better self-start in different conditions [13]. At low rotating speed, hybrid Darrieus–Savonius rotors improved Cp by 26.91%, but deflectors helped to recover efficiency at higher speeds, resulting in a 30% Cp gain [14].

Problem Framework and Resolution

Even with advancements, studies of hybrid VAWT are not tested in various climate conditions. When the temperature changes, the air's density, viscosity and what the material is made from shift, affecting turbine output. In this work, ANSYS Fluent is used to produce hybrid VAWT simulation, assessing results at different temperatures and inlet speeds, while pinpointing ideal blade angles and setting up configuration policies for different locations.

Analysis of Similar Studies

Using the Taguchi method, Zhang et al. optimized the pitch angle, diameter ratio and overlap ratio so that their Cp reached 0.2328 [15]. Farajyar et al. established the best arrangement of 3D blades to stop flow separation [16]. Chegini and colleagues boosted the efficiency of hybrid Darrieus-Savonius turbines by 26.91% with modifications to the deflector design [17]. Lakshani et al.

worked out how to make low-wind Savonius systems more efficient using advancements in deflectors [18] and Peng et al. applied Taguchi optimization to boost Cp based on the system's wind speed and TSR [19]. All of these studies together help direct the performance enhancements studied in this research for hybrid VAWTs.

3. Methodology

To understand hybrid VAWTs, researchers have used CFD, tests in the laboratory and optimization. CFD was employed by Xiaojing Sun et al. and Fausto Arpino et al. to improve how blades function in air [22, 24]. Researchers Cameron Gerrie and Sanda Budea checked that the CFD results matched the actual performance in wind tunnel tests [25, 26]. Two teams of Wendong Zhang et al. and Qiang Gao et al. developed rotor designs that solved the challenge of high negative torque at high TSR [27, 28]. Tayebi and his co-authors increased the performance of the machine by introducing active flaps together with slot blade technology [29]. Al-Bahrani found that Kline-Fogelman airfoils increased his wind turbine's efficiency by 47% at different wind speeds [30].

3.1. Project Simulation

The project uses ANSYS Fluent to perform CFD simulations as seen in previous works from Sun et al., Chaiyanupong et al. and Arpino et al. that modified the shape of hybrid blades [22–24]. Authors Gerrie et al. and Budea et al. verified the results of CFD models in wind tunnel tests [25, 26]. The rotor designs from Zhang et al. and Gao et al. boosted the output torque for elevated TSR conditions [27, 28]. Using flap-based control by Tayebi [29] and Al-Bahrani's airfoils also increased the efficiency of the design.

3.2. Numerical simulation settings

For simulations, the COUPLED algorithm and the SST k-ω turbulence model were used, together with second-order upwind schemes. Starting conditions: 9 m/s inlet speed, 1.225 kg/m^3 air density and 15°C temperature. The results consisted of torque coefficient, power coefficient and power output. The turbine design was constructed in ANSYS DesignModeler and uploaded for advanced analysis and meshing. A graphical example of the geometry can be seen in Figure 1, and the full list of data is in Table 1.

.

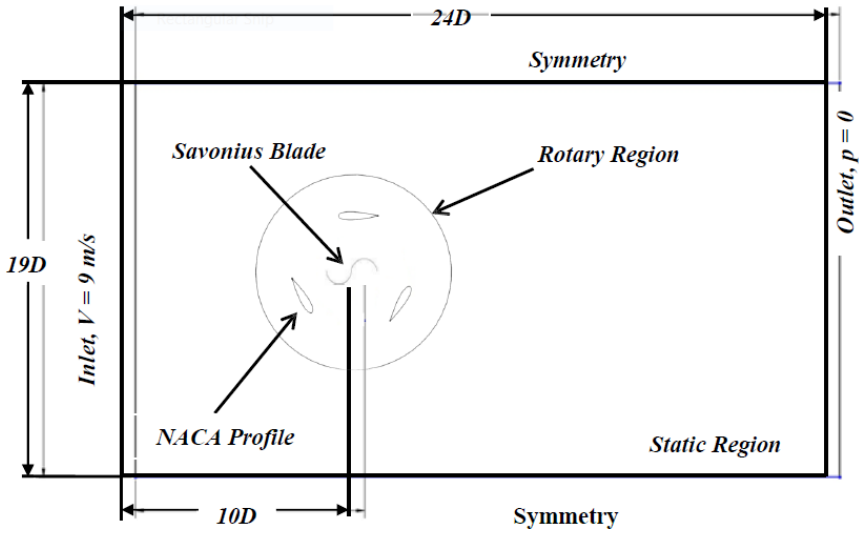

Fig. 12. Boundary Conditions and Computational Domain for Flow Simulation

Table 9. Numerical setting for CFD simulation

Parameters	**Values**
Type of Turbine	Hybrid Type
Profile of Darrieus Blade	NACA 0021
Solidity Ratio	0.5
Diameter for Darrieus Blade	3.0 m
Diameter for Savonius Blade	0.75 m
Height	4.50 m
Number of Blades	3
Aspect Ratio	1.5
Number of Stages	01
Material	Al 1060 Alloy

3.3. Boundary conditions included

The simulations involved setting inlet wind speeds from 0 to 14 m/s to represent rural and semi-urban wind patterns. With ambient temperatures going from –60°C to +60°C, this allowed for the study of how the turbine performed in every thermal extreme around the world. This analysis used a reference air density of 1.225 kg/m^3 at 15°C. The vent was opened to the pressure in the atmosphere.
SST with k-ω provided an accurate representation of the boundary layer and separation flows. The high-resolution approach to meshing (Fig. 2) guaranteed that the results were well-defined. Four sets of turbines were examined, changing the angle of the blades, how solid they were and their spacing.

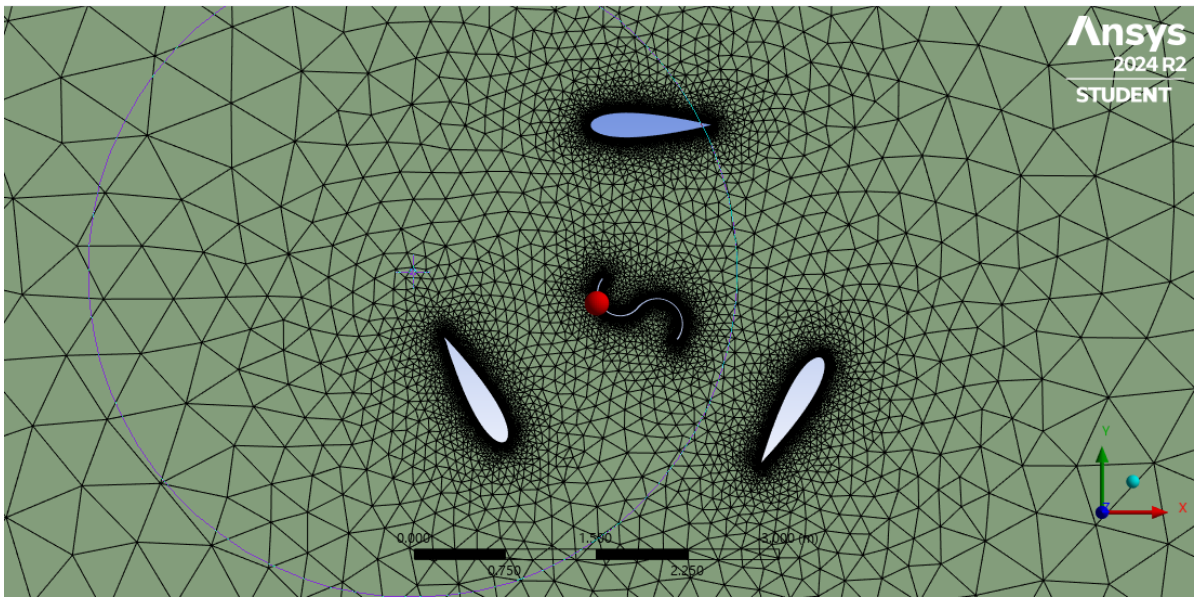

Fig. 13 Meshing of Rotor Zone

3.4. Governing equations for CFD analysis

The CFD analysis used steady/quasi-steady flow assumptions, governed by Navier-Stokes Equation for momentum conservation:

$$\frac{\partial(p\vec{v})}{\partial t} + (\vec{v}.\nabla)\vec{v}) = -\nabla p + \nabla \cdot \tau + \rho\vec{g} \quad (1)$$

where: p = pressure (Pa), τ = viscous stress tensor, g = gravitational acceleration (m/s^2).

Energy Equation for internal energy and heat transfer. RANS modelling for turbulence, with LES as a potential refinement. These equations provided insights into velocity fields, pressure distribution, and power output, essential for optimizing hybrid VAWT performance.

4. Simulation Results and Analysis

A validation study using a three-blade HVAWT with NACA 0021 airfoil, 0.5 solidity and 3 m rotor diameter was carried out to ensure the model's accuracy, matched by Hosseini et al. [21]. At 14 m/s, the k-ω SST model using COUPLED predicted Cp values that were in strong agreement with those obtained in experiments.

The study shows that the CFD model gives accurate predictions of how turbines perform. In addition, lower temperatures, which were created by the denser atmosphere, strengthened the torque and pressure fields, while the opposite occurred at higher temperatures. It confirms that the model can describe actual changes in airflow as conditions vary.

Exploring CFD allowed us to conclude that a hybrid VAWT works its best with blades between 0° and 15°, as this creates the best balance between lift and drag for maximum torque output. Overall, the results confirmed that the turbine had stable performance and efficient energy use in its hybrid format under a variety of operation parameters.

At a wind velocity of 14 m/s and an air temperature of 15°C, the turbine produced its highest torque of 90.60 Nm and generated 711 W of mechanical power. The data shows that the turbine performs well and could be used in locations with moderate wind energy. Wind and temperature changes do not affect the model's sturdiness or aerodynamics, signalling that it would handle climate differences well.

The simulations highlight that the turbine retains its functionality through various environmental variations due to its ideal blade structure and special rotor pairing in combination with the robust turbulent airflow model implemented in the k-ω SST scheme.

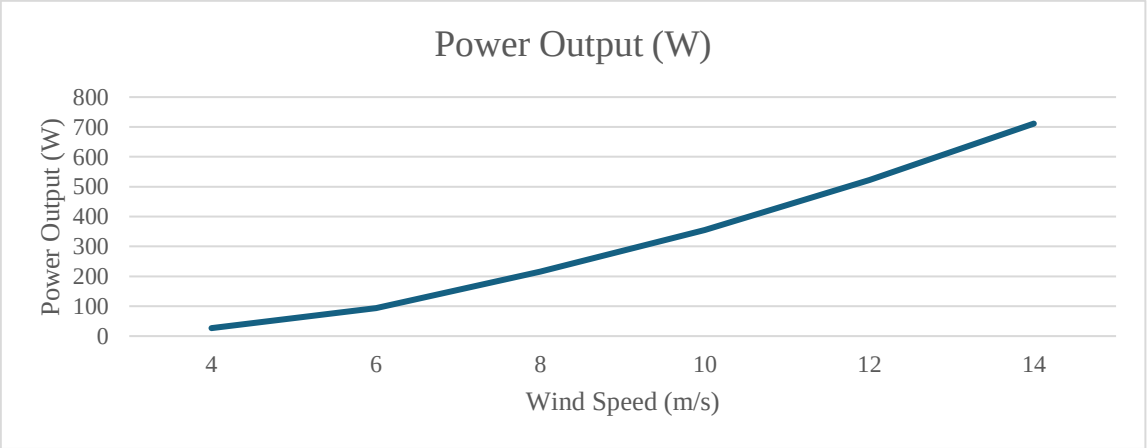

Fig. 14. Power Output VS Windspeed

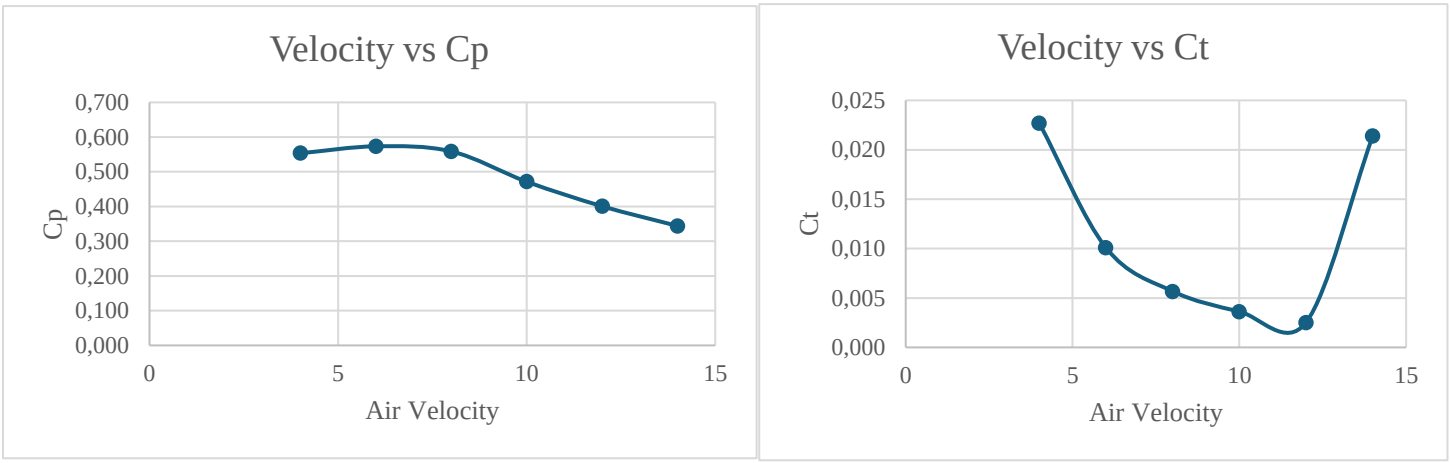

a b

Fig. 15. a – Cp at Different Inlet Velocity; b – C_t at Different Inlet Velocities

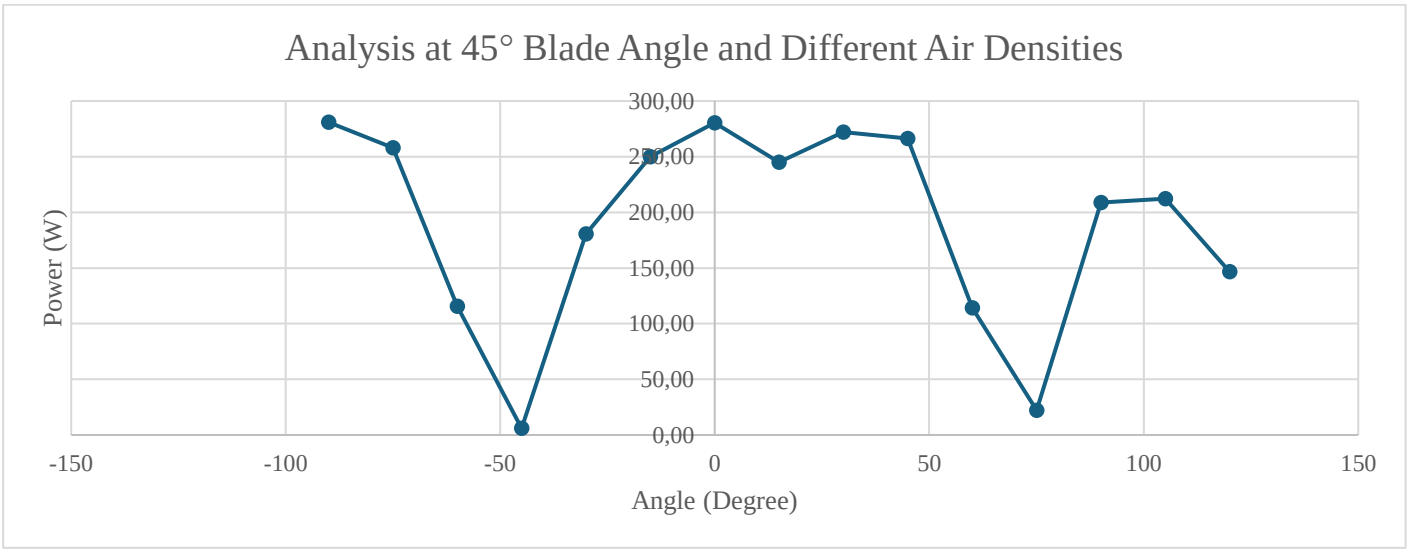

Fig. 16. Power Calculations Analysis at Different Air Densities

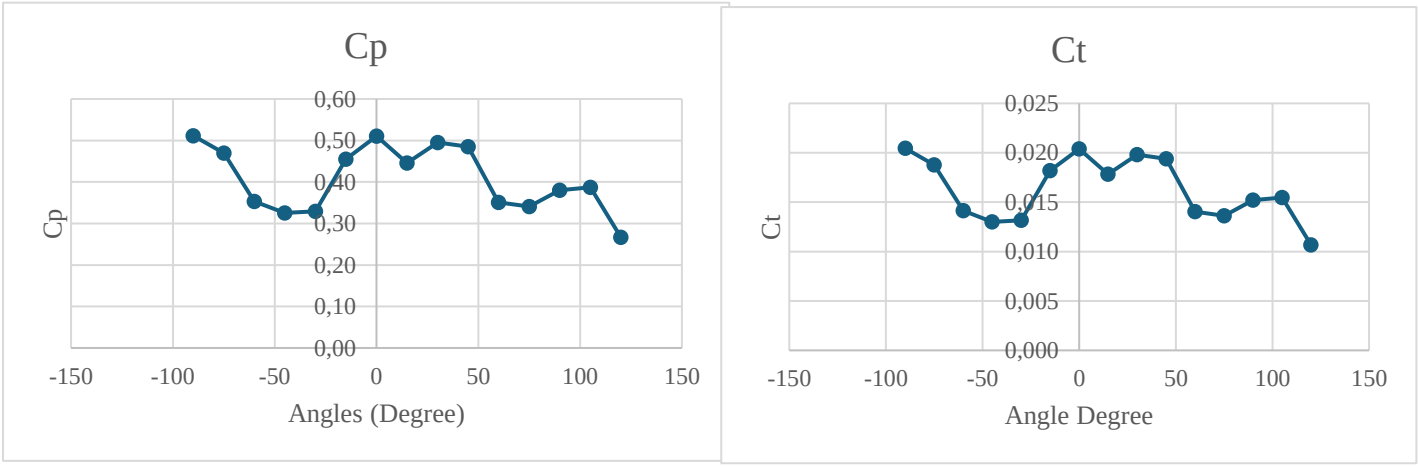

a b

Fig. 17. a – C_p at 45° Blade Angle & Different Densities; b – C_t at 45° Blade Angle & Different Densities

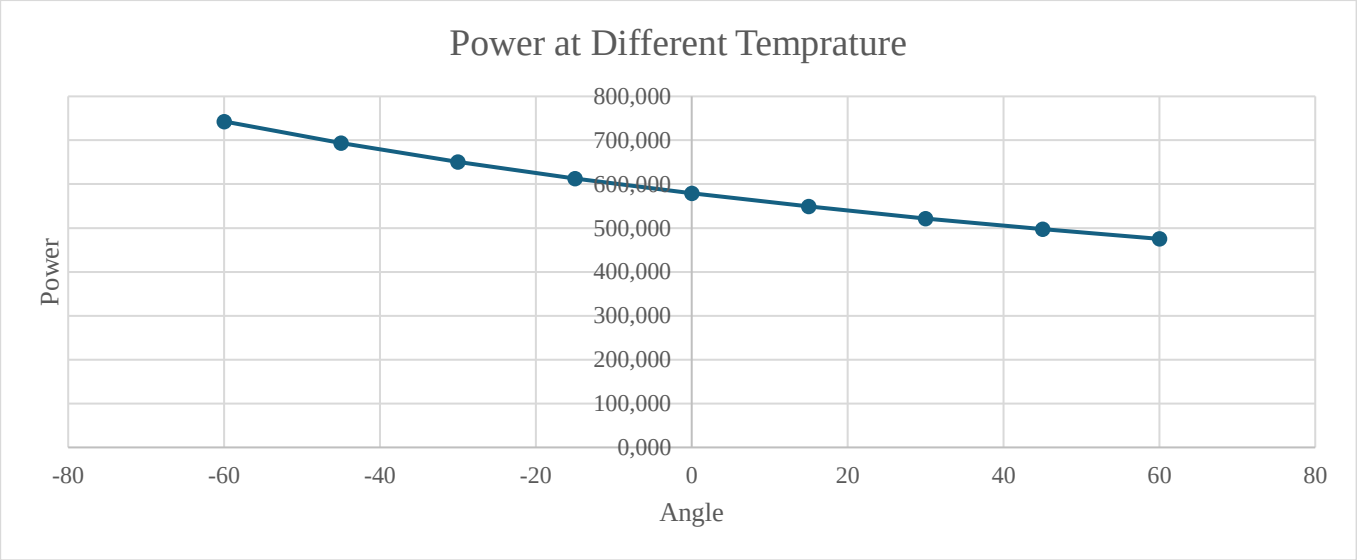

Fig. 18 Power at Different Temperatures

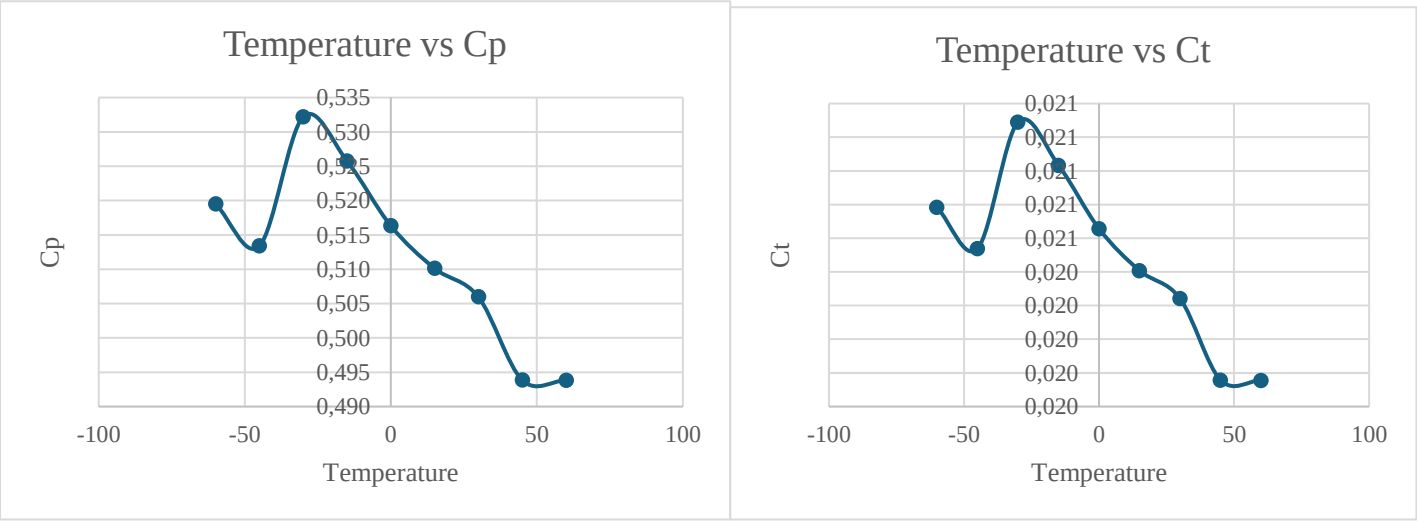

a b

Fig. 8. a – Cp Calculations at Different Temperatures; b – Ct Calculations at Different Temperatures

5. Conclusion

Simulation study using the defined parameters yielded the following important findings:

1. Results from CFD show that the best blade angle for a hybrid VAWT is between 0° and 15°, as it generates the most torque at this angle. Different configurations were used to assess the performance.
2. The turbine operated its best at a wind speed of 14 m/s and 15°C, producing a maximum torque of 90.60 Nm and 711 W of power. That means it is suitable for actual use, mainly in temperate climates.
3. Simulations and estimates reveal that the hybrid VAWT is a cost-effective way to install, operate and maintain. Although results seem positive in the initial data, full-scale deployment requires proving both technical and financial viability through experiments.

References

1. AHMAD, Muhammad, SHAHZAD, Aamer and QADRI, M Nafees Mumtaz. *An overview of aerodynamic performance analysis of vertical axis wind turbines. Energy & Environment [*online*]*. 28 August 2022. Vol.

34, no. 7, p. 2815–2857. DOI 10.1177/0958305X221121281. Available from: https://doi.org/10.1177/0958305X221121281

2. TOPTAS, Ersin, BAYRAK, Muharrem Ali and BOZ, Talha. *Vertical axis hybrid wind turbine design. Journal of Mechatronics and Artificial Intelligence in Engineering*. 30 June 2020. Vol. 1, no. 1, p. 33–40. DOI 10.21595/jmai.2020.21508.
3. BELAL, Mahmoud S., HAMDY, Osama and HUZAYYIN, Ahmed S. *Numerical Investigation of a Modified Hybrid Vertical Axis Wind Turbine*. In : *NILES 2024 - 6th Novel Intelligent and Leading Emerging Sciences Conference, Proceedings*. Institute of Electrical and Electronics Engineers Inc., 2024. p. 349–352. ISBN 9798350378511.
4. MĂLĂEL, Ion and STRĂTILĂ, Sergiu. *High-Precision Numerical Investigation of a VAWT Starting Process. Processes [*online*]*. 17 October 2024. Vol. 12, no. 10, p. 2263. DOI 10.3390/pr12102263. Available from: https://www.mdpi.com/2227-9717/12/10/2263
5. POURANSARI, Zeinab and BEHZAD, Mohadese. *Numerical investigation of the aerodynamic performance of a hybrid Darrieus-Savonius wind turbine. Wind Engineering [*online*]*. 27 July 2023. Vol. 48, no. 1, p. 3–14. DOI 10.1177/0309524X231188950. Available from: https://doi.org/10.1177/0309524X231188950
6. KUMAR, Yogesh, ROGA, Sukanta and WANMALI, Nikhil Kishor. *Experimental analysis of hybrid VAWT and the effect of semi-cylindrical attachment to the trailing edge. Energy for Sustainable Development*. 1 June 2023. Vol. 74, p. 115–126. DOI 10.1016/j.esd.2023.03.013.
7. ASADI, Mohammad and HASSANZADEH, Rahim. *Effects of internal rotor parameters on the performance of a two bladed Darrieus-two bladed Savonius hybrid wind turbine. Energy Conversion and Management*. 23 April 2021. Vol. 230, p. 114109. DOI 10.1016/j.enconman.2021.114109.
8. DIDANE, Djamal Hissein, ROSLY, Nurhayati, ZULKAFLI, Mohd Fadhli and SHAMSUDIN, Syariful Syafiq. *Numerical investigation of a novel contra-rotating vertical axis wind turbine. Sustainable Energy Technologies and Assessments [*online*]*. 1 February 2019. Vol. 31, p. 43–53. [Accessed 25 April 2025]. DOI 10.1016/J.SETA.2018.11.006. Available from: https://www.sciencedirect.com/science/article/abs/pii/S2213138818302765
9. HOSSEINI, Arian and GOUDARZI, Navid. *Design and CFD study of a hybrid vertical-axis wind turbine by employing a combined Bach-type and H-Darrieus rotor systems. Energy Conversion and Management*. 1 June 2019. Vol. 189, p. 49–59. DOI 10.1016/j.enconman.2019.03.068.
10. BIANCHINI, Alessandro, BALDUZZI, Francesco, BACHANT, Peter, FERRARA, Giovanni and FERRARI, Lorenzo. *Effectiveness of two-dimensional CFD simulations for Darrieus VAWTs: a combined numerical and experimental assessment. Energy Conversion and Management*. 2017. Vol. 136, p. 318–328. DOI 10.1016/j.enconman.2017.01.026.
11. FATAHIAN, Esmaeel, MISHRA, Rakesh, JACKSON, Frankie F. and FATAHIAN, Hossein. *Optimization and analysis of self-starting capabilities of vertical axis wind turbine pairs: A CFD-Taguchi approach. Ocean Engineering*. 15 June 2024. Vol. 302. DOI 10.1016/j.oceaneng.2024.117614.
12. KUMAR, Yogesh, SENGUPTA, A R, BISWAS, Agnimitra, MAZARBHUIYA, Hussain and GUPTA, Rajat. *CFD Analysis of the Performance of an H-Darrieus Wind Turbine Having Cavity Blades. In : .* 2021. p. 711–719. ISBN 978-981-15-7710-9.
13. MITCHELL, Samuel, OGBONNA, Iheanyichukwu and VOLKOV, Konstantin. *Improvement of self-starting capabilities of vertical axis wind turbines with new design of turbine blades. Sustainability (Switzerland)*. 1 April 2021. Vol. 13, no. 7. DOI 10.3390/su13073854.
14. CHEGINI, Sahel, ASADBEIGI, Mohammadreza, GHAFOORIAN, Farzad and MEHRPOOYA, Mehdi. *An investigation into the self-starting of darrieus-savonius hybrid wind turbine and performance enhancement through innovative deflectors: A CFD approach. Ocean Engineering [*online*]*. 2023. Vol. 287, p. 115910. DOI https://doi.org/10.1016/j.oceaneng.2023.115910. Available from: https://www.sciencedirect.com/science/article/pii/S0029801823022941
15. ZHANG, Jintao, WANG, Chao, LIU, Wenhao, ZHU, Jianyang, YAN, Yangyang and ZHAO, Hui. *Optimization of the Energy Capture Performance of the Lift-Drag Hybrid Vertical-Axis Wind Turbine Based on the Taguchi Experimental Method and CFD Simulation. Sustainability (Switzerland)*. 1 June 2023. Vol. 15, no. 11. DOI 10.3390/su15118848.
16. FARAJYAR, Shayan, GHAFOORIAN, Farzad, MEHRPOOYA, Mehdi and ASADBEIGI, Mohammadreza. *CFD Investigation and Optimization on the Aerodynamic Performance of a Savonius Vertical Axis Wind*

Turbine and Its Installation in a Hybrid Power Supply System: A Case Study in Iran. Sustainability (Switzerland). 1 March 2023. Vol. 15, no. 6. DOI 10.3390/su15065318.

17. CHEGINI, Sahel, ASADBEIGI, Mohammadreza, GHAFOORIAN, Farzad and MEHRPOOYA, Mehdi. *An investigation into the self-starting of darrieus-savonius hybrid wind turbine and performance enhancement through innovative deflectors: A CFD approach. Ocean Engineering [*online*]*. 2023. Vol. 287, p. 115910. DOI https://doi.org/10.1016/j.oceaneng.2023.115910. Available from: https://www.sciencedirect.com/science/article/pii/S0029801823022941
18. LAKSHANI, W A A, PIYATHILAKA, P and THILAKARATHNA, S. *Biomass and Sustainable Energy Optimizing Vertical-Axis Wind Turbine Performance and Determining Optimal Velocity and Deflector Configuration Based on Wind Speed*. [no date].
19. PENG, H. Y., LIU, M. N., LIU, H. J. and LIN, K. *Optimization of twin vertical axis wind turbines through large eddy simulations and Taguchi method. Energy [*online*]*. 1 February 2022. Vol. 240, p. 122560. [Accessed 25 April 2025]. DOI 10.1016/J.ENERGY.2021.122560. Available from: https://www.sciencedirect.com/science/article/abs/pii/S0360544221028097
20. SUN, Xiaojing, CHEN, Yajun, CAO, Yang, WU, Guoqing, ZHENG, Zhongquan and HUANG, Diangui. *Research on the aerodynamic characteristics of a lift drag hybrid vertical axis wind turbine. Advances in Mechanical Engineering*. 28 January 2016. Vol. 8, no. 1. DOI 10.1177/1687814016629349.
21. PINAR PÉREZ, Jesús María, GARCÍA MÁRQUEZ, Fausto Pedro, TOBIAS, Andrew and PAPAELIAS, Mayorkinos. *Wind turbine reliability analysis*. 2013. Elsevier Ltd.
22. SUN, Xiaojing, XU, Yingqiao and HUANG, Diangui. *Numerical simulation and research on improving aerodynamic performance of vertical axis wind turbine by co-flow jet. Journal of Renewable and Sustainable Energy*. 1 January 2019. Vol. 11, no. 1. DOI 10.1063/1.5052378.
23. CHAIYANUPONG, Jaruwan and CHITSOMBOON, Tawit. *Effects of turbulence models and grid densities on computational accuracy of flows over a vertical axis wind turbine. International Journal of Renewable Energy Development*. 1 October 2018. Vol. 7, no. 3, p. 213–222. DOI 10.14710/ijred.7.3.213-222.
24. ARPINO, F., CORTELLESSA, G., DELL'ISOLA, M., SCUNGIO, M., FOCANTI, V., PROFILI, M. and ROTONDI, M. *CFD simulations of power coefficients for an innovative Darrieus style vertical axis wind turbine with auxiliary straight blades*. In : *Journal of Physics: Conference Series*. Institute of Physics Publishing, 20 November 2017.
25. GERRIE, Cameron, ISLAM, Sheikh Zahidul, GERRIE, Sean, TURNER, Naomi and ASIM, Taimoor. *3D CFD Modelling of Performance of a Vertical Axis Turbine. Energies*. 1 February 2023. Vol. 16, no. 3. DOI 10.3390/en16031144.
26. BUDEA, Sanda, SIMIONESCU, Ştefan Mugur and COPĂCEANU, Valentin. *Numerical and experimental investigations on a hybrid vertical axis wind turbine*. In : *E3S Web of Conferences*. EDP Sciences, 22 January 2025.
27. ZHANG, Wendong, CAO, Yang, QIAN, Zhong, WANG, Jian, ZHU, Yixian, YANG, Yanan, WANG, Yujie and WU, Guoqing. *Research on Aerodynamic Performance of Asynchronous-Hybrid Dual-Rotor Vertical-Axis Wind Turbines. Energies*. 1 September 2024. Vol. 17, no. 17. DOI 10.3390/en17174424.
28. GAO, Qiang, LIAN, Shuai and YAN, Hongwei. *Aerodynamic Performance Analysis of Adaptive Drag-Lift Hybrid Type Vertical Axis Wind Turbine. Energies*. 1 August 2022. Vol. 15, no. 15. DOI 10.3390/en15155600.
29. TAYEBI, Ali and TORABI, Farshid. *Flow control techniques to improve the aerodynamic performance of Darrieus vertical axis wind turbines: A critical review. Journal of Wind Engineering and Industrial Aerodynamics*. 1 September 2024. Vol. 252, p. 105820. DOI 10.1016/j.jweia.2024.105820.
30. BALAMURUGAN, Rohini Janaki, AL-BONSRULAH, Hussein A.Z., RAJA, Vijayanandh, KUMAR, Lokeshkumar, KANNAN, Sri Diviyalakshmi, MADASAMY, Senthil Kumar, RASHEED, Raffik, RAJENDRAN, Parvathy and AL-BAHRANI, Mohammed. *Design and multiperspectivity-based performance investigations of H-Darrieus vertical axis wind turbine through computational fluid dynamics adopted with moving reference frame approaches. International Journal of Low-Carbon Technologies*. 2022. Vol. 17, p. 784–806. DOI 10.1093/ijlct/ctac055.

Aerodynamic Design and Performance Evaluation of Horizontal Axis Wind Turbine Blades Using QBlade

M. Usman SIKANDAR[1, 2*], Olga KHRYSTOSLAVENKO[3], Alastair DUTTON[2]

1 Kaunas University of Technology, Kaunas, Lithuania

2 Offshore Wind Learning, London, United Kingdom

3 Vilnius Tech, Vilnius, Lithuania

** Usman@spin-pack.com*

Abstract

The aerodynamic performance of a horizontal axis wind turbine (HAWT) blade was analyzed and optimized using QBlade software, incorporating XFoil for airfoil polar calculations. A three-bladed rotor with a 20m diameter was designed, featuring NACA 55xx series airfoils at r/R > 0.3 and NACA 0035 at r/R = 0.25, while maintaining a circular profile at r/R = 0.1. Aerodynamic properties, including lift and drag coefficients (CL/CD), were extracted for an angle of attack (AoA) of 5 ° and a tip speed ratio (TSR) of 6. Blade element momentum (BEM) simulations were conducted to obtain power coefficient (Cp) and thrust coefficient (Ct) variations with TSR, illustrating optimal performance around TSR = 6 with Cp peaking at approximately 0.4. The optimized blade design incorporated twist distribution and chord variation, ensuring an efficient energy conversion profile. The Reynolds number distribution along the blade confirmed aerodynamic stability, with values ranging up to 1.4×10^7. The results highlight the effectiveness of QBlade in rotor blade design and performance assessment, providing a computationally efficient approach to optimize wind turbine efficiency. Future improvements could involve increasing the number of analyzed sections

Keywords: HAWT, QBlade, XFoil, Blade Optimization, Aerodynamic Performance, Wind Turbine Efficiency

1. Introduction

Wind energy has emerged as a crucial renewable energy source, with Horizontal Axis Wind Turbines (HAWTs) being the predominant choice for efficient energy conversion. The aerodynamic performance of the wind turbine blades significantly influences the overall efficiency of the system. Computational tools such as QBlade, which incorporates XFoil for airfoil polar calculations, provide a cost-effective alternative to experimental wind tunnel testing for aerodynamic analysis and optimization (Zuhdi & Islam, 2017). Several studies have investigated the aerodynamic design, optimization, and performance evaluation of HAWT blades using QBlade, demonstrating its reliability in predicting aerodynamic forces, power coefficients, and thrust coefficients (Zahariea et al., 2019). The design of wind turbine blades involves defining the chord distribution and twist angles to maximize aerodynamic efficiency. Studies have shown that optimizing these parameters using QBlade leads to significant improvements in power coefficient (Cp) values (Nazir & Javed, 2019). The use of multi-airfoil elements in blade design has also been explored, demonstrating enhanced lift-to-drag ratios and improved wind energy capture (Xi & Zhao, 2022). Airfoil selection is critical in determining the aerodynamic performance of HAWTs. The integration of different NACA airfoils at various blade sections has been extensively investigated, with studies demonstrating that NACA 5522 and NACA 55xx airfoils provide an

optimal balance of lift and drag, enhancing overall efficiency (Davari et al., 2024). Additionally, modifications to airfoil camber and thickness have been explored to optimize aerodynamic performance at varying Reynolds numbers (Akheel et al., 2024).

The aerodynamic performance of a three-bladed rotor with a 20m diameter was analyzed using QBlade. The rotor design included circular airfoils at r/R=0.1, transitioning to NACA 0035 at r/R=0.25, and NACA 55xx series beyond r/R=0.3. The study considered different angle of attack (AoA) values, with 5° assigned for the third team in the design experiment. The rotor was evaluated at different Tip Speed Ratios (TSRs), ranging from 5.0 to 6.5, to optimize energy extraction and aerodynamic performance. The QBlade simulations provided crucial insights into the lift and drag characteristics of these airfoils and their impact on the power coefficient (Cp) and thrust coefficient (Ct).QBlade applies Blade Element Momentum (BEM) theory to simulate wind turbine blade performance. Several studies have validated BEM-based predictions of power coefficient (Cp), thrust coefficient (Ct), and torque distribution (Altmimi et al., 2022). The software's integrated XFoil module enhances the accuracy of lift and drag coefficient estimations, making it a reliable tool for wind turbine analysis (Marten et al., 2013). Optimizing the Tip Speed Ratio (TSR) is essential for maximizing wind turbine efficiency. Research has shown that selecting a TSR of around 6 yields peak power coefficients of approximately 0.40 (Abdullah et al., 2023). Additionally, Reynolds number computations for each blade section provide insights into aerodynamic force distributions, aiding in performance optimization (Guţu et al., 2021).

Despite its effectiveness, QBlade simulations rely on steady wind conditions, which may not fully capture real-world turbulence effects. Future studies should incorporate dynamic stall modeling and adaptive blade pitch control to improve aerodynamic performance (Hachim & Mahdi, 2020). Additionally, structural integrity assessments, including modal and static structural analysis, should be further explored for enhanced blade durability (Krishnanunni et al., 2020). The application of QBlade in HAWT blade design and optimization has proven to be highly effective, offering a computationally inexpensive alternative to CFD and wind tunnel testing. Studies confirm that optimized chord and twist distributions, coupled with appropriate airfoil selections, significantly enhance wind turbine performance. Further research into real-world turbulence effects and structural optimization is essential for advancing wind energy technology. Building upon these findings, this paper will carry out a detailed study to analyze the aerodynamic design and optimization of a 20m diameter, three-bladed HAWT rotor using QBlade. The research will incorporate the analysis of various airfoil transitions, chord distributions, angle of attack configurations, and Tip Speed Ratios (TSRs) to validate the effectiveness of computational optimization for wind turbine blade design.

2. Methodology

This study presents the aerodynamic design and performance evaluation of horizontal-axis wind turbine (HAWT) blades using QBlade, an open-source software for blade element momentum (BEM) analysis. The methodology encompasses airfoil selection, blade geometry definition, computational analysis, and optimization to enhance aerodynamic efficiency.

Blade Geometry and Airfoil Selection

A three-blade rotor with a diameter of 20 m was considered, with airfoil profiles varying along the span. The law of chords was derived based on blade radius fractions (r/R), with different NACA airfoil families applied. The key stations considered include r/R = 0.1, 0.25, 0.3, 0.6, 0.9, and 1.0, where:

- Circular profiles were assigned near the root (r/R = 0.1, 0.25)
- NACA 55xx series were employed at mid-sections
- NACA 5510 was utilized towards the tip

A tabulated summary of chord length, thickness-to-chord ratio (t/c), and relative velocity (V_{rel}) was extracted (Figure 1, Table 1).

r (m)	0,00	0,50	1,00	1,50	2,00	2,50	3,00	3,50	4,00	4,50	5,00	5,50	6,00	6,50	7,00	7,50	8,00	8,50	9,00	9,50	10,00
c (m)	0,80	0,80	0,80	0,90	1,10	1,20	1,20	1,08	1,00	0,95	0,90	0,85	0,80	0,75	0,70	0,65	0,60	0,55	0,50	0,42	0,30
t/c	1,00	1,00	1,00	0,80	0,60	0,40	0,34	0,32	0,30	0,28	0,26	0,24	0,22	0,20	0,18	0,16	0,14	0,12	0,10	0,10	0,10

Fig. 19. Chord and t/c Ratio Along the Blade

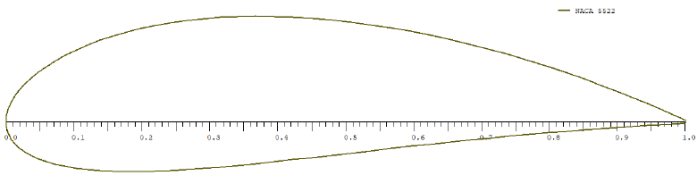

Fig. 20. NACA 5522 corresponding to t/c ratio 0.22

Table 10. Data for Sections

Sections r/R	r	c	t/c	Airfoil	Vrel	Re
0.0	0	0.8	1.00	Circular	2.7	144000
0.1	1	0.8	1.00	Circular	4.3	229333
0.25	2.5	1.2	0.40	NACA0035	8.8	704000
0.3	3	1.2	0.34	NACA5534	10.41	832800
0.6	6	0.8	0.22	NACA5522	20.29	1082133
0.9	9	0.5	0.10	NACA5510	30.28	1009333
1.0	10	0.3	0.10	NACA5510	33.62	672400

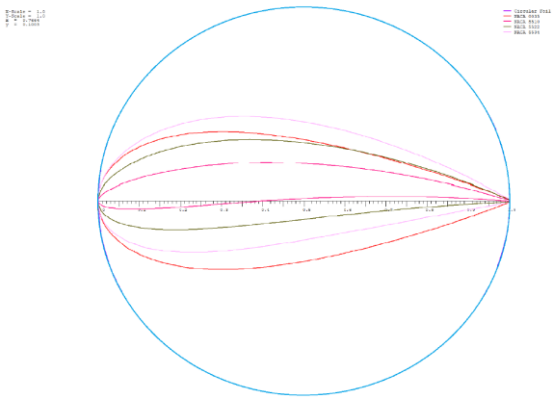

Fig. 21. Airfoils for Blades

Airfoil Performance Computation

The aerodynamic coefficients (C_L, C_D) can be computed for each airfoil using X_{FOIL} integrated within QBlade. The Reynolds number can be calculated as:

Where:

V_{rel} is the relative velocity,

C is the local chord length, and

ν_{air} is the kinematic viscosity of air (1.5×10^{-5} m^2/s).

Polar plots of C_L vs AoA and C_L/C_D vs AoA are generated for the NACA 5522 profile

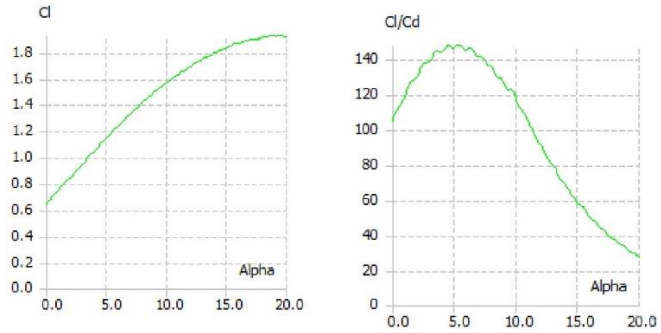

Fig. 22. Polar plots of CL vs AoA and CL/CD vs AoA

Blade Optimization & BEM Analysis

Using QBlade's blade design module, an HAWT with 3 blades and a hub radius of 0.5 m was designed. The tip speed ratio (TSR) was set to 6, and an optimal angle of attack (AoA) of 5° was used for lift-to-drag maximization. Optimization was performed using the Betz limit approach. The twist and chord distribution were refined iteratively.

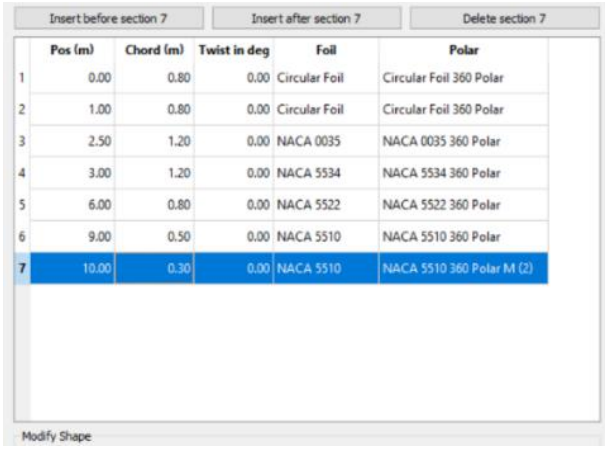

Fig. 23. Twist and chord distribution (Refined)

A BEM simulation was then conducted with correction factors applied (Prandtl tip/root loss, 3D correction, Reynolds drag correction). The simulation yielded a coefficient of power (Cp) vs TSR and thrust coefficient (C_t) vs TSR curves.

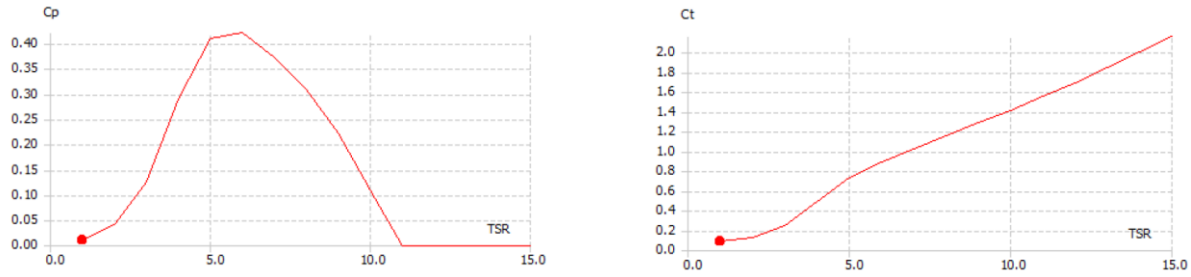

Fig. 24. C_p vs TSR & C_t vs TSR Curves

3. Results & Discussion

3.1. Airfoil Characteristics & Reynolds Number Analysis

The computed Reynolds number varied from 144,000 (root) to 1,426,260 (mid-section) and 1,008,933 (tip), confirming that the airfoils experience a transition from laminar to turbulent flow. The C_L/C_D ratio for NACA 5522 peaked at 146, validating its selection for mid-span regions. The drag coefficient (C_D) was found to be 0.0078, a critical factor in reducing torque losses.

3.2. Blade Geometry Optimization & Twist Distribution

The optimized blade geometry showed a decreasing chord length and an increasing twist angle from root to tip. After optimization, the twist at r = 2.5 m increased to 6.25°, while at r = 10 m, it reduced to -2.66°, indicating a well-balanced aerodynamic shape. Design can be improved by taking into account more stations.

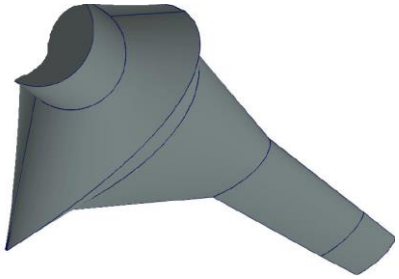

Fig. 25. Preliminary Design with 7 Stations

3.3. Rotor Performance & Power Coefficient Analysis

The BEM simulation results reveal that C_p reaches a peak value of 0.40 at TSR ≈ 6, which aligns with optimal efficiency predictions. The C_t curve shows an increasing trend with TSR, emphasizing the increasing thrust demand as rotational speed increases.

4. Conclusions

This study successfully presents the aerodynamic design and performance evaluation of a horizontal axis wind turbine (HAWT) blade using QBlade. By leveraging Blade Element Momentum (BEM) theory and computational optimization, the aerodynamic efficiency of a three-blade rotor was systematically analyzed. The investigation involved selecting NACA airfoil profiles across different blade sections, optimizing the chord length and twist distribution, and computing aerodynamic coefficients (C_L/C_D) through XFOIL simulations. The Reynolds number analysis confirmed smooth aerodynamic behavior, with airfoil performance validating the selection of NACA 5522 for mid-span and NACA 5510 near the tip.

The BEM simulation results demonstrated a peak power coefficient (Cp) of 0.40 at TSR ≈ 6, aligning with expected efficiency benchmarks. The thrust coefficient (Ct) curve showed a gradual increase with TSR, emphasizing the aerodynamic loading variations across different rotational speeds.

This research highlights the effectiveness of QBlade as a computational tool for wind turbine blade design and performance assessment. The study suggests further refinement by incorporating:

- Increased blade section resolution for improved aerodynamic accuracy.
- Advanced stall delay techniques for enhanced performance under varying wind conditions.
- CFD validation to complement BEM predictions and validate flow characteristics.

By focusing exclusively on HAWT design and analysis, this study provides valuable insights into optimizing blade aerodynamics for improved wind energy harnessing. Future work can be extended to hybrid blade configurations for enhanced efficiency in diverse operating environments e.g., harnessing tidal energy.

Acknowledgement

This research was partially supported by the European Union under Grant Agreement No. 610523-EPP-1-2019-1-BE-EPPKA1-JMD-MOB.

References

1. ABDULLAH, O., HAMZAH, A. A., AMMAR, S., AL-TAMIMI, A., ALJIBORI, H. S. S., MOHAMMED, M. N., ABED, A. M., HAMEED, M. S., & ALANI, Z. N. (2023). Design and optimization of a small horizontal axis wind turbine blade using QBlade. 2023 IEEE 8th International Conference on Engineering Technologies and Applied Sciences (ICETAS). https://doi.org/10.1109/ICETAS59148.2023.10346571
2. AKHEEL, M. M., SANKAR, B., BOOPATHI, K., PRASAD, D. M. R., SHANKAR, N. P., & RAJKUMAR, N. (2024). Optimizing efficiency and analyzing performance: Enhanced airfoil cross-sections for horizontal axis small wind turbines. Wind Engineering. https://doi.org/10.1177/0309524x241259946
3. ALTMIMI, A., AWS, A., JWEEG, M., ABED, A., & ABDULLAH, O. (2022). An investigation of design and simulation of horizontal axis wind turbine using QBlade. Measurement Science Review. https://doi.org/10.2478/msr-2022-0032
4. DAVARI, H. S., BOTEZ, R., SEIFY DAVARI, M., & CHOWDHURY, H. (2024). Enhancing the efficiency of horizontal axis wind turbines through optimization of blade parameters. Journal of Engineering. https://doi.org/10.1155/2024/8574868
5. GUȚU, M., ODAINÂI, V., MALCOCI, I., & NICOLAE, T. (2021). Aerodynamic efficiency numerical estimation of 1 kW horizontal axis wind turbine rotor. 2021 International Conference on Electromechanical and Energy Systems (SIELMEN). https://doi.org/10.1109/SIELMEN53755.2021.9600363
6. HACHIM, G. M., & MAHDI, J. A. (2020). Analytical assessment of the effects of blade cone angle on the aerodynamic performance of the horizontal axis wind turbine. IOP Conference Series: Materials Science and Engineering. https://doi.org/10.1088/1757-899X/671/1/012140
7. KRISHNANUNNI, A., DATTA, N., CHAMBHARE, H. S., & SWAROOP, D. (2020). Basic design and blade structural analysis of a small horizontal-axis wind turbine for low wind speeds. https://doi.org/10.1115/power2020-16554
8. MARTEN, D., WENDLER, J., PECHLIVANOGLOU, G., NAYERI, C. N., & PASCHEREIT, C. O. (2013). QBLADE: an open source tool for design and simulation of horizontal and vertical axis wind turbines. International Journal of Emerging Technology and Advanced Engineering, 3(3), 264-269.

a. https://www.researchgate.net/publication/275638847_QBLADE_An_Open_Source_Tool_for_Design_and_Simulation_of_Horizontal_and_Vertical_Axis_Wind_Turbines
9. NAZIR, N., & JAVED, A. (2019). Comparison of 1KW horizontal axis wind turbine rotor blade performance using numerical simulation. 2019 Sixth International Conference on Aerospace Science and Engineering (ICASE). https://doi.org/10.1109/ICASE48783.2019.9059224
10. XI, L., & ZHAO, L. (2022). Optimal design of wind turbine blades by a combination of multi-airfoil leaf elements. Journal of Physics: Conference Series. https://doi.org/10.1088/1742-6596/2235/1/012008

Performance Evaluation and Optimization of Power Take-Off (PTO) Systems for Tidal Energy Converters – Horizontal Axis Turbine (TEC-HAT)

M. Usman SIKANDAR[1,2*], Olga KHRYSTOSLAVENKO[3], Chris LLOYD[2]

1 Kaunas University of Technology, Kaunas, Lithuania

2 Offshore Wind Learning, London, United Kingdom

3 Vilnius Tech, Vilnius, Lithuania

** Usman@spin-pack.com*

Abstract

This study evaluates and optimizes the performance of Power Take-Off (PTO) systems in Horizontal Axis Tidal Turbines (HATTs) through detailed computational analysis. Using predefined values of the power coefficient (Cp = 0.32) and thrust coefficient (Ct = 1.2), the rotor and hydrodynamic parameters were computed, yielding a tip-speed ratio (TSR) of 7.81 at an operational water speed of 2.15 m/s. Rotor geometry calculations resulted in a swept area of 736.2 m^2, a rotor diameter of 30.62 m, and a rotational speed of 1.095 rad/s. The rotor torque and thrust forces were estimated at 1068 kN·m and 2092.9 kN, respectively. Gear and generator selection initially optimized performance, with a Flender Planurex P2SA gearbox and a Siemens PM-WC generator rated at 1382 kW. The computed cut-out water speed was 2.7 m/s, leading to an annual energy production (AEP) of 4810.19 MWh/year and a capacity factor (CF) of 39.7%. An optimization study was conducted by varying rotor diameter and rotational speed. The optimal configuration, featuring a 34.0 m rotor diameter and 8.5 RPM, achieved a TSR of 7.04, significantly improving the turbine's performance. This optimized design resulted in a power output of 1479.8 kW, a rotor torque of 1662.5 kN·m, an AEP of 12,963.2 MWh/year, and a high-capacity factor of 107.08%. Consequently, a generator upgrade to a 1500–1600 kW class, such as the Siemens 1FT7 or ABB M3BP 355 series, is recommended to accommodate the enhanced output. These results demonstrate the strong potential for improving the efficiency, reliability, and economic viability of tidal energy conversion systems through PTO optimization.

Keywords: Tidal Energy, Power Take-Off (PTO), Horizontal Axis Tidal Turbines (HATT), Rotor Optimization, Hydrodynamic Performance

1. Introduction

Tidal energy has emerged as a viable renewable energy source due to its predictability and high energy density. The Power Take-Off (PTO) system plays a crucial role in converting kinetic energy from tidal currents into usable electricity, and its optimization significantly impacts the overall efficiency of Horizontal Axis Tidal Turbines (HATTs). The performance of PTO systems is influenced by several factors, including hydrodynamic efficiency, rotor geometry, gear and generator selection, and advanced control strategies. Recent research has focused on improving hydrodynamic performance, as the power coefficient (C_p) and thrust coefficient (C_t) directly affect energy capture. Computational Fluid Dynamics (CFD) simulations and Blade Element Momentum (BEM) theory have been widely employed to optimize these parameters, ensuring an efficient balance between power output and structural loads [1]. Studies have demonstrated that adjusting

the tip-speed ratio (TSR) between 6 and 8 leads to optimal energy extraction, with variable pitch blades improving efficiency by up to 15% [2].
Rotor design also plays a significant role in optimizing tidal turbine efficiency. Research indicates that an increase in rotor diameter enhances power capture but necessitates robust structural reinforcements due to the higher loads acting on the system [3]. A bi-directional counter-rotating tidal turbine model has shown efficiency improvements of 8%, particularly in sites experiencing bidirectional tidal flows, as this design reduces losses caused by flow reversal [4]. Furthermore, probabilistic failure models have been developed to assess the impact of turbulent flow on PTO components, revealing that uncertainties in turbulence modelling can directly affect failure rates and operational reliability [5].

Power Take-Off system selection is equally important in optimizing performance and reducing operational losses. Direct-drive generators are increasingly being favoured as they eliminate the need for mechanical gearboxes, thus enhancing reliability and reducing maintenance costs [6]. Comparative studies between hydraulic and electromagnetic PTO systems indicate that hydraulic PTOs are better suited for high-energy tidal sites, whereas electromagnetic PTOs perform more efficiently in locations with moderate tidal velocities [7]. Additionally, a real-time emulation of PTO systems has shown that variable-speed control significantly increases energy output and system adaptability, making it a preferred approach for future tidal energy deployments [8].

Several advanced control strategies have been investigated to optimize PTO efficiency. Maximum Power Point Tracking (MPPT) algorithms dynamically adjust rotor speed to maintain maximum energy capture, while fuzzy logic-based controllers allow turbines to adapt to fluctuating flow conditions [9]. Research on Yaw-controlled tidal turbines suggests that active control of turbine orientation can enhance performance in sites where flow direction is variable [10]. These findings emphasize the importance of integrating adaptive control strategies into PTO systems to improve their operational efficiency and reliability.

Economic feasibility and environmental sustainability remain major challenges for tidal energy deployment. While levelized costs of tidal energy are declining, ongoing research aims to reduce maintenance costs and extend the operational lifespan of PTO components [11]. Environmental concerns have also been addressed, with studies highlighting the need for optimized turbine placement to reduce ecological impact while maintaining high energy yield [12]. Future improvements in component reliability, material selection, and site-specific deployment strategies are expected to enhance the economic competitiveness of tidal energy and facilitate its broader integration into national energy grids.

The purpose of this study is to advance the performance evaluation and optimization of PTO systems in TEC-HATs by integrating state-of-the-art hydrodynamic modelling, improved rotor geometries, high-efficiency PTO components, and advanced control strategies. The research will focus on enhancing energy capture efficiency, reducing failure rates, and increasing the economic viability of tidal energy. Addressing these challenges will contribute to developing cost-effective, sustainable, and highly efficient tidal energy solutions, which are essential for the future expansion of renewable marine energy systems.

2. Methodology

Since Cp and Ct are derived from a previous study, this methodology focuses on utilizing these values to compute the key parameters without redundant experimental derivation. The revised methodology follows:

- Utilize C_p = 0.32 and C_t = 1.2 as calculated via QBlade for HAWT.
- Establish the relationship between water speed and turbine performance using pre-defined C_p and C_t.
- Define rotor design parameters based on power requirements and efficiency considerations.
- Compute TSR using the given water speed relation and C_p to ensure optimal energy extraction.
- Select appropriate gear and electric generator with minimum weight constraints.
- Evaluate AEP and CF based on the given water speed distribution and turbine efficiency & optimization study.

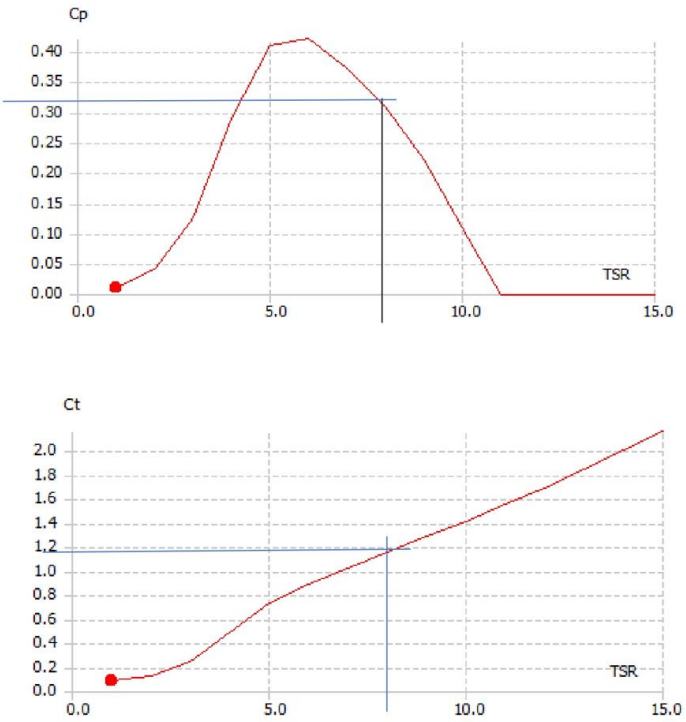

Fig. 26. C_p vs TSR & C_t vs TSR

3. Results

3.1. Rotor and Hydrodynamic Parameters

The efficiency of a tidal turbine largely depends on its tip-speed ratio (TSR), which governs the optimal energy extraction. The TSR is defined as the ratio of the blade tip speed to the free stream velocity. Higher TSR values indicate that the rotor is optimized for high-speed, low-torque applications, whereas lower TSR values favour high-torque operations.

Table 11. Rotor and Hydrodynamic Parameters

Parameter	**Formula/Value**	**Units**
Water Speed (U_{wn})	2.0 + 0.05 × TN	m/s
Team Number (T_N)	3	-
Calculated U_{wn}	2.15	m/s
Blade Tip Speed (U_{tb})	18 - 0.4 × TN	m/s
Calculated U_{tb}	16.8	m/s

Tip Speed Ratio (TSR)	U_{tb} / U_{wn}	-
Calculated TSR	7.81	-
Power Coefficient (C_p)	0.32	-
Thrust Coefficient (C_t)	1.2	-

3.2. Rotor Geometry

The rotor's swept area determines the amount of kinetic energy available for conversion. A larger rotor captures more energy but requires structural reinforcement and increased material costs. The following calculations define the rotor's key geometrical parameters.

Table 12. Rotor Geometry

Parameter	Formula/Value	Units
Rotor Area (A_{rotor})	736.2	m^2
Rotor Diameter (D_r)	30.62	m
Rotor Radius (R_r)	15.31	m

3.3. Rotational Speed and Torque

Rotational speed influences the efficiency and mechanical stability of the turbine. Too high a speed increases wear and tear, while too low a speed leads to inefficient energy capture. The rotor speed and torque are derived as follows:

Table 13. Rotational Speed and Torque

Parameter	Formula/Value	Units
Rotational Speed (Ω_{rotor})	1.095	rad/s
Rotor RPM (N_{rotor})	10.46	rpm
Torque Coefficient (C_q)	0.04	-

3.4. Rotor Torque and Thrust

The forces acting on the rotor determine the structural loads and mechanical stresses experienced by the turbine. The rotor torque and thrust are crucial for gearbox and generator design.

Table 14. Rotor Torque and Thrust

Parameter	Formula/Value	Units
Rotor Torque (Q_{rotor})	1068	kN·m
Thrust Force (T_{rotor})	2092.9	kN

3.5 Gear and Generator Selection

To ensure efficient energy conversion and mechanical reliability, the selection of appropriate gear and generator systems is crucial. The gear system must handle the torque generated by the rotor while ensuring smooth power transmission to the generator. The generator, in turn, must efficiently convert the mechanical energy into electrical power while maintaining optimal performance across varying load conditions.

Table 15. Gear and Generator Selection

Component	Chosen Model	Specifications
Gear	Flender Planurex P2SA	Nominal Output Torque: 1709 kN·m
Generator	Siemens PM-WC	800 RPM, Rated Power: 1382 kW

3.6. U_w Cutout AEP Calculation

The Annual Energy Production (AEP) estimation is an essential metric for evaluating the performance of a tidal turbine system. AEP depends on factors such as water speed variations, capacity factor, and generator efficiency. The cut-out water speed represents the maximum operational limit, beyond which the turbine ceases operation to prevent structural damage.

Table 16. U_w Cut_{out} AEP Calculation

Parameter	Formula/Value	Units
Cut-out Water Speed (U_w cut-out)	2.7	m/s
Annual Energy Production (AEP)	4810.189	MWh/year
Capacity Factor (CF)	(AEP / (Nominal Power × 8760)) × 100	%
Calculated CF	39.7	%

3.7. AEP Optimization Study

To optimize the performance of the tidal energy converter design, an optimization study was conducted. The objective was to maximize the Annual Energy Production (AEP) while maintaining the tip-speed ratio (TSR) within the optimal range of 6–8 and ensuring that the rotor torque did not exceed the gearbox limit of 1709 kNm. The optimization considered variations in rotor diameter between 28 and 34 meters (in 0.5 m increments) and rotational speed (RPM) between 8 and 12 rpm (in 0.5 rpm increments), as supported by standard tidal turbine design practices. For each design combination, key performance indicators such as TSR, power output, rotor torque, AEP, and capacity factor (CF) were calculated. Only configurations satisfying the operational constraints were considered. The results revealed that the optimal design features a rotor diameter of 34.0 meters and an RPM of 8.5, achieving a TSR of 7.04. This design produced a power output of 1479.8 kW, a rotor torque of 1662.5 kNm, an AEP of 12,963.2 MWh/year, and a remarkably high-capacity factor of 107.08%. A 3D scatter plot illustrating the relationship between rotor diameter, RPM, and AEP demonstrates the energy output landscape, highlighting the optimal region for maximum energy production. These findings confirm that strategic adjustment of rotor geometry and rotational speed can significantly enhance tidal turbine performance.

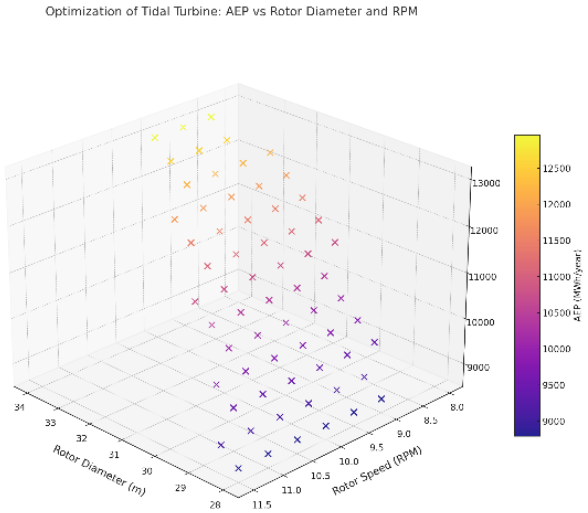

Fig. 27. Optimization of Tidal Turbine AEP as a Function of Rotor Diameter and Rotational Speed

4. Discussion

The performance of a tidal turbine is critically linked to its tip-speed ratio (TSR), with a TSR of 7.81 achieved in this study, aligning within the optimal 6–8 range to balance energy extraction and structural load management. With a power coefficient (Cp) of 0.32, a thrust coefficient (Ct) of 1.2, and an average water speed of 2.15 m/s, the turbine effectively captures tidal energy while maintaining structural stability. The rotor, with a swept area of 736.2 m^2 and a diameter of 30.62 m, coupled with an operational rotational speed of 1.095 rad/s (10.46 RPM), delivers a rotor torque of 1068 kN·m and thrust force of 2092.9 kN. A Flender Planurex P2SA gearbox and a Siemens PM-WC generator (1382 kW, 800 RPM) were initially selected to ensure efficient power transmission. The turbine's cut-out water speed was set at 2.7 m/s, resulting in an annual energy production (AEP) of 4810.19 MWh/year and a capacity factor (CF) of 39.7%. To enhance performance, an optimization study was conducted, varying rotor diameters between 28–34 meters and rotational speeds between 8–12 RPM. Key performance parameters were evaluated, identifying an optimal design with a 34.0-meter rotor diameter and 8.5 RPM, achieving a TSR of 7.04. This configuration elevated the power output to 1479.8 kW, rotor torque to 1662.5 kN·m, and AEP to 12,963.2 MWh/year, with a significantly improved capacity factor of 107.08%. A 3D scatter plot illustrated the relationship between rotor diameter, RPM, and AEP, highlighting the optimal performance region. Based on these findings, a generator upgrade to a 1500–1600 kW class, such as the Siemens 1FT7 or ABB M3BP 355 series, is recommended to accommodate the enhanced output and ensure operational reliability.

5. Conclusion

The computational analysis and optimization of the PTO system for Horizontal Axis Tidal Turbines (HATTs) demonstrate the system's ability to achieve efficient energy conversion through optimized rotor geometry, torque distribution, and power output. Initially, a TSR of 7.81, a rotor diameter of 30.62 m, and an estimated annual energy production (AEP) of 4810.19 MWh/year with a 39.7% capacity factor confirmed effective performance within structural and hydrodynamic constraints. To further enhance energy capture, an optimization study was conducted, identifying an optimal configuration with a 34.0 m rotor diameter and 8.5 RPM, yielding a TSR of 7.04. This optimized design increased AEP to 12,963.2 MWh/year and achieved a high capacity factor of 107.08%, indicating substantial performance improvement. Consequently, a generator upgrade to a 1500–1600 kW class, such as the Siemens 1FT7 or ABB M3BP 355 series, is recommended to match the enhanced output, while the existing Flender Planurex P2SA gearbox remains marginally suitable. These findings confirm the strong potential of optimized HATT systems for sustainable tidal energy generation. Future advancements in material selection, adaptive control strategies, and component durability could further enhance system efficiency.

Acknowledgment

This research was partially supported by the European Union under Grant Agreement No. 610523-EPP-1-2019-1-BE-EPPKA1-JMD-MOB.

References

1. Jo, C., Rho, Y., & Lee, K. HAT tidal current turbine design and performance test with variable loads. *Journal of the Korean Society for New and Renewable Energy*, (2012), 8(1), 44-51. Available from: https://doi.org/10.7849/KSNRE.2012.8.1.044
2. Portilla, M. P., Piñeiro, A. L., Rivas, L. N., & Guerra, E. T. Improved design of multi-rotor tidal energy converters. (2018), Volume 10: Ocean Renewable Energy. Available from: https://doi.org/10.1115/OMAE2018-78227

3. Afshar, O., Henderson, A., Walker, J. M., & Wang, X. Numerical investigation of a horizontal axis tidal turbine. *Proceedings of the International Conference on Ocean Engineering,* (2016). Available from: https://people.eng.unimelb.edu.au/imarusic/proceedings/20/492%20Paper.pdf
4. Huang, B., Zhu, G., & Kanemoto, T. Design and performance enhancement of a bi-directional counter-rotating type horizontal axis tidal turbine. *Ocean Engineering*, (2016), 128, 116-123. Available from: https://doi.org/10.1016/J.OCEANENG.2016.10.012
5. Val, D., Chernin, L., & Yurchenko, D. Updatable probabilistic evaluation of failure rates of mechanical components in power take-off systems of tidal stream turbines. *Energies*, (2021), 14(20), 6586. Available from: https://doi.org/10.3390/en14206586
6. Wani, F. Improving the reliability of tidal turbine generator systems. *Thesis, Delft University of Technology,* (2021). Available from: https://doi.org/10.4233/UUID:B5D38E9A-44AB-4BD4-9CF9-15659F7867B8
7. Hansen, R. H., Andersen, T. O., & Pedersen, H. C. Model based design of efficient power take-off systems for wave energy converters. In Proceedings of the 12th Scandinavian International Conference on Fluid Power, Tampere, Finland, (2011), 18-20. Available from: https://vbn.aau.dk/en/publications/model-based-design-of-efficient-power-take-off-systems-for-wave-e
8. Erdogan, N., Murray, D., Giebhardt, J., Wecker, M., & Donegan, J. Real-time hardware emulation of a power take-off model for grid-connected tidal energy systems. IEEE International Electric Machines & Drives Conference (IEMDC), (2019), 1368-1372. Available from: https://doi.org/10.1109/IEMDC.2019.8785358
9. Henriques, J., Gomes, R., Gato, L., Falcão, A., Robles, E., & Ceballos, S. Testing and control of a power take-off system for an oscillating-water-column wave energy converter. *Renewable Energy*, (2016), 85, 714-724. Available from: https://doi.org/10.1016/J.RENENE.2015.07.015
10. Frost, C., Morris, C. E., Mason-Jones, A., O'Doherty, D., & O'Doherty, T. The effect of tidal flow directionality on tidal turbine performance characteristics. *Renewable Energy*, (2015), 78, 609-620. Available from: https://doi.org/10.1016/J.RENENE.2015.01.053
11. Batten, W. M. J., Bahaj, A. S., Molland, A. F., & Chaplin, J. R. Power performance analysis according to the configuration and load control algorithm of power take-off system for oscillating water column type wave energy converters. *Energies*, (2022), 13(23), 6415. Available from: https://doi.org/10.3390/en13236415
12. Chan, R., Kim, K., Park, J.-Y., Park, S., Kim, K.-H., & Kwak, S. The effect of power take-off system on S-shaped vertical axis autorotation current turbine. *Journal of Marine Science and Engineering*, (2020), 10(11), 1660. Available from: https://doi.org/10.1115/omae2023-100991

Design and Fabrication of a Universal Solar Dryer with Tracking Device

Masin Muhammadu MUHAMMADU*, Muhammad SULE-SARKI

Federal University of Technology, Gidan Gwanu-Minna, Nigeria

** masin.muhammadu@futminna.edu.ng*

Abstract

A solar dryer with tracking has been developed to make maximum use of the solar energy for drying products, especially agricultural products such as tomatoes, vegetables, etc. The framework of all the parts of the dryer concept was designed, fabricated and tested using available materials that were sourced locally. Preliminary tests with no load to the dryer showed that the solar collector raised the ambient air temperature from 20 °C to 41 °C, and to a warm air of 28 °C to 64 °C between the morning and midday. This lowered the relative humidity of the air from an average of 26 % in the morning to 5 % at midday. The dryer, loaded at 5 kg/m, dried tomato slices of 8 mm thickness from the initial moisture content of 93.3% to a final moisture content of 12 % in 13 hours and 11 hours when operated under natural convection current. Using forced ventilation, the slices of tomato took 11 hours to reach final moisture contents of 12 %. The open-air, sun drying tests conducted side by side with solar drying needed an average of 20 hours to reach the same final moisture contents for tomato slices. The maximum drying rate of tomato slices attained under natural convection and forced circulation was 3.1 and 2.8 kg of water per kg of dry matter-hr. For the open-air sun drying, the maximum drying rates for tomato slices were 1.5 kg of water per kg of dry matter-hr. The dryer was able to remove 52.8% of moisture while tracking the sun, dry basis, from 4.6 kg of product in one day of 10.00 hours drying time, which is about 0.46 kg/hr drying rate. The efficiency of the dryer was 65.7%, and the solar dryer system will be useful for long-term preservation of agricultural perishable crops by farmers and stakeholders.

Keywords: tracking device, solar, dryer, universal, efficiency and convection.

1. Introduction

Drying is a simple process of removing moisture or excess water content from a product whereby the moisture content of the product is reduced to a pre-determined value, usually by the movement of heated air through the product. This value of moisture content is very much higher than the required for long preservation [1]. Due to this moisture content, bacterial and fungal growth are very fast in the crops. Bacteria and enzymes may spoil the product and reduce the nutrient content in it. The moisture content of crops, to a certain level, slows down the bacterial, enzymes and yeast effect. Therefore, it is necessary to reduce the moisture content in the product for its long preservation. Another case of drying is to remove the total excess water from the product [1-2]. These dehydrated products regain their original conditions after rehydration whenever necessary for use.

Drying is the most practical means of preserving vegetable or agricultural products by reducing their excess moisture content to a safe level, which will inhibit the growth of microorganisms. Because of that, the solar dryer technology will become an alternative method which can process

the products in a clean, safe, hygienic and produce better quality and more nutritious foods. In general, this solar dryer has saved energy, labour-intensive, time, less area for spreading the product to dry, makes the process more efficient and protects the environment and also safe the products from Rat attack to avoid the deadly disease called Lassa fever [3 – 6].

Vegetables and fruit are the main source of Vitamins such as vitamins A, B and C and also minerals such as calcium, phosphorous, iron, magnesium and to a little extent carbohydrate in our diet which are essential to the body by contributing to the requirements of the metabolic needs of the body, in view of this, vegetable like tomatoes should be accorded a rightful position in the process of feeding the nation [5]. Fruits and vegetables are not only seasonal but highly perishable and spoil more readily than other Agricultural products.

Vegetable crops such as tomatoes, okra, onions and peppers are perishable crops and are generally grown and widely eaten in Nigeria. These agricultural products are characterised by being of good quality, excessive and cheap in their seasons and scarce, costly and of bad quality out of season. Keeping these crops for some months in their fresh state (such as to retain the actual nutrients, taste and colour as when freshly harvested) has remained a problem yet unsolved because they deteriorate a few days after harvest [4]. And many problems also occur in the previous type of solar tracking system. The problem here is the solar panel that is used only in a fixed installation. Because of this problem, the power that can be generated is low. Also, there is a problem with installing more than one solar panel to produce enough power [6, 7].

2. Materials and Methods

The materials used in the fabrication of the solar dryer are listed in Table 1.

Table 1. Materials used in the fabrication of the universal solar tracker

S/No	Item	Purpose and Specification
1	Glass	Use for the reflection of light
2	Wooden frame	Use for the construction of a solar collector
3	Absorber	Use for collecting heat to generate hot air
4	D.C Fan	2 V, 0.5 A, for blowing hot air
5	Air Duct	Plastic Flexible pipe for conveying air
6	PV Module 80 W	80 W solar panel for powering the DC fan and tracking system
7	Angle Iron	1” Mild steel iron, used for the solar panel frame
8	Square Pipe	1” Mild steel pipe, used as a dryer chamber
9	Insulator	Fiber glass, used as an insulator
10	Al–sheet	Use for covering the drying chamber
11	Al–foil	Use for covering the inner chamber
12	Wire mesh	0.5 cm iron rod, used as a tray
13	Linear Actuator	For actuating the solar collector

2.1. Description and Working Principles

The schematic diagram of the solar tomatoes dryer shown in Figure 1, comprises the tracker, air flow solar collectors.

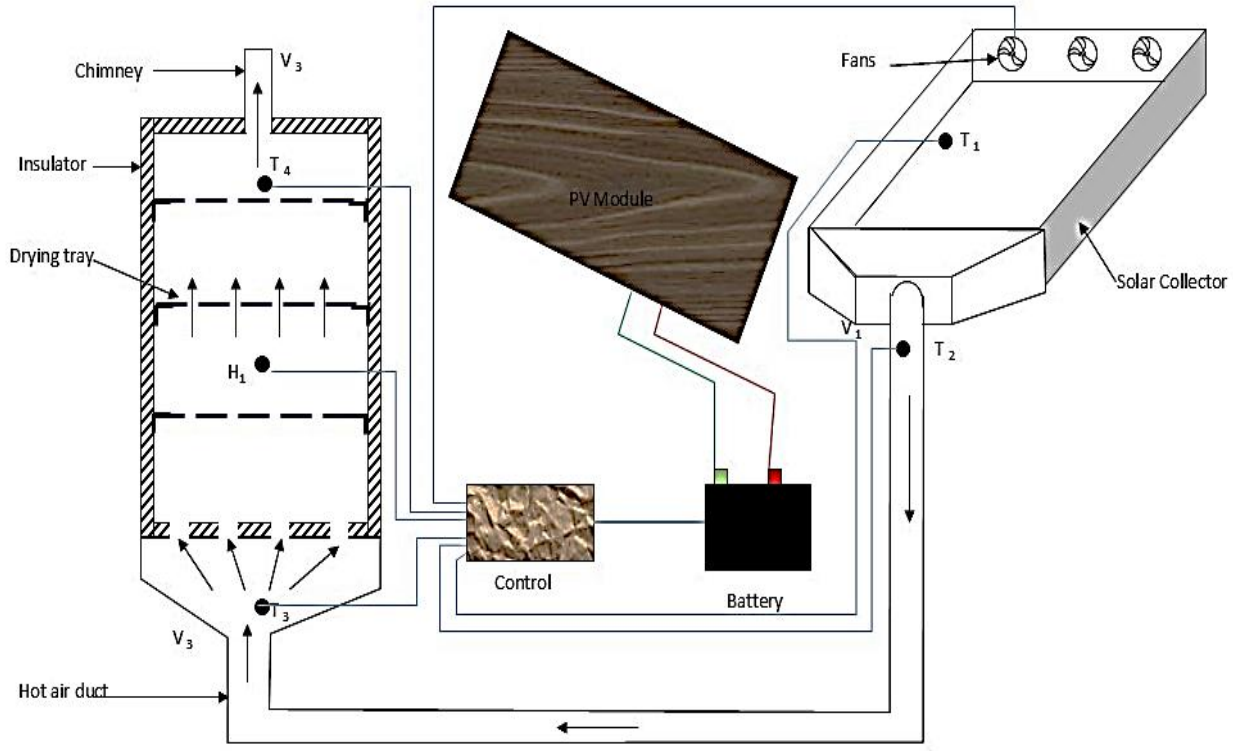

Fig. 1. Schematic layout of the universal solar dryer with tracking device, drying chamber section and chimney

The solar collector was designed to track the movement of the sun when working. The solar collector collects the solar radiation from the sun to heat up air extracted from the environment and blows the hot air flow through the transparent (glazing) into the tomatoes drying chamber via a mini-DC fan. The air is transported through an insulated air duct. The solar radiation is absorbed into the collector via a black body absorber. The collector is insulated using a fibreglass to minimized heat loss to the environment.

Air from the surrounding pass through an inlet pipe attached to the absorber plate with the aid of an air sucker and when the solar collector, collected the incoming solar radiation from the sun, it heats up the air from the surrounding and the hot air pass through the multiple pipes to exit at the outlet pipe the hot air enters the drying chamber under the effect of thermal force and is placed in shelves and passes through drying trays with tomatoes.

The hot air enters the tomato dryer from the bottom of the dryer and exits from the top of the dryer through a chimney. The hot air loses its temperature before exiting the dry chamber, and the tomatoes gain temperature from the hot air, thereby losing their moisture content to a certain level. The entire system is monitored by a control system that is capable of measuring the temperature and humidity inside the drying chamber.

2.2. Methodology of Calculations

The drying of vegetables is in two face or stages. The first stage is to raise the temperature of the wet materials to a level at which the moisture will be removed. Equations (1) and (2) were used to determine the amount of heat required to remove the moisture content.

$$Q_{Exp.} = M_T C_P (\Delta T) \quad (1)$$

where: M_T – Mass of tomatoes (kg), Cp – Specific heat capacity (kJ/Kg°C), ΔT - Change in temperature (°C), $Q_u = A_c \cdot F_c .e .IH$, Fr = heat remitter factor (0.7 for an air collector), E = Effective transmittance (0.5 for transparent white polyether), I = Total solar radiation per unit area,

Q = 40 m x 0.7 x 0.5 x 500

=7000 W

= 7.0 kJ/s

Therefore, energy required for 1 hr (3600 S), 7.0 x 3600 = 25200 kJ/hr, and for 10 hrs, 10 hr x 25200 kJ/hr = 252000 kJ/day. Therefore, the period that will be required is

$\frac{8k}{2k/d} = 4\ days$

However, determining the quantity of water or moisture to be removed in drying substances is directly connected to the amount of drying space. According to Hafez et al. [7], Equation (2) can be used to determine the quantity of water in a drying substance.

$$M_w = \frac{W_w (M_i - M_f)}{1 - M_f} \quad (2)$$

Furthermore, the average daily solar insulation of Minna is 12.58 MJ/m^2/day and for an ambient temperature of 33 °C and F = 500 W/m^2. The collector efficiency ranges between 30% to 40%. Other factors that influence the collector efficiency are temperature, air flow rate, isolation of cover material use, and absorber plate, type of insulator used. An efficiency of 30% was chosen, and this means that the expected energy production can be determined by Equation (3):

$$Q_{exp.} = I \times \eta_{collect} \quad (3)$$

$Q_{exp.} = 12.58 \times 0.38$

$Q_{exp.} = 4.7804$ MJ/m^2/day

Therefore, the collector area required is given by Equation (4)

$$A_c = \frac{Total\ drying\ energy\ required}{Solar\ energy\ product} \quad (4)$$

$A_c = \frac{718.200}{14.34}$,

$A_c = 5.0$ m^2

Therefore, the total collector area required is 5.0 m^2 and considering a collector dimension ratio of 1:1:5, the collector width = 0.8 m, while the length is 1.12 m was used.

In addition, the recommended drying temperature for the fruits and vegetables (Tomatoes inclusive) is between 37.7 °C to 54.4 °C [8]. Any temperature below this range may not effectively dry the material, and if the temperature is higher than the recommended, it may cause sugar caramelization (browning of sugar) for many fruit products.

Also, energy efficiency in drying is of obvious importance as energy consumption is such a large component of drying costs. So this adiabatic air-drying efficiency (ŋ), can be defined by: The efficiency(ŋ) of the energy efficiency in drying was calculated using Equation (5).

$$\eta = \frac{T_1 - T_2}{T_1 - T_a}\ x\ 100 \quad (5)$$

where: T_1 is the inlet (high) air temperature into the dryer, T_2 is the outlet air temperature from the dryer, and T_a is the ambient air temperature. The numerator, the gap between T_1 and T_2, is a major factor in the efficiency.

Then, the rate of mass transfer is proportional to the potential (pressure or concentration) difference and to the properties of the transfer system, characterised by a mass-transfer coefficient, we have

$$\frac{dw}{dt} = k'_g . A . \Delta Y \quad (6)$$

where: dw is the mass (moisture) being transferred kgs^{-1} in time dt, A is the area through which the transfer is taking place, kg' is the mass transfer coefficient in this case in units $kgm^{-2}\,s^{-1}$, and ΔY is the humidity difference in $kgkg^{-1}$

So also, air flow rate affects the performance of the dryer, therefore, determining air flow rate in the dryer is a function of the cross-sectional area of a duct and the distance the air travels with time. Then the cross-sectional area can be easily determined and the volumetric flow calculated.

$$Q = A . V \ (m^3/s) \quad (7)$$

where: A = area (m^2) and V = air velocity m/s.

This comprised the supporting frame, the jack that provides the linear motion and the mechanism for translating the linear motion into a rotary motion for the flat solar collector. Therefore, the position, velocity and torque equations of the tracking mechanism are given by Equations (8) - (10).

$$Xd = b . cos\theta + (a^2 - b^2 sin\theta)^{1/2} \quad (8)$$

$$V_d = -\left[bsin\theta + \frac{bcos\theta\ sin\theta}{a^2 - b^2 sin^2\theta}\right]\dot{\theta} \quad (9)$$

$$\text{and } T = m_1 ga \times cos\theta + m_2 ga \times cos\theta \times sin\theta \quad (10)$$

where: a – Jack length (cm), b – half of collector length (m) and c – angle that the jack makes with horizontal (degree).

Fabrication Procedure - PV Module Stand: The 80 W solar use has a side of 0.8 m x 1.2 m, and there from 1" angle iron (mild steel) was cut using a hacksaw and joined together with the aid of a bolt and nut to form the frame for the PV module. The supporting stand of the PV module was also fabricated using a 1" mild steel equal angle iron. The stand was also bolted together using an M5 bolt and nut. The PV-module frame and PV-module stand were coupled via a pivoted pin joint.

To determine the air flow rate required for drying, the useful energy has to be estimated. The volumetric flow rate of the air at the drying section is

$$V = \frac{Ma}{\rho} \quad (11)$$

Procedure Experimental: The solar dryer setup was placed outside in an open space having direct sunlight, as shown in Figure 4. The drying chamber, the solar tracker and the solar panel were all connected to the control unit, having four (4) temperature sensors to measure both the inlet and outlet temperature of the solar collector and drying chamber, respectively. A DC fans were fixed to the collector for air axial flow through the collector. The experiments were conducted in May 2023 during the rainy season, from 9 am to 5 pm. The solar radiation was measured using a pyranometer. The temperature of the four sensors was read directly from the display at an interval of 10 minutes at a controlled air velocity. The weight of the drying samples was measured using a digital weighing device each time the is recorded. All the experiments were repeated to confirm the repeatability of the data obtained. Figure 2 indicates the experimental setup.

Fig. 2. Experimental Setup

3. Results and Discussion

The amount of heat required to remove the moisture content of the tomato from 80% to 20% was computed to be 332640 joules at a device drying efficiency of 65.52%. the drying area of the drying chamber was computed to be 0.264 m^2 with a drying space of 0.2123 m^3. The air flow rate is 0.732 m^3/s. while the mass of the water removed is 7.62 Kg during the drying period, when drying tomatoes.

The results of the tracking device show a maximum velocity and acceleration of 0.2 m/s and 0.05 m^2/s, while the positioner is tracking the sun. The velocity of the collector increases steadily, while the acceleration remains almost constant. Fig. 3 indicates the angular position of the Solar Collector.

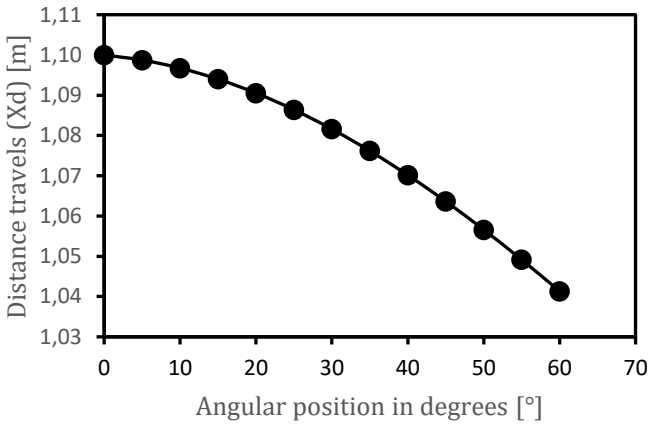

Fig. 3. Angular position of the Solar Collector

3.1 Experimental Results

Figure 4 indicates experimental results conducted for one week from morning to evening (7:00 am to 3:00 pm) in hourly variation of the dryer concerning the ambient temperatures, and this rate was corrected with results of [2 – 4] and was plotted graphically as indicated. The temperatures at the inlet and outlet of both the solar collector and the drying chamber were recorded while varying the velocity or flow rate of the forced convection over the solar collector. Also, the ambient temperature was recorded simultaneously. However, (T_1[°C] to T_4[°C]) were the repeated values within an hour as indicated in Fig.4. The average temperatures of the solar collector inlet and outlet were 34.7 °C and 56.4 °C, while those of the drying chamber were 52.4 °C and 46.3 °C, respectively. Therefore, the heating temperature inside the dryer was higher than the ambient temperature by an average of 21.6 °C (37.7%) throughout the daylight and up to 31 °C (75%) between 13.00 and 15.00 hours, which indicates a prospect for better performance than open-air sun drying.

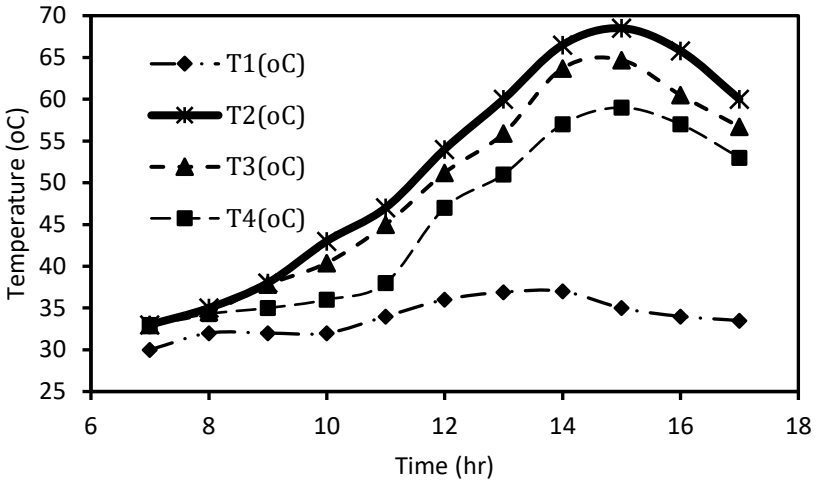

Fig. 4. Hourly variation of the dryer and the ambient temperatures

It was observed that the drying rate increased due to an increase in temperature between 10.00h and 14.00h but decreased thereafter, which shows the earlier and faster removal of moisture from the dried item.

4. Conclusions

The following conclusions were drawn:

1. A universal solar tracker dryer for drying tomatoes was successfully designed.
2. The designed machine was successfully fabricated.
3. The efficiency of the solar tracker was found to be 75.52%.
4. The dryer was able to remove 52.8% of moisture, dry basis, from 4.6 kg of product in one day of 10.00 hours drying time, which is about 0.46 kg/hr drying rate.
5. This rate compares well with the rate obtained from other dryers.

References

1. UDOMKUN, P., ROMULI, S., SCHOCK, S., MAHAYOTHEE, B., SARTAS, M., WOSSEN, T., NJUKWE, E., VANLAUWE, B., and Müller, J. Review of solar dryers for agricultural products in Asia and Africa: An innovation landscape approach. *Journal of Environmental Management,* 268, 2020, 110730.
2. REZA, M. S. and HOSSAIN, M. A. Development and performance assessment of a hybrid solar cabinet dryer for fish drying. *Energy and Thermofluids Engineering,* 3, 2023, 29-38.
3. ELWAKEEL, A. E., WAPET, D.E.M., MAHMOUD, W. E. A. M, ABDALLAH, S. E., MAHMOUD, M. M., ARDJOUN, S. A. E. M. and TANTAWY, A. A. Design and implementation of a PV-integrated solar dryer based on internet of things and date fruit quality monitoring and control. *International Journal of Energy Research,* 2023, no. 1, 7425045.
4. ADETAN, D. A., OLADEJO, K. A. and OBAYOPO, S. O. Development of a Multipurpose Solar Dryer. *FUOYE J Eng Technol.,* 1(1), 2016, 78-82.
5. BOYO, A. and BOYO, H. Development of a solar fish dryer. *Biological Sciences-PJSIR,* 52(4),2009, 228-230.
6. American Society of Heating, Refrigerating and Air-Conditioning Engineers (ASHRAE). ASHRAE, Handbook, 1977. Atlanta, Georgia, USA.
7. HAFEZ, A. Z., YOUSEF, A. M. and Harag, N. M. Solar tracking systems: Technologies and trackers drive types–A review. *Renewable and Sustainable Energy Reviews,* 91, 2018, 754-782.
8. SCANLIN, D. The design, construction and use of an indirect, through-pass, solar food dryer. *Homebrew Appalachian*. 1997, Vol. 57, 22.

SUSTAINABLE URBAN AND RURAL DEVELOPMENT

A Multi-Criteria Decision-Making Approach for Sustainable Landscape Management in Urban and Rural Development

Sulaksha WIMALASENA*, Jūratė ŠLIOGERIENĖ, Thilina Ganganath WEERAKOON

Vilnius Gediminas Technical University, Vilnius, Lithuania

** sulaksha-wimalasena.didde-cottalbadde-vithange@stud.vilniustech.lt*

Abstract

Sustainable landscape management is crucial for balancing environmental, social, and economic problems in both urban and rural growth. As increasing urbanization and climate change continue to affect land-use patterns, decision-makers want sophisticated frameworks to evaluate and prioritize landscape management solutions. This study employs the Analytic Hierarchy Process (AHP), a widely used Multi-Criteria Decision-Making (MCDM) method, to examine sustainable landscape management choices in Sri Lanka. Three important strategies – Green Infrastructure, Urban Farming, and Sustainable Forest Management – were selected and evaluated as alternatives based on four fundamental criteria including Environmental Sustainability, Socio-Cultural Impact, Economic Viability, and Governance & Policy Frameworks.

A structured AHP method was used to develop a hierarchical decision-making model, perform pairwise comparisons, and compute priority weights for each criterion and sub-criterion. The results reveal that Urban Farming is the most desired alternative, having the highest total weight (0.4068), followed by Green Infrastructure (0.3735) and Sustainable Forest Management (0.2196). The findings emphasize the usefulness of AHP in incorporating several sustainability criteria into the decision-making process, giving policymakers and urban planners a structured framework for optimizing landscape management. By including environmental protection, socio-economic advantages, and governance considerations, this study contributes to the rising discourse on sustainable urban and rural development.

Keywords: multi-criteria decision-making, decision support system, sustainable landscape management, urban development, rural planning, analytic hierarchy process.

1. Introduction

Sustainable landscape management plays a crucial role in balancing ecological, economic, and social concerns in both urban and rural development. As growing urbanization and climate change transform land-use patterns, decision-makers require comprehensive frameworks to maximize resource allocation, assure environmental sustainability, and increase social well-being [1, 2]. A Multi-Criteria Decision-Making (MCDM) approach has evolved as a useful way for handling these challenges by incorporating multiple criteria to evaluate and prioritize landscape management methods [3]. This research intends to explore the application of MCDM in sustainable landscape management, focusing on urban and rural development concerns, by synthesizing recent breakthroughs in decision-support systems, optimization models, and participatory frameworks.

The issue of making educated landscape management decisions is increased by competing needs for green infrastructure, agricultural land, and urban expansion [4]. Conventional decision-making procedures typically fail to account for the multidimensional trade-offs involved,

necessitating an integrated process that combines ecological, economic, and social aspects [5]. Recent studies have proved the efficacy of MCDM in numerous areas, including urban agriculture optimization [2], forest ecosystem sustainability [3], and pedestrian infrastructure planning [4]. These techniques employ mathematical modelling, multi-objective optimization (MOO), and qualitative assessment tools such as Analytical Hierarchy Process (AHP), Technique for Order Preference by Similarity to Ideal Solution (TOPSIS), and *VIšekriterijumsko KOmpromisno Rangiranje* (VIKOR) to evaluate landscape options [6, 7].

The methodological approach employed in this study incorporates a systematic evaluation of current literature on MCDM applications in landscape management, coupled with an examination of essential decision-support (DSS) systems. Several studies have proven that integrating MOO with MCDM promotes decision quality by addressing spatial, economic, and environmental limitations [1, 2]. Additionally, participatory decision-making frameworks, such as multi-lens governance models [5] and interactive scenario-based techniques [8], have been proposed to promote stakeholder involvement in landscape planning. The findings indicate that MCDM methods greatly contribute to optimizing landscape management by balancing environmental conservation with urban growth objectives. For instance, Xu and Chang [1] found a 16.23% increase in green space with MCDM-based design, while Haloui et al. [2] demonstrated its usefulness in lowering CO_2 emissions and improving urban agricultural sites. Similarly, Shavazipour, Podkopaev, and Miettinen [8] emphasized how MCDM enables long-term forest landscape design under severe uncertainty. These observations underline the importance of adaptive and context-specific decision-making frameworks to handle rising sustainability concerns in urban and rural areas.

In summary, this paper presents a complete evaluation of MCDM applications in sustainable landscape management, stressing their importance in improving urban and rural development. By merging advanced decision-support approaches, spatial planning tools, and participatory governance models, this research contributes to the evolving debate on sustainable landscape decision-making. The succeeding sections will further explore specific case studies, techniques, and policy implications for promoting landscape sustainability through multi-criteria approaches.

2. Methodology

The Analytic Hierarchy Process (AHP), originally pioneered by Thomas L. Saaty in 1971, stands as one of the most powerful and widely embraced methodologies for addressing complex Multi-Criteria Decision-Making (MCDM) challenges across an impressive spectrum of domains – including political strategy, economic policy-making, socio-cultural evaluations, and management science [9]. Renowned for its exceptional adaptability and intuitive structure, AHP advocates the careful integration of decision-makers' ideas, preferences, and judgments by meticulously deconstructing difficult, diverse problems into an elegant and accessible hierarchical model.

At the center of its methodology lies the building of a structured, tiered framework that cascades logically from the ultimate decision aim to an extensive network of criteria and sub-criteria, ending in a foundation of particular alternatives or possibilities. This sophisticated design begins with a clearly stated, overall purpose at the top of the hierarchy, which then branches downward into progressively intricate and nuanced levels of decision criteria. Figure 1 which is developed by the author vividly illustrates this hierarchical design in the context of identifying the Best Sustainable Landscape Management Strategy – where high-level considerations such as environmental sustainability dominate the upper echelons, while their more granular, contributing sub-criteria are carefully distributed across the intermediate levels. This methodical

approach not only encourages clarity and logic but also helps decision-makers to traverse and solve otherwise overwhelming decision scenarios with confidence and precision.

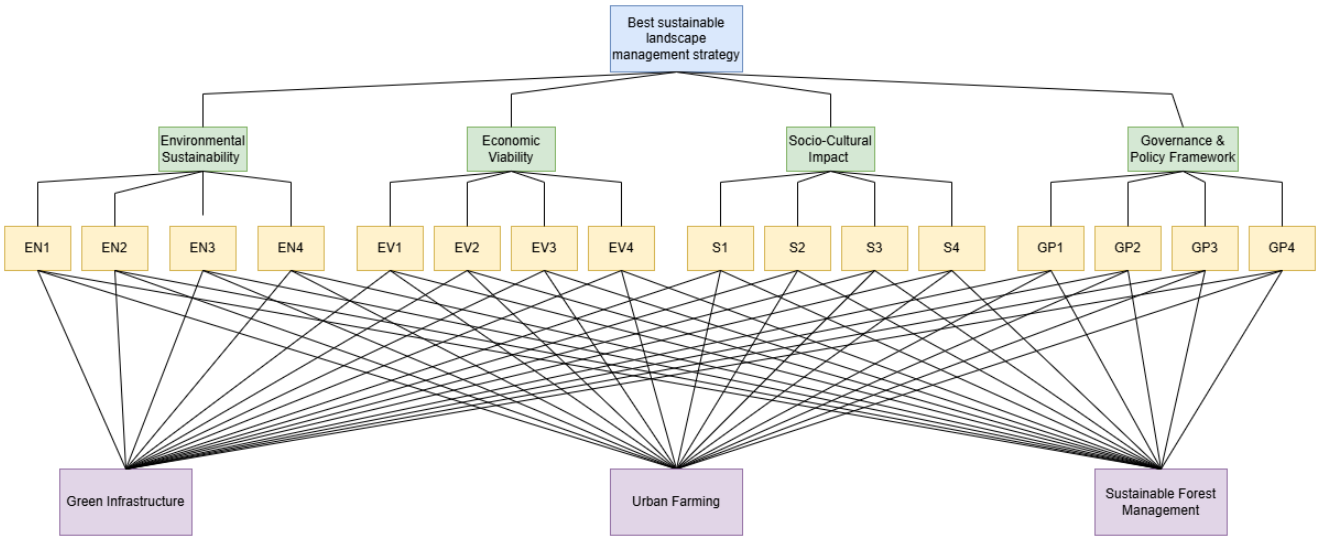

Fig. 1. AHP hierarchical structure for decision-making factors influencing sustainable landscape management (developed by the author)

The first and most important phase in the AHP process is the creation of the hierarchical structure, as was previously mentioned. The relative value or preference of pieces within the same tier is then evaluated by pairwise comparisons at each hierarchical level. Based on their expertise and judgment, stakeholders or subject matter experts offer numerical values that represent a level of preference. Using a matrix, this technique ranks components at each level according to their links to lower ones. A standardized nine-point Saaty scale that represents degrees of importance is used to quantify preferences. This scale is described and interpreted in depth in Table 1.

Table 1. Fundamental scale use for pairwise comparison [9]

Intensity of Importance	Definition
1	Equally importance
3	Moderate importance
5	Strong importance
7	Demonstrated importance
9	Extreme importance
2,4,6,8	Intermediate values

To be able to calculate overall rankings or weights for items at each hierarchy level, priorities from pairwise comparisons are synthesized. A lower CR score denotes greater reliability, and consistency analysis guarantees logical and congruent preferences [10]. Equations 1 and 2 can be used to get the consistency index and ratio:

$$CI = \frac{(\lambda_{max} - n)}{n - 1}, \tag{1}$$

$$CR = \frac{CI}{RI}. \tag{2}$$

In this case, n denotes the matrix's size or order, while λ_{max} represents the eigenvalue of a particular decision matrix. According to Saaty (10), each matrix's Random Index (RI) is determined by the number of criteria it includes. Table 2 gives the corresponding RI values based on the matrix order n.

Table 2. Average random index (RI) dependent on matrix size [10]

n	1	2	3	4	5	6	7	8	9	10
RI	0	0	0.52	0.89	1.11	1.25	1.35	1.40	1.45	1.49

The value of CR that is lower than 0.10 indicates that the consistency is satisfactory, whereas a value that is higher indicates that the pairwise comparisons should be revised.

3. Case study

A case study was performed to illustrate the utilization of the AHP in decision-making for sustainable landscape management. The study focused on a project in Sri Lanka, where the purpose was to discover the best-suited technique for sustainable landscape development in both urban and rural areas. Three principal Alternatives were assessed, including Green Infrastructure, Urban Agriculture, and Sustainable Forest Management. The options were pre-selected for their importance to environmental protection, socio-economic advantages, and policy alignment. The study intended to establish the most effective way by analyzing many variables, including environmental sustainability, socio-cultural impact, economic viability, and governance & policy frameworks. Through AHP, a structured decision-making process was carried out to enable policymakers and urban planners to make informed decisions for sustainable development. The pairwise comparison of the goal is as shown in Table 3.

Table 3. Pairwise comparison matrix

Goal	Environmental Sustainability	Socio-Cultural Impact	Economic Viability	Governance & Policy Framework	Priority Vector
Environmental Sustainability	1	3	5	7	0.56381
Socio-Cultural Impact	0.33333	1	3	5	0.26339
Economic Viability	0.2	0.33333	1	3	0.11779
Governance & Policy Framework	0.14286	0.2	0.33333	1	0.05502

After computation, the maximum eigenvalue (λ_{max}) is found to be 4.117, with a consistency index (CI) of 0.039 and a random index (RI) of 0.89 (for (n = 4), as indicated in Table 2). The consistency ratio (CR) is estimated as 0.043, which is below the threshold of 0.1, suggesting that the decision-makers' judgments are consistent. The weights allocated to each primary criterion are presented in Table 4.

Table 4. Main criteria weights

Main Criteria	Weight
Environmental Sustainability	0.5377
Socio-Cultural Impact	0.2992
Economic Viability	0.1237
Governance & Policy	0.0394

Similarly, the pairwise comparison of all the sub-criteria was undertaken to ensure a full evaluation of the options. The performance of Green Infrastructure, Urban Farming, and

Sustainable Forest Management with respect to each important criterion was examined and is provided in Table 5. From Table 5, it can be noticed that Urban Farming has the highest overall weight, making it the most preferable option for sustainable landscape management. This implies that Urban Farming performs best across major sustainability parameters, considering environmental effect, socio-cultural advantages, economic feasibility, and governance support.

Table 5. Main criteria weights

Main Criteria	Green Infrastructure	Urban Farming	Sustainable Forest Management
Environmental Sustainability	0.27895	0.64912	0.07193
Socio-Cultural Impact	0.63699	0.10473	0.25828
Economic Viability	0.32364	0.07459	0.60177
Governance & Policy Framework	0.18839	0.08096	0.73064

The final overall weights and ranking of the alternatives were established by averaging the ratings assigned to each sub-criterion. The weights were computed by first multiplying each sub-criteria with its corresponding main criterion weight and the respective performance rating of each alternative. The values obtained from all sub-criteria were then summed to get the final weight of each alternative. These AHP calculations offered unambiguous and structured weights for the criterion, sub-criteria, and alternative ranks in a crisp numerical form. Table 6 displays the final weight calculations along with the associated ranking of the alternatives, showing the best suitable technique for sustainable landscape management in urban and rural development.

Table 6. Final Weight calculations and ranking

Alternative	Final Score	Final Ranking
Urban Farming	0.4068	1
Green Infrastructure	0.3736	2
Sustainable Forest Management	0.2196	3

The AHP study found that Urban Farming emerged as the most suitable method for sustainable landscape management, gaining the highest total weight among the alternatives. Green Infrastructure followed closely in second place, exhibiting good performance in socio-cultural and economic dimensions. Sustainable Forest Management, while valuable for long-term ecological stability, was placed lowest due to substantially lower scores in governance and economic feasibility.

4. Conclusions

1. This study demonstrates the importance of the Analytic Hierarchy Process (AHP) in sustainable landscape management for urban and rural development. Among the alternatives, Urban Farming (0.4068) ranked highest, followed by Green Infrastructure (0.3735) and Sustainable Forest Management (0.2196).
2. The analysis identifies Environmental Sustainability as the most influential factor (0.5377), underlining its influence in decision-making. Urban Farming emerged as the best balanced solution, excelling in environmental, socio-cultural, and economic aspects.
3. While AHP provides a disciplined and systematic decision-making framework, its dependence on expert judgment involves subjectivity. Future studies should combine fuzzy logic or machine learning to enhance objectivity.
4. Practically, this study gives insights for urban planners and politicians, pushing for integrating Urban Farming and Green Infrastructure to meet sustainability goals. Strengthening governance systems is critical for effective implementation.

5. This research contributes to MCDM approaches in landscape design, emphasizing the value of AHP in optimizing sustainable decisions. Future studies could explore more participative decision-support systems to solve developing sustainability challenges.

References

1. XU, Yiwen, and Jiang CHANG. The practice of multi-criteria decision analysis modeling in decision support for landscape planning. Online. Applied Mathematics and Nonlinear Sciences, vol. 9 (January 2024), no. 1. ISSN 2444-8656.
2. HALOUI, Doha, Kenza OUFASKA, Mustapha OUDANI, Khalid El YASSINI, Amine BELHADI, et al. Sustainable urban farming using a two-phase multi-objective and multi-criteria decision-making approach. Online. International Transactions in Operational Research, April 2024. ISSN 1475-3995.
3. KPADÉ, Cokou Patrice, Lota D. TAMINI, Steeve PEPIN, Damase P. KHASA, Younes ABBAS, et al. Evaluating multi-criteria decision-making methods for sustainable management of forest ecosystems: a systematic review. Online. Forests, vol. 15 (September 2024), no. 10, p. 1728. ISSN 1999-4907.
4. REYES-NORAMBUENA, Pedro, Javier MARTINEZ-TORRES, Alireza NEMATI, Sarfaraz HASHEMKHANI ZOLFANI, and Jurgita ANTUCHEVICIENE. Towards sustainable urban futures: integrating a novel grey multi-criteria decision-making model for optimal pedestrian walkway site selection. Online. Sustainability, vol. 16 (May 2024), no. 11, p. 4437. ISSN 2071-1050.
5. COLE, Beth, Andrew V. BRADLEY, Simon WILLCOCK, Emma GARDNER, Ewan ALLINSON, et al. Using a multi-lens framework for landscape decisions. Online. People and Nature, May 2023. ISSN 2575-8314.
6. YUAN, Zheng, Baohua WEN, Cheng HE, Jin ZHOU, Zhonghua ZHOU, et al. Application of Multi-Criteria Decision-Making Analysis to Rural Spatial Sustainability Evaluation: A Systematic Review. Online. International Journal of Environmental Research and Public Health, vol. 19 (May 2022), no. 11, p. 6572. ISSN 1660-4601.
7. LANGENHEIM, Nano, and Marcus WHITE. Green Infrastructure and Urban-Renewal Simulation for Street Tree Design Decision-Making: Moderating Demands of Stormwater Management, Sunlight and Visual Aesthetics. Online. International Journal of Environmental Research and Public Health, vol. 19 (July 2022), no. 13, p. 8220. ISSN 1660-4601.
8. SHAVAZIPOUR, Babooshka, Dmitry PODKOPAEV, and Kaisa MIETTINEN. Interactive decision support and trade-off analysis for sustainable forest landscape planning under deep uncertainty. Online. Canadian Journal of Forest Research, August 2022. ISSN 1208-6037.
9. SAATY, Thomas L. A scaling method for priorities in hierarchical structures. Online. Journal of Mathematical Psychology, vol. 15 (June 1977), no. 3, pp. 234–281. ISSN 0022-2496.
10. SAATY, Thomas L. Decision making with the analytic hierarchy process. Online. International Journal of Services Sciences, vol. 1 (2008), no. 1, p. 83. ISSN 1753-1454.

Implementation of Circular Economy Measures in Jonava Municipality Using the "Living Lab" Approach

Akvilina PIPINYTĖ[1]*, Visvaldas VARŽINSKAS[2]

1 Kaunas University of Technology, Faculty of Mechanical Engineering and Design, Kaunas, Lithuania

2 Kaunas University of Technology, Institute of Environmental Engineering, Kaunas, Lithuania

** akvilina.pipinyte@ktu.edu*

Abstract

A "Living Lab" models real-life scenarios in combination with the communities, researchers, businesses, and governance to reach long-term goals in the circularity of cities. It is important to have precise steps of what can be done at a municipality (urban) level to reach circularity measures, as the lack of data or methods used today is not efficient enough to reach national circularity goals. This work aims to prepare a circular economy-oriented roadmap for Jonava municipality to increase the efficiency of materials consumption, implement circular practices, and reduce environmental impact. This study was carried out in 39 public organisations from 7 sectors – public governance, education, culture, social, health, sports, and municipal services. A survey was conducted regarding the material flows (materials or energy inputs and outputs) from the organisations to analyse the highest concern areas. An analysis of current good and bad practices regarding circularity (circular consumption, circular procurement, etc.) from organisations was carried out to understand the current situation. From the results, a strategic framework was created for the municipality, which consists of recommendations regarding urban circularity measures that public organisations may implement in their work areas.

Keywords: living lab, circularity, innovation, public organisations.

1. Introduction

Urban activities significantly contribute to climate change, with urban areas accounting for 70 percent of global CO_2 emissions [1]. This figure is projected to rise, as 2008 marked the first time in history when more individuals resided in cities than in rural locations. By 2050, two-thirds of the global population is expected to inhabit urban settings [2]. Given that cities are already major players in climate change, it is crucial to implement sustainable development goals within communities before reaching an environmental tipping point. A shift towards urban circularity is essential, where community members, local governance, businesses, and researchers collaborate to address circularity challenges in a municipality.

Research problem. Lithuania aims to achieve a completely circular economy by 2050 [3]. Yet, the existing approaches utilized by municipalities are ineffective due to inadequate data and insufficient communication among stakeholders. Therefore, it is essential to create a definitive circularity framework to fulfil national circularity objectives.

Research aim. To analyse the current problematic areas of Jonava municipality regarding circularity, get acquainted with the good and bad practices, and to prepare an urban circular-economy-oriented roadmap for Jonava municipality.

Research tasks:

1. Analyse the concept of urban circular economy and the current situation of Jonava municipality regarding circularity.

2. Conduct a study in which data on Jonava municipality public organizations' material and energy inputs and outputs, barriers, and implemented circularity projects in organizations are collected and interpreted.
3. Create an urban circularity-oriented framework for Jonava municipality.

Research methods. Assessment of literature sources, implementation of research to gather and analyse data related to material and energy movements, along with other sustainability information, and the execution of a focus group method to obtain insights.

2. Analysis of the urban circularity economy concept and its significance

The prevailing economic model today is the linear economy, where resources are obtained, utilized to create products, consumed, and then discarded as waste. This approach leads to significant harm to the planet as valuable finite resources are wasted after a single use. A circular model aims to retrieve resources once consumers have finished using them, thereby preserving their value rather than letting them go to waste. One effective strategy to achieve this is by promoting the development of circular cities. A circular city operates as an integrated system to decouple resources, maintaining the value and quality of products, components, materials, and nutrients for as long as possible. The advantages of a circular city include closing the material loop, utilizing less hazardous resources, generating less waste, creating a safer environment for both humans and biodiversity, and reducing emissions [4].

A circular model is more than just reusing or recycling products and materials; it is also:

- elimination of hazardous substances in manufactured products;
- eco-design implementation in products (reuse, remanufacture, repair, and recycle);
- raising environmental awareness and changing consumption patterns;
- development of new business models (for example, leasing materials and products) [5].

To shift towards a circular economy, various strategies can be observed in the figure below (Fig. 1). Actions can be categorized into different levels (micro, meso, and macro) and involve varying degrees of participation from national, regional, and local authorities. The micro level focuses on consumers and individual businesses, while the meso level establishes connections within industrial ecosystems. At the macro level, more extensive changes can be implemented through policy modifications at the national, regional, and local levels [6].

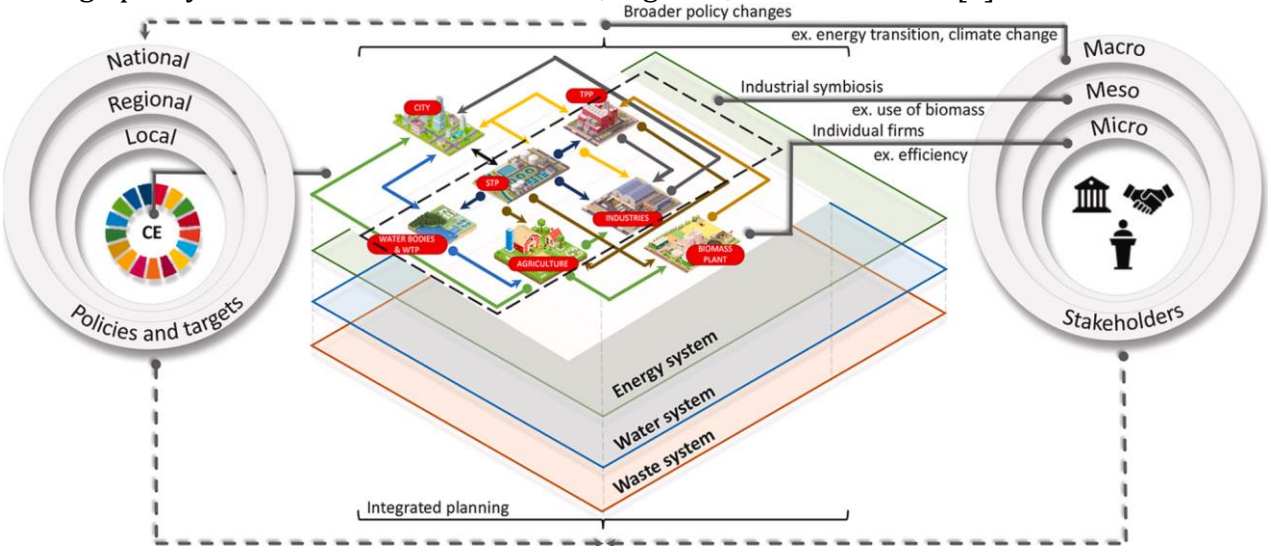

Fig. 1. Conceptual framework for a circular economy approach to integrating local and national targets and policies [6]

For a city to effectively transition to a circular model, it is crucial to integrate and consider the social, economic, and environmental aspects. One approach that facilitates this connection across all dimensions is the "Living Lab" method. The "Living Lab" method addresses dynamic challenges by employing innovative strategies that engage various stakeholders, including residents, universities, businesses, and governmental entities. Unlike conventional approaches, the "Living Lab" utilizes end-users to test solutions within real-world contexts. The main features of a "Living Lab"[7]:

- the end-user is at the centre of attention, and all solutions should cater to the needs of the end-user;
- Testing of the solutions in a real-time environment;
- Contributions for solutions are usually from different sectors of expertise;

Regular feedback from end-users, leading to ongoing enhancements of the solutions and improvements of the solutions [7].

3. Research methodology

The research examines 39 public organizations situated in the Jonava municipality. The evaluation of the material inputs and outputs of these public organizations was based on a survey conducted in 2023. An additional survey assessed the current state, including the circularity methods currently in use and the barriers encountered. The findings from these surveys were analysed, leading to the identification of key problem areas. Recommendations were provided regarding research paper analysis, end-user requirements, and national policies for the areas that contribute the most harm. Additional research was done using the program STAN to understand the waste flows in Jonava municipality.

The survey examines seven different sectors within the municipality: public governance, education, culture, social services, health, sports, and municipal services (Table 1). The education sector is the largest, comprising 20 out of the 39 public organizations surveyed. The survey identifies six procurement categories: food, electronics, furniture, household items, vehicles, and repair services. The survey questions focus on material and energy flows, as well as aspects such as the organization's area, employee and vehicle count, and the number of computers, among other details. This data aids in understanding the correlation between the size of an organization and its consumption patterns.

Organisation distribution by sectors (Table 1).

Table 1. Public organisations by sectors

Sector	Public organisation	No. of public organisations
Public governance	Municipality administration	1
	Municipality control and audit office	1
	Education support service	1
Education	School	10
	School-multifunctional centre	3
	Art school	1
	Kindergarten	6
Culture	Library	1
	Culture centre	1
Social	Social services centre	1
	Activity centre for people with disabilities	1
	Temporary care housing	2
	Public health office	1
Health	Primary healthcare centre	1

Sector	Public organisation	No. of public organisations
	Hospital	1
Sport	Sport centre	1
	Swimming pool	1
Municipal service	Water supply	1
	Fire service	1
	Public transport	1
	Heating	1
	Cleaning and maintenance	1

4. Results

It has been observed from the public organisations' collected data that the "Education" sector accounts for 50.86% of the total budget allocated for purchasing new items and for repairs. This indicates that while the "Education" sector is utilizing more funds than other sectors, it is also focusing more on repairing items instead of acquiring new ones.
The top 15 categories across all the sectors were observed, which contributed the most to the quantity of items bought and the "Food and Beverage" sector recorded the highest volume at 267,205 kg purchased in 2023 (Fig. 2). The predominant portion is attributed to fruits and vegetables, accounting for 25% of the entire category, followed by dairy products at 16%, and animal products at 14%. The second category, "Printing and Publishing," totalled 150,266 kg of materials. The largest quantities in this category were attributed to books, publications, and printing paper. The significance of the "Printing and Publishing" category stems largely from the Education sector, which utilizes a substantial amount of printed materials.

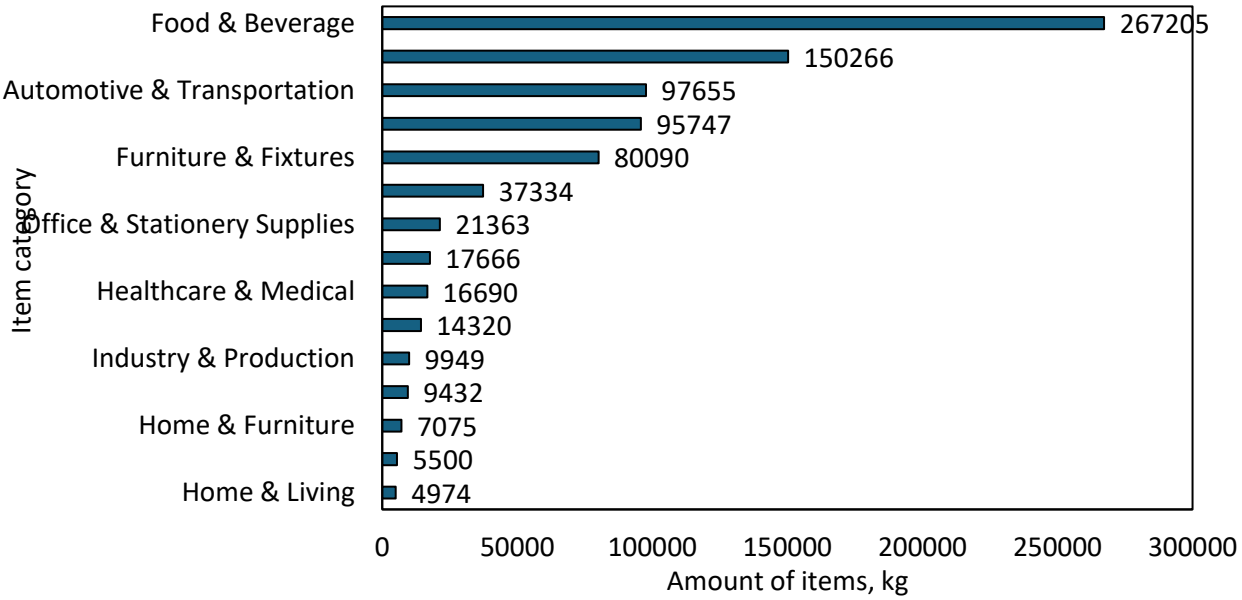

Fig. 2. Number of items bought in kilograms

The Jonava municipality has a waste management system that is part of the Kaunas region waste management center (Fig. 3). As reported by the Environmental Protection Agency, Jonava municipality produced a total of 12,091 tons of waste in 2023, with most of it being collected as mixed municipal waste [8]. Of this amount, 4,652 tons were incinerated to generate energy, resulting in the production of 3.35 GWh of electricity and 8.19 GWh of heat, based on the statistics of the burned waste to energy ratio [9]. Regarding biological waste, food waste comprised 1,078 tons, making up 8.92% of the total waste generated in the municipality [10]. Overall, biological

waste amounted to 4,671 tons, which was converted into technical compost and used at the landfill. If technical compost is regarded as having a purpose and is not considered landfilled waste, then only 187.08 tons of waste were being landfilled, which represents 1.55% of the total waste. However, if technical compost is included in waste calculations, then 38.8% is subject to landfilling. Additionally, the landfill produces biogas, and 208.71 tons of waste were used to generate biogas, resulting in 271.3 kWh of electricity and 1043.6 kWh of heat [11].

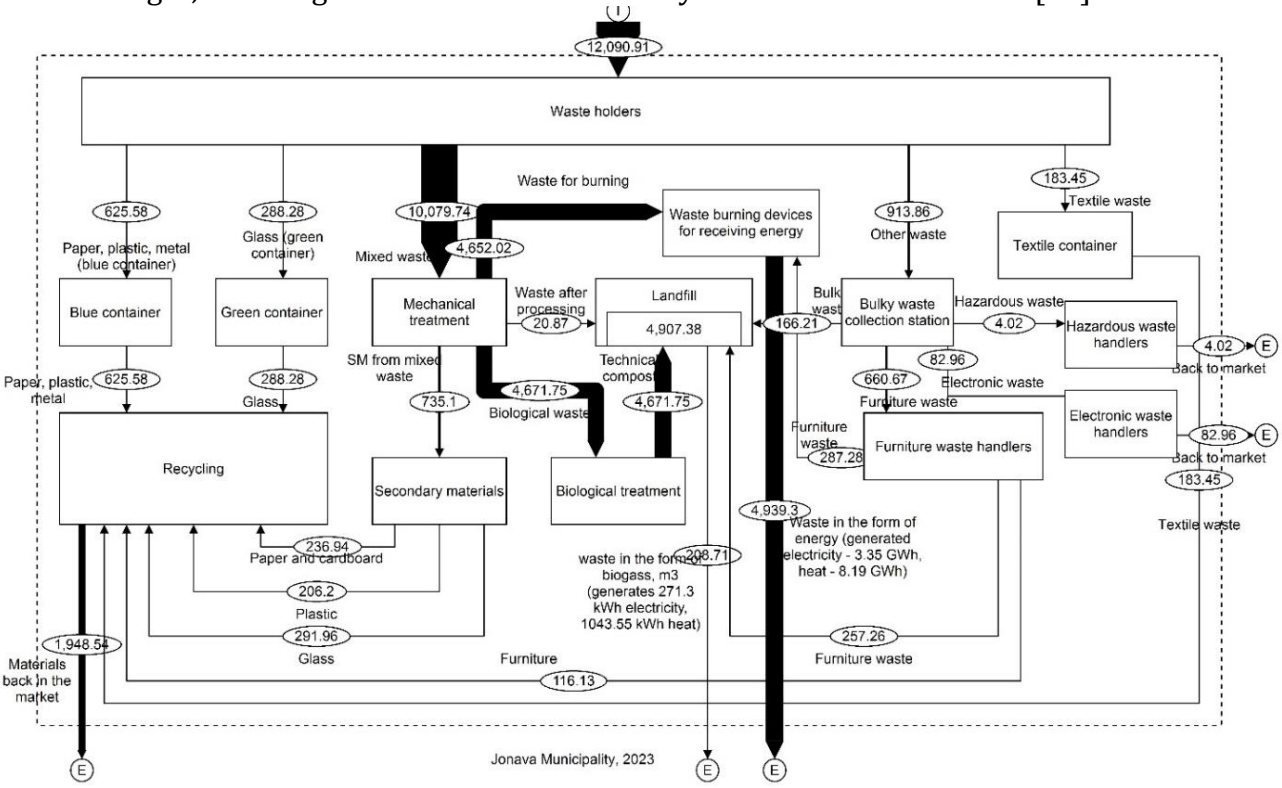

Fig. 3. Jonava municipality waste management system, 2023

Based on the focus group method conducted with 50 management employees from public organisations, the primary reasons for the incomplete implementation of circular activities in Jonava municipality public organisations include:

- insufficient funding for circular initiatives;
- limited awareness regarding circularity;
- challenges in altering established habits (for instance, using paper and digital copies);
- over-regulation (such as catering larger food portions than necessary).

From the overall results, it is seen that major areas of concern are “Food and beverages” category, which could be solved by removing regulatory barriers and implementing a self-catering system where it is appropriate (schools, social homes, etc.). Another area worth of focus is “Printing and publishing”, which can be solved by using green procurement principles, using electronic signatures, and saving material in electronic form rather than paper. Lastly, the social dimension needs to be considered, where environmental awareness is raised in the community. Social initiatives could be implemented, for example, the sharing of items between organisations, events for the community regarding environmental issues that are important in the area, with giving knowledge on what each person could implement in their daily life.

5. Conclusions

1. Categories with the highest amounts of materials are "Food and Beverages" – 267,205 kg, "Printing and Publishing" – 150,266 kg, and "Automotive and Transportation" – 97,655 kg.
2. In 2023, Jonava municipality generated 12 090 tons of waste, from which 10 079 tons were from mixed municipal waste and only 2 011 were from sorting containers and stations.
3. The primary challenges for executing circular initiatives are a lack of awareness, insufficient finances, over-regulation, and absence of a systematic approach.
4. It is recommended that the municipality organises environmental awareness events, implements food saving initiatives (self-catering system), implements green public procurement in their working environment, and eliminates using paper when possible.

References

1. United Nations. *Sustainable Cities and Human Settlements | Department of Economic and Social Affairs.* [2024. Available from: https://sdgs.un.org/topics/sustainable-cities-and-human-settlements. [viewed Jan 11, 2025].
2. DODMAN, David; HAYWARD, Bronwyn; PELLING, Mark; BROTO, Vanesa C.; CHOW, Winston T. L., et al. Cities, settlements and key infrastructure *In: Climate Change 2022: Impacts, adaptation, and vulnerability*, pp. 907–1040 Cambridge: Cambridge University Press, 2022. Available from: https://ink.library.smu.edu.sg/cis_research/33. [viewed Jan 11, 2025].
3. Lietuvos Respublikos Seimas. *XIV-490 Dėl Nacionalinės Klimato Kaitos Valdymo Darbotvarkės Patvirtinimo.* e-seimas.lrs.lt: June 30, 2021. Available from: https://e-seimas.lrs.lt/portal/legalAct/lt/TAD/7eb37fc0db3311eb866fe2e083228059?positionInSearchResul %20-. [viewed Jan 11, 2025].
4. Circular Cities Declaration. *Circular Cities Declaration | Home.* circularcitiesdeclaration.eu: Available from: https://circularcitiesdeclaration.eu/. [viewed Jan 15, 2025].
5. ENENKEL, Kathrin; MOOREN, Caro; TALMAN-GROSS, Larissa; ECKARTZ, Katharina; OSTERTAG, Katrin, et al. *Regulatory Barriers for the Circular Economy.* Technopolis Group. June 30, 2016. Available from: https://ec.europa.eu/docsroom/documents/19742.
6. BELLEZONI, Rodrigo A.; ADEOGUN, Ayoola Paul; PAES, Michel Xocaira and DE OLIVEIRA, José Antônio Puppim. Tackling climate change through circular economy in cities*. Journal of Cleaner Production*, vol. 381 (2022). Available from: https://www.sciencedirect.com/science/article/pii/S095965262204700X.
7. POLYDOROPOULOU, Amalia; BOUHOURAS, Efstathios; PAPAIOANNOU, Georgios and KARAKIKES, Ioannis. Living labs for the resilience of ports against climate change disruptions*. Ocean & Coastal Management*, vol. 261 (2025), pp. 107528. Available from: https://www.sciencedirect.com/science/article/pii/S0964569124005131.
8. Aplinkos Apsaugos Agentūra. *Informacija Apie Komunalinių Atliekų Tvarkymo Sistemas Lietuvos Savivaldybėse* [2025-02-27]. Available from: https://aaa.lrv.lt/lt/veiklos-sritys/atliekos/atlieku-apskaita/informacija-apie-komunaliniu-atlieku-tvarkymo-sistemas-lietuvos-savivaldybese/. [viewed March 25, 2025].
9. Kauno kogeneracinė jėgainė. *UAB Kauno Kogeneracinė Jėgainė 2023 M. Metinis Pranešimas.* Kauno kogeneracinė jėgainė. 2023. Available from: https://ignitisgrupe.lt/sites/default/files/public/inline-files/10.%20KKJ%20Finansin%D8%B3s%20ataskaitos%202023%20KKJ.pdf. [viewed Apr 25, 2025].
10. Aplinkos Apsaugos Agentūra. *Mišrių Komunalinių Atliekų Sudėties Tyrimai Ir Biologiškai Skaidžių Atliekų Vertinimas.* [2025-03-21]. Available from: https://aaa.lrv.lt/lt/veiklos-sritys/atliekos/atlieku-apskaita/misriu-komunaliniu-atlieku-sudeties-tyrimai-ir-biologiskai-skaidziu-atlieku-vertinimas/. [viewed March 3, 2025].
11. ŠALČIŪNAITĖ, Brigita and PLIOPAITĖ BATAITIENĖ, Ingrida. Forecast of biogas generation in Lithuanian regional land fills*. Mokslas – Lietuvos Ateitis / Science – Future of Lithuania*, vol. 7 (2015), no. 4, pp. 392–398. Available from: https://file:///C:/Users/User/Downloads/2726-Article%20Text-5922-1-10-20180613.pdf. [viewed Apr 25, 2025].

Life Cycle Assessment of Small Wastewater Treatment Plants in the Baltic Sea Region

Varun KEMPARAJU*, Jolanta DVARIONIENĖ**

Kaunas University of Technology, Kaunas, Lithuania

**varkem@ktu.lt ,*

***jolanta.dvarioniene@ktu.lt*

Abstract

Environmental pressure on the Baltic Sea is intensifying due to increased nutrient pollution and micro-pollutants resulting from growing human activity. Small Wastewater Treatment Plants (WWTPS) are vital in mitigating these impacts, but their efficiency varies based on size or Population Equivalent (PE). Facilities serving fewer than 2,000 PE are often less effective, partly due to the absence of standardized regulations. Despite their small scale, these plants are frequently located in tourist-heavy areas that contribute significantly to nutrient loads, making their environmental impact difficult to assess. This study uses Life Cycle Assessment (LCA) to evaluate and compare the performance of small-scale wastewater treatment technologies through a selected case study in the Baltic Sea region. The findings show that upgrading small WWTPS with tertiary nutrient removal technologies significantly improves the elimination of suspended solids, nitrogen, and phosphorus. However, this improvement comes with increased energy consumption, emphasizing the need to explore alternative energy sources such as renewable energy.

Keywords: Small WWTPS, Life Cycle Assessment (LCA), Nutrient Reduction, Environmental Impacts, EU UWWTD, Suspended Solids (SS), Nitrogen (N), Phosphorus (P).

1. Introduction

Water is life, and wastewater treatment is critical in the protection of environmental and public health. Wastewater treatment before it is discharged into receiving waters saves aquatic life by preventing detrimental pollutants from entering water bodies [1]. Wastewater contains excess nutrients like phosphorus, nitrogen, and suspended solids that cause eutrophication, algal growth, and loss of oxygen. [2]. Wastewater plants can also generate energy. Methane is obtained during the anaerobic process in the wastewater sludge. This Methane is captured and converted to heat and electricity [3]. In the sludge produced during this process, the water is filtered, and the solid sludge can be used as a useful fertilizer for agricultural activities [4]. Eutrophication is a significant issue in the Baltic Sea region. Eutrophication occurs when excess nutrients, particularly phosphorus and nitrogen, accumulate in the water, leading to the overgrowth of algae and other undesirable aquatic plants. This nutrient pollution has resulted in severe consequences, including oxygen depletion, harmful algal blooms, and a loss of biodiversity.

2. Water Policy and Wastewater Treatment

Effective management of wastewater must be ensured in order to uphold levels of sustainability within the EU and globally. There are several important directives and strategies which play an important role in water resources management in the EU:

- **Urban Wastewater Treatment Directive (UWWTD)**: The Urban Wastewater Treatment Directive (UWWTD) 91/271/EEC, launched by the EU in 1991, regulates the collection, treatment, and discharge of urban wastewater to prevent water pollution. It mandates EU member states to implement primary practices to manage wastewater, especially in developed regions, focusing on municipal sewage treatment [6].
- **Nitrates Directive:** The Nitrate Directive (91/676/EEC), established by the EU in 1991, is intended to protect water quality through addressing nitrate pollution from agriculture. It is primarily a water protection legislation, complementing other directives like the Water Framework Directive and the Urban Wastewater Treatment Directive [7].
- **HELCOM Baltic Sea Action Plan:** The HELCOM Baltic Sea Action Plan (BSAP) 2007 and updated in 2021 is one of the primary instruments to restore ecological balance in the Baltic Sea. It addresses concerns such as eutrophication, pollution, biodiversity loss, and climate change. The BSAP 2021 contains targets to be achieved by 2030 [8].

Small wastewater treatment plants (WWTPS) (Fig. 1) play a crucial role in managing wastewater in rural areas around the Baltic region [5].

Fig. 1. Compact WWTPS [9]

Small-scale wastewater treatment plants (WWTPS) are prone to numerous issues that impact efficiency and performance and have potential implications for the environment and public health. Some of the significant issues include ageing systems, high operational costs (energy, labour, chemicals), and staying up to date with evolving regulatory standards. The systems also struggle with peak flows, effective sludge disposal, and lack of skilled labour – issues that influence maximum utilization and compliance [10].

3. Methodology

Life Cycle Assessment (LCA) is used to compare the environmental effects of wastewater treatment plants (WWTPS) across categories to maximize design, operation, and resource utilization. LCA addresses effects from raw material production to disposal, such as energy usage and emissions. LCA reveals latent disadvantages, including increased energy and GHG emissions as a result of high-level nutrient removal. LCA also promotes energy efficiency, chemical

evaluation, and resource recovery. ISO 14040:2006 and ISO 14044:2006 formulate the basis and guidelines for the application of LCA in WWTPS (Fig. 2).

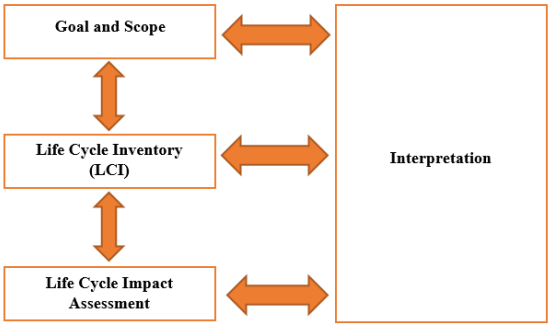

Fig. 2. Major phases of LCA using ISO 14040 [11]

The Assessment was done considering only the operation stage considering the energy consumption, usage of chemicals, discharge and emissions, generation of waste, maintenance of the treatment plant, and monitoring.

4. Results and Discussions

The results of the environmental impact assessment using LCA approach for the small wastewater treatment plant in the selected case study – Scenario 1 (S1) and Scenario 2 (S2) – are presented in Figure 3. The results are expressed as a single environmental impact score, measured in environmental points (Pt) per 1 m^3 of treated wastewater, and include energy consumption.

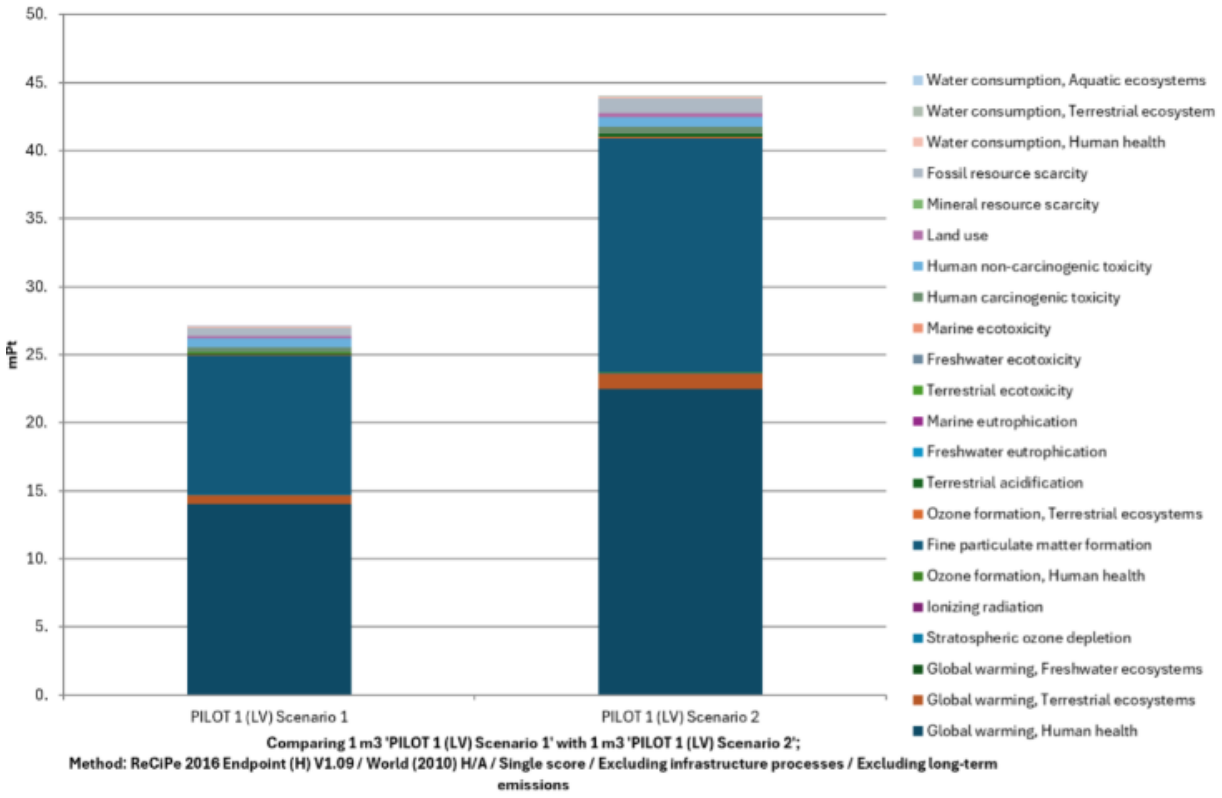

Fig. 3. Environmental impact comparison for the small wastewater treatment plant in selected case study in Baltic Sea region.

The results present the environmental impact assessment of treating 1 m^3 of wastewater in a selected small wastewater treatment plant (WWTP) in the Baltic Sea region, including the energy consumption. The analysis reveals that energy use is a significant contributor to the environmental impact in both scenarios. Scenario 1 (S1) results in 27 mPt of environmental burdens, whereas Scenario 2 (S2) leads to 44 mPt. In S1, the primary impact category is Global warming (Human health), contributing 14 mPt (over 52%). This is followed by Fine particulate matter formation at 10 mPt (more than 37%). Additional contributions include Human Carcinogenic toxicity at 0.68 mPt, Human non-carcinogenic toxicity at 0.35 mPt, and other categories with smaller shares. Similarly, S2 shows the highest contribution to Global warming (Human health) with 23 mPt (over 55%), followed by Fine particulate matter formation with 17 mPt (more than 40%). Other impacts include Human carcinogenic toxicity at 0.71 mPt, Human non-carcinogenic toxicity at 0.45 mPt, and minor contributions from other categories. Electricity consumption is clearly the dominant factor driving CO_2 emissions in both treatment scenarios. According to the life cycle assessment (LCA), the main contributor to environmental damage in the wastewater treatment processes at selected small WWTP (S1 and S2) is electricity usage. The adoption of renewable energy sources in the future could significantly reduce these environmental burdens.

5. Conclusion

Small wastewater treatment plants (WWTPS) in the Baltic Sea region play a significant role in managing nutrient pollution, especially in tourist-heavy areas. Upgrading these facilities with tertiary nutrient removal technologies significantly enhances the removal of suspended solids, nitrogen, and phosphorus, meeting the requirements set by EU directives and HELCOM targets. Life Cycle Assessment (LCA) indicates that electricity consumption is a major contributor to the environmental impact of these systems, highlighting the potential benefits of integrating renewable energy sources. To protect the Baltic Sea ecosystem, coordinated policy efforts, investment in infrastructure upgrades, and the adoption of cleaner energy technologies are essential.

Acknowledgement: This work was supported by the NURSECOAST-II project “Model Nutrients Reduction Solutions in Near-Coast Touristic Areas” (Nr #C015) co-funded by the European Union by the INTERREG Baltic Sea Region Program 2021–2027.

References

1. RSB Environmental. *Environmental benefits of wastewater treatment plant: Preserving ecosystems and water conservation*. 2023, July 11. https://rsbenv.com/what-are-the-environmental-benefits-of-wastewater-treatment-plant
2. PALATSI J, RIPOLL F, BENZAL A, PIJUAN M, ROMERO-GÜIZA MS. Enhancement of biological nutrient removal process with advanced process control tools in full-scale wastewater treatment plant. *Water Res.* 2021 Jul 15;200117212. doi: 10.1016/j.watres.2021.117212. Epub 2021 May 21. PMID: 34029870.
3. HALLAJI, S.M., KUROSHKARIM, M. & MOUSSAVI, S.P. Enhancing methane production using anaerobic co-digestion of waste activated sludge with combined fruit waste and cheese whey. *BMC Biotechnol* 19, 19 (2019). https://doi.org/10.1186/s12896-019-0513-y
4. SUGURBEKOVA, G., NAGYZBEKKYZY, E., SARSENOVA, A., DANLYBAYEVA, G., ANUARBEKOVA, S., KUDAIBERGENOVA, R., FROCHOT, C., ACHERAR, S., ZHATKANBAYEV, Y., & MOLDAGULOVA, N. Sewage Sludge Management and Application in the Form of Sustainable Fertilizer. *Sustainability,* 2023. https://doi.org/10.3390/su15076112.

5. Eutrophication – the Greatest Threat to the Baltic Sea. https://www.bsag.fi/en/the-baltic-sea/eutrophication
6. European Commission. (n.d.). Revision of the Urban Waste Water Treatment Directive. Retrieved February 14, 2025, from https://environment.ec.europa.eu/topics/water/revision-urban-waste-water-treatment-directive_en
7. European Commission. (n.d.). Nitrates. Environment. Retrieved February 21, 2025, from https://environment.ec.europa.eu/topics/water/nitrates_en
8. HELCOM. (n.d.). *Wastewater*. HELCOM. https://helcom.fi/action-areas/industrial-municipal-releases/waste-water/
9. ALAMY. (n.d.). Aerial view of a small sewage treatment plant. Retrieved February 23, 2025, from https://www.alamy.com/aerial-view-of-a-small-sewage-treatment-plant-image151815710.html
10. SUSBIO. (n.d.). Common challenges in sewage treatment plants and their solutions. Retrieved March 6, 2025, from https://susbio.in/common-challenges-in-sewage-treatment-plants-and-their-solutions/
11. ZHANG, Y., LI, X., WANG, J., & CHEN, H. Life cycle assessment of sewage sludge treatment: A review. *Chemosphere*, (2023), 344, 139894. https://doi.org/10.1016/j.chemosphere.2023.139894

TRANSPORT ENGINEERING AND SUSTAINABLE MOBILITY

Human Error: Implementing Safety Features in AoA Systems

Benas LITVINAVIČIUS
Kaunas University of Technology, Kaunas, Lithuania
benas.litvinavicius@ktu.edu

Abstract

This paper addresses the risks associated with uncalibrated aircraft angle-of-attack (AoA) sensors. The problems often arise due to improper maintenance or documentation failure. The study presents the different types of stall warning systems and AoA sensors and their working principle, as well as two viable solutions to the problem. The first solution involves the use of unique verification codes embedded in the sensor itself to track fault and maintenance history, as well as the aircraft's ability to recognize when the sensor was changed. The second solution is based on Built-In-Test-Equipment and proposes the use of an additional rotor inside the paddle chamber of the sensor. The paper also discusses the optimization process of the second solution by using principles from simpler stall warning systems and the integration of a reference map to compare the output with experimental data. The research was successful, but further prototyping and research are needed to check the validity of the solutions provided.

Keywords: AoA sensors, aviation safety, calibration, fail-safe, self-diagnosis

1. Introduction

AoA sensors play a vital role in aviation by ensuring the aerodynamic safety of aircraft. These sensors measure the angle between the wing of the chord line of the wing and the direction of the airflow. Exceeding the critical AoA leads to a wing stall, which can potentially lead to a catastrophe [1]. Despite their importance, AoA sensors are prone to failure, especially after maintenance or replacement. This was tragically demonstrated in the 2019 Boeing 737 MAX crash, where a newly installed, uncalibrated AoA sensor misled the MCAS (Maneuvering Characteristics Augmentation System), contributing to the incident [2]. This research aims to provide two plausible solutions to the problem of improper AoA sensor calibration.

2. Methods and Sensor Analysis

The methodology of this paper can be split into two major parts: technical literature analysis and conceptual engineering design. Firstly, a thorough review of existing literature on AoA systems was conducted. Sources included academic publications, books and aviation safety reports. This provided a detailed understanding of the intricacies of both stall warning systems and AoA sensors. Secondly, a problem-focused analysis was performed to identify common causes of calibration-related errors, particularly those introduced during sensor replacement. Real-world aviation accidents were examined to inform the analysis.

Simple stall warning systems use mechanisms such as vibrating reeds or mechanical flaps located on the leading edge of the wing, where low-pressure airflow shifts when the critical AoA is reached [3]. The figure shows how the location of the flapper switch changes when the AoA is changed (Fig. 1). These components either produce an audible sound due to the air being sucked out or close a circuit with a buzzer.

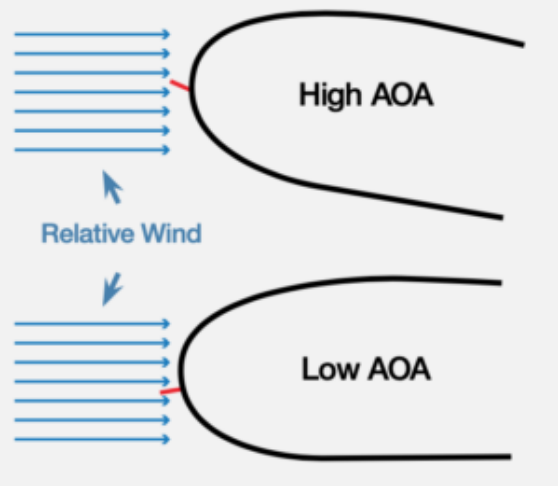

Fig. 28. Flapper Switch Stall Warning System's Working Principle [4]

On the other hand, more advanced AoA sensors, such as vane-type or slotted probe-type, use potentiometers to convert analogue signals to electrical ones. When the angle of attack is changing, the airflow moving around the vane also changes. Therefore, the angle at which the vane is pointing to the airflow is changing, and the potentiometer changes the resistance of the circuit[5]. The slotted probe calculates the difference between the upper and the lower holes. This is done by having an internal paddle which is moved by the difference in pressure from the holes in the probe [3]. The figure displays the insides of a slotted probe- type AoA sensor (Fig. 2). These paddles are mechanically connected to a potentiometer. As the paddles shift to compensate for the pressure difference, the potentiometer adjusts the circuit resistance, allowing for accurate calculation of the AoA. They require periodic calibration and recalibration after replacement. Following maintenance, if a sensor is not correctly tested or its change is not recorded, critical failures may occur. Autopilot systems, which rely heavily on AoA data, lack the contextual awareness to question faulty readings.

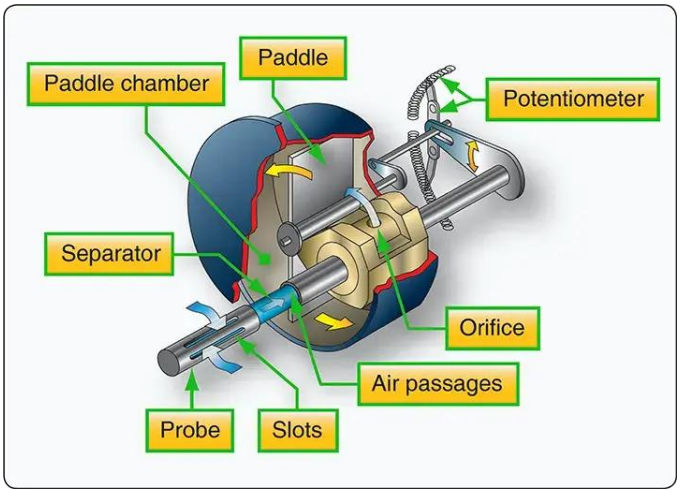

Fig. 29. Slotted Probe Type AOA Sensor [3]

Then, based on the findings, two design solutions were conceptualized. The first being an electronic identification system, and the second being a built-in test feature. These solutions were conceptualized by analyzing the mechanical and electrical capabilities of current AoA sensors, along with stall warning systems, to find components that could be repurposed. Throughout the

process, the fail-safe principle served as the foundation for all of the proposed solutions. *Fail-safe* is a concept where, in the event of a malfunction, the failure of one component does not cause harm to other systems or to the system itself [6]. The fail-safe principle can be implemented through redundant systems, physical laws, or other methods. For example, if a system relies on *N* sensors providing matching data, then *N+1* sensors should be installed to create a tolerance for failure [7]. A good example is the airbag system in vehicles during a crash. The airbags must always be deployed during a crash. No failure is acceptable, it would prevent deployment. Therefore, more than one sensor is used, and the system is designed to activate the airbags only if all sensors, or all except one, indicate deployment is needed [8]. If even one sensor fails or provides inconsistent data, the processor detects the discrepancy and ignores the faulty sensor's input and signals the need for its replacement.

3. Proposed Fail-Safe Solutions

3.1. Unique Identification System

Since the aircraft's AoA sensor is an electronic device whose measurements are based on changes in electrical voltage within a circuit, it is possible to implement a unique identification code into the system. This code would allow the aircraft to detect when the sensor has been replaced. Furthermore, the unique identifier could store information about the sensor's maintenance history, including any past failures or repairs. When a new sensor is connected to the aircraft system, it should not be trusted blindly. Instead, a warning message and an audible signal about the need for calibration should appear on the aircraft's control panel. This message could only be cleared by an authorized technician logging into the system and entering a security code. While this solution would not fully eliminate the issue of improper documentation, it would create an additional layer of accountability. Technicians would no longer be able to simply neglect proper procedures without detection. Moreover, if the procedures were skipped entirely, the pilot would be made aware of the problem through the visible warning, potentially preventing a dangerous situation. This concept is like how unique VIN codes are used in the automobile industry or how Apple implements part-specific identifiers in their mobile devices. VIN codes allow access to databases that store vehicle mileage, accident history, usage in ride-sharing services, and much more [9]**.** Apple's security system prevents certain device functionalities unless each internal component's unique code is verified by a certified technician. For example, if a component like the camera is replaced with a non-genuine part or without proper authorization, the phone will disable related functions until an Apple-certified technician confirms the repair [10]. These measures help prevent unauthorized modifications and spying attempts [11]. Applying similar technology to aviation would likely require significant investment, because the production of these systems would need to be changed a lot. Even then, the problem would not be completely solved.

3.2. Self-Test Rotor Mechanism

Since AoA sensors that measure the AoA have rotating parts, it would be plausible to use an electrical rotor. If calibration is needed due to the malfunction of the potentiometer, then we can measure its resistance and determine whether they are correct for a given angle-of-attack. Installing a rotor inside the paddle chamber parallel to the main shaft can give us an opportunity to rotate the shaft to the wanted position with the help of a belt system. For example, the rotor could rotate the shaft to the predefined maximum, minimum and neutral positions. Then, using a voltmeter we could measure the voltage and, therefore, resistance of the potentiometer and compare it with known values. If the values do not match, then a signal would be sent straight to the cockpit to inform the pilots of a malfunction. This accurate rotation of the rotor needs us to know the voltage needed to rotate it the correct amount. Therefore, a system would need

additional periodic calibration. These kinds of systems are already used in other fields and other parts of the aircraft, and they are called BITE (Built-In Test Equipment). These systems are based on passive fault detection and self-diagnosis principles [12]. While implementing such a system would involve increased costs due to added components and calibration requirements, it could significantly enhance safety. If a simpler and more cost-effective version of this system could be developed, it could be successfully optimized and implemented in real-world aviation applications.

4. System Enhancement and Integration

One of the ways to make the system more reliable could be to install additional electrical circuits inside of the mechanical stops in the AoA sensor. This way, it would be possible to rotate the rotor to the predetermined positions manually from inside the cockpit. The paddle would close the circuit, and a light would flash on the panel. Therefore, the pilot would be able to check whether the sensor accurately displays the minimum, maximum and neutral positions and decide whether it is safe to operate the aircraft. A similar principle is used in basic stall warning systems, where a flapper switch detects high AoA conditions. However, in this case, the concept is repurposed as a diagnostic tool that does not require a second person to perform the test, as the electric rotor replaces the manual input of a technician. Another way to optimize this system could be to calculate the theoretical AoA. By using other onboard sensors' data, such as speed, climb rate and others, the processor could use theoretical formulas to calculate the AoA and determine whether the sensor is working properly. If not, then the output of the sensor would be ignored, and a signal would be sent to the cockpit to inform the flight crew of the malfunction. To reduce the computational load on the computer it is plausible to use a value reference map. In the aircraft's development stage, experiments would be done to establish correlations between flight conditions and the AoA. Then, a reference value map would be created and installed on the main computer, allowing for quick comparison during flight. This kind of system is already used in fuel-injection systems on motorcycles [13]. The computer takes data from temperature, velocity, altitude and other sensors on the motorcycle and searches for the closest match on the reference map and injects the most optimal amount of fuel.

5. Conclusions

1. AoA sensors play a vital role in aviation, but to this day, they are susceptible to calibration-related errors.
2. The first solution is a unique identification system embedded in the AoA sensor, enabling aircraft systems to detect when the sensor is changed and track fault history. This would enforce calibration and improve accountability among the technicians. However, its integration would involve significant manufacturing changes.
3. The second solution involves a built-in rotor mechanism, capable of rotating the sensor shaft to a predetermined reference position. By measuring the potentiometer values and comparing them to expected outputs, the system could self-diagnose, but it would require additional periodic calibration.
4. The second solution can be made more reliable and the cost could be lowered by implementing reference maps and/or repurposing the stall warning system's working principles.
5. These findings suggest a shift toward self-monitoring equipment. However, further research and prototyping are needed to fully test reliability, viability and cost-effectiveness in real-world aviation applications.

References

1. AKULAVIČIUS, Pranas and Algimantas SKURDENIS. *Aerodinamika ir skrydžių dinamika: mokymo priemonė.* Kaunas: Rosma, 2002.
2. WAGMAN David. Human Error, Lax Reporting and MCAS All Contributed to Fatal Boeing Crash. *GlobalSpec* (2019). Available from: https://insights.globalspec.com/article/12909/human-error-lax-reporting-and-mcas-all-contributed-to-fatal-boeing-crash. [viewed 2025-04-08].
3. FORENZ Thomas; Kurt C. GIBSON; Charles L. RODRIGUEZ and Peter VOSBURY. *Turbine Aeroplane Structures and Systems: Module 11A (B1).* Aircraft Technical Book Company, 2021. Available from: https://aerospaceengineering.softecks.in/878/>. [viewed 2025-04-08].
4. BURNSIDE, Joseph E. Stall Warning Systems. *Aviation safety* (2021). Available from: https://aviationsafetymagazine.com/aircraft/stall-warning-systems/. [viewed 2025-04-10].
5. *A Complete Guide to Potentiometers.* 2023-01-17. Available from: https://uk.rs-online.com/web/content/discovery/ideas-and-advice/potentiometers-guide/. [viewed 2025-04-06].
6. *Audio English.* Available from: https://www.audioenglish.org/z/fail_safe.htm. [viewed 2025-04-06].
7. RUTHERFORD Jr., David B. What do You Mean It's Fail Safe? Evaluating Fail-Safety in Processor-Based Vital Control Systems. *In: American Public Transit Association 1990 Rapid Transit Conference*. Available from: https://web.archive.org/web/20111008021648/http://www.billpetit.com/Papers/Petit017.pdf. [viewed 2025-04-06].
8. KOMAKI, Hiroyuki; Syusaku KURODA; Toshinari NIOKA; Hiroyuki HONISHI and Masataka WAKAMOTO. Development of the Electronic "Safing" System for Airbag ECUs. *Jujitsu Ten Tech* (2005), no. 24. Available from: https://www.denso-ten.com/business/technicaljournal/pdf/24-3.pdf. [viewed 2025-04-06].
9. National Highway Traffic Safety Administration (NHTSA). *VIN Decoder.* Available from: https://www.nhtsa.gov/vin-decoder. [viewed 2025-04-06].
10. GROVE Owen. We Repaired an iPhone to See if iOS 18 Fixes iPhone Repair. The Verge. *The Verge* (2024). Available from: https://www.theverge.com/24325804/apple-iphone-ios-18-right-to-repair. [viewed 2025-04-06].
11. KEACH, Sean. . I-CLONE? Hidden iPhone Menu Reveals if You've Been Sold a Dodgy Model – and There's a Costly Sign You Shouldn't Ignore. *The Sun* (2024). Available from: https://www.thesun.co.uk/tech/31450990/apple-iphone-genuine-parts-fake-unknown-warning-message/. [viewed 2025-04-06].
12. Skybrary. *Built-in Test Equipment (BITE).* Available from: https://skybrary.aero/articles/built-test-equipment-bite. [viewed 2025-04-06].
13. CAMERON Kevin. How Does a Motorcycle Fuel Injector Work? *CycleWorld* (2018). Available from: https://www.cycleworld.com/how-does-motorcycle-fuel-injector-work/. [viewed 2025-04-06].

Experimental Research of High-Aspect Ratio Wing Flutter at Low Reynolds Numbers

Paulina KILNAITĖ*, Martynas LENDRAITIS

Kaunas University of Technology, Kaunas, Lithuania

** paulina.kilnaite@ktu.edu*

Abstract

High-aspect ratio wings are flexible and particularly prone to aeroelastic phenomena such as flutter. This issue is even more significant for modern unmanned aerial vehicles operating at low Reynolds numbers, where maintaining structural integrity while minimising weight is a constant challenge. Experimental research of high-aspect ratio wing flutter at low Reynolds numbers is essential for developing lighter aircraft designs while maintaining safety.

This article focusses on investigating flutter phenomena in high-aspect ratio wings at low Reynolds numbers. A slender composite wing is equipped with an accelerometer and a gyroscopic sensor and is placed inside a wind tunnel. A laser vibrometer placed outside the wind tunnel is also used, enabling a comparison of different measurement methods. While one method provides useful data on vibrations and orientation, the other offers higher precision and more detailed insight into multiple vibration modes.

Keywords: flutter, inertial sensors, optical methods.

1. Introduction

A flutter phenomenon in high-aspect ratio wings presents a complex aeroelastic challenge which remains not so widely researched due to limitations in both modelling and experimental techniques [1]. This evaluation of aeroelastic phenomena is important and relevant to lightweight and thin-wing structures used in super-light, high-performance unmanned aerial vehicles. In these types of aircraft, the wings are prone to oscillations and high deformations, particularly at high speeds, where varying aerodynamic forces can excite multiple vibration modes. These oscillations can grow in amplitude under certain conditions, potentially leading to aeroelastic instabilities.

As the aviation industry evolves, it not only raises a need to experimentally investigate and apply improvements to already existing research techniques, but also creates possibilities to combine measurement methods by integrating and applying new ways of thinking. Classical aeroelastic research may rely on various complicated sensor systems or modal analysis in idealised environments [2], in contrast, new studies are shifting to applying minimal equipment needs or even non-contact methods to the research area [3, 4]: inertial sensors and optical methods are introduced to study aeroelasticity.

Although optical methods and inertial sensors have been used in aeroelasticity research for some time, the potential of their combined application is still growing. This integrated approach enables the collection of high-resolution, real-time, and non-intrusive data, extensively enhancing the ability to analyse complex aeroelastic phenomena. Optical techniques offer precise deformation measurements, while inertial sensors accurately capture vibration frequencies across multiple axes, providing a more detailed understanding of aeroelastic phenomena.

The experimental methodology that involves inertial sensors and optical methods is increasingly seen as the future of research in aeroelasticity and related fields, as these methods are especially well suited for use with laboratory-scale models, where detailed monitoring of dynamic processes is essential. By combining inertial sensors with optical methods, researchers can gain deeper insights into aeroelastic phenomena, enabling safety predictions for aviation vehicles and systems. In general, the integration of new methods represents a significant step forward in the experimental research on the aeroelasticity topic.

2. Experimental setup

To conduct the research, a highly flexible wing model is required. The model should be thin, with a short chord and a large span to achieve a high aspect ratio. Additionally, it must fit within the available wind tunnel chamber and enable the observation of aeroelastic phenomena at reasonable flow velocities.

A wing was designed and manufactured using aramid fabric (see Fig. 1), featuring a chord length of 32.7 $\cdot 10^{-3}$ m and a total spanwise length of 0.33 m. The structure consists of three layers arranged in a symmetrical and balanced composite layup, with the aramid fabric impregnated with epoxy resin, resulting in a final thickness of 0.877 $\cdot 10^{-3}$ m.

Although the full manufactured half-wingspans are 0.33 m, only 0.27 m is exposed to the airflow during experiments, as the remaining length is used to secure the wing model during the experiments. This results in an aspect ratio of approximately 16.5 for the full-span wing.

Fig. 1 Research wing model

Inside the wing, between the layers of composite material, four wires without an insulating material are laid. Wires are used to connect the inertial measurement sensor to the microcontroller, as incorporating a battery and wireless sensor at this scale would significantly alter the wings' dynamic behaviour.
The experimental part of the high-aspect ratio wing flutter research consists of two parts: using an accelerometer and a gyroscope sensor placed on the end of the wing, and a laser vibrometer for non-contact measurements. The experimental equipment (see Fig. 2) was used to take both measurements simultaneously, enabling a direct comparison of the data.

Fig. 2 View of experimental equipment

The experimental setup view includes a manufactured wing positioned in the AEROLAB wind tunnel as a cantilever wing, with one side fully fixed to the wind tunnel wall and the other exposed to the freestream. An MPU6050 sensor is mounted at the wingtip, while a laser vibrometer is positioned at a fixed location.

2.1. Research conducted with accelerometers and gyroscope sensor

The flutter research is conducted with accelerometers and gyroscope sensor MPU6050 that uses a standard Arduino UNO R3 microcontroller and a computer for data collection. The MPU6050, which is used to analyse vibrations from the wingtip, is a versatile sensor with wide applications in various fields.
One of the main advantages of this sensor is its high reliability, precision, and compact size at a low cost. The MPU6050 integrates two main sensors: an accelerometer, which measures acceleration forces, and a gyroscope, which measures rotations. Both the accelerometer and the gyroscope are capable of measuring linear acceleration and angular velocity over a wide dynamic range along three axes [5].
The programme used to record the measurements was configured to set the accelerometer range to ±4g and the gyroscope range to ±500°/s. These settings were chosen to prioritise the detection of the initial onset of flutter and the determination of critical speed, rather than to capture peak amplitudes. Selecting such a range improves sensitivity to small vibrations and subtle oscillations, enabling a more accurate analysis of the early stages of aerodynamic phenomena.
The sensor is designed to be mounted on the wingtip. In this configuration, the sensor is assembled (see Fig. 3), the accelerometer measurements capture bending oscillations, while the gyroscope measurements capture torsional rotations.

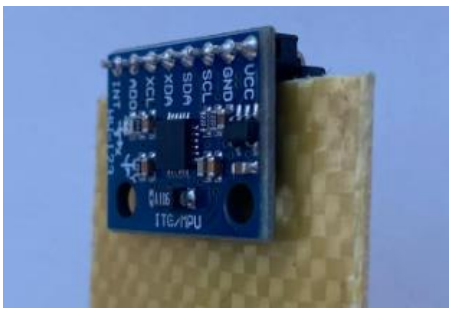

Fig. 3 Placement of the MPU6050 sensor at the wingtip

The wing model with the sensor is fixed in the test chamber of a wind tunnel. The setup is arranged so that the desired wingspan lies within the airflow. Once the wing is mounted, it must be allowed to come to a complete rest to eliminate any residual vibrations or disturbances that could interfere with the accuracy of aeroelastic measurements. The experiment begins by gradually increasing the airflow in the wind tunnel up until the critical point is reached and continues even after the flutter phenomenon is observed.
The results are presented in a graphical form, including both standard plots and a spectrogram to illustrate the frequency and amplitude content of the measured vibrations.
By looking at the plot of accelerometer and gyroscope (see Fig. 4), it can be identified that flutter phenomenon is observed when the airflow velocity reaches 20 m/s mark. The flutter can be identified by observation of the growing amplitudes in all the measurements.
The accelerometer data show that the wingtip experiences only low vibration amplitudes until the airflow reaches 18 m/s. Beyond this point, the wingtip begins to bend, with vibrations gradually increasing up until the critical point at 20 m/s is reached, where the amplitudes of the wingtip vibrations increase rapidly, signalling the observance of flutter.

A similar trend can be identified by looking at the gyroscope data (see Fig. 4), which tracks the rotation of the wingtip. Up to 19 m/s, there is minimal rotation of the wingtip, but once the critical velocity of 20 m/s is passed, the torsion motion increases, further confirming the presence not only of the flutter phenomenon, but also the possible observation of divergence.

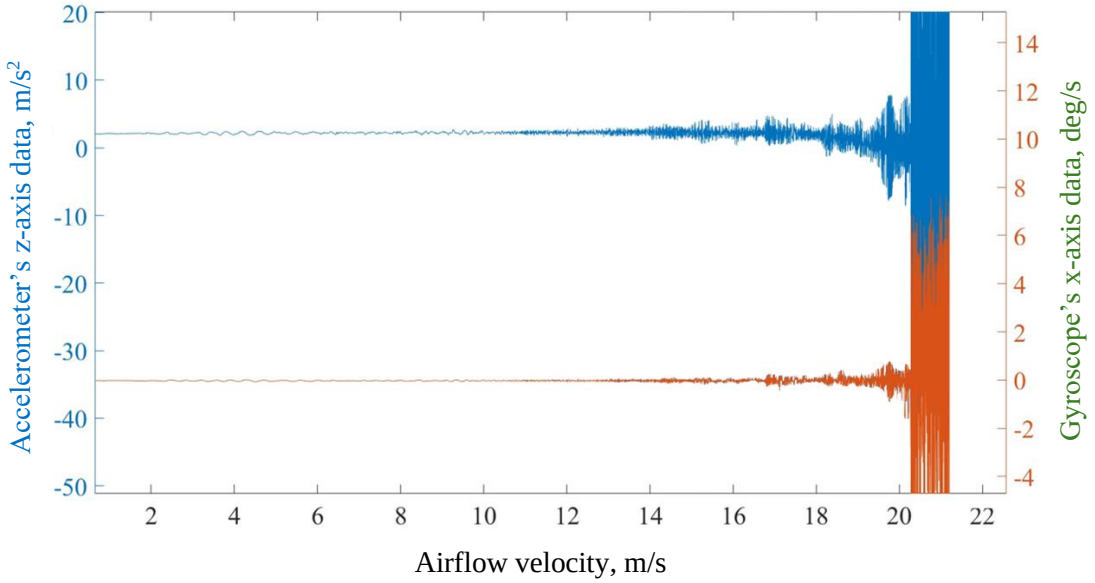

Fig. 4 Inertial measurements of wingtip bending and torsional motion, obtained from a mounted sensor

From the data gathered by the accelerometer, the FFT analysis is performed and plotted on a spectrogram (see Fig. 5), providing additional insights into the experiment. A plot of frequency versus airflow velocity is used to track changes in the wingtip dynamic response, revealing how the bending and torsional modes shift with increasing flow speed. The spectrogram reveals that the main frequency of the observed phenomenon is equal to around 35 Hz.

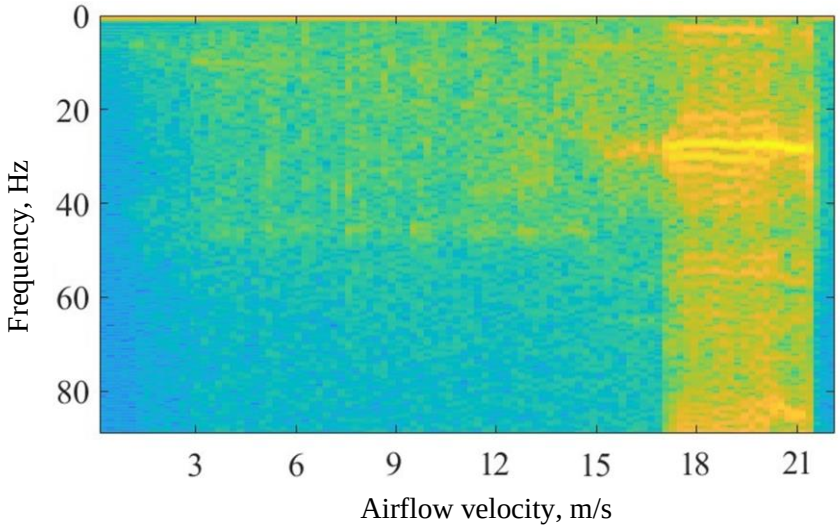

Fig. 5 Wingtip bending vibration frequency response to increasing airflow velocity, obtained from a mounted sensor

As the frequency remains constant despite increasing airflow, it indicates that the system has reached a resonant frequency where the aerodynamic forces and structural vibrations are in sync, reinforcing the onset of aeroelastic instability, further confirming the presence of flutter.

2.2. Research conducted with laser vibrometer

For the extension and validation of the research, flutter analysis is conducted in parallel using the laser vibrometer OMETRON. This advanced measurement tool is designed for non-contact measurement of vibrations and operates using the principle of a laser Doppler vibrometer, where a laser beam is directed at the vibrating surface of the object being studied [6].
While the MPU6050 accelerometer and gyroscope sensor capture multiaxis motion and provide real-time feedback on the dynamic behaviour of the wingtip, the OMETRON laser vibrometer enables more precise measurement of vibration frequencies and mode shapes without physical contact.
An FFT analysis is performed on the measurements obtained from the laser vibrometer and plotted on a frequency versus time spectrogram to visualise the frequency content (see Fig.6).
The data from the laser vibrometer confirms similar findings, with the frequency of the observed phenomenon levelling around 35 Hz. However, as the data are more refined, a more comprehensive understanding of the phenomenon can be done by comparing it with inertial sensor results. It can be said that as time progresses and airflow velocity increases, the flutter frequency of the wing decreases. This suggests that airflow exerts a damping effect on the frequency of flutter while simultaneously increasing the amplitude.

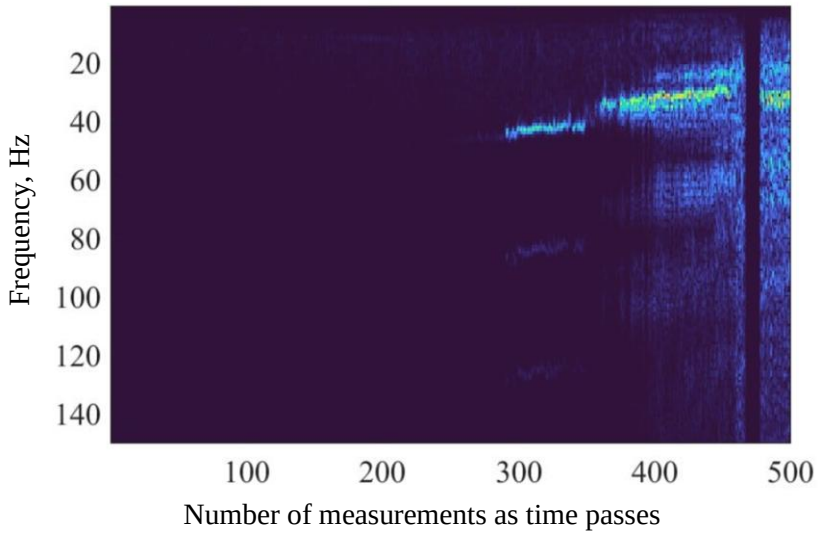

Fig. 6. Wingtip bending vibration frequency response to increasing airflow velocity, based on sequential measurements using a laser vibrometer

Additionally, the laser vibrometer data reveal repetitive patterns at higher frequencies, suggesting the presence of different modes of the same vibration. This indicates that multiple vibrational modes are interacting, which further supports the onset of aeroelastic instability.
The consistency of the primary frequency, along with the appearance of higher frequency modes, demonstrates that the system has reached a resonant state where aerodynamic forces and structural vibrations are coupled.

3. Results and discussion

The use of inertial sensors, such as accelerometers and gyroscopes sensor, and non-contact measurement techniques, such as laser vibrometers, enabled tracking of wingtip vibrations, which resulted in the possibility to analyse the flutter and its prediction. The accelerometer and gyroscope data can provide critical insights into the onset of not only the flutter phenomenon but also divergence. On the other hand, the laser vibrometer not only offers flutter prediction

capability but also gives a more detailed view of the vibration modes and their interactions. The complementary nature of these methods enhances the understanding of aeroelastic instability, revealing both damping effects and the coupling of aerodynamic forces with structural vibrations. Experimental research on the flutter phenomenon shows that the wing exhibits vibrational modes, with the onset of instability occurring at a specific airflow velocity, leading to aeroelastic instability. Using the accelerometer-gyroscope sensor and the laser vibrometer, the research successfully identified the critical airflow velocity at which flutter instability occurs, it equals around 20 m/s, as the wing experiences a significant increase in vibration amplitudes and torsional motion after this critical point is reached.
The spectrogram analysis showed a broader view of the flutter phenomenon and revealed its frequency of 35 Hz, this value was confirmed by application of both methods. The findings of this research may contribute to the development of safer and more stable experimental research designs, particularly for applications involving a high-aspect ratio structure.

4. Conclusions

1. Experimental measurement methods were performed by applying inertial sensors and non-contact techniques used to investigate the flutter phenomenon in the designed wing model. The accelerometer and gyroscope sensor data indicate divergence at 19 m/s, with flutter occurring at 20 m/s, marked by increasing vibration amplitudes and torsional motion. The laser vibrometer confirms these findings, showing levelled frequencies around 35 Hz, with additional insights into the interaction of higher-frequency modes. Both methods provide consistent results, with the laser vibrometer offering a detailed view of vibrational modes and the inertial sensors capturing dynamic responses related to the onset of flutter.
2. The experimental results demonstrate that divergence occurs at lower velocities, while flutter can be observed at a higher critical velocity. Comparing the methods emphasises the advantage of using advanced tools like the laser vibrometer, which provides a more detailed detection of different vibration modes and the onset of flutter. The method choice depends on the level of accuracy needed and the equipment available, with a laser vibrometer offering a clearer understanding of how the structure behaves and flutter begins, but an inertial sensor being more affordable with easier availability.

References

1. FAHAD LATIF, Rana, et al. *Semi-Analytical Flutter Analysis of a Light UAV Wing*. In: Proceedings of the 17th International Bhurban Conference on Applied Sciences and Technology. Islamabad, 2020. pp. 88-98. DOI: 10.1109/IBCAST47879.2020.9044521.
2. KHIZER ALI KHAN, Muhammad, et al. *An overview of methods for investigation of aeroelastic response on high aspect ratio fixed-winged aircraft*. In: Proceedings of the 3rd Pak-Turk International Conference on Materials Science and Engineering. Topi, 2020. pp. 6-18. DOI: 10.1088/1757-899X/899/1/012002.
3. FIGUEIREDO, Helosman Valente, et al. Aeroelastic Vibration Measurement Based on Laser and Computer Vision Technique. *Experimental Techniques*, vol. 45 (2020), no. 2, pp. 95-107. DOI: 10.1007/s40799-020-00399-0.
4. MERTENS, Christoph, 2023. *Experimental Aeroelastic Characterization Based on Integrated Optical Measurements*. Doctoral dissertation. Delft University of Technology, Delft. Available at: https://www.researchgate.net/publication/371984821_Experimental_Aeroelastic_Characterization_Based_on_Integrated_Optical_Measurements.
5. InvenSense, 2013. *MPU-6000 and MPU-6050 Product Specification Revision 3.4 Datasheet*. (PDF). InvenSense. [viewed 27 February 2025].
6. ROTHBERG, Steve J., et al. An international review of laser Doppler vibrometry: Making light work of vibration measurement. *Optics and Lasers in Engineering*, vol. 99 (2017), pp. 11-22. Available at: https://doi.org/10.1016/j.optlaseng.2016.10.023.

International Young Researchers' Conference
INDUSTRIAL ENGINEERING 2025
Conference Proceedings
ISSN 2538-6727 (online)
SL xxx. xxx printer's sheets. Order No. xxx
Publisher Kaunas University of Technology, K. Donelaičio 73, LT-44029 Kaunas
Publishing House Technologija, Studentų 54, LT-51424 Kaunas